9

ACS SYMPOSIUM SERIES 1106

Advances in Fluorine-Containing Polymers

EDITED BY

Dennis W. Smith, Jr., Scott T. Iacono, Dylan J. Boday, and Sharon C. Kettwich

18.9984032

Downloaded by 89.163.34.136 on August 28, 2012 | http://pubs.acs.org
Publication Date (Web): August 16, 2012 | doi: 10.1021/bk-2012-1106.fw001

Advances in Fluorine-Containing Polymers

In Advances in Fluorine-Containing Polymers; Smith, D., et al.;
ACS Symposium Series; American Chemical Society: Washington, DC, 2012.

Downloaded by 89.163.34.136 on August 28, 2012 | http://pubs.acs.org
Publication Date (Web): August 16, 2012 | doi: 10.1021/bk-2012-1106.fw001

ACS SYMPOSIUM SERIES **1106**

Advances in Fluorine-Containing Polymers

Dennis W. Smith, Jr., Editor
The University of Texas at Dallas
Richardson, Texas, United States

Scott T. Iacono, Editor
United States Air Force Academy
USAF Academy, Colorado, United States

Dylan J. Boday, Editor
IBM Materials Engineering
Tucson, Arizona, United States

Sharon C. Kettwich, Editor
United States Air Force Academy
USAF Academy, Colorado, United States

Downloaded by 89.163.34.136 on August 28, 2012 | http://pubs.acs.org
Publication Date (Web): August 16, 2012 | doi: 10.1021/bk-2012-1106.fw001

Sponsored by the
ACS Division of Polymer Chemistry, Inc.

American Chemical Society, Washington, DC

Distributed in print by Oxford University Press, Inc.

Downloaded by 89.163.34.136 on August 28, 2012 | http://pubs.acs.org
Publication Date (Web): August 16, 2012 | doi: 10.1021/bk-2012-1106.fw001

Library of Congress Cataloging-in-Publication Data

Advances in fluorine-containing polymers / Dennis W. Smith, Jr., editor, the University of Texas at Dallas, Richardson, Texas, United States, Scott T. Iacono, editor, United States Air Force Academy, USAF Academy, Colorado, United States, Dylan J. Boday, editor, IBM Materials Engineering, Tucson, Arizona, United States, Sharon C. Kettwich, editor, United States Air Force Academy, USAF Academy, Colorado, United States ; sponsored by the ACS Division of Polymer Chemistry, Inc.
pages cm. -- (ACS symposium series ; 1106)
Includes bibliographical references and index.
ISBN 978-0-8412-2792-7
1. Fluoropolymers. I. Smith, Dennis W., Jr., editor of compilation. II. American Chemical Society. Division of Polymer Chemistry.
QD383.F48A38 2012
547′.84--dc23
2012026988

The paper used in this publication meets the minimum requirements of American National Standard for Information Sciences—Permanence of Paper for Printed Library Materials, ANSI Z39.48n1984.

Copyright © 2012 American Chemical Society

Distributed in print by Oxford University Press, Inc.

All Rights Reserved. Reprographic copying beyond that permitted by Sections 107 or 108 of the U.S. Copyright Act is allowed for internal use only, provided that a per-chapter fee of $40.25 plus $0.75 per page is paid to the Copyright Clearance Center, Inc., 222 Rosewood Drive, Danvers, MA 01923, USA. Republication or reproduction for sale of pages in this book is permitted only under license from ACS. Direct these and other permission requests to ACS Copyright Office, Publications Division, 1155 16th Street, N.W., Washington, DC 20036.

The citation of trade names and/or names of manufacturers in this publication is not to be construed as an endorsement or as approval by ACS of the commercial products or services referenced herein; nor should the mere reference herein to any drawing, specification, chemical process, or other data be regarded as a license or as a conveyance of any right or permission to the holder, reader, or any other person or corporation, to manufacture, reproduce, use, or sell any patented invention or copyrighted work that may in any way be related thereto. Registered names, trademarks, etc., used in this publication, even without specific indication thereof, are not to be considered unprotected by law.

PRINTED IN THE UNITED STATES OF AMERICA

Downloaded by 89.163.34.136 on August 28, 2012 | http://pubs.acs.org
Publication Date (Web): August 16, 2012 | doi: 10.1021/bk-2012-1106.fw001

Foreword

The ACS Symposium Series was first published in 1974 to provide a mechanism for publishing symposia quickly in book form. The purpose of the series is to publish timely, comprehensive books developed from the ACS sponsored symposia based on current scientific research. Occasionally, books are developed from symposia sponsored by other organizations when the topic is of keen interest to the chemistry audience.

Before agreeing to publish a book, the proposed table of contents is reviewed for appropriate and comprehensive coverage and for interest to the audience. Some papers may be excluded to better focus the book; others may be added to provide comprehensiveness. When appropriate, overview or introductory chapters are added. Drafts of chapters are peer-reviewed prior to final acceptance or rejection, and manuscripts are prepared in camera-ready format.

As a rule, only original research papers and original review papers are included in the volumes. Verbatim reproductions of previous published papers are not accepted.

ACS Books Department

Downloaded by 89.163.34.136 on August 28, 2012 | http://pubs.acs.org
Publication Date (Web): August 16, 2012 | doi: 10.1021/bk-2012-1106.pr001

Preface

Fluorine containing polymer science and technology is nearly 70 years old, and fluoropolymer commercial markets maintain a growth rate above the US GDP. Advances in the ability to tailor fluoropolymer properties continue to forge a wide range of technologies to better control their unique optical, electronic, processing, environmental stability, and surface properties.

The purpose of this book is to publish new discoveries from leading international laboratories including academia, government, and industrial institutions. The multidisciplinary nature of fluoropolymer research lends their development to applications including, but not limited to, automotive, aerospace, biomedical, and defense technologies.

This timely collection is based on the international symposium, *Fluroine Containing Polymers*, which was held at the 230th National ACS Meeting (Washington, DC), 238th National ACS Meeting (Washington, DC), and 242nd National ACS Meeting (Denver, CO) in 2005, 2009, and 2011, respectively. Many exciting new findings have been reported in these past symposia that include fundamental structure/property relationships, new polymerization methodologies for emerging applications, energy conversion, photonics, coatings, and processing.

The book is targeted for academic and industrial scientists and engineers who are engaged in research and developments of fluoropolymer synthesis, characterization, and materials processing.

We thank the authors for their timely contributions and revisions throughout this publication process. We would also acknowledge the reviewers for providing important and judicious feedback. We express appreciation to the past organizers and session chairs of this symposium series for their support. Finally, we thank the ACS Division of Polymer Chemistry and Division of Fluorine Chemistry for sponsoring and funding the symposia over the years.

Dennis W. Smith, Jr., Professor & Welch Chair
Department of Chemistry & The Alan MacDiramid NanoTech Institute
The University of Texas at Dallas
Richardson, Texas 75080

Scott T. Iacono, Associate Professor
Department of Chemistry
United States Air Force Academy
USAF Academy, Colorado 80840

In Advances in Fluorine-Containing Polymers; Smith, D., et al.;
ACS Symposium Series; American Chemical Society: Washington, DC, 2012.

Dylan J. Boday, Senior Scientist
IBM Materials Engineering
9000 S. Rita Road
Tucson, Arizona 85744

Sharon C. Kettwich, Research Scientist
Department of Chemistry
United States Air Force Academy
USAF Academy, Colorado 80840

Downloaded by 89.163.34.136 on August 28, 2012 | http://pubs.acs.org
Publication Date (Web): August 16, 2012 | doi: 10.1021/bk-2012-1106.pr001

Downloaded by COLUMBIA UNIV on August 28, 2012 | http://pubs.acs.org
Publication Date (Web): August 16, 2012 | doi: 10.1021/bk-2012-1106.ot001

Editors' Biographies

Dennis W. Smith, Jr.

Dennis joined The Dow Chemical Company Central Research Laboratory as Sr. Research Chemist in 1993 working primarily on the synthesis and characterization of high performance thermosets for thin film microelectronics applications. He then joined Clemson in 1998 and was promoted to Professor of Chemistry in 2006, and in 2010, he joined The University of Texas at Dallas as Robert A. Welch Professor of Chemistry and was elected as Fellow of The American Chemical Society. His research interests focus Broad research interests include synthesis, mechanism, structure/property relationships, and applications of polymeric materials and composites. Dr. Dennis W. Smith, Jr. received his BS from Missouri State University and his Ph.D. from the University of Florida under the guidance of Prof. Ken Wagener on the scope and mechanism of acyclic diene metathesis (ADMET) polymerization.

Scott T. Iacono

Since 2002, Scott was a research chemist at the Air Force Research Laboratory at Edwards Air Force Base synthesizing inorganic-organic hybrid fluoropolymers for solid rocket motor propulsion components. In 2010, he joined the Department of Chemistry at the United States Air Force Academy and has since been promoted to associate professor and concurrently serves as the Chemistry Research Center Director. His current research efforts focus on organofluorine methodologies for monomer development, fluorosiloxane polymers, metalized fluoropolymer composites, and fulvene-based conjugated polymers. He has authored collectively over 60 journal papers, conference papers, and contributed book chapters. Scott Iacono completed his BS at Louisiana State University and PhD studies with emphasis organic and polymer chemistry at Clemson University.

In Advances in Fluorine-Containing Polymers; Smith, D., et al.;
ACS Symposium Series; American Chemical Society: Washington, DC, 2012.

Dylan J. Boday

Dylan's research at IBM focuses on creating inventive pathways toward the development of polymers, composites, surface science, nanoparticles, and hybrid materials. He also established and now leads a global team focused on the development of sustainable materials for use within IBM products. His technical contributions have led to more than 30 patent filings and numerous published articles. For these efforts, Dylan was named an IBM Master Inventor. Dylan holds a B.S. degree in Chemistry and a Ph.D. degree in Materials Engineering from the University of Arizona.

Downloaded by COLUMBIA UNIV on August 28, 2012 | http://pubs.acs.org
Publication Date (Web): August 16, 2012 | doi: 10.1021/bk-2012-1106.ot001

Sharon C. Kettwich

Sharon is CEO of Fortiori Scienta, Inc., a scientific research and development company that specializes in contracting with government agencies to perform basic research investigations that aim to produce products and materials for military applications. Sharon has worked at the United States Air Force Academy in the Chemistry Department's Research Center since 2010 on polymer research with an emphasis on fluorosiloxane polymer systems, fluoropolymers, and metalized structural energetic composites. Prior research was focused on low temperature chemical physics studies. Sharon received a B.S. in Chemistry, a B.A. in Spanish from the University of New Mexico, and a Ph.D. from the University of Wyoming in Physical Chemistry.

Chapter 1

The State of Fluoropolymers

Dylan J. Boday*

IBM Materials Engineering, Tucson, Arizona 85744
***E-mail: dboday@us.ibm.com**

Downloaded by 89.163.34.136 on August 28, 2012 | http://pubs.acs.org
Publication Date (Web): August 16, 2012 | doi: 10.1021/bk-2012-1106.ch001

This overview provides a brief summary of the current state for the fluoropolymer field. It includes fundamental fluorpolymer chemistry, fluorinated coatings, biomedical applications, fluorinated materials in composites, fluorinated elastomers and copolymer synthetic strategies. The above mentioned research areas are an example of this field which is rapidly growing due to the fact that inclusion of fluorine can impart such significant changes to a bulk materials physical properties. This ACS Symposium Series book will highlight the advances in the fluoropolymer field, which will include contributions from the national Fluorine-Containing Symposium series.

Introduction

Fluorine containing polymer science and technology is approaching its dodranscentennial anniversary from the accidental discovery of poly(tetrafluoroethyene) marketed as Teflon (*1*). At its infancy, the research in this field was directed towards poly(tetrafluorethylene) (PTFE), with focus on developing and understanding the synthetic pathways to prepare PTFE and the bulk physical properties associated with PTFE. Today fluoropolymers can be found in nearly every major industry market. In 2010, the fluorpolymer industry had a revenue of $5.8 billion with uses ranging from non-stick cooking surfaces to use in clothing apparel. The outstanding properties and chemical inertness of PTFE has lead to significant research to incorporate fluorine into other polymers and additives. Several reviews in the area of fluoropolymers highlight the field's decorated past (*2–8*)). The research in this filed has transitioned from PTFE centric towards new growth fields for fluoropolymers. This transition, is leading to an estimated compounded annual growth rate of 6.5% through 2016 (*9*). This growth can not only be identified by tracking the financials of the fluoropolymer

In Advances in Fluorine-Containing Polymers; Smith, D., et al.;
ACS Symposium Series; American Chemical Society: Washington, DC, 2012.

field, but also through the scientific impact of the field. In 2011, the fluorpolymer field received in excess of 4000 citations. Tracking the number of citations per year from 1993 to present, the number of citations is growing exponentially demonstrating the rapid growth in scientific impact of this research field (Figure 1) (*10*).

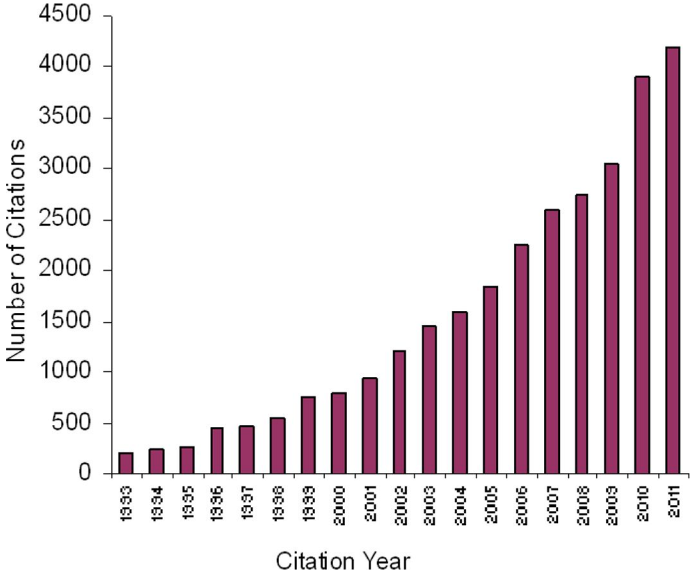

Figure 1. Number of citations per year for fluorine containing polymers.

The fluorpolymer field is not the only fluorine containing research area seeing significant growth. The use of fluorine, outside of the fluoropolymer field, is rapidly expanding in other areas such as in the pharmaceutical and agrochemical fields. Fluorine containing molecules have seen use in bioactive compounds to moderate metabolism, drug delivery and retention within biological systems (*11*). The pharmaceutical field in 2011 noticed significant growth where 7 out of 35 drugs approved contained fluorine and 3 of the 10 best selling drugs contained fluorine. This has lead to a significant amount of work surrounding the organofluorine field with new approaches to add fluorine functionalities to compound targets for use in the pharmaceutical and agrochemical fields. It is expected the field of fluoropolymers will benefit significantly from the increased attention in these other fields and that the growth of the fluorpolymer field will only continue to expand as the synthetic tool box expands to add fluorine.

The latest research in the field of fluorine containing materials was presented during the 2011 Fall American Chemical Society National meeting in Denver, Colorado. Following a very successful ACS symposium, the symposium organizers decided that to aid the growth of the fluoropolymer field, a book highlighting the research presented at this meeting would be beneficial. Within this ACS symposium series book, the field of fluoropolymer science and technology has been partioned to the following major themes:

Downloaded by 89.163.34.136 on August 28, 2012 | http://pubs.acs.org
Publication Date (Web): August 16, 2012 | doi: 10.1021/bk-2012-1106.ch001

1. Fluorine containing homo and copolymer synthesis
2. Biomedical applications
3. Fluoropolymer composites
4. Fluorinated materials in energy applications
5. Low energy fluoropolymer surfaces
6. Characterization of fluorinated materials

In this introductory chapter, each of these subsets of the fluorpolymer field is briefly reviewed. A large majority of the examples highlighted are from recent contributions to the national Fluorine-Containing Symposium series sponsored by the ACS Division of Polymer Chemistry.

Downloaded by 89.163.34.136 on August 28, 2012 | http://pubs.acs.org
Publication Date (Web): August 16, 2012 | doi: 10.1021/bk-2012-1106.ch001

Fluorine-Containing Homo and Copolymer Synthesis

Core to the fluoropolymer field is the synthesis of polymers containing fluorine. Without the significant work and attention towards this area, the applications made possible by these polymers as detailed *vida infra* would not be possible. Initial work in fluorine containing polymers focused on homo polymer synthesis with the primary focus on PTFE (*12*). This work has progressed towards the development of new polymerization methods and processes for new polymer networks such as controlled radical polymerizations (*13*) and cationic polymerizations (*14*). Initial work on copolymers focused on improving the solubility of the fluoropolymer (*15*) and has recently shifted towards the development of materials for advanced applications such as foul-resistant coatings (*16*) and lithography applications (*17*), which utilize the properties of fluorine which has been added to the polymer.

Within this book, several recent advances in the synthesis of fluoropolymers are highlighted. Loy et. al. discusses the use of semi-fluorinated polyarylene copolymers. These polymers were prepared via copolymerization of a fluorinated diethynylbenzene and 1,4-(biscyclopentadienone). The monomer ratio was varied to determine the effect on the polymer bulk properties as the fluorine concentration changes. Iacono et. al. demonstrates preparation of new fluorinated arylene vinylene ether polymers via step-growth polymerization of bishydroxy monomers with trifluorovinylethers. Optimization of the polymerization allows for tailored linear, block and network polymers. Asandeii et. al. explores various free radical initiators in various solvent systems to determine the effects on the vinylidene fluoride polymerization. Lastly, Aoshima et. al. discusses the preparation of well defined fluorine containing vinyl ether star polymers. These star polymers were prepared by base-assisted living cationic polymerization. The vinyl ether star polymers demonstrate sensitive upper critical solution temperature phase separation in organic solvents.

Biomedical Applications

Fluoropolymers demonstrate excellent inertness to various chemicals and biological environments as well as hydrophobicity and lipophilicity. Fluoropolymers have been used in biomedical applications such as ultrasound contrast agents (*18*), prosthetics (*19*), fluorinated amphiphile-colloids (*20*), contact lens (*21*) and drug delivery (*22*). As mentioned above, fluorine is currently the functionality of choice for the pharmaceutical industry. As this field continues to use fluorine containing molecules, the use of fluoropolymers in biomedical applications will continue to increase.

Perahia et. al. detail the development of responsive interfaces within a thin film through the development of perfluorocyclobutyl (PFCB) polyhedral oligomeric silisesquioxanes (POSS) composites. The responsive interface is demonstrated via exposure of the composite to humidity and monitoring the composites response using neutron reflectometry. From these results, it was determined that the fluorinated segment controls the POSS interactions within the composite. The results provide insight into how these thin films behave in various environments commonly found in medical applications.

Downloaded by 89.163.34.136 on August 28, 2012 | http://pubs.acs.org
Publication Date (Web): August 16, 2012 | doi: 10.1021/bk-2012-1106.ch001

Fluoropolymer Composites

Fluoropolymer composites have been extensively investigated to increase the mechanical properties of fluoropolymers or to add functionality to a fluoropolymer. Several key reviews in the area demonstrate the progress made in fluoropolymer composites (*23*, *24*). Specific examples of additives to fluoropolymers include carbon nanofibers (*25*) and carbon nanotubes (*26*) adding electrical conductivity and sensor applications, silica nanoparticles in proton exchange membranes (PEM) to extend the operating temperatures (*27*) and $CaF_2:Er^{3+}$ to PFCB for active optical devices (*28*). Other examples of composites include the dramatic improvements in the oleophobic properties of PFCB polymers and were observed from the addition of fluoroalkyl polyhedral oligomeric silisesquioxanes (F-POSS) (*29*).

Mabry et. al. describes the preparation of incompletely-condensed F-POSS and subjecting them to react with a variety of functional dichlorosilanes. This reaction adds a functionality which can be passive or reactive allowing for various interactions with the polymer matrices or improving the solubility of the F-POSS. Klapper et. al. details the optimization of fluoropolymer amphiphiles as surface active compounds. The fluorinated amphiphile block copolymers were prepared by free and controlled radical copolymerizations. This work demonstrates a simple and efficient procedure to prepare perfluorinated amphiphiles for use in modifying liquid-liquid or liquid-solid interactions. Lastly, Crouse describes a fluoropolymer composite formulation for energetic materials. These composites use the abundant amount of fluorine that serve as the oxidizer for strong electropositive metals which serve as the fuel. Not only do the fluoropolymer serve as the oxidizer, but serve as the polymer matrix. The composites prepared allow for simple processing and high energetic activity.

Fluorinated Materials in Energy Applications

With the increased demand for power required to meet society's needs currently and in particular the future, new advanced materials are necessary. A particular advanced material finding use in alternative energy applications are fluorine containing polymers (*30*). The most commonly investigated fluoropolymer for use in PEMs has been polyperfluorsulfonic acids (*31*). The fluorinated backbone of polyperfluorsulfonic acids allows for improved oxidation resistance and reduced water dissolution while maintaining ion conducting functionalities. It is also believed that fluorine within polyperfluorsulfonic acids drives phase separation thus allowing for ionic conducting domains to form (*32*). To improve energy conversion in PEMs, operating temperatures above 100 °C are targeted (*33*). Many of the polymers that are being evaluated in these elevated temperature applications are fluoropolymers with the excellent properties detailed above (*34*).

Ameduri et. al. describes the preparation of fluorinated copolymers containing a carbonate or ether pendent chains by radical polymerizations. These polymers were prepared by copolymerizing fluoroalkenes with vinyl monomers containing ether or carbonate functionalities. These fluoropolymers demonstrate excellent chemical inertness and thermal stability while containing pendent ether and carbonate functionalities which could find use in polymer electrolytes for lithium ion battery applications. As discussed above, Loy et. al. discusses the synthesis of fluorinated polyarylene copolymers which potentially can be used as proton exchange membranes.

Low Energy Fluoropolymer Surfaces

During the initial discovery of PTFE, it was noted that the polymer had inherent lubricity. This lubricity led to one of the most well established areas where fluoropolymers are used. These areas range from additives in conventional thermoplastics for reducing surface friction to non-stick surfaces (*35*). The low surface energy observed in fluorinated materials has led to their use in the development of super hydrophobic surfaces as either a neat fluorpolymer film (*36*) or using fluoropolymers as an additive (*37*). Not only have fluoropolymers displayed hydrophobicity, but they can also demonstrate oleophobic properties (*38*). Adding surface roughness and re-entrant surface texture to fluoropolymer films can increase the oleophobicity of the films with contact angles greater that 150° for both water and organic liquids with significantly lower surface tensions (*39*).

In this book, Tuteja et. al. described their recent work on developing oleophobic surfaces for oil-water separations. The surfaces were prepared by dip-coating a stainless steel mesh in a polyethylene glycol diacrylate and 20wt% fluorodecyl-POSS solution. Upon exposing the coated mesh to water and oil, the water absorbs into the mesh while the oil sits on the surface. This demonstrates a hydrophilic/oleophobic surface that may have applications in oil-water separations.

Downloaded by 89.163.34.136 on August 28, 2012 | http://pubs.acs.org
Publication Date (Web): August 16, 2012 | doi: 10.1021/bk-2012-1106.ch001

Downloaded by 89.163.34.136 on August 28, 2012 | http://pubs.acs.org
Publication Date (Web): August 16, 2012 | doi: 10.1021/bk-2012-1106.ch001

Characterization of Fluorinated Materials

The development of polymers containing fluorine is dictated by the ability to characterize these materials. This allows for further insight into the polymers microstructure and the affect with which the microstructure has on the bulk polymers structure-property relationship. Commonly used techniques to characterize fluoropolymers include mass spectroscopy (*40*), thermal techniques (*41*) and NMR (*42*). NMR is a characterization technique which is particularly useful due to the sensitivity, better dispersion resonances, natural abundance and magnetogyric ratio of ^{19}F compared to ^{1}H.

Within this book, Rinaldi et. al. details the use of 2-D NMR to characterize the microstructure of polyvinylidene fluoride (PVDF). ^{19}F NMR is particularly useful in fluoropolymer characterization due to the sensitivity of ^{19}F and large chemical shift dispersion. The information discussed provides insight into the structure-property relationship of PVDF and information on the polymerization process to prepare PVDF.

Conclusion

The above areas which the field of fluorine containing polymers has been parsed in to for this ACS symposium series books demonstrates the breadth of the field. It also shows how quickly the field is emerging into new directions and will continue to do so for the foreseeable future. This book is meant to highlight the contributions in the fluoropolymer field at the ACS national meetings and the ACS Division of Polymer Chemistry Workshops and catalyze it going forward by finding synergy in areas within the fluoropolymer field.

References

1. Plunket, R. J. Tetrafluoroethylene Polymers. U.S. Patent 2230654, 1941.
2. Genzer, J.; Efimenko, K. *Biofouling* **2006**, *46*, 297.
3. Souzy, R.; Ameduri, B. *Prog. Polym. Sci.* **2005**, *30*, 644.
4. Kang, E. T.; Zhang, Y. *Adv. Mater.* **2000**, *12*, 1481.
5. Imae, T. *Curr. Opin. Colloid Interface Sci.* **2003**, *8*, 307.
6. Ameduri, B.; Boutevin, B.; Guida-Pietrasanta, F.; Rousseau, A. *J. Fluorine Chem.* **2001**, *107*, 397.
7. Xu, T. W. *J. Membr. Sci.* **2005**, *263*, 1.
8. Ameduri, B. *Macromolecules* **2010**, *43*, 10163.
9. Fluoropolymers Market Analysis by Product Types, Applications & Geography - Trends & Global Forecasts (2011−2016). Markets and Markets, 2012. http://www.marketsandmarkets.com/Market-Reports/fluor-polymer-market-497.html.
10. Data was aquired from Web of Science using search string fluorine, polymer.
11. Ritter, S. K. *Chem. Eng. News* **2012**, February, 10.
12. Bixler, G. H. *Ind. Eng. Chem.* **1951**, *22*, 1085.
13. Jankova, K.; Hvilsted, S. *J. Fluorine Chem.* **2005**, *126*, 241.

14. Shimomoto, H.; Fukami, D.; Irita, T.; Katsukawa, K.; Nagai, T.; Kanaoka, S.; Aoshima, S. *J. Polym. Sci., Part A: Poly. Chem.* **2012**, *8*, 1547.
15. Imae, T. *Curr. Opin. Colloid Interface Sci.* **2003**, *8*, 307.
16. Wang, Y. P.; Bettes, D. E.; Finlay, J. A.; Brewer, L.; Callow, M. E.; Callow, J. A.; Wendt, D. E.; DeSimone, J. M. *Macromolecules* **2011**, *44*, 878.
17. Ito, H.; Truong, H. D.; Okazaki, M.; DiPietro, R. A. *J. Photopolym. Sci. Technol.* **2003**, *16*, 523.
18. Cosgrove, D. *Eur. J. Radiol.* **2006**, *60*, 324.
19. Kannan, R. Y.; Salacinski, H. J.; Butler, P. E.; Hamilton, G.; Seifalian, A. M. *J. Biomed. Mater. Res., Part B* **2005**, *74B*, 570.
20. Krafft, M. P.; Riess, J. G. *Biochimie* **1998**, *80*, 489.
21. Nicolson, P. C.; Vogt, J. *Biomaterials* **2001**, *22*, 3273.
22. Riess, J. G.; Krafft, M. P. *Biomaterials* **1998**, *19*, 1529.
23. Souzy, R.; Ameduri, B. *Prog. Polym. Sci.* **2005**, *30*, 644.
24. Coulson, S. R.; Woodward, I.; Badyal, J. P. S.; Willis, C. *J. Phys. Chem. B* **2000**, *104*, 8836.
25. Das, A.; Schutzius, T. M.; Bayer, I. S.; Megaridis, C. M. *Carbon* **2012**, *50*, 1346.
26. Wang, J.; Musameh, M. *Anal. Chem.* **2003**, *75*, 2075.
27. Harmer, M. A.; Farneth, W. E.; Sun, Q. *J. Amer. Chem. Soc.* **1996**, *118*, 7708.
28. Kumar, G. A.; Chen, C. W.; Riman, R.; Chen, S.; Smith, D. W., Jr.; Ballato, J. *Appl. Phys. Lett.* **2005**, *86*, 241105.
29. Iacono, S. T.; Budy, S. M.; Smith, D. W., Jr.; Mabry, J. M. *J. Mater. Chem.* **2010**, *20*, 2979.
30. Hickner, M. A.; Ghassemi, H.; Seung Kim, Y.; Einsla, B. R.; McGrath, J. E. *Chem. Rev.* **2004**, *104*, 4587.
31. Mauritz, K. A.; Moore, R. B. *Chem. Rev.* **2004**, *104*, 4535.
32. Kreuer, K. D. *J. Mater. Sci.* **2001**, *185*, 29.
33. Li, Q. F.; He, R. H.; Jensen, J. O.; Bjerrum, N. J. *Chem. Mater.* **2003**, *15*, 4896.
34. Doyle, M.; Choi, S. K.; Proulx, G. *J. Electrochem. Soc.* **2000**, *147*, 34.
35. Ashokkumar, S.; Adler-Nissen, J. *J. Food Eng.* **2011**, *105*, 537.
36. Agarwal, S.; Horst, S.; Bognitzki, M. *Macromol. Mater. Eng.* **2006**, *291*, 592.
37. Yilgor, I.; Bilgin, S.; Isik, M.; Yilgor, E. *Polymer* **2012**, *6*, 1180.
38. Han, D. W.; Steckl, A. J. *Langmuir* **2009**, *26*, 9454.
39. Tuteja, A.; Tuteja, A.; Ma, M. L.; Mabry, J. M.; Mazzella, S. A.; Rutledge, G. C.; McKinley, G. H.; Cohen, R. E. *Science* **2007**, *318*, 1618.
40. Romack, T. J.; Danel, l A. S.; Cottone, T. M.; Dutta, S. K. *Rapid Commun. Mass Spectrom.* **2008**, *22*, 930.
41. Fleszar, M. F. *Thermochim. Acta* **2000**, *357*, 279.
42. Li, L.; Rinaldi, P. L. *Macromolecules* **1996**, *29*, 4808.

Downloaded by 89.163.34.136 on August 28, 2012 | http://pubs.acs.org
Publication Date (Web): August 16, 2012 | doi: 10.1021/bk-2012-1106.ch001

Downloaded by PENNSYLVANIA STATE UNIV on August 28, 2012 | http://pubs.acs.org
Publication Date (Web): August 16, 2012 | doi: 10.1021/bk-2012-1106.ch002

Chapter 2

Recent Advances in Partially Fluorinated Arylene Vinylene Ether (FAVE) Polymers

Sharon C. Kettwich,[1] Benjamin R. Lund,[2] Dennis W. Smith Jr.,[*,2] and Scott T. Iacono[*,1]

**[1]Department of Chemistry, United States Air Force Academy,
2355 Fairchild Drive, Suite 2N225, USAF Academy, Colorado 80840
[2]Department of Chemistry and The Alan G. MacDiarmid NanoTech Institute, The University of Texas at Dallas, Richardson, Texas 75080
[*]E-mail: scott.iacono@usafa.edu (S.T.I.); dwsmith@utdallas.edu (D.W.S.)**

A new, facile step-growth polymerization of diols/bisphenols and aryl trifluorovinylethers has been established to afford fluorinated arylene vinylene ether (FAVE) polymers. Kinetic and mechanistic studies produced optimized polymerization methodologies that have led to the development of tailorable FAVE polymer systems to include linear polymers, telechelomers, segmented block polymers, and networks. The combination of tailroability, processablility, and thermal stability has promoted interest in light emissive materials, chemical sensors, and proton exchange membranes. This timely review will provide a comprehensive account of this new FAVE polymer system.

Introduction

Perfluoropolyethers (PFPEs) are a class of low molecular weight fluoropolymers that are typically liquid at room temperature. They possess similar thermal and chemical stabilities as poly(tetrafluoroethylene) (PTFE). PFPEs are advantageous to use as high service temperature fluids because of their low volatility, no shear thinning (near Newtonian behavior), and viscosity that is nearly independent of temperature (*1*). Very few examples of liquids compare to PFPEs stability in liquid phase behavior over a wide temperature range (−100 to 400 °C).

In Advances in Fluorine-Containing Polymers; Smith, D., et al.;
ACS Symposium Series; American Chemical Society: Washington, DC, 2012.

PFPEs are prepared by a variety of commercial processes. They can be prepared by reaction of fluoroolefins with elemental oxygen in the presence of UV light, ring-opening anionic polymerization of tetrafluorooxetane, or by ring-opening polymerization of hexafluoropropene oxide. Some notable examples of commercial PFPEs from these polymerization conditions include Fomblin® Z, Demnum®, and Krytox® (Scheme 1). PFPEs are currently used for diffusion pump fluids, lubricants, greases, low dielectric fluids, and protective environmental coatings. Other uses included segmenting PFPEs in polyurethanes, epoxy resins, polyesters, and paint additives for improving mechanical properties over the virgin polymer material.

While the thermal stability of PFPEs exceeds 400 °C in oxygen-rich environments, they suffer severely from metal-catalyzed degradation. For PFPEs, the formation of metal fluorides is thermodynamically favored which renders them unstable in the presence of metals, metal oxides, or metal salts at elevated temperatures. The mechanism of metal-catalyzed degradation of PFPE involves primarily chain scission of the ether linkage. It is noted that most degradation is limited to specific classes of PFPEs with particular metal compounds.

Downloaded by PENNSYLVANIA STATE UNIV on August 28, 2012 | http://pubs.acs.org
Publication Date (Web): August 16, 2012 | doi: 10.1021/bk-2012-1106.ch002

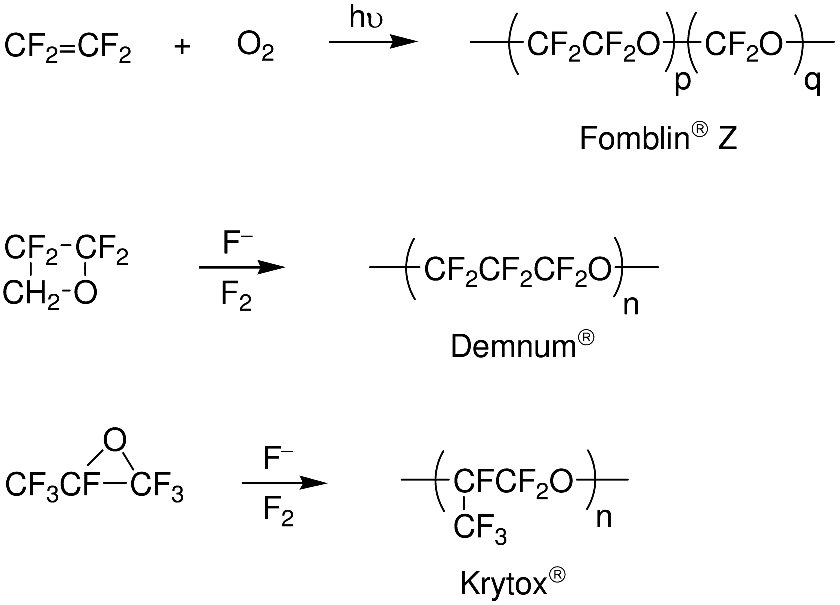

Scheme 1. Commercial preparation of perfluoropolyethers (PFPEs).

Nucleophile addition to fluorinated alkenes is widely known in organofluorine chemistry. It is also of major commercial importance to the fluoroelastomer industry where, for example, phenols and amines are used to crosslink unsaturated fluoropolymers (*2*). Furthermore, Feiring et al. has developed step-growth polymer chemistry based on this transformation to produce an alternative route

Downloaded by PENNSYLVANIA STATE UNIV on August 28, 2012 | http://pubs.acs.org
Publication Date (Web): August 16, 2012 | doi: 10.1021/bk-2012-1106.ch002

to prepare aliphatic PFPEs that exhibit low surface energy, exceptional thermal and chemical resistance, and excellent electrical insulating properties (Scheme 2) (*3*, *4*). It was also shown that amorphous fluoropolymers and liquid crystalline polymers were prepared employing this polymerization methodology (*5*, *6*). Utilizing this scheme affords PFPEs without the requirement to use high pressures, temperatures, or gaseous starting materials like those conditions typically used in commercial preparation.

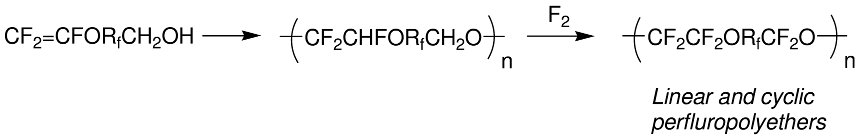
$CF_2{=}CFOR_fCH_2OH$
$-\!\!(CF_2CHFOR_fCH_2O)_n\!\!-$
F_2
$-\!\!(CF_2CF_2OR_fCF_2O)_n\!\!-$
Linear and cyclic perfluropolyethers

Scheme 2. Self-condensation, step-growth polymerization of fluorinated vinyl ether alcohols affording linear and cyclic PFPEs after fluorination.

Based on the preliminary work by Feiring et al., it is clear that the development of partially fluorinated PFPEs based on an aromatic polymer backbone is a feasible means to address not only performance limitations, but also to develop new polymer systems with modular utility in mind. This account is primarily concerned with the facile preparation of partially fluorinated arylene vinylene ether (FAVE) polymers and via base-promoted, step-growth polymerization of commercial aryl bis(triflurovinyloxy) ethers with bisphenols (Scheme 3).

Aryl trifluorovinyl ethers (TFVE) are a class of fluorinated alkenes that are prepared from readily available phenoic precursors. They can be functionalized employing common, operationally simple techniques suited for desired applications (Scheme 3, top). To date, two general polymerization routes using aryl TFVE have been employed in order to prepare tailorable advanced materials. A third general route utilizing octafluorocyclopentene has recently been discovered and is presented at the end of this discussion. Aryl TFVEs undergo condensate-free, thermal [2 + 2] cyclodimerization (*7*) to afford perfluorocyclobutyl (PFCB) aryl ether polymers (*8*). On the other hand, base-catalyzed, step-growth polymerization of aryl TFVEs with bisphenols afford FAVE polymers (Scheme 3, bottom) (*9*–*12*). The resulting polymers possess dual functionality and are telechelic in nature with intact TFVE endgroups and well-defined 1,2-difluoroethylene (Z = CF=CF) or 1,2,2-hydrofluoroethane (Z = $CHFCF_2$) enchainment. These polymers can be modularly tailored by functionalization of the aryl group (the functional spacer) for applications including thermally crosslinkable fluoroelastomer additives, (*9*, *13*) proton exchange membranes (PEMs) for hydrogen-based fuel cells, (*10*) polymer light emitting diodes (PLEDs), (*11*) and chemical sensors (*12*, *14*). Recent work involving copolymerization of bisfunctional *C*-, *P*-, *N*-, and *S*- monomers and functionalizing heterogeneous silica supports (denoted *X* in Scheme 3) with aryl TFVE will also be discussed.

Downloaded by PENNSYLVANIA STATE UNIV on August 28, 2012 | http://pubs.acs.org
Publication Date (Web): August 16, 2012 | doi: 10.1021/bk-2012-1106.ch002

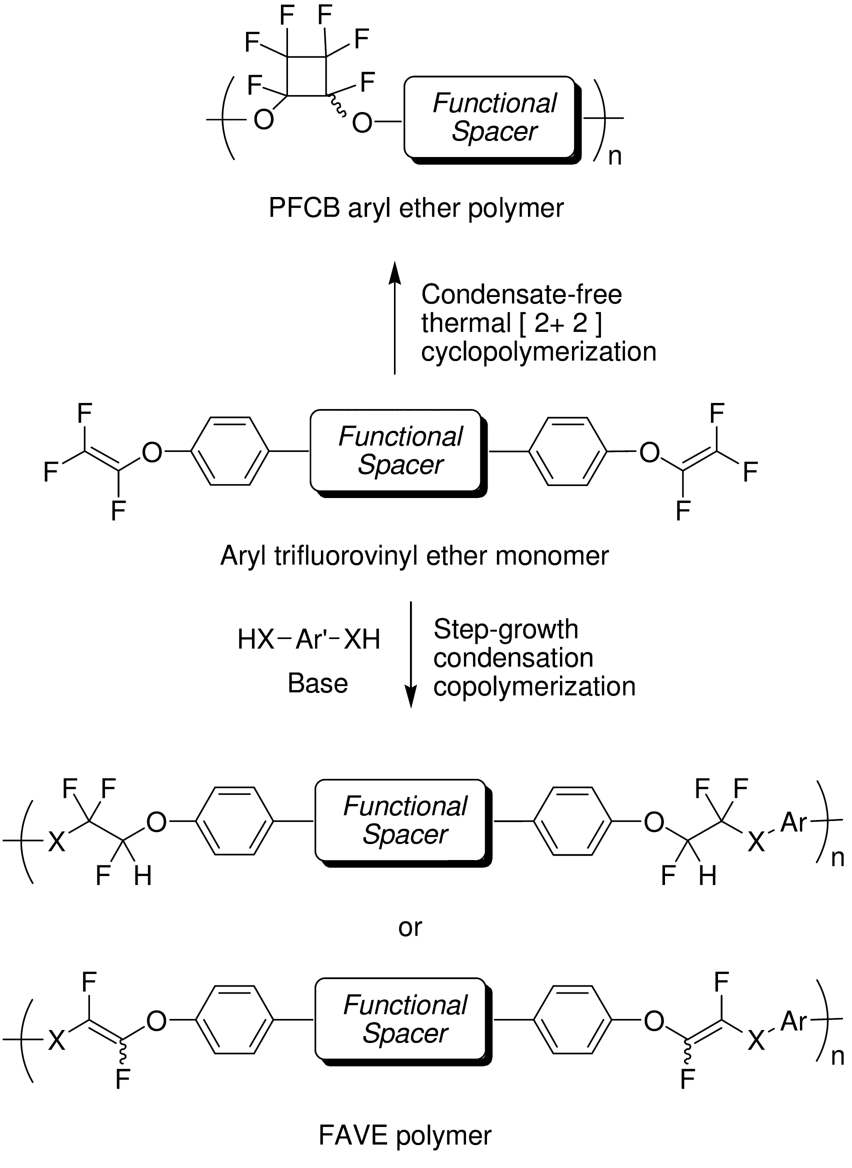
PFCB aryl ether polymer
Functional Spacer
Condensate-free thermal [2+ 2] cyclopolymerization
Aryl trifluorovinyl ether monomer
HX−Ar'−XH
Base
Step-growth condensation copolymerization
or
FAVE polymer

Scheme 3. Two distinct routes to functionalized step-growth, semifluorinated aryl ether polymers from aryl TFVE monomers: (top) thermal [2 + 2] cyclodimerization to afford PFCB aryl ether polymers and (bottom) by base-catalyzed nucleophilic addition of bisphenols to produce semifluorinated aryl heteroether polymers.

Downloaded by PENNSYLVANIA STATE UNIV on August 28, 2012 | http://pubs.acs.org
Publication Date (Web): August 16, 2012 | doi: 10.1021/bk-2012-1106.ch002

Results and Discussion

Step-Growth Polymers

Methodology

The initial work in this arrangement focuses on employing the step-growth polymerization of commercially available aryl TFVEs with bisphenols in a 1:1 molar ratio affording transparent, film-forming FAVE polymers, as shown in Scheme 4. One of the optimized polymerization pathways involved generation of the bisphenoxide sodium salt using NaH in DMF followed by stoichiometric addition of aryl TFVE monomer, while stirring at 60−80 °C for 3−6 h. This method produced polymers possessing primarily 1,2-difluoroethylene (Z = CF=CF) from the elimination of sodium fluoride. Residual 1,2,2-hydrofluoroethane groups (Z = $CHFCF_2$) are a result of protonation of the intermediate anion by free phenol or adventitious water. Alternatively, Cs_2CO_3 (50 mol %) was used to prepare FAVE polymers where up to 80% of the polymer backbone was enriched with 1,2,2-hydrofluoroethane groups (Z = $CHFCF_2$). This result is consistent with the observation that the 1,1,2-trifluoroethane anion intermediate (Z = CF_2CFC^-) is protonated and regenerates the carbonate base. It is noted that when Z = $CHFCF_2$, the unit is directional in accordance to the order of the diaryl spacer group (X with respect to Y). Therefore, the order should represent −X−Ar−O−$CHFCF_2$−O−Ar−Y− as a repeat unit. A small molecule methodology was recently reported (*15*). Here, the ability to tailor FAVE polymers from monofunctionalized aryl TFVEs or bisphenols offers an additional opportunity to design PFPE-based materials from an experimental, bottom-up approach.

Overall, the preparation of FAVE polymers proceeded in high isolated yields (50−80%), often producing fibrous white to pale yellow solids after purification. The purified polymers are solution processable in common organic solvents ($CHCl_3$, THF, DMSO, or cyclopentanone) to afford optically transparent, flexible films. The simplicity of the polymerization is also realized by the operationally simple method of purification. FAVE polymers are precipitated from the crude polymerization mixture in deionized water or methanol. The precipitated solid polymer is then collected by vacuum filtration followed by successive washings with deionized water, methanol, and hexanes. The polymers can be reprecipitated in methanol or soxlet extraction in order to remove lower molecular weight fractions.

For the polymers enriched with the internal fluoroolefins (Z = CF=CF), approximately a 1.2:1 (*Z*):(*E*)-isomer ratio was typically observed by ^{19}F NMR in all cases. This observation is consistent with single molecule phenol additions to aryl trifluorovinyl ether (TFVEs) and also perfluorovinyl alkyl ethers studied by Feiring (*3*, *16*). The degree of unsaturation was also shown to be controlled by substitution of the spacer group (X or Y). Substitution with electron withdrawing groups (e.g., X or Y = $C(CF_3)_2$) seemed to retard the degree of unsaturation. These results were repeatable over multiple polymerizations while rigorously controlling reaction conditions (e.g., measuring precise stoichiometry, controlling temperature, and using the same solvent batch).

Downloaded by PENNSYLVANIA STATE UNIV on August 28, 2012 | http://pubs.acs.org
Publication Date (Web): August 16, 2012 | doi: 10.1021/bk-2012-1106.ch002

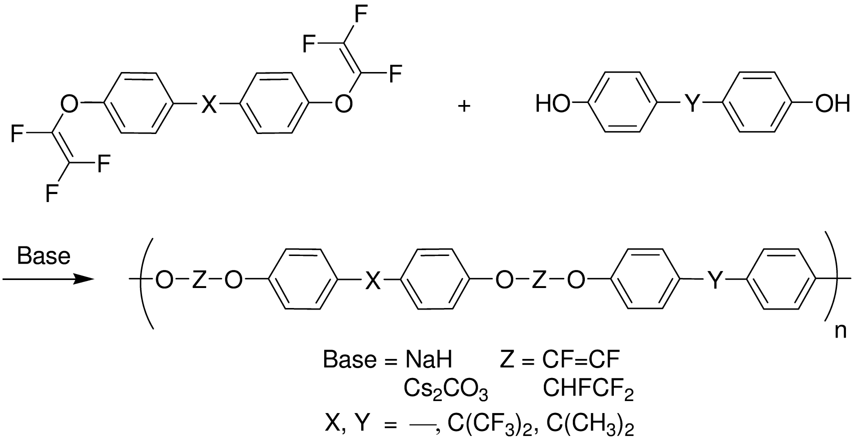
F
F
F
O
X
O
F
F
F
+
HO
Y
OH
Base
O–Z–O
X
O–Z–O
Y
n
Base = NaH
Cs2CO3
Z = CF=CF
CHFCF2
X, Y = —, C(CF3)2, C(CH3)2

Scheme 4. Step-growth condensation polymerization of aryl TFVE with bisphenols affording FAVE polymers.

Attempts to prepare the more obvious polymer system with the biphenyl aryl ether backbone from 4,4′-dihydroxydiphenyl and the 4,4′-bis(4-trifluorovinyloxy)biphenyl produced an insoluble solid (Scheme 5). No further characterization was attempted to confirm the proposed structure. However, it is presumed that rigid nature of the biphenyl polymer backbone renders this chain extended system insoluble. This result may indicate that in order to solubilize the polymer, a flexible segment may be required in the monomers with substitution in the X or Y position, where X or Y = $C(CH_3)_2$ or $C(CF_3)_2$.

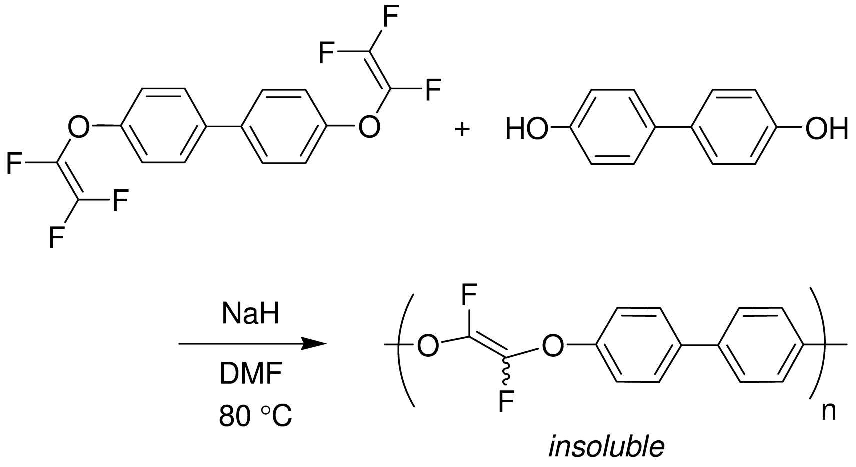
F
F
F
O
O
F
F
F
+
HO
OH
NaH
DMF
80 °C
F
O
O
F
n
insoluble

Scheme 5. Polymerization of 4,4'-bis(4-trifluorovinyloxy)biphenyl and 4,4'-dihydroxyphenol.

FAVE polymers with alternating aryl/alkyl backbones (Scheme 6) were successfully prepared. Number-average molecular weight (M_n) of the polymers ranged 900–6800. Although with low molecular weight, these polymers still produced free-standing films. The flexibility of the alkyl segments in the FAVE polymer backbone lowered the glass transition temperature (T_g) significantly compared with the aryl segmented polymers (*vida infra*).

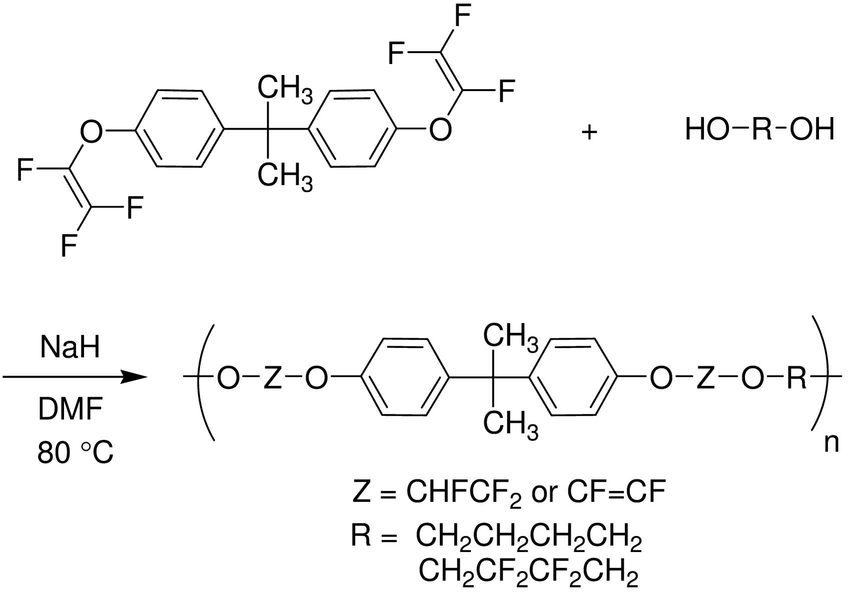

Scheme 6. Polymerization of alkyl diols with 4,4'-bis(4-trifluorovinyloxy)-biphenyl afforded FAVE polymers with alternating aryl/alkyl ether backbones.

Thermal Properties

Differential scanning calorimetry (DSC) studies on FAVE polymers demonstrated a broad range of glass transition temperatures (T_g) of 3–122 °C. The lowest T_g of 3 °C was observed for fluoroalkyl polymer (R = $CH_2CF_2CF_2CH_2$). Introducing flexible, fluorinated alkyl or aryl segments, as a general trend, induces more polymer chain slippage thereby lowering T_g among the FAVE polymers.

Similar thermal activation of the internal fluoroolefin was observed by calorimetry analysis. The thermal crosslinking of the internal fluoroolefin (Z = CF=CF) was observed via DSC analysis, which gave exotherm onsets at 220–300 °C. DSC data for FAVE polymers before and after heating to 300 °C in nitrogen showed an initial T_g of the amorphous FAVE thermoplastics. However, after crosslinking the polymer revealed no T_g indicating a densely, insoluble cross-linked network.

Downloaded by PENNSYLVANIA STATE UNIV on August 28, 2012 | http://pubs.acs.org
Publication Date (Web): August 16, 2012 | doi: 10.1021/bk-2012-1106.ch002

Thermogravimetric analysis (TGA) of FAVE polymers exhibited two discret onset decomposition temperatures (T_d) in nitrogen, whereas only a single T_d was observed in air. Figure 1 shows two the decomposition events. No greater than 5% mass loss was observed after the first T_d in nitrogen among the FAVE polymer studied. A single T_d is observed in air and may be the result of oxidation of the internal fluoroolefin. This would be consistent with earlier work that reports that fluorinated vinyl ethers oxidize in air at elevated temperatures and undergo stabilizing skeletal rearrangement before decomposition (*17*). Overall char yields ranged from 30−40% at 900 °C in nitrogen, producing black, glass-like solids.

Downloaded by PENNSYLVANIA STATE UNIV on August 28, 2012 | http://pubs.acs.org
Publication Date (Web): August 16, 2012 | doi: 10.1021/bk-2012-1106.ch002

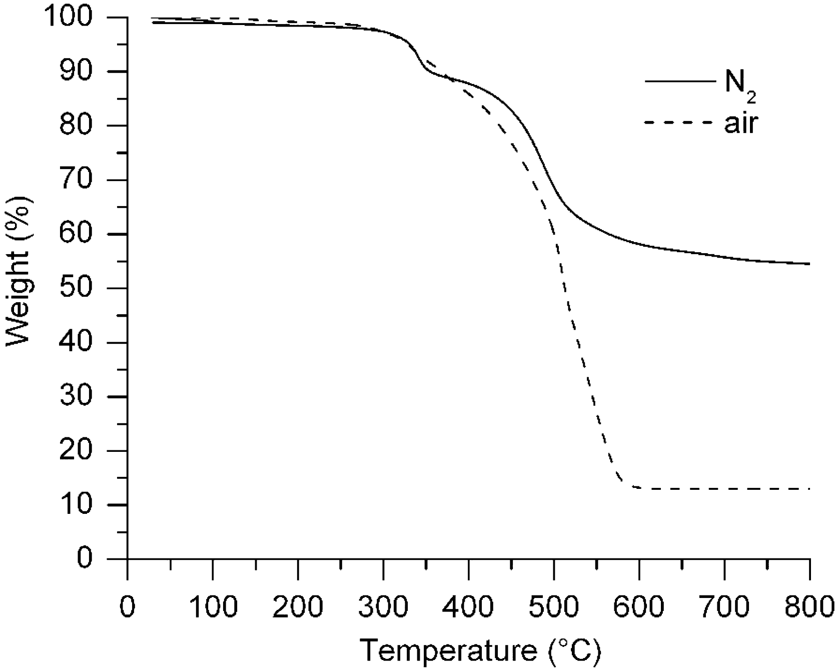

Figure 1. TGA analysis of a FAVE polymer in N_2 and air where a noticeable step-wise degradation is only present in N_2.

Attempts to chemically activate the internal difluorodioxyvinylene groups with hν or chemical initiators such as AIBN, BF_3 etherate, or benzoyl peroxide failed to induce reactivity. Both enchained Z segments (Z = CF=CF and $CHFCF_2$) remained intact by ^{19}F NMR analysis. As previously reported, even aryl TFVEs do not undergo radical-initiated polymerizations under such conditions (*18*).

An experimental correlation was observed from TGA analysis that showed that the amount of initial weight loss of FAVE polymers heated in N_2 to 350 °C is proportional to the amount of internal fluoroolefin content (Z = CF=CF) (Figure 2). As such, higher internal fluoroolefin content FAVE polymers showed greater weight loss upon heating than those with less internal fluoroolefin content. Gas chromatography coupled with mass spectroscopy (GC−MS) of chloroform-soluble fractions after polymer samples were heated to 350 °C revealed the presence of bisphenol fragments. Based on this observation, it appears the activation of the internal fluoroolefins to form polymer networks proceeds with the expulsion of phenol, indicating that chain scission of the ether linkages is likely. The nature of the bond scission, wheter homo- or heterolytic, remains unclear.

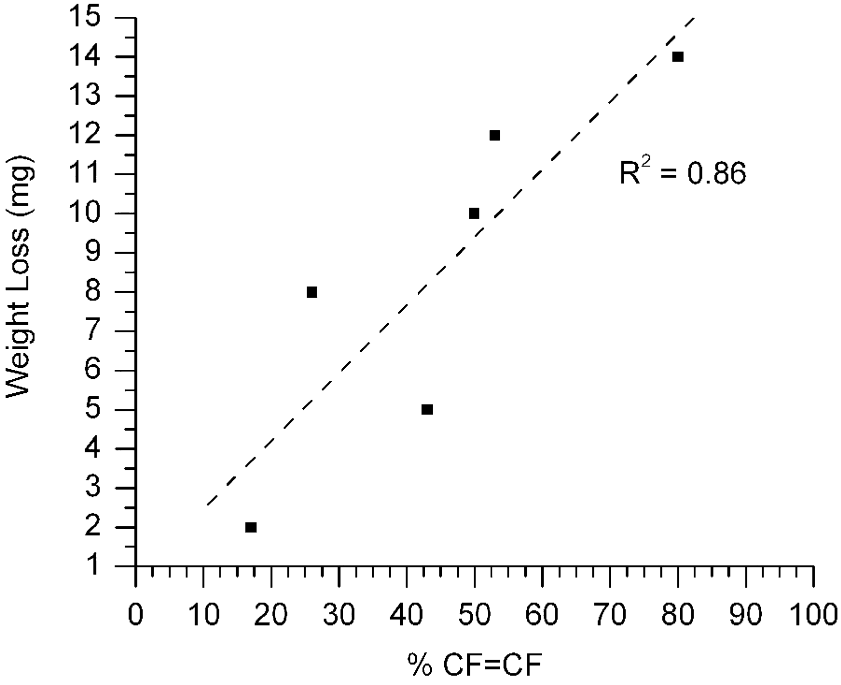

Figure 2. Plot of onset weight loss versus percent of Z = CF=CF in selected FAVE polymers heated in N_2 to 350 °C.

Polymerization Kinetics

The novel nature of the step-growth polymerization to afford FAVE polymers prompted investigation into understanding the kinetics of this system. An extended account was recently published detailing polymerization kinetics and mechanistic understanding (*19*). The biphenol AF derived FAVE polymer (X = Y = $C(CF_3)_2$) was used as a model system to understand the kinetics using NaH or catalytic Cs_2CO_3. ^{19}F NMR served as a suitable tool to evaluate polymerization kinetics. The polymerization, specifically the conversion, can be quantitatively monitored by relative peak integration of the ^{19}F peak signals of the aryl TFVE groups compared with the formation of the internal fluroolefins, where Z = CF=CF. Among polymerization temperature ranges 50−90 °C there is no evidence of the aryl TFVE signals in the ^{19}F NMR after 180 min. The *n*-th order kinetic model was used to determine rate constants over a series of programmed temperatures. Polymerization using stoichiometric NaH resulted in second order kinetics with

Downloaded by PENNSYLVANIA STATE UNIV on August 28, 2012 | http://pubs.acs.org
Publication Date (Web): August 16, 2012 | doi: 10.1021/bk-2012-1106.ch002

Downloaded by PENNSYLVANIA STATE UNIV on August 28, 2012 | http://pubs.acs.org
Publication Date (Web): August 16, 2012 | doi: 10.1021/bk-2012-1106.ch002

an activation energy of 59 kJ/mol. Compared with common routes of step-growth polymerizations using bisphenol monomers, FAVE polymerizations demonstrate analogous activation energies when compared with poly(carbonate)s (77 kJ/mol), poly(urethane)s (31−35 kJ/mol), or poly(ester)s (41−188 kJ/mol) (*20*).

Functionalized Polymers

While fluoropolymers possess superior material property advantages over their hydrogen-containing analogs, they have shown little utility for light emissive applications. This is primarily due to poor solution processablility because of their high crystalline nature and their lack of extended π−π conjugation. It has been shown, however, that introducing fluorine into conjugated polymers diminishes their susceptibility to light induced oxidation, thus improving their resistance to photobleaching (*21*). An extension of the aforementioned work was done by preparing amorphous FAVE polymers functionalized with various chromophore units (Scheme 7). By choice of chromophore bisphenol segment, tunable photoluminescence was achieved. Other optical properties were investigated including solution/thin film photoemission phenomena, electroluminescence, selective anion detection, and preparation of metallopolymers for metal ion sensing applications. Based on the selection chromophore, these polymers can be prepared for specific applications encompassing a modular family of sensors. Precursory studies have shown these polymers possess unique capabilities for optical sensing (*12*, *14*).

Of notable mention, the performance of thiophene-modified polymer as a F^- sensor was evaluated in terms of the of the Z-substituted ether linkage. As shown in the previous sections of this chapter, flexibility imparted by the Z = CF=CF or $CHFCF_2$ did not affect solution quantum yields. However, compared with thiophene-modified FAVE polymers enriched with mostly Z = CF=CF (52% and 83%), the predominately Z = $CHFCF_2$ (with 7% residual CF=CF) enriched analog only produced only a 0.8-fold emission enhancement upon the addition of 1 equiv F^-. Nonetheless, selectivity was still preferential for F^- and showed less than a 20% variation in integration emission with other anion titrations. Therefore, the presence of 1,2-difluoroethylene enrichment is required to facilitate efficient sensing capability of the polymer. This may be due to the rigidity imparted by the −CF=CF− groups, which is known to strongly influence the fluorescence of polymers. More flexible materials are known to have lower quantum yields due to increased vibrational effects (such as intramolecular vibrational energy redistribution) to nonradiative decay pathways (*22*, *23*).

A new sulfonated PFCB aryl ether containing polymer was prepared as a transparent, film-forming polymer via the condensation of commercial bisphenols and bis(trifluorovinyloxyether)biphenyls for the preparation of proton exchange membranes for hydrogen fuel cells (Figure 3) (*10*). The highest degree of sulfonation determined by measuring the ion exchange capacity (IEC) value was 27% before rendering it water-soluble. Conductivity tests revealed a maximum conductivity of 0.011 S/cm at 100% relative humidity (RH) comparable to Nafion® at 40% RH.

Downloaded by PENNSYLVANIA STATE UNIV on August 28, 2012 | http://pubs.acs.org
Publication Date (Web): August 16, 2012 | doi: 10.1021/bk-2012-1106.ch002

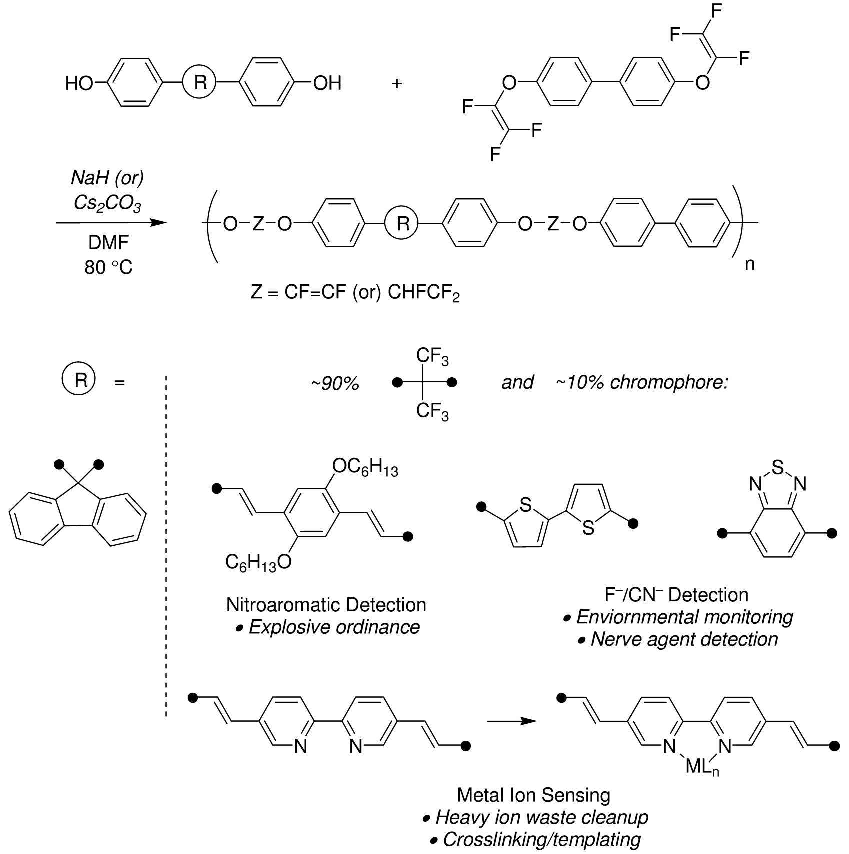
HO
R
OH
+
O
F
F
F
O
F
F
F
NaH (or)
Cs_2CO_3
DMF
80 °C
O–Z–O
R
O–Z–O
n
Z = CF=CF (or) $CHFCF_2$
R =
~90%
CF_3
CF_3
and ~10% chromophore:
OC_6H_{13}
$C_6H_{13}O$
S
S
N
S
N
Nitroaromatic Detection
• Explosive ordinance
F⁻/CN⁻ Detection
• Enviornmental monitoring
• Nerve agent detection
N
N
N
N
ML_n
Metal Ion Sensing
• Heavy ion waste cleanup
• Crosslinking/templating

Scheme 7. Modular family of chromophore-modified FAVE based polymers and potential applications.

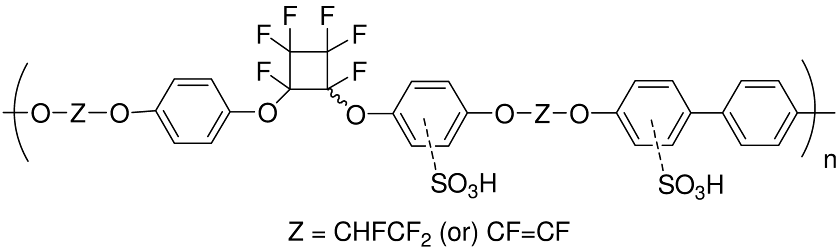
F
F
F
F
F
F
O–Z–O
O
O
O–Z–O
SO_3H
SO_3H
n
Z = $CHFCF_2$ (or) CF=CF

Figure 3. Sulfonated FAVE/PFCB polymer for proton exchange membranes.

Downloaded by PENNSYLVANIA STATE UNIV on August 28, 2012 | http://pubs.acs.org
Publication Date (Web): August 16, 2012 | doi: 10.1021/bk-2012-1106.ch002

Telechelomers

Telechelic FAVE polymers were prepared as shown in Scheme 8 using a similar methodology for the preparation of polymers in the previous section using NaH as the base. Using a slight modification, the addition of excess bis(trifluorovinyloxy) aryl ethers to sodium salt of bisphenol, produced endcapped telechelic polymers. Telechelomers contained up to 92% fluoroolefin (Z = CF=CF) content; this high fluoroolefin content was not achieved with polymers in the previous sections. While the molecular weights were intentionally limited for the telechelics, this strategy provided convenient access to processable PFCB aryl ether polymers via thermal chain extension and without crosslinking, as illustrated in Scheme 8 and pictorially in Scheme 9.

Chain extension of FAVE telechelomers can be thermally controlled to initially induce step-growth aryl TFVE cyclopolymerization at 210 °C, producing linear perfluorocyclobutyl (PFCB) aryl ether polymers. Further heating to > 325 °C induces crosslinking of the internal fluoroolefin groups (Scheme 9). These exothermic events were recorded by DSC analysis of a typical FAVE telecholomer and are shown in Figure 4. The network polymers formed from these heat treatments were insoluble materials with no observable T_g below 350 °C. It is also important to note the 1,2,2-hydrofluoroethane groups (Z = $CHFCF_2$) do not undergo thermal dehydrofluorination under these conditions based on ^{19}F NMR.

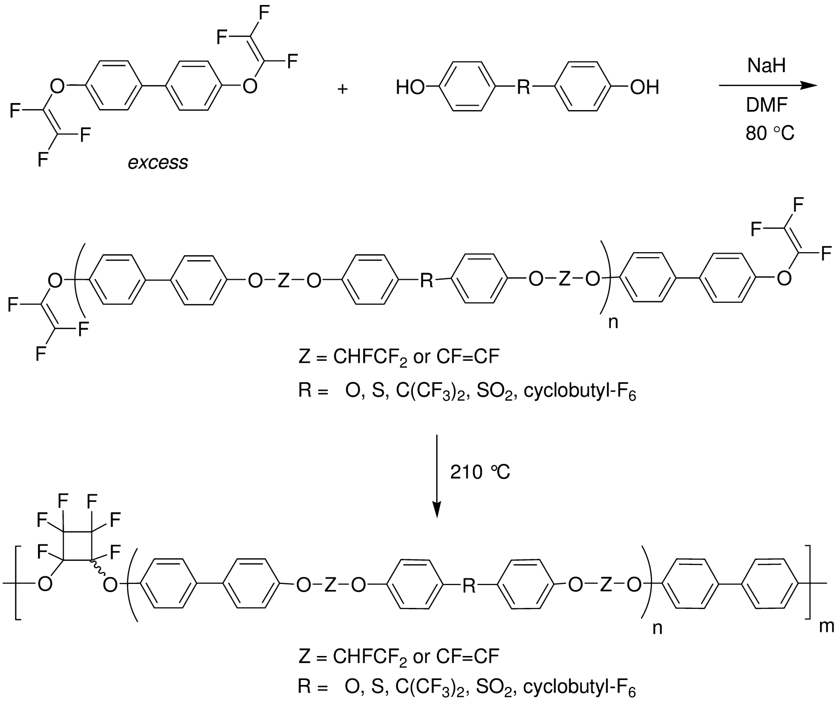
excess
+
HO
R
OH
NaH
DMF
80 °C
n
Z = CHFCF2 or CF=CF
R = O, S, C(CF3)2, SO2, cyclobutyl-F6
210 °C
n
m
Z = CHFCF2 or CF=CF
R = O, S, C(CF3)2, SO2, cyclobutyl-F6

Scheme 8. Chain extension of telechelomers to PFCB aryl ether polymers.

Downloaded by PENNSYLVANIA STATE UNIV on August 28, 2012 | http://pubs.acs.org
Publication Date (Web): August 16, 2012 | doi: 10.1021/bk-2012-1106.ch002

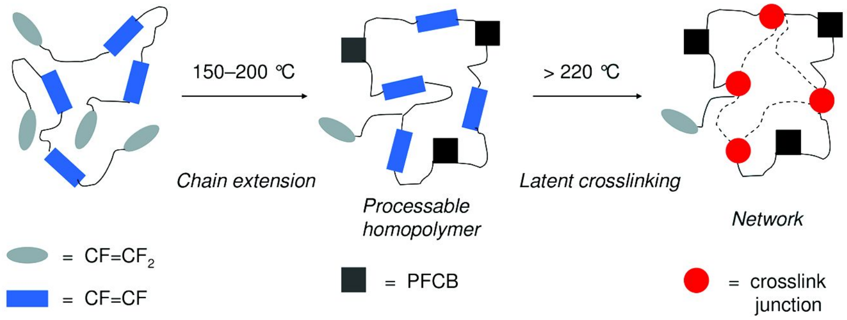
150–200 °C
Chain extension
Processable homopolymer
> 220 °C
Latent crosslinking
Network
= CF=CF2
= CF=CF
= PFCB
= crosslink junction

Scheme 9. Cartoon illustration of dual thermal reactivity of telechelomers: (1) chain extension to solution processable PFCB aryl ether polymers followed by (2) thermal crosslinking via the internal fluoroolefins, producing insoluble network polymers.

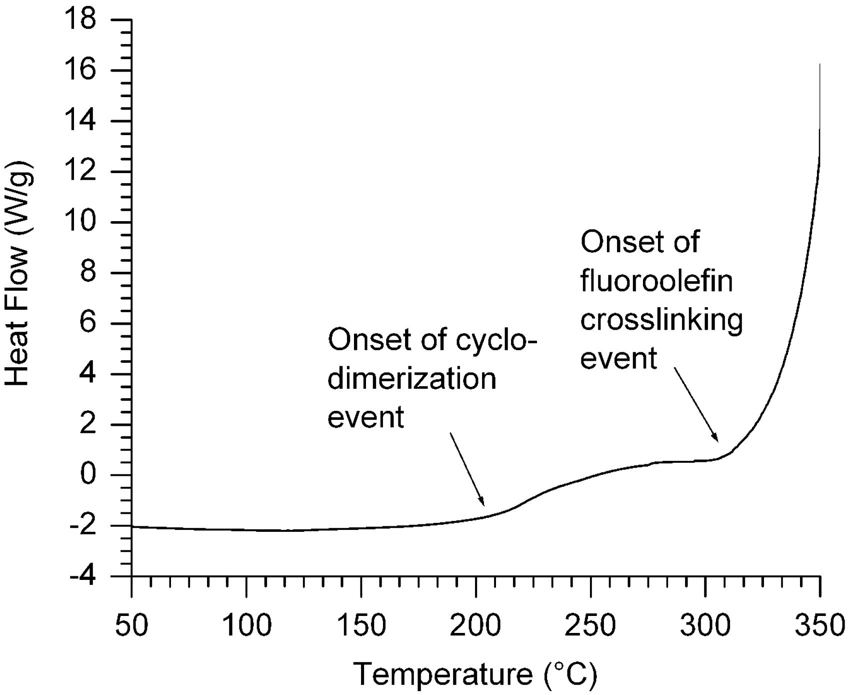

Figure 4. DSC trace of FAVE telechelomer heated to 350 °C showing two exotherms due to the onset of cyclodimerization of the aryl TFVE endgroups at ca. 210 °C and onset of internal fluoroolefin crosslinking, ca. 325 °C.

Downloaded by PENNSYLVANIA STATE UNIV on August 28, 2012 | http://pubs.acs.org
Publication Date (Web): August 16, 2012 | doi: 10.1021/bk-2012-1106.ch002

Network Polymers

FAVE network polymers were prepared by polymerization of PFCB aryl ether prepolymers with crosslinking agents (Scheme 9) (*24*). Attempts to use crosslinking agents included 1,1,1-tris(4-hydroxyphenyl)ethane, cyclopentyl POSS triol, poly(4-vinylphenol), aniline, and 4,4′-dithiolphenol. The PFCB aryl ether prepolymer that was used in this example had a number-average molecular weight (M_n) of ca. 13000 by ^{19}F NMR analysis. Addition of 1,1,1-tris(4-hydroxyphenyl)ethane (40 mol % relative to prepolymer) and Cs_2CO_3 (20 mol %) to a solution of PFCB aryl ether prepolymer in DMF at 60 °C immediately produced the gelled network material after 30 min. Filtering, followed by sequential washings with DI H_2O, MeOH, and hexanes, and vacuum drying at 60 °C for 24 h afforded a pale white insoluble solid. Swelling of network polymer was achieved only with DMSO and DMF. Following similar conditions, but using *iso*-butyl POSS triol and aniline failed to produce the desired network polymers. ^{19}F NMR of POSS triol (40 mol %) showed 52% conversion of aryl TFVE groups, whereas aniline (40 mol %) showed no conversion. However, when using NaH (2 equiv per aniline) as the base, the reactivity of aniline showed 91% conversion of the aryl TFVE moieties. Nevertheless, no network polymer was produced because NaH may lead to ether cleavage of the PFCB aryl ether prepolymer, as ^{19}F NMR indicates. Using 40 mol % poly(4-vinylphenol) (Aldrich, M_w of 8000) as a crosslinking reagent in the presence of 20 mol % Cs_2CO_3 and PFCB aryl ether prepolymer produced an insoluble gel after 24 h in DMF at 60 °C.

Segmented Block Copolymers

Attempts were made to incorporate functional polymer/oligomer segments into the FAVE polymer backbone using the biphenyl PFCB aryl ether prepolymer described in the previous section (*24*). Incorporation of block polymer segments included poly(ethyleneglycol) (PEG-400, M_w 400), poly(etheramine)s such as Jeffamine® D-400 (Huntsman, M_w 430), and perfluoropolyethers such as Fomblin® ZDOL 2000 (Solvay Solexis, M_n 1600) (Figure 5). In all cases, a stoichiometric equivalent of prepolymers was reacted with PFCB aryl ether prepolymer using 50 mol % Cs_2CO_3 in DMF at 60 °C. PEG segments were successfully incorporated and ^{19}F NMR showed quantitative consumption of aryl TFVE producing primarily 1,2,2-hydrofluoroethane (Z = $CHFCF_2$) units. Functionalization with Jeffamine® D-400 using NaH as the base also resulted in near quantitative consumption of aryl TFVE, according to ^{19}F NMR. However, ^{1}H NMR analysis did not reveal the presence of diagnostic functional groups representative of the poly(etheramine) backbone. At present, this result remains inconclusive as to whether successful incorporation was achieved. Employing the same conditions, copolymerization with Fomblin® ZDOL 2000 produced a phase separated mixture in DMF solution at 60 °C. Analysis by ^{19}F NMR reveals the aryl TFVE groups of the PFCB aryl ether prepolymer were unabated. Future studies should entail that polymerization with Fomblin® ZDOL 2000 prepolymers could be carried out solely in fluorinated solvents (or in a mixture of fluorinated solvents) to induce solution phase compatibility.

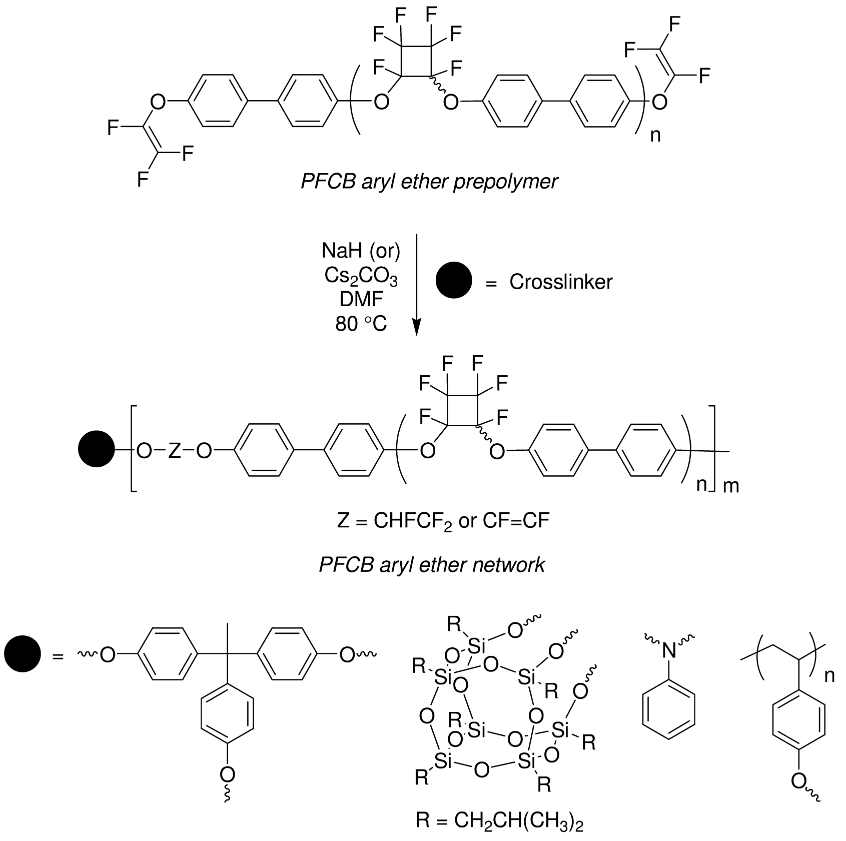
PFCB aryl ether prepolymer
NaH (or) Cs2CO3 DMF 80 °C
= Crosslinker
Z = CHFCF2 or CF=CF
PFCB aryl ether network
R = CH2CH(CH3)2

Scheme 10. Preparation of FAVE network polymers using various crosslinkers.

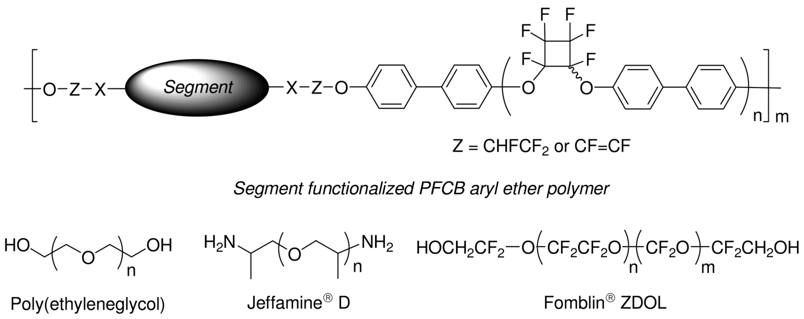
Segment
Z = CHFCF2 or CF=CF
Segment functionalized PFCB aryl ether polymer
Poly(ethyleneglycol)
Jeffamine® D
Fomblin® ZDOL

Figure 5. FAVE polymers functionalized with segments from commercially available prepolymers.

Downloaded by PENNSYLVANIA STATE UNIV on August 28, 2012 | http://pubs.acs.org
Publication Date (Web): August 16, 2012 | doi: 10.1021/bk-2012-1106.ch002

Downloaded by PENNSYLVANIA STATE UNIV on August 28, 2012 | http://pubs.acs.org
Publication Date (Web): August 16, 2012 | doi: 10.1021/bk-2012-1106.ch002

New Directions

While FAVE chemistry is by no means depleted in its depth or scope, the search for new, unique systems which are able to embrace the "semifluoroinated aryl ether polymer" motif are of current interest. Perfluorocycloalkenes are a class of such molecules (Figure 6). In particular, octafluorocyclopentene (OFCP) has been of studied for some time and reactions with a range of nucleophiles have been reported (*25*, *26*). Although containing a vinyl moiety, OFCP does not homopolymerize under radical conditions. With few exceptions, radical and step-growth methodologies towards copolymers of OFCP have resulted in either low molecular weight polymers or poor incorporation of OFCP into the backbone. Due to the similarity of OFCP to TFVE and the literature precedent towards nucleophilic addition, polycondensation was attempted with OFCP and commercial bisphenols.

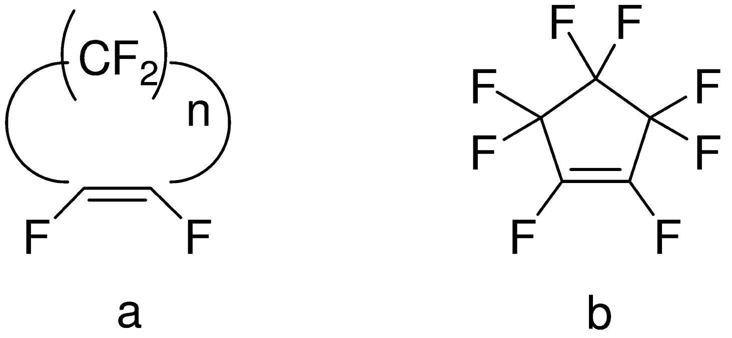

Figure 6. General perfluorocycloalkene (a) and octafluorocuclopentene (OFCP)(b).

Initial polymerizations were attempted utilizing traditional FAVE conditions where the sodium salt of bisphenol AF was generated *in situ via* NaH and then reacted with PFCP in a 1:1 molar ratio at 80 °C for 10 h; however, only low molecular weight oligomers were recovered (Scheme 11). The use of an organic base, triethylamine (TEA), was then explored. Initial polymerizations were much more promising and moderate molecular weight polymers were obtained (M_n = 9100). Higher molecular weight polymers were achieved under longer reaction times (24 h). Polymerization was also achieved using bisphenol A and biphenol in good yield and M_n of 9600 and 15400, respectively (Scheme 12). A recent consolidated accounts reports the details of these PFCP polymers (*27*).

Spectroscopic analyses of the crude reaction mixtures show that these polymerizations are very clean with no byproducts or branching. Further, spectroscopic data do not show the presence of any chiral carbons as typically seen in FAVE and PFCB chemistry. This suggests that the double bond of the fluoroalkene remains completely intact through the polymerization reaction

Downloaded by PENNSYLVANIA STATE UNIV on August 28, 2012 | http://pubs.acs.org
Publication Date (Web): August 16, 2012 | doi: 10.1021/bk-2012-1106.ch002

via a double addition-elimination mechanism. While FAVE polymers form fluoroalkanes in the presence of electrophilic H^+ (Cs_2CO_3 as base), PFCP polymers show no such behavior under similar conditions (TEA as a base). Further, although OFCP shows multiple additions occurring with methoxide anions (when used in excess), PFCP polymers show no branching or crosslinking, despite the presence of vinyl groups in the backbone and reactive phenolic species in the reaction mixture. While this behavior is not well understood, it does offer a unique opportunity to study the reactivity of the PFCP alkene functionality post polymerization. Elucidation of the reaction mechanism and exploration of the reactivity of the PFCP alkene should provide new and varied post polymerization chemistries including crosslinking and functionalization.

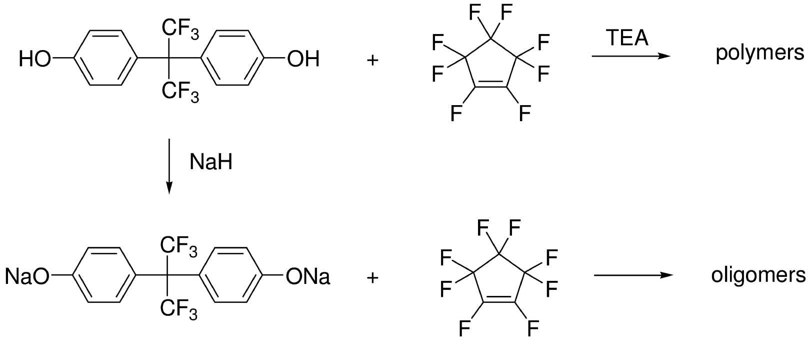

Scheme 11. Reaction of Bisphenol AF and OFCP using NaH or TEA.

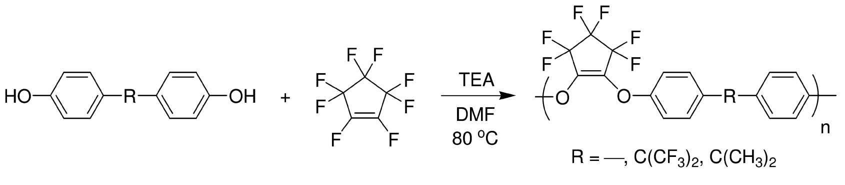

Scheme 12. General polymerization scheme of OFCP with Bisphenols.

Thermal analyses of these polymers *via* differential scanning calorimetry show glass transitions ranging 89−124 °C. Further, DSC thermograms show unique crystallinity for the bisphenol AF polymer with a polymorphic melt around 250 °C. While observed in the PFCB aryl ether polymer of bisphenol AF, this crystallinity is unique from all other PFCB and FAVE aryl ether systems. It may be that the combination of a cyclic perfluoro moiety, coupled with bisphenol AF produces this unique crystallinity.

Finally, the thermal stability of these PFCP polymers was explored *via* thermogravimetric analysis in nitrogen. The degradation temperature for these polymers at 5 wt % ranges 432−483 °C with approximately 30−50 % mass retention at 800 °C. Uniquely, bisphenol AF-derivitized PFCP loses only 15% of its mass at 800 °C, leaving 85% of its mass intact. This exceptional thermal stability may be due to rearrangement of the PFCP ring, formation of a ladder polymer structure, and interchain crosslinking.

Conclusion

This account presented the step-growth polymerization of bisphenols to bis(trifluorovinyloxy) aryl ethers thereby producing a new class of fluoropolymers, namely, fluorinated arylene vinylene ether (FAVE) polymers from commercial feedstocks. The telechelomers possess dual functionality which enable thermal chain extension and tandem crosslinking to afford network polymers without the aid of curing agents. These amorphous fluoropolymers may find application as crosslinking additives for fluoroelastomers as well as melt or solution processable resins for other thermosetting applications.

The details of the polymerization kinetics presented herein suggest a very facile addition elimination−substitution process. Therefore, other more benign bases should be explored. Transition metal-mediated or organic bases (i.e., amines) were not studied in substantial detail for this polymerization methodology. These should be considered for future work, particularly with emphasis on the catalytic nature and production of condensate.

The mechanistic details of crosslinking via thermal activation of the internal fluoroolefins still remain inconclusive. More so, the presence of biphenol segments as a result of thermal crosslinking may suggest reversibility of the aryl ether linkages with two-electron transfer. Therefore, investigations to understand the crosslinking phenomena are warranted.

The details of the polymerization kinetics presented herein suggest a very facile, base-promoted addition polymerization with subsequent elimination and/or substitution from newly adjoined moieties along the backbone. Based on the ease of nucleophilic addition to fluoroolefins, it is conceivable that bases soluble in organic solvents to improve diffusion could be investigated to include catalytic amines or organometallic complexes. Using such bases should circumvent the use of stoichiometric base or high catalytic loadings using hydride or carbonate bases, respectively.

Interest in FAVE polymers is anticipated to grow due to the ability to modularly functionalize their backbone for tailored applications, as mentioned in this account. Therefore, the polymerization kinetics between aryl TFVEs and bisphenols would be of interest in order to study their reaction sensitivity based on monomer functionality. Many functionalized aryl TFVE and bisphenol monomers are either commercially available or easily prepared. Furthermore, additions to aryl TFVE are not limited to phenols, but may also include bifunctional *C*-, *P*-, *N*-, and *S*-nucleophiles. The results of these studies are ongoing and will be reported elsewhere.

Downloaded by PENNSYLVANIA STATE UNIV on August 28, 2012 | http://pubs.acs.org
Publication Date (Web): August 16, 2012 | doi: 10.1021/bk-2012-1106.ch002

Acknowledgments

The authors wish to acknowledge past and on-going contributors to include Prof. Rhett Smith (Clemson University), Dr. Jianyong "Jack" Jin (The University of Auckland), Mr. Dirk Ewald (Hexion Specialty Chemical), Mr. Stephen Budy (University of Arizona), Mr. John Buquoi (USAFA), and Dr. Justin Moody. Partial financial support through the Welch Foundations is recognized by DWS. We thank Tetramer Technologies, L.L.C. for donation of aryl TFVE monomers, which are commercially available and distributed through Oakwood Chemicals, Inc. DWS recognizes the Robert A. Welch Foundation for partial support.

Downloaded by PENNSYLVANIA STATE UNIV on August 28, 2012 | http://pubs.acs.org
Publication Date (Web): August 16, 2012 | doi: 10.1021/bk-2012-1106.ch002

References

1. Scheirs, J. In *Modern Fluoropolymers: High Performance Polymers for Diverse Applications*; Scheirs, J., Ed.; Wiley: Chichester, 1997; p 435.
2. Schmiegel, W. W. *Angew. Makromol. Chem.* **1979**, *76/77*, 39.
3. Hung, M.-H.; Farnham, W. B.; Feiring, A. E.; Rozen, S. *J. Am. Chem. Soc.* **1993**, *115*, 8954.
4. Feiring, A. E.; Rozen, S.; Wonchoba, E. R. *J. Fluorine Chem.* **1998**, *89*, 31.
5. Yang, Z. Y.; Feiring, A. E.; Smart, B. E. *J. Am. Chem. Soc.* **1994**, *116*, 4135.
6. Rodenhouse, R.; Percec, V.; Feiring, A. E. *J. Polym. Sci. Part C: Polym. Lett.* **1990**, *28*, 345.
7. Spraul, B. K.; Suresh, S.; Jin, J.; Smith, D. W., Jr. *J. Am. Chem. Soc.* **2006**, *128*, 7055.
8. Iacono, S. T.; Budy, S. M.; Jin, J.; Smith, D. W., Jr. *J. Polym. Sci., Part A: Polym. Chem.* **2007**, *45*, 5705.
9. Iacono, S. T.; Budy, S. M.; Ewald, D.; Smith, D. W., Jr. *Chem. Commun.* **2006**, 4844.
10. Iacono, S. T.; Ewald, D.; Sankhe, A.; Rettenbacher, A.; Smith, D. W., Jr. *High Perform. Polym.* **2007**, 581.
11. Iacono, S. T.; Budy, S. M.; Moody, J. D.; Smith, R. C.; Smith, D. W., Jr. *Macromolecules* **2008**, *41*, 7490.
12. He, S.; Iacono, S. T.; Budy, S. M.; Dennis, A. E.; Smith, D. W., Jr.; Smith, R. C. *J. Mater. Chem.* **2008**, *18*, 1970.
13. Tackett, K. N.; Iacono, S. T.; Smith, D. W., Jr. *Polym. Prepr.* **2008**, *49*, 01.
14. Gilliard, R. J., Jr.; Iacono, S. T.; Budy, S. M.; Moody, J. D.; Smith, D. W., Jr.; Smith, R. C. *Sens. Actuators, B* **2009**, *143*, 1.
15. Moody, J. M.; VanDerveer, D.; Smith, D. W., Jr.; Iacono, S. T. *Org. Biomol. Chem.* **2011**, *9*, 4842.
16. Feiring, A. E.; Wonchoba, E. R. *J. Am. Chem. Soc.* **1992**, *57*, 7014.
17. Corley, R. S.; Lal, J.; Kane, M. W. *J. Am. Chem. Soc.* **1956**, *78*, 3489.
18. Pummer, W. J.; Wall, L. A. *SPE Trans.* **1963**, *3*, 220.
19. Buquoi, J. Q.; Smith, D. W., Jr.; Iacono, S. T. *J. Polym. Sci., Part A: Polym. Chem.* **2011**, *49*, 4441.
20. Odian, G. *Principles of Polymerization*, 4th ed.; John Wiley & Sons, Inc.: Hoboken, NJ, 2004.
21. Kim, Y.; Swager, T. M. *Chem. Commun.* **2005**, 372.

22. Brédas, J.-L.; Cornil, J.; Heeger, A. J. *Adv. Mater.* **1996**, *8*, 447.
23. Lemmer, U.; Heun, S.; Mahrt, R. F.; Scherf, U.; Hopmeier, M.; Siegner, U.; Göbel, E. O.; Bässler, H. *Chem. Phys. Lett.* **1995**, *240*, 373.
24. Iacono, S. T. Ph.D. Thesis, Clemson University, 2008.
25. Yamada, S.; Ishii, E.; Konno, T.; Ishihara, T. *Org. Biomol. Chem.* **2007**, *5*, 1442.
26. Yamada, S.; Ishii, E.; Konno, T.; Ishihara, T. *Tetrahedron* **2008**, *64*, 4215.
27. Cracowski, J.-M.; Sharma, B.; Brown, D. K.; Christensen, K.; Lund, B. R.; Smith, D. W., Jr. *Macromolecules* **2011**, *45*, 76.

Downloaded by PENNSYLVANIA STATE UNIV on August 28, 2012 | http://pubs.acs.org
Publication Date (Web): August 16, 2012 | doi: 10.1021/bk-2012-1106.ch002

Downloaded by COLUMBIA UNIV on August 28, 2012 | http://pubs.acs.org
Publication Date (Web): August 16, 2012 | doi: 10.1021/bk-2012-1106.ch003

Chapter 3

Synthesis and Characterization of Semi-Fluorinated Polyarylene Copolymers

Stephen M. Budy[1] and Douglas A. Loy*,[1,2]

[1]Department of Chemistry and Biochemistry, University of Arizona, Tucson, Arizona 85721
[2]Department of Materials Science and Engineering, University of Arizona, Tucson, Arizona 85721
***E-mail: daloy@email.arizona.edu**

A series of semi-fluorinated Diels–Alder polyarylenes copolymers were synthesized by copolymerization of 1,4-bis(2,4,5-triphenylcyclopentadienone)benzene with 1,4-diethynyl-2,3,5,6-tetrafluorobenzene and 1,4-diethynylbenzene as co-monomers. We varied the feed ratio of the fluorinated and fluorine-free diethynylbenzene co-monomers to allow systematic variation in the level of fluorination in the resulting polyarylenes. The semi-fluorinated polyarylene copolymers were characterized by ^{1}H and ^{19}F NMR, ATR–FTIR, elemental analysis, TGA, DSC, GPC, and water contact analysis. ^{19}F NMR spectroscopy confirmed the addition of fluorine into the copolymers, while FTIR spectroscopy and elemental analysis established a linear correlation with increasing fluorine content as the feed ratio of the fluorinated monomer increased. Thermal analysis showed little change in the series of copolymers for onset of decomposition (T_d = 550 °C), however, the char yield increased dramatically (55 to 75%). Water contact analysis showed a minimal surface effects for **P6** as compared to **P1** (90° versus 88°, respectively).

Downloaded by COLUMBIA UNIV on August 28, 2012 | http://pubs.acs.org
Publication Date (Web): August 16, 2012 | doi: 10.1021/bk-2012-1106.ch003

Introduction

High performance polymers, such as polyimides, polyaramides, and polybenzimidazoles, possess high glass transition temperatures (T_g), thermal stability, and superior mechanical properties (*1*–*5*). In spite of having these excellent properties, most of these high performance polymers have major drawbacks, such as insolubility in common organic solvents, intractability, infusibility, and low transparency (*6*). It has been observed that addition of fluorine substituents to a polymer can increase its solubility in organic solvents and processability (*7*). Fluorinated polymers typically have high thermal stability, improved chemical resistance, and lower surface energy when compared to their non-fluorinated counterparts (*8*). The strong C–F bond strength (490 kJ/mol) leads to high thermal and chemical stabilities (*9*). The small size and low polarizability of fluorine leads to a low surface energy, hydrophobicity, and a low dielectric constant for fluorinated materials (*6*). Because of these superior properties, fluorinated polymers are more attractive than non-fluorinated for a range of applications (*10*–*14*), including pharmaceuticals (*15*, *16*), crop protection agents (*17*, *18*), tracers for positron emission tomography (PET) (*19*, *20*), transistors (*21*), light emitting diodes (LEDs) (*22*, *23*), photovoltaic (PV) cells (*24*, *25*), gas separation membranes (*26*–*29*), and proton exchange membranes (PEMs) for fuel cells (*30*–*32*).

Stille *et al.* (*33*, *34*) successfully synthesized high molecular weight polymers affording Diels–Alder (DA) polyarylenes (*35*). Rusanov *et al.* (*36*, *37*) and Kumar and Neenan (*38*) have synthesized fluorine-containing polyphenylenes combining good solubility in common organic solvents with high thermal stability and low dielectric constants (*36*). Deck *et al.* (*39*–*42*) has shown preliminary or proposed work by preparing fluoroarylated cyclopentadienes (CPDO). We have also previously synthesized fluorine-containing polyphenylenes and tested them for gas separation membranes (*43*). In this study, we have chosen to extend this earlier work by examining the Diels-Alder co-polymerization of 1,4-bis(2,4,5-triphenylcyclopentadienone)benzene with varying amounts of 1,4-diethynylbenzene and 1,4-diethynyl-2,3,5,6-tetrafluorobenzene (Scheme 1) to permit systematic control over the level of fluorination and fine tuning of properties between the fluorinated and non-fluorinated polyarylenes. Because the pendant phenyl groups shield much of the polymer backbone from the outside environment, the four fluoride groups are hidden enough to cause minimal changes to polymer solubility while still allowing thermomechanical and optical properties to be influenced.

Experimental Section

Materials

Chemicals and solvents used were purchased from Sigma and used without purification unless otherwise stated. 1,4-diethynylbenzene (**1**, see Scheme 1) was purchased from TCI and purified by sublimation before use. 1,4-Diethynyl-2,3,5,6-tetrafluorobenzene (**2**) was prepared according to the literature (*44*, *45*). 1,3-Bis(2,4,5-triphenylcyclopentadienone)benzene (bistetracyclone) (**3**) was prepared according to literature procedure (*46*). Glassware was oven-dried (24 h) prior to use. Solvents and reagents were purchased from Sigma Aldrich and used without further purification. All reactions were carried out under an atmosphere of argon.

General Polymerization Procedures

To a dry round bottom flask with stir bar, 0.8294 g (1.2 mmol) bistetracyclone (**3**) and 0–0.1515 g diethynylbenzenes **1** (0–1.2 mmol) and/or 0–0.2379 g **2** (0–1.2 mmol) were added in various proportions (designated by mole percent composition of **2**, 0 mol% (**P1**), 5 mol% (**P2**), 10 mol% (**P3**), 20 mol% (**P4**), 50 mol% (**P5**), 100 mol% (**P6**)). Polymerizations were performed in 10 mL diphenyl ether (Ph_2O) as solvent. The reaction vessel was equipped with a reflux condenser and heated with an oil bath at 180 °C for 72 h under an argon atmosphere. Care must be taken to exclude oxygen from the reaction due to the reactivity of the diethynyl monomers. Similarly, their reactivity with light and air makes it important to sublime the diethynyl monomers *before* conducting the polymerizations. The reaction was cooled to room temperature and titurated into acetone (~750 mL). Additional purification of the polymers were performed by dissolving dry polymers in minimal amounts of tetrahydrofuran (THF) and precipitated in methanol (MeOH), and repeated three times. The tan polymers (79–86% yield) were collected by filtration and dried in a vacuum oven at 80 °C for 24 h.

Downloaded by COLUMBIA UNIV on August 28, 2012 | http://pubs.acs.org
Publication Date (Web): August 16, 2012 | doi: 10.1021/bk-2012-1106.ch003

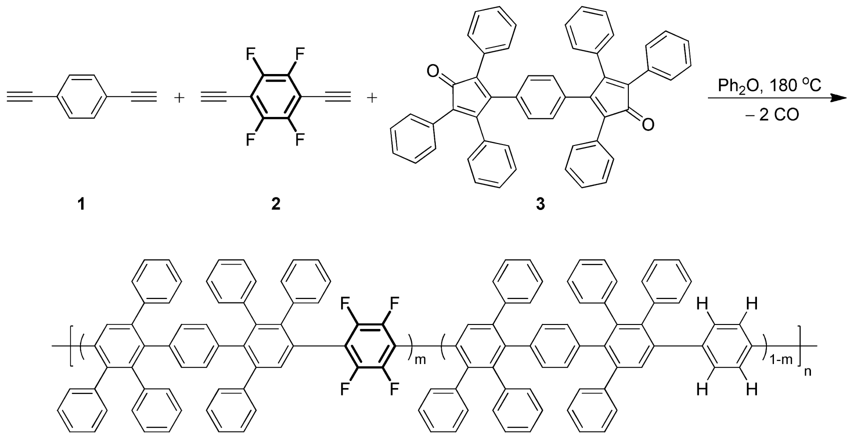

Scheme 1. Diels–Alder polymerization of semi-fluorinated polyarylene copolymers.

P1

86% yield; ^{1}H NMR (CDCl$_3$, 400 MHz): δ 7.48–7.40 (m), 7.35–7.31 (m), 7.20–6.55 (m), 6.36–6.17 (m); ^{13}C NMR (CDCl$_3$, 100 MHz): δ 132.4, 131.9, 131.6, 131.6, 130.3, 129.6, 129.3, 127.6, 127.0, 126.7, 125.7, 121.7; ATR–FTIR (neat): 3060-2852 (aromatic C–H stretching, sp^3 C–H stretching), 1598, 1073, 1024, 756, and 695 (C=C bending), 836 (aromatic C–H bending) cm^{-1}; GPC in THF relative to polystyrene, M_n = 41,600 g/mol ($M_\mathrm{w}/M_\mathrm{n}$ = 2.3); Anal. Calcd: C, 94.68; H, 5.32. Found: C, 88.98; H, 5.15.

P2

79% yield; ^{1}H NMR (CDCl$_3$, 400 MHz): δ 7.47–7.39 (m), 7.36–7.30 (m), 7.20–6.58 (m), 6.36–6.17 (m); ^{13}C NMR (CDCl$_3$, 100 MHz): δ 132.4, 132.0, 130.8, 129.9, 129.6, 129.3, 127.7, 127.0, 126.7, 125.7, 123.4, 119.0; ^{19}F NMR (CDCl$_3$, 376 MHz): δ –140.8, –140.9; ATR–FTIR (neat): 3060-2852 (aromatic C–H stretching, sp^3 C–H stretching), 1598, 1073, 1024, 756, and 695 (C=C bending), 1236 (aromatic C–F stretching), 836 (aromatic C–H bending), 722 (aromatic C–F bending) cm^{-1}; GPC in THF relative to polystyrene, M_n = 22,500 g/mol ($M_\mathrm{w}/M_\mathrm{n}$ = 1.9); Anal. Calcd: C, 94.23; H, 5.27; F, 0.50. Found: C, 93.90; H, 4.93; F, 0.52.

P3

82% yield; ^{1}H NMR (CDCl$_3$, 400 MHz): δ 7.47–7.39 (m), 7.35–7.30 (m), 7.20–6.58 (m), 6.37–6.17 (m); ^{13}C NMR (CDCl$_3$, 100 MHz): δ 132.4, 132.0, 131.7, 130.6, 130.1, 129.6, 129.3, 127.7, 127.0, 125.5, 123.3, 119.3; ^{19}F NMR (CDCl$_3$, 376 MHz): δ –140.8, –140.9; ATR–FTIR (neat): 3060-2852 (aromatic C–H stretching, sp^3 C–H stretching), 1598, 1073, 1024, 756, and 695 (C=C bending), 1236 (aromatic C–F stretching), 836 (aromatic C–H bending), 722 (aromatic C–F bending) cm^{-1}; GPC in THF relative to polystyrene, M_n = 27,500 g/mol ($M_\mathrm{w}/M_\mathrm{n}$ = 2.1); Anal. Calcd: C, 93.76; H, 5.25; F, 0.99. Found: C, 89.43; H, 5.15; F, 0.97.

P4

85% yield; ^{1}H NMR (CDCl$_3$, 400 MHz): δ 7.45–7.39 (m), 7.36–7.30 (m), 7.21–6.55 (m), 6.38–6.16 (m); ^{13}C NMR (CDCl$_3$, 100 MHz): δ 132.4, 132.0, 131.7, 130.8, 130.6, 130.3, 130.1, 129.6, 129.3, 127.6, 127.0, 125.6; ^{19}F NMR (CDCl$_3$, 376 MHz): δ –140.8, –140.9; ATR–FTIR (neat): 3060-2852 (aromatic C–H stretching, sp^3 C–H stretching), 1598, 1073, 1024, 756, and 695 (C=C bending), 1236 (aromatic C–F stretching), 836 (aromatic C–H bending), 722 (aromatic C–F bending) cm^{-1}; GPC in THF relative to polystyrene, M_n = 34,200 g/mol ($M_\mathrm{w}/M_\mathrm{n}$ = 2.1); Anal. Calcd: C, 92.92; H, 5.12; F, 1.96. Found: C, 92.30; H, 4.76; F, 1.81.

Downloaded by COLUMBIA UNIV on August 28, 2012 | http://pubs.acs.org
Publication Date (Web): August 16, 2012 | doi: 10.1021/bk-2012-1106.ch003

P5

81% yield; ^{1}H NMR ($CDCl_3$, 400 MHz): δ 7.45–7.39 (m), 7.36–7.30 (m), 7.23–6.56 (m), 6.39–6.16 (m); ^{13}C NMR ($CDCl_3$, 100 MHz): δ 132.4, 131.8, 131.6, 130.2, 130.0, 129.6, 129.3, 127.7, 127.0, 126.5, 125.8, 123.5; ^{19}F NMR ($CDCl_3$, 376 MHz): δ –140.8, –140.9; ATR–FTIR (neat): 3060-2852 (aromatic C–H stretching, sp^3 C–H stretching), 1598, 1073, 1024, 756, and 695 (C=C bending), 1236 (aromatic C–F stretching), 836 (aromatic C–H bending), 722 (aromatic C–F bending) cm^{-1}; GPC in THF relative to polystyrene, M_n = 39,100 g/mol (M_w/M_n = 2.0); Anal. Calcd: C, 90.40; H, 4.83; F, 4.77. Found: C, 90.90; H, 4.69; F, 3.39.

P6

85% yield; ^{1}H NMR ($CDCl_3$, 400 MHz): δ 7.46–7.39 (m), 7.36–7.30 (m), 7.29–6.54 (m), 6.40–6.17 (m); ^{13}C NMR ($CDCl_3$, 100 MHz): δ 132.4, 132.1, 131.7, 130.8, 130.6, 130.3, 130.0, 129.6, 127.7, 127.1, 126.8, 126.5; ^{19}F NMR ($CDCl_3$, 376 MHz): δ –140.8, –140.9; ATR–FTIR (neat): 3060-2852 (aromatic C–H stretching, sp^3 C–H stretching), 1598, 1073, 1024, 756, and 695 (C=C bending), 1236 (aromatic C–F stretching), 836 (aromatic C–H bending), 722 (aromatic C–F bending) cm^{-1}; GPC in THF relative to polystyrene, M_n = 48,500 g/mol (M_w/M_n = 2.2); Anal. Calcd: C, 86.50; H, 4.38; F, 9.12. Found: C, 83.05; H, 4.06; F, 7.54.

Characterization

Nuclear Magnetic Resonance (NMR) Spectroscopy

^{1}H and ^{19}F NMR data were obtained on a Bruker AVIII-400 NMR spectrometer (400 MHz for ^{1}H and 376 MHz for ^{19}F) and chemical shifts were reported in part per million (δ ppm). ^{1}H NMR was internally referenced to tetramethylsilane (TMS) (δ 0.0) and ^{19}F NMR was internally referenced to trichlorofluoromethane ($CFCl_3$) (δ 0.0). The NMR spectrometer is equipped with a BBOF (Broadband 5mm Direct Z-Gradient) probe and SampleJet autosampler. Operation of the instrument is fully automated, using ICON-NMR software and automatic lock, tune/match, and ^{2}H gradient shimming. Data were processed using MestReNova software (version 6.0.4) and Origin (version 6.1).

Fourier Transform Infrared (FTIR) Spectroscopy

Attenuated total reflectance Fourier transform infrared (ATR–FTIR) analysis of neat samples was performed on a Thermo Nicolet-FTIR Spectrometer iS10 with a ZnSe ATR crystal apparatus. Bare ATR crystal substrate was used as reference before each sample. Neat samples were pressed against the ATR prism to maximize interfacial contact. Spectra were recorded at 4 cm^{-1} resolution with 64 scans using OMNIC software. Data were processed using Origin (version 6.1).

Downloaded by COLUMBIA UNIV on August 28, 2012 | http://pubs.acs.org
Publication Date (Web): August 16, 2012 | doi: 10.1021/bk-2012-1106.ch003

Downloaded by COLUMBIA UNIV on August 28, 2012 | http://pubs.acs.org
Publication Date (Web): August 16, 2012 | doi: 10.1021/bk-2012-1106.ch003

Elemental Analysis

Elemental analysis was performed by Columbia Analytical Services (Tucson, AZ). The CH analysis was performed on a Perkin Elmer 2400. Samples were combusted at 950 °C and the gases analyzed by infrared (IR) spectroscopy. The fluorine analysis was performed by combustion in an oxygen charged Schoniger flask. A scrubber solution and oxygen were added to the flask before the sample was burned in a platinum basket that was attached to the top of the flask. After the flask had sat for one hour, the solution was brought up to 100 mL with Nanopure water and then analyzed by ion chromatography.

Gel Permeation Chromatography (GPC)

Gel permeation chromatography was performed in a tetrahydrofuran (THF) mobile phase with a Waters 1515 eluted through three 5 µm PLgel columns (Polymer Labs, pore sizes 102, 103, 104 Å) at 35 °C with a Waters 2414 differential refractometer and Waters 2487 dual wavelength UV-Vis spectrometer (● = 254 nm). Molar masses were calculated using the Empower software (Waters) calibrated against low polydispersity linear polystyrene (PS) standards (Polymer Labs EasiCal PS-2).

Thermal Analysis

Differential scanning calorimetry (DSC) analysis was performed on a 2920 Modulated DSC instrument in nitrogen at a heating rate of 10 °C/min. Samples weighed approximately 5 mg. The heating cycle was run from 25 °C to 450 °C and cycled three times. Data were processed using TA Universal Analysis. Thermal gravimetric analysis (TGA) was performed on a Hi-Rest TGA 2950 Thermogravimetric Analyzer instrument in nitrogen at a heating rate of 10 °C/min. Samples weighed 5–10 mg. The temperature was started at room temperature and ramped up to 700 °C. The onset of the degradation temperature (T_d) and char yield was determined using TA Universal Analysis. Data were processed using Origin (version 6.1).

Goniometery Measurements

Contact angle analysis was performed on a First Ten Angstroms 200 instrument. Water contact angle (10 µL, HPLC-grade water) was determined using the graphical software (version 2.0) from the captured image. Static contact angle values reported were an average of two values measured on different areas of the spin cast surface with an average standard deviation of ±1 degree

(°). Samples were prepared by dissolving polymers in tetrahydrofuran (THF) or cyclohexanone (5–10 wt%) and spin cast (P-6000 Spin Coater, Specialty Coating System (SCS)) at 2000–2500 rpm on a glass substrate. Films were dried in a vacuum oven at 80 °C for 24 h.

Results and Discussion

Diels–Alder polymerization of bistetracyclone (**3**) and 1,4-diethynylbenzene (**1**) has been synthesized previously to afford polyarylene (*33–35*, *37*, *47*, *48*), whereas polymerization of **3** and both 1,4-diethynylbenzene (**1**) and 1,4-diethynyl-2,3,5,6-tetrafluorobenzene (**2**) has not been investigated. The polymer of **3** and 1,3-diethynyl-2,4,5,6-tetrafluorobenzene has been made and investigated, but to a lesser degree than the unfluorinated polyarylenes (*38*). The Diels Alder polymerizations are very colorful with the deep purple color of the biscyclone monomer making the initial polymerization solution completely opaque to light. The purple color gradually fades away to a to the transparent tea brown of the product polymers. The polymerizations are conducted in diphenyl ether because both monoemrs and all of the polymers we have made to date are soluble. Introduction of the fluorine groups (0-7.5.4 wt% F) has no noticable effect on the rate of the reaction or the appearance of the products to the eye. After re-precipitation all of the polymers were tan in color and soluble in the same solvents (THF, toluene, diphenyl ether, chloroform and cyclohexanone). The fluorinated polymers appeared to be slightly less soluble in cyclohexanone than the non-fluorinated polyarylene of similar molecular weight.

Diels–Alder step-growth polymerization of biscyclopentadienones with bisacetylenes can produce either *para* or *meta* substitution in the polymer backbone during the benzene ring formation via expulsion of carbon monoxide (CO). Stille and Noren showed with a model reaction study that both were present and the ratios (*para* to *meta*) varied with temperature from 0.55 at 100 °C to 1.0 at 255 °C (*49*). However, Shifrina et al. used a different model reaction and showed at 240 °C the major isomeric product was meta, meta-isomer (83% yield, separation by crystallization) (*35*). More work in this area is necessary to elucidate a clear depiction of the backbone architecture for linear polyarylenes. The incorporation of fluorine-containing monomers may give an advantage in this area due to the cleanliness of the ^{19}F NMR spectra and eliminate the possibility of overlapping signals that often complicate proton spectra (*50–52*). To assist with our NMR characterizations, we prepared the two model compounds, (**4**) and 2,2″,3,3″,4,4″,5,5″-octaphenyl-1,1′:4′,1″-terphenyl and 2′,3′,5′,6′-tetrafluoro-2,2″,3,3″,4,4″,5,5″-octaphenyl-1,1′:4′,1″-terphenyl (**5**) from the Diels-Alder cycloadditions of 2,3,4,5-tetraphenylcyclopentadienone with **1** and **2**, respectively (*53*).

The un-fluorinated polyarylene has been characterized previously. Our spectra (Figure 1a) were consistent with the earlier reports but shed no new light on the *meta* versus *para* regiochemistry assignments. The ^{1}H NMR spectra change little between **P1** (0 wt% F polymer content) and **P6** (7.54 wt% F polymer content), as shown in Figure 1. Assignments were made based on the work of

Downloaded by COLUMBIA UNIV on August 28, 2012 | http://pubs.acs.org
Publication Date (Web): August 16, 2012 | doi: 10.1021/bk-2012-1106.ch003

Downloaded by COLUMBIA UNIV on August 28, 2012 | http://pubs.acs.org
Publication Date (Web): August 16, 2012 | doi: 10.1021/bk-2012-1106.ch003

Shifrina et. al. The environment remains relatively constant for protons H_1–H_4, however, the interaction with the fluorine co-monomer changes the shape but not the position for protons H_5–H_7.

Proton H_8 is the most sensitive to the fluorine addition as it shifts upfield by approximately 0.3 ppm units in **P6** as compared to **P1**. The sharp doublet of doublets at 7.38 ppm is due to the tetracyclone end group. The singlet at 7.26 ppm is due to $CDCl_3$. All the ^{19}F NMR spectra show the same two peaks at –140.8 and –140.9 ppm confirming the presence of **2** in the polymer backbone for polymers **P2**–**P6** (Figure 2a–e). The shape and position are constant, however the intensity increases as the feed ratio increases across the copolymer series going from Figure 2a to Figure 2e.

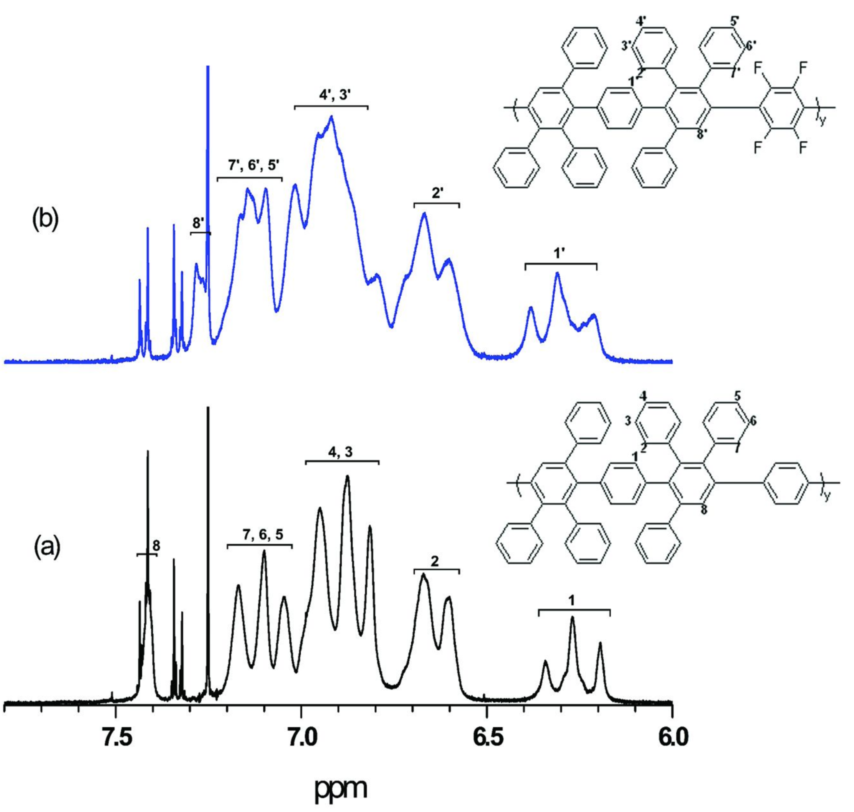

*Figure 1. ^1H NMR spectra of (a) **P1** and (b) **P6** in $CDCl_3$.*

Attenuated total reflectance Fourier transform infrared (ATR–FTIR) spectroscopy was also used to characterize the polyarylene copolymers, as shown in the overlaid spectra in Figure 3. Prominent spectral features include many aromatic vibrations at 1073, 1024, 756, and 695 cm^{-1}; numerous bands of variable intensity are present in the range of 1250–950 cm^{-1} assigned to aromatic C–H in-plane vibrations, and one or more strong bands are present in the range of 900–650 cm^{-1} due to aromatic C–H out-of-plane vibrations (*54*). The spectra of the semi-fluorinated copolymers showed increasing absorptions at 1236 and 722 cm^{-1} due to aromatic C–F vibrations (*55*, *56*). The characteristic absorption at 1236 cm^{-1} can also be used to elucidate the effects of the increase in the **2** feed ratio, which is shown in Figure 4 as a linear relationship. Copolymers containing fluorine show few differences in these overlaid spectra, however, the intensity differences in the aromatic vibrations are presumed to be from the differences in the morphology and dihedral angle in the polymer backbone, and possibly from different penetration depth and wavelength dependence from the ATR crystal.

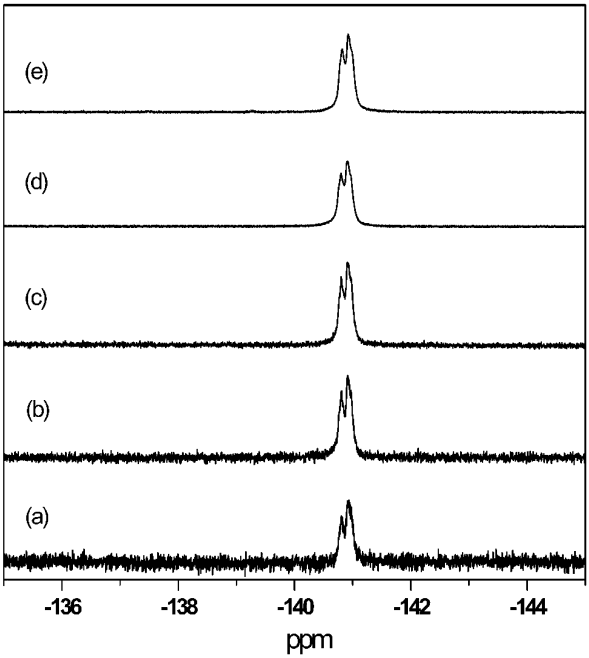

Figure 2. ^{19}F NMR spectra of (a) ***P2****, (b)* ***P3****, (c)* ***P4****, (d)* ***P5****, and (e)* ***P6*** *in $CDCl_3$.*

Diels–Alder polymerization reactions were monitored by gel permeation chromatography (GPC) and found to produce reasonably high molecular weight materials with typical step-growth polydispersities (PDI). Table 1 illustrates the chemical structures and properties of **P1**–**P6** with different amounts of fluorine (from 0 to 7.54 wt%) in the polyarylene copolymer backbone. The number average molecular weight (M_n) and polydispersities ranged from 22,500 to 48,500 g/mol and 1.9 to 2.3, respectively. Without fluorine groups, the repeat unit molecular weight is 775 g/mole and for the M_n of 41,600 g/mole for the polymer, there should be 53 repeat units in the average macromolecule. With 4 fluorine groups, the repeat unit molecular weight is 847 g/mole, so for a 48,500 g/mole number average molecular weight, there should be 57 repeat units per chain. The lowest molecular weight sample, prepared with 10mol% **2**, was calculated to have about 29 repeat units per chain. Even in this case, the concentration of ethynylbenzene end-groups would be infinitesimal by ^{1}H NMR.

Downloaded by COLUMBIA UNIV on August 28, 2012 | http://pubs.acs.org
Publication Date (Web): August 16, 2012 | doi: 10.1021/bk-2012-1106.ch003

The effect of the relative reactivity of the diethynyl monomers' (**1** and **2**) on their incorporation into the copolymers (**P2**-**P5**) was not examined in the present study. While quantitative studies on the influence of the fluorine groups on the reactivity of the ethynyl groups in these polymerizations have not been performed, the homopolymerizations (**P1** and **P6**) appeared to proceed at similar rates. If this can be verified, it means that the incorporation of **1** and **2** into the copolymers may be homogeneous. However, additional experiments need to be performed to determine the relative reactivities of the monomers.

As mentioned previously, the presence of only four fluorine atoms can have benefits in the overall final properties of the material, such as lowering the optical loss at telecommunication wavelengths (*57*). Therefore, the ability to tune the properties of materials using feed ratios in a controlled fashion with predictable results is of interest in many fields. In Figure 5, elemental analysis results for fluorine content in the polyarylene copolymer series have been presented in relation to **2** feed ratios. The solid line shows the calculated results based on the feed ratios and the solid circles show the experimental results determined from elemental analysis. The lower incorporation of the fluorine-containing monomer (**2**) is evident by these results, but still shows good tailorability among the final materials.

Downloaded by COLUMBIA UNIV on August 28, 2012 | http://pubs.acs.org
Publication Date (Web): August 16, 2012 | doi: 10.1021/bk-2012-1106.ch003

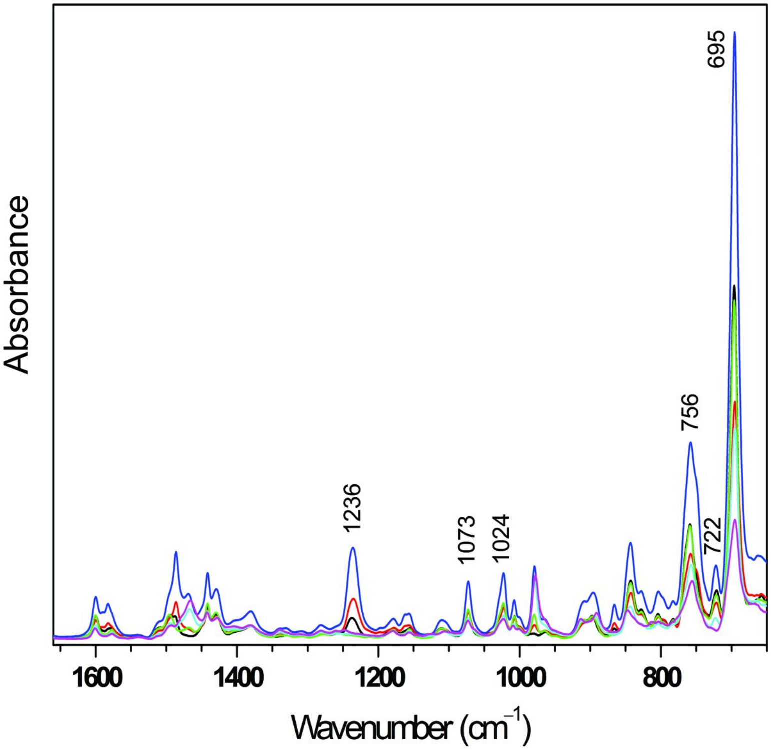

*Figure 3. Overlay of ATR–FTIR spectra of semi-fluorinated polyarylene copolymers with 4 cm^{-1} resolution. Absorbance intensity increases from **P1** to **P6** over the range 1650 to 650 cm^{-1}.*

Downloaded by COLUMBIA UNIV on August 28, 2012 | http://pubs.acs.org
Publication Date (Web): August 16, 2012 | doi: 10.1021/bk-2012-1106.ch003

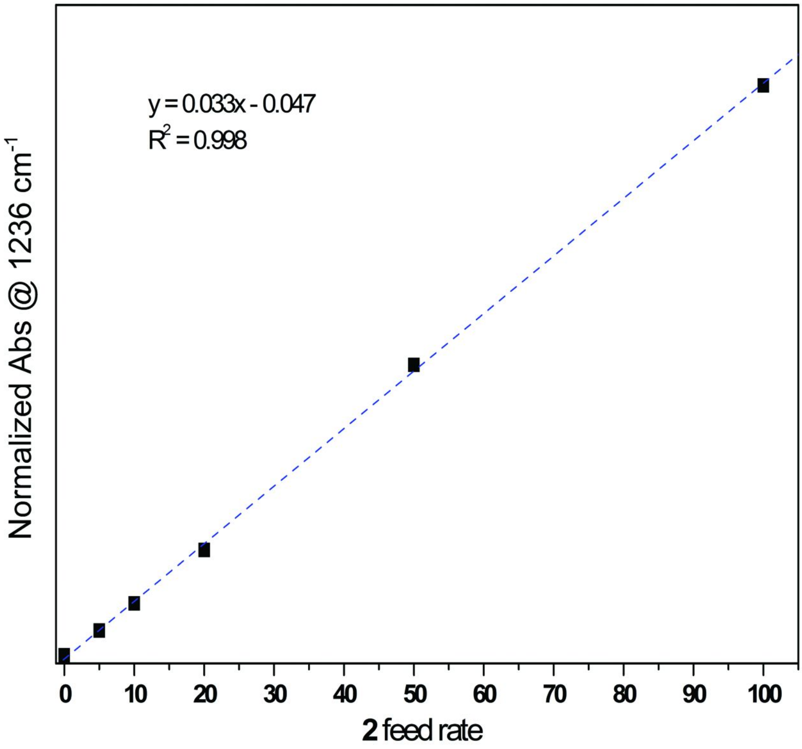

Figure 4. Normalized ATR–FTIR absorbance at 1236 cm^{-1} versus ***2*** *feed ratio.*

Thermal analysis was performed on the entire semi-fluorinated polyarylene copolymer series (**P1**–**P6**). DSC showed no melting or glass transition temperature in the range 25 to 450 °C for any of the samples at a heating rate of 10 °C/min. Dynamic thermal mechanical analysis may give more information about the glass transition temperature and will be investigated in further studies. Thermal gravimetric analysis (TGA) was used to investigate the thermal stability of the series (Figure 6) under nitrogen atmosphere. The onset for thermal degradation temperature (T_d) for all the samples was approximately 550 °C. The fluorine content did not change the overall thermal stability in the semi-fluorinated polyarylene copolymers; however, the char yield present at 700 °C did change quite dramatically going from 0 wt% fluorine (**P1**) to 7.54 wt% fluorine (**P6**); 55 to 75%, respectively (Table 1). The thermal stability and char yield were initially adequate for many high-temperature and high-performance applications, but controlling the fluorine content in the polyarylene copolymers allows for possible applications in flame retardant polymeric materials (*58*). Also of interest is the potential use of these highly aromatic polymers as carbon precursor materials. A number of polymers can be carbonized where carbon-carbon composites have been used for numerous structural applications at elevated temperatures because of their light weight, high strength and modulus, low coefficient of thermal expansion, and thermal stability (*59–61*).

Downloaded by COLUMBIA UNIV on August 28, 2012 | http://pubs.acs.org
Publication Date (Web): August 16, 2012 | doi: 10.1021/bk-2012-1106.ch003

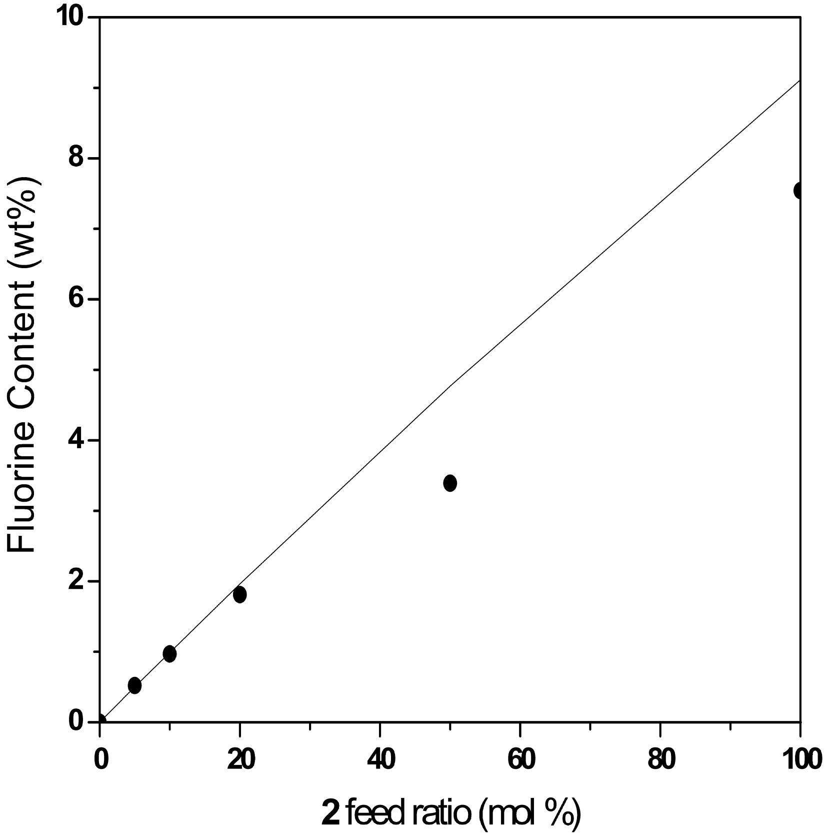

*Figure 5. Fluorine content as determined by elemental analysis versus feed ratio of **2**; solid line represents the calculated amount and solid circles represents experimental results.*

It is well known that fluoropolymers, such as polytetrafluoroethylene (PTFE), have superior hydrophobic and non-stick characteristics as compared to its non-fluorinated analogue (*62*). In this manner, the pristine spun cast film surface of **P1** and **P6** were studied by sessile drop analysis to determine the water contact angle for each polymer. The contact angle and surface energy are related using Young's equation (*63*). Figure 7 shows representative images captured for each sample with the measured contact angle changing very little with the addition of 7.54 wt% fluorine as compared to no fluorine; 90 and 88 degrees, respectively. It is assumed that because the fluorines are on the backbone phenylene group surrounded by additional phenyl rings along the polymer backbone they are hidden from the surface of the rigid rod polymer. This might also explain the similarity in solubility of the polyarylenes in organic solvents despite variation in fluorine content. If this hypothesis tests true, this could be a viable strategy for modifying the optical and thermal properties of polymers without changing their solubility in solvents or other polymers. Thus, these polymers could be more readily incorporated into multilayer optical coatings or mirrors. However, surface roughness also comes into play according to Cassie (*64*) and Wenzel (*65*). Further work in this area will involve increasing the fluorine content in polyarylene and processing, or adding nanocomposites, to increase the surface roughness.

Downloaded by COLUMBIA UNIV on August 28, 2012 | http://pubs.acs.org
Publication Date (Web): August 16, 2012 | doi: 10.1021/bk-2012-1106.ch003

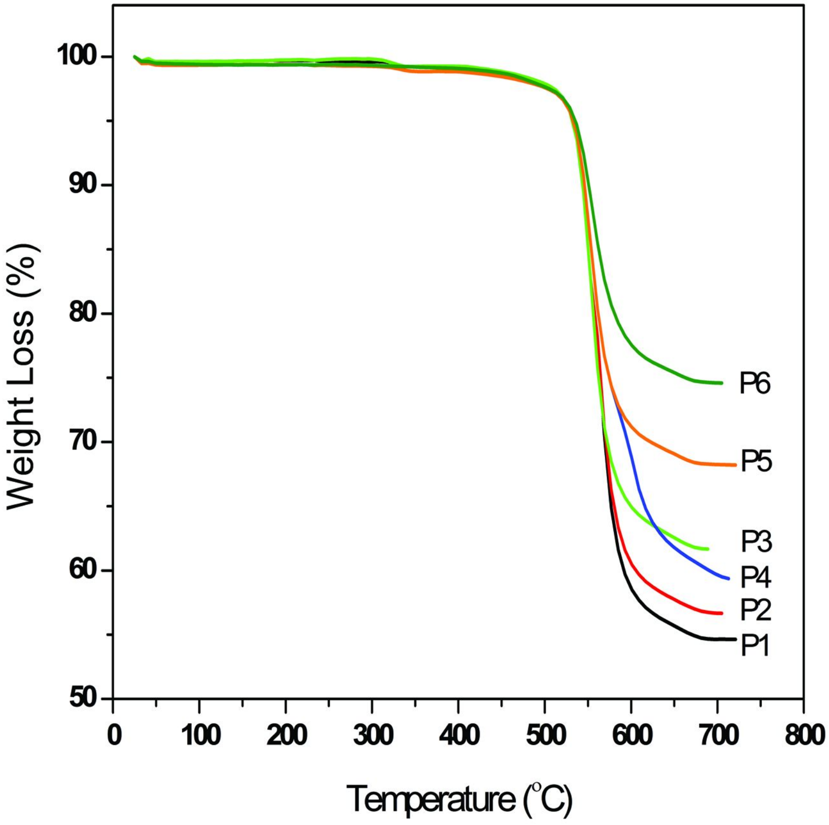

*Figure 6. Thermal gravimetric analysis results for **P1**–**P6** at a heating rate of 10 °C/min in nitrogen.*

Downloaded by COLUMBIA UNIV on August 28, 2012 | http://pubs.acs.org
Publication Date (Web): August 16, 2012 | doi: 10.1021/bk-2012-1106.ch003

Table 1. Summary of Polymer Properties for the Semi-fluorinated Polyarylene Copolymers

Sample	***1***:***2***[a]	*Yield (%)*	*F content (wt%)*[b]	$M_n \times 10^{-3}$ *(g/mol)*[c]	$M_w \times 10^{-3}$ *(g/mol)*[c]	*PDI* (M_w/M_n)[c]	*Char Yield (%)*[d]
P1	100:0	86	0	42	96	2.3	55
P2	95:5	79	0.52	22	42	1.9	57
P3	90:10	82	0.97	27	57	2.0	62
P4	80:20	85	1.81	34	73	2.1	60
P5	50:50	81	3.39	39	77	1.9	68
P6	0:100	85	7.54	48	105	2.1	75

[a] Molar feed ratio. [b] Determined by elemental analysis. [c] Determined from GPC, using PS standards in THF. [d] Determined from TGA with a heating rate of 10 °C/min in nitrogen at 700 °C, using Universal Analysis 2000 software.

Downloaded by COLUMBIA UNIV on August 28, 2012 | http://pubs.acs.org
Publication Date (Web): August 16, 2012 | doi: 10.1021/bk-2012-1106.ch003

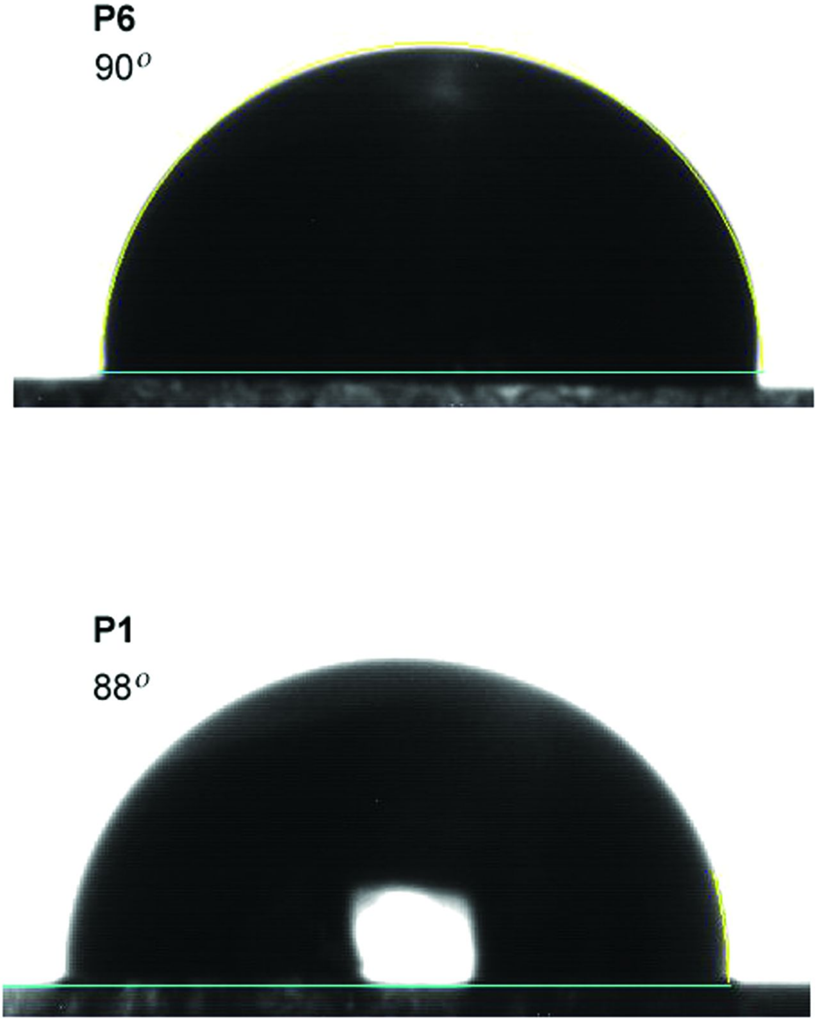

*Figure 7. Captured images from sessile drop analysis show water contact angles for **P1** = 88° and **P6** = 90°.*

Conclusion

The potential to fabricate enriched semi-fluorinated polyarylene copolymers has been demonstrated. The feed ratios from mixtures of non-fluorinated (**1**) and fluorinated monomers (**2**) lead to a series of semi-fluorinated polyarylene copolymers easily tailoring the amount of fluorine in the backbone of the polymer. This strategy allows for facile tuning of fluorine-containing polyarylene coatings, films, and bulk materials. These studies have shown incorporation of fluorine in the backbone of polyarylene via ^{19}F NMR spectroscopy, while

ATR–FTIR spectroscopy and elemental analysis elucidated the linear correlation of fluorine composition increase as the feed ratio increased. Future endeavors will include synthesis and characterization of new semi-fluorinated polyarylene block copolymers, as well as alternative methods for incorporating higher levels of fluorine in polyarylene.

Acknowledgments

S. Iacono (USAFA) provided assistance with contact angle measurements. S. Budy specifically recognizes the *Diversity Fellowship for Underrepresented Students*. The authors thank the University of Arizona's Nuclear Magnetic Resonance (NMR) Facility, Small Facility Laboratory, W. M. Keck Center for Surface and Interface Imaging, and Mass Spectrometry (MS) Facility. This research was funded by Energy Materials Corporation (EMC) and the University of Arizona.

References

1. Cassidy, P. E. *Thermally Stable Polymers: Synthesis and Properties*; Marcel Dekker: New York, 1980.
2. Yates, C. R.; Hayes, W. *Eur. Polym. J.* **2004**, *40*, 1257–1281.
3. Vandezande, P.; Gevers, L. E. M.; Vankelecom, I. F. J. *Chem. Soc. Rev.* **2008**, *37*, 365–405.
4. Meador, M. A. *Annu. Rev. Mater. Sci.* **1998**, *28*, 599–630.
5. Chae, H. G.; Kumar, S. *J. Appl. Polym. Sci.* **2006**, *100*, 791–802.
6. Dhara, M. G.; Banerjee, S. *Prog. Polym. Sci.* **2010**, *35*, 1022–1077.
7. Cassidy, P. E.; Amiabhavi, T. M.; Reddy, V. S.; Fitch, J. W. *Eur. Polym. J.* **1995**, *31*, 353–361.
8. Imae, T. *Curr. Opin. Colloid Interface Sci.* **2003**, *8*, 307–314.
9. Critchley, J. P.; Knight, G. J.; Wright, W. W. *Heat Resistat Polymers: Technologically Useful Materials*; Plenum Press: New York, 1983.
10. Iacono, S. T.; Budy, S. M.; Jin, J. Y.; Smith, D. W. *J. Polym. Sci., Part A: Polym. Chem.* **2007**, *45*, 5705–5721.
11. Iacono, S. T.; Budy, S. M.; Jin, J.; Dennis, W.; Smith, J. *J. Polym. Sci., Part A: Polym. Chem.* **2009**, *47*, 3454.
12. Bruma, M.; Fitch, J. W.; Cassidy, P. E. *J. Macro. Sci., Rev. Macro. Chem. Phys.* **1996**, *36*, 119–159.
13. Hedrick, J. L.; Labadie, J. W.; Ueda, M. Poly(aryl ether) Synthesis. In *Step Growth Polymers for High Performance Materials: New Synthetic Methods*; Hedrick, J. L., Labadie, J. W., Eds.; ACS Symposium Series 624; American Chemical Society: Washington, DC, 1996; pp 210−225.
14. Shimizu, M.; Hiyama, T. *Angew. Chem., Int. Ed.* **2005**, *44*, 214–231.
15. Muller, K.; Faeh, C.; Diederich, F. *Science* **2007**, *317*, 1881–1886.
16. Purser, S.; Moore, P. R.; Swallow, S.; Gouverneur, V. *Chem. Soc. Rev.* **2008**, *37*, 320–330.
17. Jeschke, P. *ChemBioChem* **2004**, *5*, 570–589.

Downloaded by COLUMBIA UNIV on August 28, 2012 | http://pubs.acs.org
Publication Date (Web): August 16, 2012 | doi: 10.1021/bk-2012-1106.ch003

18. Maienfisch, P.; Hall, R. G. *Chimia* **2004**, *58*, 93–99.
19. Ametamey, S. M.; Honer, M.; Schubiger, P. A. *Chem. Rev.* **2008**, *108*, 1501–1516.
20. Phelps, M. E. *Proc. Natl. Acad. Sci. U.S.A.* **2000**, *97*, 9226–9233.
21. Kobayashi, S.; Nishikawa, T.; Takenobu, T.; Mori, S.; Shimoda, T.; Mitani, T.; Shimotani, H.; Yoshimoto, N.; Ogawa, S.; Iwasa, Y. *Nat. Mater.* **2004**, *3*, 317–322.
22. Gurge, R. M.; Sarker, A. M.; Lahti, P. M.; Hu, B.; Karasz, F. E. *Macromolecules* **1997**, *30*, 8286–8292.
23. Kang, I. N.; Shim, H. K.; Zyung, T. *Chem. Mater.* **1997**, *9*, 746–749.
24. Son, H. J.; Wang, W.; Xu, T.; Liang, Y. Y.; Wu, Y. E.; Li, G.; Yu, L. P. *J. Am. Chem. Soc.* **2011**, *133*, 1885–1894.
25. Liang, Y. Y.; Feng, D. Q.; Wu, Y.; Tsai, S. T.; Li, G.; Ray, C.; Yu, L. P. *J. Am. Chem. Soc.* **2009**, *131*, 7792–7799.
26. Mohr, J. M.; Paul, D. R.; Tam, Y.; Mlsna, T. E.; Lagow, R. J. *J. Membr. Sci.* **1991**, *55*, 149–171.
27. Mohr, J. M.; Paul, D. R.; Mlsna, T. E.; Lagow, R. J. *J. Membr. Sci.* **1991**, *55*, 131–148.
28. Xu, Z.-K.; Dannenberg, C.; Springer, J.; Banerjee, S.; Maier, G. *J. Membr. Sci.* **2002**, *205*, 23–31.
29. Yampolskii, Y. P.; Bespalova, N. B.; Finkelshtein, E. S.; Bondar, V. I.; Popov, A. V. *Macromolecules* **1994**, *27*, 2872–2878.
30. Miyatake, K.; Zhou, H.; Matsuo, T.; Uchida, H.; Watanabe, M. *Macromolecules* **2004**, *37*, 4961–4966.
31. Kim, D. S.; Robertson, G. P.; Guiver, M. D.; Lee, Y. M. *J. Membr. Sci.* **2006**, *281*, 111–120.
32. Ghassemi, H.; McGrath, J. E.; Zawodzinski, J. T. A. *Polymer* **2006**, *47*, 4132–4139.
33. Stille, J. K.; Harris, F. W.; Rakutis, R. O.; Mukamal, H. *J. Polym. Sci., Part B: Polym. Lett.* **1966**, *4*, 791–793.
34. Stille, J. K.; Rakutis, R. O.; Mukamal, H.; Harris, F. W. *Macromolecules* **1968**, *1*, 431–436.
35. Shifrina, Z. B.; Averina, M. S.; Rusanov, A. L.; Wagner, M.; Müllen, K. *Macromolecules* **2000**, *33*, 3525–3529.
36. Rusanov, A. L.; Keshtov, M. L.; Khokhlov, A. R.; Keshtova, S. V.; Peregudov, A. S. *Vysokomolekulyarnye Soedineniya, Seriya A i Seriya B* **2001**, *43*, 581–587.
37. Rusanov, A. L.; Likhachev, D. Y.; Kostoglodov, P. V.; Belomoina, N. M. *Polym. Sci. Ser. C* **2008**, *50*, 39–62.
38. Kumar, U.; Neenan, T. X. *Macromolecules* **1995**, *28*, 124–130.
39. Cargagna, C. S.; Deck, P. A. *Polym. Prepr.* **2009**, *50*, 160.
40. Evans, J. P.; Deck, P. A. *Polym. Prepr.* **2009**, *50*, 166.
41. Sen, S.; Deck, P. A. *Polym. Prepr.* **2009**, *50*, 161.
42. Sen, S.; Deck, P. A. *Polym. Prepr.* **2011**, *52*, 737.
43. Fujimoto, C. H.; Loy, D. A.; Wheeler, D. R.; Jamison, G. M.; Cornelius, C. J. *Polym. Prepr.* **2002**, *43*, 1376.
44. Neenan, T. X.; Whitesides, G. M. *J. Org. Chem.* **1988**, *53*, 2489–2496.

Downloaded by COLUMBIA UNIV on August 28, 2012 | http://pubs.acs.org
Publication Date (Web): August 16, 2012 | doi: 10.1021/bk-2012-1106.ch003

45. Waugh, F.; Walton, D. R. M. *J. Organomet. Chem.* **1972**, *39*, 275–278.
46. Ogliaruso, M. A.; Becker, E. I. *J. Org. Chem.* **1965**, *30*, 3354–3360.
47. Lebedev, B. V.; Kulagina, T. G.; Bykova, T. A.; Smir, N. N.; Shifrina, Z. B.; Averina, M. S.; Rusanov, A. L. *Oxid. Commun.* **2005**, *28*, 131–142.
48. Fujimoto, C. H.; Hickner, M. A.; Cornelius, C. J.; Loy, D. A. *Macromolecules* **2005**, *38*, 5010–5016.
49. Stille, J. K.; Noren, G. K. *Macromolecules* **1972**, *5*, 49–55.
50. Seco, J. M.; Quinoa, E.; Riguera, R. *Chem. Rev.* **2004**, *104*, 17–118.
51. Danielson, M. A.; Falke, J. J. *Annu. Rev. Biophys. Biomol. Struct.* **1996**, *25*, 163–195.
52. Gakh, Y. G.; Gakh, A. A.; Gronenborn, A. M. *Magn. Reson. Chem.* **2000**, *38*, 551–558.
53. Budy, S. M.; Nichol, G. S.; Loy, D. A. *Acta Cryst. C* **2011**, accepted.
54. Silverstein, R. M.; Webster, F. X.; Kiemle, D. J. *Spectrometric Identification of Organic Compounds*, 7th ed.; John Wiley & Sons: Hoboken, NJ, 2005.
55. Pretsch, E.; Buhlmann, P.; Affolter, C. *Structure Determination of Organic Compounds*, 3rd ed.; Spring: New York, 2000.
56. Irvin, J. A.; Neef, C. J.; Kane, K. M.; Cassidy, P. E.; Tullos, G.; St. Clair, A. K. *J. Polym. Sci., Part A: Polym. Chem.* **1992**, *30*, 1675–1679.
57. Pitois, C.; Wiesmann, D.; Lindgren, M.; Hult, A. *Adv. Mater.* **2001**, *13*, 1483–1487.
58. Wilkie, C. A.; Morgan, A. B. *Fire Retardancy of Polymeric Materials*, 2nd ed.; CRC Press: Boca Raton, FL, 2010.
59. Gilbert, J. B.; Kipling, J. J.; McEnaney, B.; Sherwood, J. N. *Polymer* **1962**, *3*, 1–10.
60. Ruland, W. *Carbon* **1965**, *2*, 365–378.
61. Sastri, S. B.; Armistead, J. P.; Keller, T. M. *Carbon* **1993**, *31*, 617–622.
62. Fox, H. W.; Zisman, W. A. *J. Colloid Sci.* **1950**, *5*, 514–531.
63. Young, T. *Philos. Trans. R. Soc. London* **1805**, *95*, 65–87.
64. Cassie, A. B. D.; Baxter, S. *Trans. Faraday Soc.* **1944**, *40*, 0546–0550.
65. Wenzel, R. N. *Ind. Eng. Chem.* **1936**, *28*, 988–994.

Downloaded by COLUMBIA UNIV on August 28, 2012 | http://pubs.acs.org
Publication Date (Web): August 16, 2012 | doi: 10.1021/bk-2012-1106.ch003

Downloaded by STANFORD UNIV GREEN LIBR on August 28, 2012 | http://pubs.acs.org
Publication Date (Web): August 16, 2012 | doi: 10.1021/bk-2012-1106.ch004

Chapter 4

Towards Metal Mediated Radical Polymerization of Vinylidene Fluoride

Alexandru D. Asandei,[*] Christopher P. Simpson, Olumide I. Adebolu, and Yanhui Chen

**Department of Chemistry and Institute of Materials Science,
University of Connecticut, 97 N. Eagleville Rd.,
Storrs, Connecticut 06269, USA
[*]E-mail: asandei@ims.uconn.edu**

As a prelude to metal mediated systems, a series of typical free radical initiators were first evaluated in the thermal or UV-mediated VDF polymerization in glass tubes, at room temperature (rt) in a variety of solvents. Better polymerization results were obtained with initiators which generate the most reactive radicals (TBPO), in solvents that minimize chain transfer (ACN). The effect of UV irradiation was subsequently investigated to reveal a photocontrolled free radical polymerization. Finally, a series of epoxides, aldehydes, halides and peroxides, known to initiate both styrene and diene polymerizations in the presence of $Cp_2TiCl^•$, were tested as potential rt VDF initiators. However, regardless of reaction conditions, no polymer was obtained. This is most likely due to the incompatibility of solvents appropriate for Cp_2TiCl_2 reductions with those conducive of VDF polymerizations. Thus, polar solvents favored by Cp_2TiCl_2 are strong chain transfer agents towards VDF (dioxane, THF, diglyme, acetone), while solvents that limit chain transfer to $PVDF^•$ (ACN), react with $Cp_2TiCl^•$.

In Advances in Fluorine-Containing Polymers; Smith, D., et al.;
ACS Symposium Series; American Chemical Society: Washington, DC, 2012.

Downloaded by STANFORD UNIV GREEN LIBR on August 28, 2012 | http://pubs.acs.org
Publication Date (Web): August 16, 2012 | doi: 10.1021/bk-2012-1106.ch004

Introduction

Fluorinated (co)polymers are fundamental specialty materials endowed with wide morphological versatility, high thermal, chemical, ageing and weather resistance, as well as low surface energy, dielectric constant, flammability, refractive index, and moisture absorption. As such, their applications range anywhere from paints and coatings, pipe liners, transmission fluids, O-rings for extreme temperatures, fuel cell membranes and antifouling layers to optical fibers and high power capacitors (*1*). A well know example is poly(vinylidene fluoride) (PVDF) (*2*) which due to its excellent chemical inertness, acid resistance, low water absorptivity, weatherability, low dielectric constant and piezoelectric properties (*3*–*5*), is a widely used high-performance material for coatings, membranes for fuel cells and Li ion batteries (*6*), as well as semiconductor and nuclear applications. To overcome the PVDF high crystallinity and low solubility, various copolymers, especially with non homopolymerizable (*7*, *8*) hexafluoropropene (*8*, *9*) (HFP) are also used. PVDF is obtained by the high pressure (bp_{VDF} = -86 °C, bp_{HFP} = -29.6 °C) peroxide initiated VDF radical polymerization in metal reactors at 50-100°C (*10*, *11*).

Conversely, controlled radical polymerizations (CRPs) which limit termination and other side reactions *via* atom transfer (ATRP) (*12*, *13*) dissociation-combination (DC) or degenerative transfer (DT) mechanisms and enable control over molecular weight and polydispersity, have been widely applied in the synthesis of complex macromolecular structures (*13*). However, while they have recently seen remarkable developments (*12*), and ATRP, nitroxide or addition-fragmentation methods were successful with acrylates or styrenes, their applicability towards very reactive monomers such as main chain fluorinated alkenes, still awaits demonstration. Moreover, all metal based systems employ only late transition metals and provide initiation only from activated halides or thermal initiators. Thus, a broader selection of initiators and catalysts would be desirable, especially since they might provide access to novel chain ends derived either from the initiator or catalyst or both.

Thus, as (co)polymers of main chain fluorinated monomers (*e.g.* VDF) are important, the study of their CRPs and the synthesis of the complex polymer architectures thereby derived, is a worthy undertaking (*14*, *15*). Conversely, such polymerizations are quite challenging, especially on a laboratory scale, in view of the low bp of the monomers and the high-pressure metal reactor requirement. As such, while styrene or acrylate CRPs can be conveniently sampled repeatedly from the side arm of a Schlenk tube on a 1 g scale, kinetic studies of VDF polymerizations involve many one-data-point experiments. This is a very time-consuming and expensive process due to the typical lab unavailability of a large number of costly metal reactors, which moreover still require 10-100 g of monomer. Thus, development of methods that would allow few grams-scale polymerizations to proceed at room temperature (rt) in inexpensive, low-pressure glass tubes, would be highly desirable, especially since such procedures would easily lend themselves to the fast screening of a wide range of catalysts and reaction conditions.

Downloaded by STANFORD UNIV GREEN LIBR on August 28, 2012 | http://pubs.acs.org
Publication Date (Web): August 16, 2012 | doi: 10.1021/bk-2012-1106.ch004

VDF polymerization can proceed at rt under organic free radical initiation (*16*), but only very low molecular weight VDF telomers (DP < 1-3) may be obtained, and only at high temperatures (> 100 °C) from transition metal salts and polyhalides by redox catalysis (*15*, *17*). Moreover, while the 1:1 metal catalyzed addition of R_F-I derived perfluoroalkyl radicals to alkenes using Cu (*18*), Zn (*19*), Pd (*20*), $SnCl_2/CH_3COOAg$ (*21*, *22*) Cp_2TiCl (*23–25*) occurs readily at high temperatures, the metal *catalyzed* addition of such electrophilic radicals to electrophilic fluorinated alkene substrates (FMs) at T < 100 °C, and especially at ambient temperatures is to the best of our knowledge, conspicuously absent from the literature. Moreover, there are no reports on metal-mediated VDF polymerizations, let alone VDF-CRP. Consequently, the ability to initiate and control VDF using a transition metal system under mild conditions would be of great synthetic value.

The paramagnetic Cp_2TiCl (*26*) available in situ by Zn reduction of Cp_2TiCl_2 (*27*) is a mild one electron transfer agent which catalyzes a variety of radical reactions (*28*), including epoxide radical ring opening (RRO (*29*),), aldehyde SET reduction and halide abstraction. We have demonstrated the Cp_2TiCl-catalyzed LRP of styrene (*30–39*) initiated by epoxides, aldehydes (*40*, *41*), halides (*42*), and peroxides (*43*), as well as that of dienes (*44*) initiated from halides (*45–65*) epoxides (*45*, *46*, *51*), and aldehydes (*47*, *48*). The effect of ligands, reducing agents, solvents, additives, reagent ratios and temperature was investigated (*30–39*). This methodology was applied in the synthesis of branched and graft copolymers (*66*), and Ti alkoxides generated in-situ from epoxides and aldehydes were also shown to catalyze the living ring opening polymerization of cyclic esters epoxides and anhydrides (*67–69*).

Encouraged by these results, we decided to evaluate such alternative methods of polymerization initiation and control (*70*), and explore the scope and limitations of transition metal catalysts in the rt VDF radical polymerization.

Experimental

Materials

Vinylidene fluoride (VDF, 98% min.) and hexafluoropropene (HFP, 99% min.), 1-iodononafluorobutane (PFBI, 98%) and heptafluoro-2-iodopropane (PFipI, 97%), 1, 8-dichloroperfluorooctane (DCPfO, 99%) (all from Synquest Laboratories). Activated Zn powder (Zn, 99+%), glycidyl 4-methoxyphenyl ether (MPEG, 99%), 1,2,7,8-Diepoxyoctane (DEO, 97%), 1,4-butanediol diglycidyl ether (BDE, 95%), Benzaldehyde (BA, 99.5%), 1,10-Dibromodecane (DBD, 97%), methyl iodide (CH_3I, 99.5%), 1-(bromoethyl)benzene (BEB, 95%), azobisisobutyronitrile (AIBN, 98%), H_2O_2 (50% in H_2O), benzoyl peroxide (BPO, 97%), tert-butylperoxy benzoate (TBPB, 95%), t-butyl peroxide (TBPO, 98%), 2,5-bis-(tert-butylperoxy)-2,5–dimethylhexane (BTBDMH, 90%), dicumyl peroxide (DCPO, 99%), and dimethyl carbonate (DMC, ≥ 99%, anhydrous) (all from Aldrich), dilauryl peroxide (DLPO, 99%) methoxybenzene sulfonyl chloride (MBSC, 99%), bis(cyclopentadienyl)titanium dichloride (Cp_2TiCl_2, 97%), bromotrichloromethane ($BrCCl_3$, 99%), ethylene carbonate (EC, 99%)

(all from Acros) and carbon tetrachloride (CCl_4, 99%, Fisher) were used as received. Methanol (MeOH, 99%) acetonitrile (ACN, 99%), anisole (99.7%), α,α,α-trifluorotoluene (TFT, 99%), pyridine (Pry, 99%), N-methyl-2-pyrrolidinone (NMP, 99%) (all from Aldrich), N,N′-dimethylacetamide (DMAC, 99%), dioxane (99.7, %), dimethyl sulfoxide (DMSO, 99.8%), benzonitrile (BzN, 99%), and ε-caprolactone (CL, 99%) (all from Acros), diglyme (99.5%, Fluka), N,N′-dimethylformamide (DMF, 99.9%), toluene (Tol, 99.8%) (both from Fisher), and tetrahydrofuran (THF, 99%, J. T. Baker), were dried over CaH_2 overnight. Acetone (99.9%, J. T. Baker) was dried over anhydrous $MgSO_4$.

Downloaded by STANFORD UNIV GREEN LIBR on August 28, 2012 | http://pubs.acs.org
Publication Date (Web): August 16, 2012 | doi: 10.1021/bk-2012-1106.ch004

Techniques

^{1}H NMR (500 MHz) spectra were recorded on a Bruker DRX-500 at 24°C in acetone-d_6. GPC analyses were performed on a Waters gel permeation chromatograph equipped with a Waters 2414 differential refractometer and a Jordi 2 mixed bed columns setup at 80°C. DMAc (Fisher, 99.9% HPLC grade) was used as eluent at a flow rate of 1 mL/min. Number-average (M_n) and weight-average molecular weights (M_w) were determined from calibration plots constructed with polymethylmethacrylate standards. All reported polydispersities are those of water precipitated samples.

Polymerizations

A 35-mL Ace Glass 8648 # 15 Ace-Thread pressure tube equipped with bushing and a plunger valve was charged with TBPO (0.16 mL, 0.85 mmol), ACN (3 mL) and degassed. The tube was then cooled, opened under He and charged with VDF (1.1g, 17.18 mmol), re-degassed and the reaction mixture was warmed up to room temperature on a stir plate under UV irradiation at about 15-20 cm from a UV lamp (Fisher, model B-100AP with a spot bulb, 100W) behind a protective shield. After required amount of time, the tube was cooled in liquid nitrogen, opened and the excess VDF and HFP was allowed to boil off in the hood under maximum air flow. The reaction mixture was precipitated into deionized water. The polymer was centrifuged and dried.

A 35-mL Ace Glass 8648 # 15 Ace-Thread pressure tube equipped with bushing and a plunger valve containing Cp_2TiCl_2 (21.4 mg, 0.09 mmol), Zn (4.2 mg, 0.07 mmol) and dioxane (3.0 mL) was degassed and the Ti reduction was carried out at rt. The tube was then cooled in liquid nitrogen, opened under He and charged with MPEG (15.5 mg, 0.09 mmol) and VDF (1.10 g, 17.18 mmol), re-degassed and held at 25 °C. Conversions were determined gravimetrically.

Results and Discussion

Before evaluating the metal catalyzed systems, we decided to first verify our ability to perform the reactions in glass tubes at rt by carrying out conventional free radical VDF polymerizations. Thus, it is known that UV radiation mediates VDF (*2*) telomerization with (perfluoro)alkyl iodides (*71*) or H_2O_2 (*72*), but

Downloaded by STANFORD UNIV GREEN LIBR on August 28, 2012 | http://pubs.acs.org
Publication Date (Web): August 16, 2012 | doi: 10.1021/bk-2012-1106.ch004

there are very few reports on the use of conventional free radical initiators either at mild temperatures or under UV irradiation or on the solvent effect in VDF polymerizations. Thus, we started (*73–81*) by exploring VDF homo and copolymerizations under such conditions.

Previous investigations of solution properties (*82–87*) indicated that the best PVDF solvents are polar aprotic and H-bonding capable, and that HH sequences decrease solubility (*85*). A common structural motif is a favorable interaction of the polar Y=O bond (Y = C, S, P) of the solvent, with the mildly acidic Hs in $-CF_2-C\mathit{H}_2-CF_2-$. Accordingly, 2-pentanone, propionitrile, BN, nitrobenzene, $(MeO)_3P$, $(NEt_2)SO_2$, sulfolane, and metylpyridines were classified as bad solvents. $(BuO)_3P=O$ only swells PVDF, whereasγ-butyrolactone, propylenecarbonate, cyclohexanone, CH_3COPh and $Ph_2C=O$ solutions gel on annealing at rt. Short chain phosphates ($(RO)_3P=O$; R = Me, Et, and $(CH_3)(MeO)_2P=O$) are good solvents, whereas tertiary amides ($HCONR_2$; R = Me (DMF), Et, DMAC, N-formylmorpholine, NMP) and DMSO are very good solvents. Finally, cyclopentanone, N-alkyl cyclic urethanes as well as linear and cyclic ureas ($(Me_2N)_2C=O$, $[-N(CH_3)-(CH_2)_{2-3}-N(CH_3)-]C=O$, DMEU and DMPU) dissolve PVDF even at rt, with $[(CH_3)_2N]_3P=O$ (HMPA) and $(CH_3)[(CH_3)_2N]_2P=O$ considered excellent solvents.

However, while VDF "solution" polymerizations are typically carried out in ACN (*88*), a non-solvent weak chain transfer (CT) agent (*89*), there is in fact very little data (*90–92*) on the solvent effect in VDF polymerizations. Thus, we decided to scan a few common solvents, using typical free radical initiators, noting that while good monomer/polymer solubilization would be desirable, minimization of solvent CT outweighs solubility considerations. Thus, the trends discussed below are the combined result of the solvent CT transfer and swelling ability.

Table I. Free Radical VDF Polymerizations and Solvent Effect

Exp	*Initiator*	*[VDF]/[I]*	*Solvent*	*Temp (°C)*	M_n	*PDI*	*Time (hr)*	*Conv %*
1	AIBN	100/1	ACN	60	-	-	15	0
2	AIBN	100/1	ACN	60	-	-	19	0
3	AIBN	20/1	ACN	60	-	-	72	0
4	AIBN	40/1	Dioxane	60	-	-	18	0
5[a]	AIBN	25/1	ACN	25	-	-	40	0
6[b]	AIBN	20/1	Dioxane	25	-	-	20	0
7	BPO	20/1	ACN	60	-	-	72	0
8	BPO	100/1	ACN	80	-	-	14	0
9	BPO	100/1	ACN	80	-	-	24	0
10	BPO	100/1	ACN	90	-	-	27	0

Continued on next page.

Table I. (Continued). Free Radical VDF Polymerizations and Solvent Effect

Exp	*Initiator*	*[VDF]/[I]*	*Solvent*	*Temp (°C)*	M_n	*PDI*	*Time (hr)*	*Conv %*
11	BPO	10/1	ACN	90	-	-	24	0
12	BPO	100/1	ACN	90	-	-	14	0
13	BPO	20/1	ACN	90	-	-	20	0
14	BPO	100/1	ACN	90	-	-	3	0
15	BPO	50/1	ACN	90	-	-	4	0
16	BPO	100/1	ACN	90	-	-	14	0
17[b]	BPO	20/1	ACN	25	3,265	1.57	20	15
18	DCPO	50/1	ACN	60	3,092	1.14	16	7
19	DLPO	20/1	ACN	90	-		20	0
20[b]	DLPO	20/1	ACN	25	-		20	3
21	H_2O_2	25/1	ACN	25	-		14	0
22	H_2O_2	100/1	ACN	25	-		27	0
23	TBPB	20/1	ACN	90	-		20	0
24[b]	TBPB	20/1	ACN	25	-		20	3
25[a]	TBPO	25/1	BzN	25	-		48	0
26[a]	TBPO	20/1	ACN	25	17,187	1.55	15	37
27[a]	TBPO	25/1	DMAc	25	1,002	1.42	40	10
28[a]	TBPO	25/1	DMF	25	804	1.31	40	17
29[a]	TBPO	25/1	NMP	25	517	1.74	40	17
30[a]	TBPO	25/1	Pyridine	25	-	-	38	0
31[b]	TBPO	25/1	ACN	25	6,300	1.91	22	33
32[b]	TBPO	10/1	ACN	25	-	-	23	47
33[b]	TBPO	20/1	ACN	25	7,074	2.31	20	34
34[b]	TBPO	20/1	BzN	25	-	-	15	0
35[b]	TBPO	20/1	Dioxane	25	-	-	17	0
36[b]	TBPO	25/1	DMSO	25	-	-	48	0
37[b]	TBPO	25/1	TFT	25	-	-	48	0
38[b]	TBPO	25/1	THF	25	-	-	48	0
39[b]	TBPO	25/1	Toluene	25	-	-	48	0

[a] Oriel Xenon arc lamp. [b] High Intensity UV Lamp 365 nm.

Downloaded by STANFORD UNIV GREEN LIBR on August 28, 2012 | http://pubs.acs.org
Publication Date (Web): August 16, 2012 | doi: 10.1021/bk-2012-1106.ch004

Downloaded by STANFORD UNIV GREEN LIBR on August 28, 2012 | http://pubs.acs.org
Publication Date (Web): August 16, 2012 | doi: 10.1021/bk-2012-1106.ch004

As seen from Table I, no polymer was obtained from AIBN, dilauryl peroxide or TBPB under either thermal (< 90 °C) or irradiation conditions. However, while BPO was also unsuccessful thermally, some polymer was obtained under UV. Dicumyl peroxide was the only initiator which provided polymer at ~ 60 °C. While H_2O_2 can initiate under UV (*72*), it generated no polymer at 25 °C. Finally, TBPO decomposes thermally or under UV with the formation of methyl radicals which are reactive enough to add to VDF even at ambient temperatures, and was the most efficient of the series. Dialkyl peroxides have quite a long half lifetime (*e.g.* $t_{1/2,TBPO}^{90°C} = 543$ h) (*43*), and thus their rt thermal dissociation is negligible. Therefore, any possible rt initiation can only be due to the UV-induced decomposition.

The rest of the experiments evaluated the solvent effect and indicated that unfortunately, good PVDF solvents (DMF, DMAC) are not necessarily satisfactory for polymerizations, due to their high chain transfer ability. Conversely, ACN reactions are in fact heterogeneous, precipitation polymerizations. Thus, the prospect of VDF homogeneous solution polymerization without chain transfer under radical conditions appears unlikely.

Several sets of one data point experiments were then conducted to investigate the effect of UV irradiation on the polymerization kinetics. While HFP does not hompolymerize radically, to confirm that VDF does not self-initiate and that the polymerization is photocontrolled, we compared (Figure 1a) the kinetics of VDF polymerization under continuous UV exposure with experiments where the UV was turned off after 2 h and respectively 8 h, but the reaction was monitored for longer times.

Similarly, VDF-HFP copolymerizations were also carried out (Figure 1b) where TBPO continuous irradiation experiments (each sample irradiated until stopped at different times) were compared with reactions using BTBDMH, where all polymerizations were stopped after the same amount of time (24 h), but where each sample was irradiated for progressively longer times. As seen in Figure 1b, first order kinetics were observed for both initiators. Consistent with the results from Figure 1a, under continuous UV irradiation (TBPO), conversion increases with reaction time. Similarly, for the same total reaction time, conversion increases with UV exposure time (BTBDMH). The two apparent polymerization rate constants are $k_{p,TBPO}^{app} = 0.053$ h^{-1} and respectively, $k_{p,BTBDMH}^{app} = 0.111$ h^{-1}. The rate doubling for BTBDMH at the same molar ratios is a reflection of the fact that BTBDMH is tetrafunctional, whereas TBPO is difunctional. Thus, as expected, an uninterrupted increase in conversion is observed under continuous irradiation. By contrast, no conversion increase occurs at longer reaction times in the absence of UV assistance. This indicates that UV irradiation is necessary for the continuous generation of peroxide derived radicals, which support the polymerization.

Figure 2 illustrates the M_n and PDI profiles vs. conversion in the VDF/HFP copolymerizations from Figure 1b. The relative independence of M_n and PDI of conversion indicates that as expected, the polymerization is simply free radical.

Downloaded by STANFORD UNIV GREEN LIBR on August 28, 2012 | http://pubs.acs.org
Publication Date (Web): August 16, 2012 | doi: 10.1021/bk-2012-1106.ch004

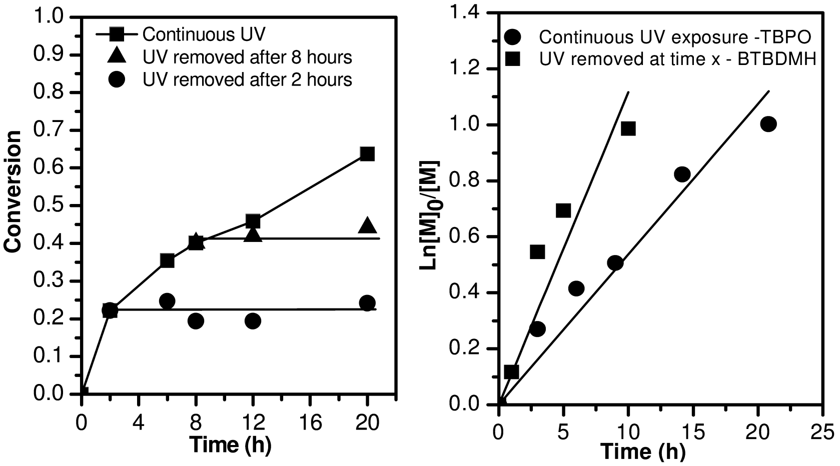

Figure 1. (a) Kinetics of VDF rt homopolymerization under UV irradiation. VDF/TBPO = 10/1. (b) Kinetics of VDF/HFP rt copolymerizations under UV irradiation: VDF/HFP/(TBPO or BTBDMH) = 10/5/1. The x axis represents total reaction time for TBPO under continuous irradiation and respectively irradiation time for BTBDMH, with all reactions stopped after 24h.

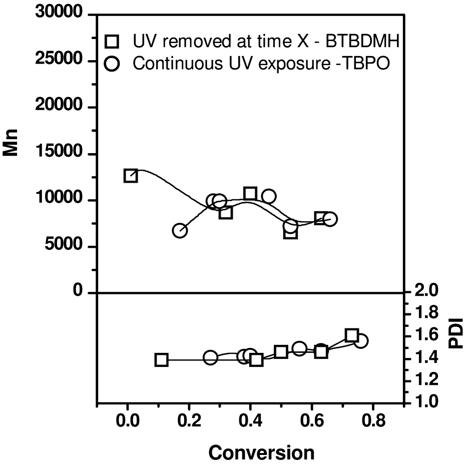

Figure 2. Dependence of M_n and PDI on conversion in VDF-HFP copolymerization at rt under UV irradiation.

Downloaded by STANFORD UNIV GREEN LIBR on August 28, 2012 | http://pubs.acs.org
Publication Date (Web): August 16, 2012 | doi: 10.1021/bk-2012-1106.ch004

Having evaluated the conventional VDF-FRP in glass tubes at rt, we then attempted a transition metal mediated radical initiation approach. Similarly to the results we have previously observed with styrene and dienes (*30–66*), we expected the VDF polymerization to follow the mechanism outlined in Scheme 1. As such, the Zn reduction of Cp_2TiCl_2 occurs readily in dioxane and in many polar solvents to generate $Cp_2Ti(III)Cl$ (eq. 1). Subsequent radical ring opening of epoxides (RRO, eq. 2,3), SET reduction of aldehydes (eq. 4), halide abstraction (eq. 5) or redox reactions with peroxides (eq. 6, 7) provide radical species which add to alkenes, thereby initiating radical polymerizations. Additionally, polymerization control (eq. 8), can be afforded by the reversible termination of the growing chains with a second equivalent of $Cp_2Ti(III)Cl$ *via* a combination of DC and DT mechanisms (eqs. 9, 10).

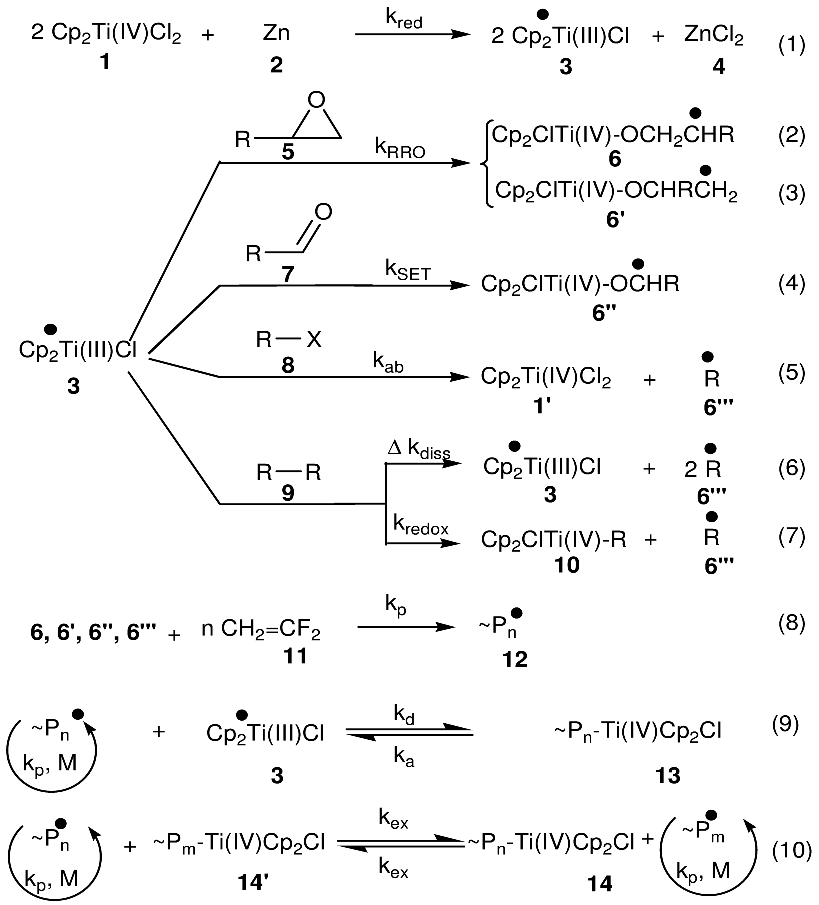
2 Cp2Ti(IV)Cl2 + Zn → 2 Cp2Ti(III)Cl + ZnCl2 (1)
1
2
kred
3
4
R 5 kRRO
Cp2ClTi(IV)-OCH2CHR (2)
6
Cp2ClTi(IV)-OCHRCH2 (3)
6'
R 7 kSET
Cp2ClTi(IV)-OCHR (4)
6''
Cp2Ti(III)Cl
3
R—X 8 kab
Cp2Ti(IV)Cl2 + R (5)
1'
6'''
R—R 9
Δ kdiss
Cp2Ti(III)Cl + 2 R (6)
3
6'''
kredox
Cp2ClTi(IV)-R + R (7)
10
6'''
6, 6', 6'', 6''' + n CH2=CF2 → ~Pn (8)
11
kp
12
~Pn kp, M + Cp2Ti(III)Cl ⇌ ~Pn-Ti(IV)Cp2Cl (9)
kd
ka
3
13
~Pn kp, M + ~Pm-Ti(IV)Cp2Cl ⇌ ~Pn-Ti(IV)Cp2Cl + ~Pm kp, M (10)
kex
kex
14'
14

Scheme 1. Cp_2TiCl-mediated VDF polymerization mechanism.

Table II. Cp_2TiCl-Mediated Initiating Systems

Exp	*[VDF]/[I]/ [Cp_2TiCl_2]/[Zn]*	*[I]*	*Solvent*	*Temp °C*	*Time (hr)*
1	7.25/0/1/1	-	DMC	50	24
2	0/0/1/0.75	-	DMC	25	24
3	3/0/1/0.6	-	Dioxane	25	24
4[a,b]	5/0/1/0	-	DMC	40	42
5	100/1/2/4	BPO	ACN	60	14
6	100/1/1/1	BPO	ACN	90	24
7[c]	20/1/.05/.25	TBPB	Anisole	25	40
8[c]	100/1/.25/.25	TBPO	Dioxane	25	21
9[c]	100/1/1/1	TBPO	Dioxane	25	27
10[c]	100/1/1.5/1.5	TBPO	Dioxane	25	99
11	100/1/2/4	TBPO	DMF	110	40
12	100/1/1.9/0.95	DEO	Dioxane	25	18
13	100/1/2/2	BDE	DMF	130	62
14	50/1/2/1.1	BDE	Acetone	40	60
15	200/1/1/0.75	MPEG	Dioxane	60	48
16	100/1/1/2	BA	DMF	150	62
17	100/1/1/0.6	BA	ACN	90	48
18	50/1/1/0.6	MBSC	ACN	60	12
19	50/1/0.1/1	MBSC	Anisole	25	164
20	100/1/2/1	DBD	ACN	25	20
21	25/1/1/0.6	CCl_4	DMC	25	43
22	100/1/3/6	CCl_4	DMC	40	21
23	50/1/0.3/5	CCl_4	DMC	40	48
24	10/1/0.015/0.05	CCl_4	DMC	50	43
25	50/1/3/1.6	CCl_4	DMC	60	46
26	50/1/3/1.5	CCl_4	DMC	60	62
27	25/1/0.02/1	CCl_3Br	Acetone	40	60
28[a,d]	50/1/1/0	CH_3I	ACN	25	24
29	50/1/0.1/2	BEB	Diox	25	25
30	50/1/2/1.1	DCPfO	DMC	50	24
31	50/1/0.05/0.6	PFBI	DMF	25	24

Continued on next page.

Downloaded by STANFORD UNIV GREEN LIBR on August 28, 2012 | http://pubs.acs.org
Publication Date (Web): August 16, 2012 | doi: 10.1021/bk-2012-1106.ch004

Downloaded by STANFORD UNIV GREEN LIBR on August 28, 2012 | http://pubs.acs.org
Publication Date (Web): August 16, 2012 | doi: 10.1021/bk-2012-1106.ch004

Table II. (Continued). Cp_2TiCl-Mediated Initiating Systems

Exp	*[VDF]/[I]/ [Cp_2TiCl_2]/[Zn]*	*[I]*	*Solvent*	*Temp °C*	*Time (hr)*
32	50/1/1/0.6	PFBI	Dioxane	25	24
33	25/1/0.2/0.4	PFBI	MeOH	25	24
34	25/1/0.1/1	PFBI	H_2O	40	44
35	25/1/0.1/1	PFBI	CL	40	44
36	50/1/2/1.1	PFBI	Acetone	40	60
37[b]	50/1/0.2/1	PFBI	DMC	40	72
38	50/1/0.2/0.1	PFBI	DMC	40	48
39	75/1/3/6	PFBI	DMC	40	14
40[b]	50/1/0.4/0.21	PFBI	Diglyme	40	18
41[b]	25/1/0.2/0.4	PFBI	Anisole	40	72
42	25/1/0.5/0.6	PFBI	DMC	45	48
43	25/1/0.2/0.4	PFBI	EC	5	48
44	25/1/1.1/2	PFBI	EC	45	48
45	50/1/3/1.6	PFBI	DMC	60	46
46	50/1/3/1.5	PFBI	DMC	60	62
47[a],[b]	50/1/0.1/0	PBFI	DMC	40	42
48	50/1/0.1/0.1	PFIpI	DMAC	25	120
49[c]	50/1/0.1/0.6	PFIpI	DMAC	25	96
50	25/1/0.1/1	PFIpI	ACN/Diox.	25	63

[a] no reducing reagent. [b] 30W CFL. [c] High Intensity UV Lamp 365nm. [d] Oriel Xe Arc Lamp.

Selected examples of the attempts at Cp_2TiCl-mediated radical initiation of VDF from four different classes of initiators (epoxides, aldehydes, halides and peroxides) are presented in Table II. However, in none of these experiments was polymer obtained. Nonetheless, the corresponding radicals can clearly be produced even at rt, as evidenced by the green to red color change upon the injection of their precursor into a Cp_2TiCl solution, and by their initiation of the polymerization of styrene and dienes (*30–67*). Conversely, the radical polymerization of VDF can proceed at rt as seen above with UV or with other radial generation systems (*16*, *70*).

Hence, what are the reasons for the lack of polymerization? Possible explanations include the absence of a solvent compatible with both VDF polymerizations and with $Cp_2TiCl^•$, the inability of the initiator radicals to add to VDF at rt, as well as potential organometallic side reactions such as Zn insertion into the carbon halide bond of the initiator (*93*, *94*) or the irreversible deactivation of the chain ends and of the catalyst via either β-H (Cp_2TiClH) or β-F (Cp_2TiClF) elimination, assuming initiation does occur. Indeed, in the presence of Zn, perfluoroalkyl iodides may add to the carbonyls of alkyl carbonates such as DMC *via* the intermediary formation of a Grignard-like R_F-Zn-I species (*93*, *94*). However, Cp_2TiCl does not abstract F from R_F-X, but mediates the addition $R_F^•$ to regular alkenes such as isoprene (*23–25*).

While one can argue that perhaps the radicals derived from aldehydes and sulfonyl or benzyl halides may not be reactive enough for rt initiation, the primary radicals derived from epoxide RRO and those obtained from CH_3-I, CCl_4 and R_F-I are definitely capable of initiation (*70*). Thus, the dominant reason is most likely, the solvent effect.

In solution, Cp_2TiCl consist of an equilibrium mixture of the monomer with the dominating $Cp_2Ti(\mu\text{-}Cl)_2TiCp_2$ chloride-bridged dimer (*95–99*), and the relative reactivity of these two species is solvent dependent. While polar, coordinating solvents readily dissociate the dimer (*95*), aromatic, less polar solvents have a lower ability to promote reduction and dimer dissociation. However, too strong of a solvent coordination may also translate in a poor polymerization performance due to blocking of the Ti active site. Amide-based solvents such as DMF, DMAC and NMP and strong nitrogen donors like pyridine and ACN may act as ligands that coordinate $Cp_2TiCl^•$ too strongly and irreversibly, or similarly to the SET reduction of aldehydes and ketones, could directly deactivate the catalyst *via* the SET reduction and addition of $Cp_2TiCl^•$ to the C=O (*28*, *40*), S=O (*100*), or CN (*101*) groups. Conversely, $Cp_2TiCl^•$ can transfer H from water and alcohols and would thus act as CT agents in a polymerization in such -OH solvents (*102*).

Under these conditions, for styrene polymerizations (*33*), the best results were obtained with aliphatic ethers such as THF, dioxane and diglyme which coordinate reversibly, and easily stabilize $Cp_2Ti(III)Cl$ (*95–99*). The solvent suitability in terms of PDI was: dioxane ≥ THF > diglyme > PhOMe > Ph_2O ≥ bulk > toluene >> pyridine > DMF > NMP, DMAC > ethylene carbonate, acetonitrile. One can already see that the best solvents for VDF polymerizations are actually at the bottom of this list.

Thus, in retrospect, the above VDF/Cp_2TiCl requirements practically disqualify all the experiments, such as those carried out in anisole, dioxane, and diglyme for VDF, and those in acetone, ACN, BN, DMC, EC, CL, TMP, H_2O and MeOH for Cp_2TiCl, with DMF, DMAC, being unsuitable for both. It appears therefore, that unfortunately, the preferred solvents for the polymerization are incompatible with the ones for the catalyst.

Downloaded by STANFORD UNIV GREEN LIBR on August 28, 2012 | http://pubs.acs.org
Publication Date (Web): August 16, 2012 | doi: 10.1021/bk-2012-1106.ch004

Downloaded by STANFORD UNIV GREEN LIBR on August 28, 2012 | http://pubs.acs.org
Publication Date (Web): August 16, 2012 | doi: 10.1021/bk-2012-1106.ch004

Conclusions

A series of typical free radical initiators such AIBN, BPO, TBPB, TBPO, DCPO, DLPO, and H_2O_2 were evaluated in the thermal or UV-mediated VDF polymerization in TFT, Py, NMP, DMAC, dioxane, THF, DMSO, BN, DMF, and toluene. Better polymerization results were obtained with initiators which generate the most reactive radicals (TBPO) in solvents that minimize chain transfer (ACN), which however, are not necessarily good PVDF solvent as well.

The effect of UV irradiation was investigated in the homo and copolymerization of VDF with HFP initiated from TBPO and BTBDMH. For a given total reaction time, a continuous increase in conversion was observed with increasing irradiation time, and faster rates were observed for the tetrafunctional BTBDMH than for the difunctional TBPO. M_n and PDI remained relatively constant, as expected in a free radical polymerization. Conversely, further kinetic sampling at longer times after the UV source was turned off, revealed no conversion increase. This indicates that UV irradiation is essential for the generation of initiator derived radicals at rt, but does not induce pure photopolymerization in the absence of the initiator.

Finally, a series of epoxides, aldehydes, halides and peroxides, known to initiate both styrene and diene polymerizations in the presence of $Cp_2TiCl^•$, were tested as potential rt VDF initiators. However, regardless of reaction conditions, no polymer was obtained. This is most likely the combined outcome of a series of factors including lower reactivity of the initiating radicals by comparison with the propagating chain, transfer to the solvent or catalyst, low reaction temperature and of several possible organometallic side reactions. The key reason for the failure of these polymerizations is most likely the solvent effect, *i.e.* the incompatibility of solvents appropriate for Cp_2TiCl_2 reductions with those conducive of VDF polymerizations. Thus, the polar solvents that promote a fast and efficient reduction of Cp_2TiCl_2 are strong chain transfer agents towards VDF (dioxane, THF, diglyme, acetone), while solvents that limit chain transfer to $PVDF^•$ (ACN, DMC), will react with $Cp_2TiCl^•$.

Acknowledgments

Financial support from the University of Connecticut is gratefully acknowledged.

References

1. Ameduri, B. *Macromolecules* **2010**, *43*, 10163–10184.
2. Ameduri, B.; Boutevin, B. *Well-Architectured Fluoropolymers: Synthesis, Properties and Applications*; Elsevier: The Netherlands, 2004.
3. Souzy, R.; Ameduri, B.; Boutevin, B. *J. Polym. Sci., Part A: Polym. Chem.* **2004**, *42*, 5077.
4. Shi, Z.; Holdcroft, S. *Macromolecules* **2004**, *37*, 2084.
5. Guiot, J.; Ameduri, B.; Boutevin, B. *Macromolecules* **2002**, *35*, 8694.
6. Yang, Z.; Rajendran, R. G. *Angew. Chem., Int. Ed.* **2005**, *44*, 564.

Downloaded by STANFORD UNIV GREEN LIBR on August 28, 2012 | http://pubs.acs.org
Publication Date (Web): August 16, 2012 | doi: 10.1021/bk-2012-1106.ch004

7. Chambers, R. D.; Fuss, R. W.; Spink, R. C. H.; Greenhall, M. P.; Kenwright, A. M.; Batsanov, A. S.; Howard, J. A. K. *J. Chem. Soc., Perkin Trans.* **2000**, *1*, 1623.
8. Souzy, R.; Ameduri, B.; Boutevin, B. *Macromol. Chem. Phys.* **2004**, *205*, 476.
9. Apostolo, M.; Arcella, V.; Storti, G.; Morbidelli, M. *Macromolecules* **1999**, *32*, 989.
10. Guiot, J.; Neouze, M. A.; Sauguet, L.; Ameduri, B.; Boutevin, B. *J. Polym. Sci., Part A: Polym. Chem.* **2005**, *43*, 917.
11. Kostov, G.; Petrov, P. *J. Polym. Sci., Part A: Polym. Chem.* **1992**, *30*, 1083.
12. Di Lena, F.; Matyjaszewski, K. *Prog. Polym. Sci.* **2010**, *35*, 959–1021.
13. *Handbook of Radical Polymerization*; Matyjaszewski, K., Davis, T. P., Eds.; Wiley-Interscience: New York, 2002; pp 361−462.
14. Ameduri, B. *Chem. Rev.* **2009**, *109*, 6632–6686.
15. Hansen, N.; Jankova, K.; Hvilsted, S. *Eur. Polym. J.* **2007**, *43*, 255.
16. Zhang, Z. C.; Chung, T. C. *Macromolecules* **2006**, *39*, 5187–5189.
17. Balague, J.; Ameduri, B.; Boutevin, B.; Caporiccio, G. *J. Fluorine Chem.* **1995**, *70*, 215–223.
18. Nguyen, B. V.; Yang, Z. Y.; Burton, D. J. *J. Org. Chem.* **1998**, *63*, 2887.
19. Li, A. R.; Chen, Q. Y. *J. Fluorine Chem.* **1997**, *81* (2), 99–101.
20. Chen, M. Y.; Yang, Z. Y.; Zhao, C. X.; Qiu, Z. M. *J. Chem. Soc., Perkin Trans. 1* **1988**, *3*, 563–567.
21. Metzerg, J. O.; Linker, U. *Liebigs Ann. Chem.* **1992**, *3*, 209–16.
22. Ishihara, T.; Kuroboshi, M. *Synth. Commun.* **1989**, *19* (9&10), 1611–1617.
23. Hu, C.; Qiu, Y. L. *J. Chem. Soc., Perkin Trans. 1* **1992**, *13*, 1569.
24. Xiao, F.; Wu, F.; Yang, X.; Shen, Y.; Shi, X. *J. Fluorine Chem.* **2005**, *126*, 319.
25. Kitazume, T.; Ishikawa, N. *J. Am. Chem. Soc.* **1985**, *107*, 5186.
26. Spencer, R. P.; Schwartz, J. *Tetrahedron* **2000**, *56*, 2103–2112.
27. Green, M. H.; Lucas, C. R. *J. Chem. Soc., Dalton Trans.* **1972**, *8*, 1000.
28. Barden, M. C.; Schwartz, J. *J. Am. Chem. Soc.* **1996**, *118*, 5484.
29. Rajanbabu, T. V.; Nugent, W. *J. Am. Chem. Soc.* **1994**, *116*, 986.
30. Asandei, A. D.; Moran, I. W.; Chen, Y.; Saha, G. *J. Organomet. Chem.* **2007**, *692*, 3174–3182.
31. Asandei, A. D.; Moran, I. W.; Saha, G.; Chen, Y. Ti-Catalyzed Living Radical Polymerization of Styrene Initiated by Epoxide Radical Ring Opening. In *Controlled/Living Radical Polymerization: From Synthesis to Materials*; Matyjaszewski, K., Ed.; ACS Symposium Series 944; American Chemical Society: Washington, DC, 2006; pp 125−139.
32. Asandei, A. D.; Moran, I. W.; Saha, G.; Chen, Y. *J. Polym. Sci., Part A: Polym. Chem.* **2006**, *44*, 2156.
33. Asandei, A. D.; Moran, I. W.; Saha, G.; Chen, Y. *J. Polym. Sci., Part A: Polym. Chem.* **2006**, *44*, 2015.
34. Asandei, A. D.; Moran, I. W. *J. Polym. Sci., Part A: Polym. Chem.* **2006**, *44*, 1060.
35. Asandei, A. D.; Moran, I. W. *J. Polym. Sci., Part A: Polym. Chem.* **2005**, *43*, 6039.

36. Asandei, A. D.; Moran, I. W. *J. Polym. Sci., Part A: Polym. Chem.* **2005**, *43*, 6028.
37. Asandei, A. D.; Moran, I. W. *J. Am. Chem. Soc.* **2004**, *126*, 15932.
38. Asandei, A. D.; Moran, I. W.; Castro, M. A. *Polym. Prepr.* **2003**, *44* (1), 829.
39. Asandei, A. D.; Chen, Y.; Saha, G.; Moran, I. W. *Tetrahedron* **2008**, *64*, 11831.
40. Asandei, A. D; Chen, Y. *Macromolecules* **2006**, *39*, 7549.
41. Asandei, A. D.; Saha, G. *Polym. Prepr.* **2007**, *48*, 272.
42. Asandei, A. D.; Chen, Y. *Polym. Mater.: Sci. Eng.* **2007**, *97*, 450.
43. Asandei, A. D.; Saha, G. *J. Polym. Sci., Part A: Polym. Chem.* **2006**, *44*, 1106.
44. Asandei, A. D.; Simpson, C. P.; Yu, H. S.; Adebolu, O. I.; Saha, G.; Chen, Y. Cp_2TiCl-Mediated Controlled Radical Polymerization of Isoprene Initiated by Epoxide Radical Ring Opening. In *Controlled/Living Radical Polymerization: Progress in RAFT, DT, NMP & OMRP*; Matyjaszewski, K., Ed.; ACS Symposium Series 1024; American Chemical Society: Washington, DC, 2009; pp 149−166.
45. Asandei, A. D.; Saha, G. *Polym. Prepr.* **2005**, *46* (2), 474.
46. Asandei, A. D.; Simpson, C. *Polym. Prepr.* **2008**, *49* (1), 452.
47. Asandei, A. D.; Simpson, C. P.; Yu, H. S. *Polym. Prepr.* **2008**, *49* (2), 73.
48. Asandei, A. D.; Adebolu, O.; Yu, H. S; Simpson, C. P.; Gilbert, M. *Polym. Prepr.* **2009**, *50* (1), 177.
49. Asandei, A. D.; Simpson, C. P. *Polym. Prepr.* **2008**, *49* (2), 75.
50. Asandei, A. D.; Yu, H. S; Adebolu, O.; Simpson, C. P.; Duong, O. *Polym. Mater.: Sci. Eng.* **2009**, *100*, 366.
51. Asandei, A. D.; Yu, H. S *Polym. Prepr.* **2009**, *50* (2), 601.
52. Asandei, A. D.; Yu, H. S; Adebolu, A. *Polym. Mater.: Sci. Eng.* **2009**, *101*, 1377.
53. Asandei, A. D.; Yu, H. S; Simpson, C. P. *Polym. Mater.: Sci. Eng.* **2009**, *101*, 1379.
54. Asandei, A. D.; Yu, H. S.; Simpson, C. P. *Polym. Prepr.* **2010**, *51* (1), 545.
55. Asandei, A. D.; Yu, H. S.; Simpson, C. P. *Polym. Mater.: Sci. Eng.* **2010**, *103*, 511.
56. Asandei, A. D.; Yu, H. S.; Simpson, C. P. *Polym. Prepr.* **2010**, *51* (2), 584.
57. Asandei, A. D.; Yu, H. S.; Simpson, C. P. *Polym. Prepr.* **2010**, *51* (2), 586.
58. Asandei, A. D.; Simpson, C. P.; Olumide, A.; Yu, H. S. *Polym. Mater.: Sci. Eng.* **2010**, *102*, 425.
59. Asandei, A. D.; Yu, H. S.; Simpson, C. P. *Polym. Mater.: Sci. Eng.* **2010**, *102*, 68.
60. Asandei, A. D.; Yu, H. S. *Polym. Prepr.* **2011**, *52* (1), 415.
61. Asandei, A. D.; Yu, H. S. *Polym. Prepr.* **2011**, *52* (1), 413.
62. Asandei, A. D.; Yu, H. S. *Polym. Mater.: Sci. Eng.* **2011**, *104*, 619.
63. Asandei, A. D.; Yu, H. S. *Polym. Mater.: Sci. Eng.* **2011**, *104*, 627.
64. Asandei, A. D.; Simpson, C. P.; Olumide, A.; Yu, H. S. *Polym. Prepr.* **2010**, *51* (1), 553.
65. Asandei, A. D.; Simpson, C. P.; Olumide, A.; Yu, H. S. *Polym. Prepr.* **2010**, *51* (1), 498.

Downloaded by STANFORD UNIV GREEN LIBR on August 28, 2012 | http://pubs.acs.org
Publication Date (Web): August 16, 2012 | doi: 10.1021/bk-2012-1106.ch004

66. Asandei, A. D.; Saha, G. *Macromolecules* **2006**, *39*, 8999.
67. Asandei, A. D.; Saha, G. *Macromol. Rapid Commun.* **2005**, *26*, 626.
68. Asandei, A. D.; Chen, Y.; Adebolu, O. I.; Simpson, C. P. *J. Polym. Sci., Part A: Polym. Chem.* **2008**, *46*, 2869.
69. Asandei, A. D.; Chen, Y.; Adebolu, O. I.; Simpson, C. P. *Polym. Prepr.* **2008**, *49* (2), 740.
70. Asandei, A. D.; Adebolu, O. I.; Simpson, C. P. *J. Am. Chem. Soc.* **2012**, *134*, 6080−6083.
71. Haszeldine, R. N.; Steele, B. R. *J. Chem. Soc.* **1954**, 923.
72. Saint-Loup, R.; Ameduri, B. *J. Fluorine Chem.* **2002**, *116*, 27.
73. Asandei, A. D.; Chen, Y. *Polym. Mater.: Sci. Eng.* **2008**, *98*, 346.
74. Asandei, A. D.; Chen, Y. *Polym. Prepr.* **2007**, *48* (2), 452–453.
75. Asandei, A. D.; Chen, Y. *Polym. Mater.: Sci. Eng.* **2007**, *97*, 270–271.
76. Asandei, A. D.; Chen, Y. *Polym. Prepr.* **2005**, *46* (2), 633.
77. Asandei, A. D.; Weiss, R. A.; Moran, I. W.; Chen, Y.; Saha, G. *Polym. Prepr.* **2004**, *45* (1), 1010.
78. Asandei, A. D.; Yu, S. H.; Adebolu, O.; Simpson, C. P. *Polym. Prepr.* **2011**, *52* (2), 470–471.
79. Asandei, A. D.; Simpson, C. P.; Adebolu, O.; Chen, Y. *Polym. Prepr.* **2011**, *52* (2), 759–560.
80. Asandei, A. D.; Simpson, C. P.; Adebolu, O.; Chen, Y. *Polym. Prepr.* **2011**, *52* (2), 728–729.
81. Asandei, A. D.; Simpson, C. P.; Adebolu, O.; Chen, Y. *Polym. Prepr.* **2011**, *52* (2), 732–733.
82. Galin, M.; Maslinkot, L. *Macromolecules* **1985**, *18*, 2192–2196.
83. Galin, J. C.; Lutringer, G.; Galin, M. *J. Appl. Polym. Sci.* **1989**, *37*, 487–498.
84. Kutringer, G.; Weill, G. *Polymer* **1991**, *32*, 877–883.
85. Lutringer, G.; Meurer, B.; Weill, G. *Polymer* **1991**, *32*, 884–891.
86. Bottino, A.; Campanelli, G.; Munari, S.; Turturro, A. *J. Polym. Sci., Part B: Polym. Phys.* **1988**, *26*, 785–794.
87. W. H. Lee In *Chemistry of Nonaqueous Solvents*; Lagowski, J. Ed.; Academic Press: New York, 1976; Vol. 4, p 167.
88. Ameduri, B.; Boutevin, B. *Top. Curr. Chem.* **1997**, *192*, 165–233.
89. Wormald, P.; Ameduri, B.; Harris, R. K.; Hazendonk, P. *Polymer* **2008**, *49*, 3629–3638.
90. Doll, W. W.; Lando, J. B. *J. Appl. Polym. Sci.* **1970**, *14*, 1767–73.
91. Russo, S.; Behari, K.; Chengji, S.; Pianca, M.; Barchiesi, E.; Moggi, G. *Polymer* **1993**, *22*, 4777–4781.
92. Duc, M.; Ameduri, B.; Boutevin, B.; Kharroubi, M.; Sage, J. M. *Macromol. Chem. Phys.* **1998**, *199*, 1271–1289.
93. Benefice, S.; Blancou, H.; Commeyras, A. *Tetrahedron* **1984**, *40*, 1541.
94. Yang, Z. Y.; Burton, D. J. *J. Org. Chem.* **1991**, *56*, 1037–1041.
95. Spencer, R. P.; Schwartz, J. *Tetrahedron* **2000**, *56*, 2103.
96. Jungst, R.; Sekutowski, D.; Davis, J.; Luly, M.; Stucky, G. *J. Inorg. Chem.* **1977**, *16*, 1645.
97. Enemaerke, R. J.; Larsen, J.; Skrydstrup, T.; Daasbjerg, K. *J. Am. Chem. Soc.* **2004**, *126*, 7853.

Downloaded by STANFORD UNIV GREEN LIBR on August 28, 2012 | http://pubs.acs.org
Publication Date (Web): August 16, 2012 | doi: 10.1021/bk-2012-1106.ch004

98. Enemaerke, R. J.; Larsen, J.; Skrydstrup, T.; Daasbjerg, K. *Organometallics* **2004**, *23*, 1866.

99. Enemaerke, R.; Larsen, J.; Hjollund, G. H.; Skrydstrup, T.; Daasbjerg, K. *Organometallics* **2005**, *24*, 1252–1262.

100. Yoo, B. W.; Choi, K. H.; Lee, S. J.; Yoon, C. M.; Kim, S. H.; Kim, J. H. *Synth. Commun.* **2002**, *32*, 63.

101. Fernandez-Mateos, A.; Madrazo, S. E.; Teijon, P. H.; Gonzalez, R. R. *J. Org. Chem.* **2009**, *74*, 3913–3918.

102. Paradas, M.; Campana, A. G.; Marcos, M. L.; Justicia, J.; Haidour, A.; Robles, R.; Cardenas, D. J.; Oltra, J. E.; Cuerva, J. M. *Dalton Trans.* **2010**, *39*, 8796–8800.

Downloaded by STANFORD UNIV GREEN LIBR on August 28, 2012 | http://pubs.acs.org
Publication Date (Web): August 16, 2012 | doi: 10.1021/bk-2012-1106.ch004

Downloaded by PENNSYLVANIA STATE UNIV on August 28, 2012 | http://pubs.acs.org
Publication Date (Web): August 16, 2012 | doi: 10.1021/bk-2012-1106.ch005

Chapter 5

Well-Defined Fluorine-Containing Star Polymers of Vinyl Ethers: Precision Synthesis by Base-Assisting Living Cationic Polymerization and Thermoresponsive Solubility Transitions

Shokyoku Kanaoka, Hiroaki Shimomoto, Dai Fukami,
and Sadahito Aoshima[*]

Department of Macromolecular Science, Graduate School of Science,
Osaka University, Toyonaka 560-0043, Japan
[*]E-mail: aoshima@chem.sci.osaka-u.ac.jp

A variety of fluorine-containing polymers of vinyl ethers with well-defined structures were synthesized by base-assisting living cationic polymerization. Well-controlled reactions were achieved in various fluorinated solvents, which had not been examined as solvents for cationic polymerization. Excellent living nature of the reactions allowed precision synthesis of block and star-shaped polymers with controlled sequences. The resulting fluorinated polymers with appropriate fluorine content underwent highly sensitive upper critical solution temperature (UCST)-type phase separation in organic solvents with a range of polarities including perfluoro versions. The unique solubility permitted thermoresponsive physical gelation with solutions of star block or heteroarm star polymers.

Introduction

Fluorinated polymers have unique properties such as low surface energy, large hydrophobicity and lipophobicity, high thermostability and chemical inertness (*1–3*), hence a variety of fluorine-containing polymers have been extensively investigated from academic and industrial viewpoints. The development of more advanced well-defined fluoropolymers such as block copolymers (*4–8*) have

In Advances in Fluorine-Containing Polymers; Smith, D., et al.;
ACS Symposium Series; American Chemical Society: Washington, DC, 2012.

Downloaded by PENNSYLVANIA STATE UNIV on August 28, 2012 | http://pubs.acs.org
Publication Date (Web): August 16, 2012 | doi: 10.1021/bk-2012-1106.ch005

been recently achieved due to the significant progress of the living/controlled polymerization methods in the past few decades. However, the synthetic routes for well-defined fluorinated polymers are limited because of their low solubility toward conventional common solvents for polymerization reactions. As a result, few systematic studies have been reported on the synthesis and characterization of well-defined fluorinated polymers for their unique characteristics.

We have synthesized various thermoresponsive polymers mostly from vinyl ethers by living cationic polymerization using a metal halide in the presence of an added base (*9*). Despite the great progress, there are few polymers undergoing upper critical solution temperature (UCST)-type phase separation in solvents with a wide range of polarities (*10*). The unique incompatibility of fluoroalkyl groups (*11*, *12*) with common organic counterparts would be a great advantage for realizing temperature responsive phase separation, especially UCST-type transition, in organic solvents. Since vinyl ether polymers with oxyethylene side chains usually exhibit good solubility to various organic solvents, sensitive thermoresponsive phase separation in various organic solvents was expected with a polymer consisting of such a vinyl ether skeleton and fluorinated pendant groups due to their lipophilic/lipophobic balance. However, no such polymers have been reported, although there were several examples of fluorinated vinyl ether polymers with well controlled structures (*4*, *5*, *13–15*). These backgrounds motivated us to synthesize various well-defined linear and branched fluorinated polymers.

This article describes a new series of fluorine-containing polymers with well-defined architectures by base-assisting living cationic polymerization (*9*). First, we investigated the feasibility of living cationic polymerization of fluorinated vinyl ethers (Chart 1) in several fluorinated solvents as new media. Then, we focused on the solubility characteristics and phase separation behavior of the resulting fluorinated polymers. Furthermore, various types of fluorine-containing star-shaped polymers were synthesized. Star-shaped polymers are branched macromolecules containing multiple arms radially connected to a central core. The synthesis of well-defined star polymers has been achieved by living polymerization techniques (*16–18*). However, only a few studies have been published on fluorinated star polymers.

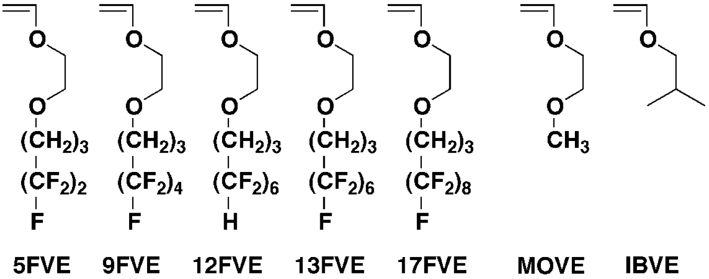

Chart 1. Structures of the vinyl ether monomers examined in this study.

Downloaded by PENNSYLVANIA STATE UNIV on August 28, 2012 | http://pubs.acs.org
Publication Date (Web): August 16, 2012 | doi: 10.1021/bk-2012-1106.ch005

Results and Discussion

Living Cationic Polymerization in Fluorinated Solvents

Fluorinated polymers with high content of fluorine atoms are known to be insoluble in non-fluorinated common organic solvents. To obtain well-defined polymers, it is preferable to keep the growing polymer chains in solution without phase separation. Thus, cationic polymerization of fluorinated monomers were examined in various fluorinated solvents. Table I lists the fluorinated solvents employed: HCFC, HFC, HFE, and TFT are all commercially available reagents.

Table I. Physical properties of fluorine-containing solvents

	HCFC	*HFC*	*HFE*	*TFT*
formula	$CF_3CF_2CHCl_2$/ CF_2ClCF_2CFHCl (45/55, w/w)	$F(CF_2)_6(CH_2)_2H$	$C_4F_9OCH_3$	$CF_3C_6H_5$
boiling point (ºC)	54	114	61	102
melting point (ºC)	-131	-76	-135	-29
density (g/ml)	1.55	1.55	1.52	1.19
fluorine content (%)[a]	46.8	70.9	68.4	39.0
dielectric constant	4.1	5.1	7.5	9.2

[a] Percentage by molecular weight.

Cationic polymerization of IBVE as a model system was first examined in various fluorinated solvents. Polymerization was conducted using a $CH_3CH(O\mathit{i}Bu)OCOCH_3$(IBEA)/$Et_{1.5}AlCl_{1.5}$ initiating system in various fluorinated solvents in the absence or presence of 1,4-dioxane as an added base at 0 ºC (Figure 1) (*19*). The reaction in HCFC in the absence of an added base reached quantitative conversion in a few seconds, yielding a polymer with a broad molecular weight distribution (MWD). In contrast, the reaction with 1,4-dioxane as an added base became slower, and took 10 min to reach about 90%. Similarly, ill-defined polymerization in HFC and HFE without a base turned well controlled reaction in the presence of 1,4-dioxane, although the reaction mixtures turned opaque shortly after initiation in contrast to those in HCFC. TFT has been used as a (co)solvent for radical polymerization of fluorinated methacrylates and styrenes (*7*). However, it may not be suitable for cationic polymerization, because it is known that TFT reacts with $AlCl_3$ at ambient temperature (*20*). In fact, a colorless transparent solution turned green shortly after the addition of the catalyst in the polymerization in TFT without any base. In sharp contrast, the presence of 1,4-dioxane permitted homogeneous polymerization in a living fashion even in TFT. The molecular weights determined by size exclusion chromatography (SEC) were in good agreement with the calculated ones, and the MWDs were invariably

In Advances in Fluorine-Containing Polymers; Smith, D., et al.;
ACS Symposium Series; American Chemical Society: Washington, DC, 2012.

very narrow. An additional feature that should be noted is the nonnecessity of the distillation of HCFC and HFE for living polymerization due to the low solubility of water (< 100 ppm, wt).

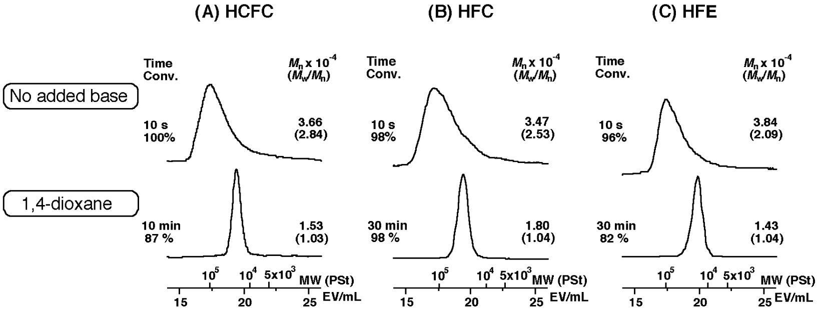

Figure 1. SEC curves of poly(IBVE)s obtained in (A) HCFC, (B) HFC, and (C) HFE in the absence or presence of 1,4-dioxane ($[IBVE]_0$ = 0.76 M, $[IBEA]_0$ = 4.0 mM, $[Et_{1.5}AlCl_{1.5}]_0$ = 20 mM, [1,4-dioxane] = 0 or 1.2 M, at 0 °C).

The living nature of the IBVE polymerization in HCFC was confirmed by monomer addition experiments (Figure 2). The livingness was examined by adding a fresh feed of IBVE to the polymerization solution when the first dose was almost consumed. The M_n of the product polymers increased proportionally to the IBVE conversion even in the second stage, and the MWD of the polymer, remaining narrow throughout the reaction, shifted toward higher molecular weight.

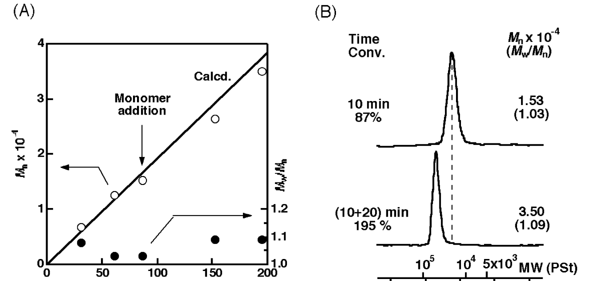

Figure 2. (A) M_n and M_w/M_n, and (B) SEC curves of poly(IBVE)s ($[IBVE]_0$ = $[IBVE]_{add}$ = 0.76 M, $[IBEA]_0$ = 4.0 mM, $[Et_{1.5}AlCl_{1.5}]_0$ = 20 mM, [1,4-dioxane] = 1.2 M, in HCFC at 0 °C).

Next, the polymerization of fluorinated vinyl ether monomers was conducted in fluorinated solvents. Figure 3 shows time-conversion curves for the polymerization of a series of fluorine-containing vinyl ether monomers in HCFC in the presence of 1,4-dioxane at 0 °C. With all the monomers, no induction period was observed in the initial stage, and the polymerization proceeded smoothly in a homogeneous system throughout the reaction. The polymerization rate slightly

Downloaded by PENNSYLVANIA STATE UNIV on August 28, 2012 | http://pubs.acs.org
Publication Date (Web): August 16, 2012 | doi: 10.1021/bk-2012-1106.ch005

Downloaded by PENNSYLVANIA STATE UNIV on August 28, 2012 | http://pubs.acs.org
Publication Date (Web): August 16, 2012 | doi: 10.1021/bk-2012-1106.ch005

decreased in the order: 5FVE > 9FVE ~ 13FVE > 12FVE. The differences in the polymerization rate would stem from the bulkiness of side chains as well as electron density on a β-vinyl carbon [^{13}C NMR in $CDCl_3$, δ (ppm): 5FVE (86.7), 9FVE (86.7), 13FVE (86.8), 12FVE (87.1)].

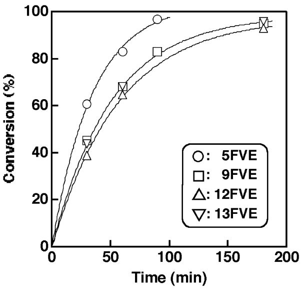

Figure 3. Time-conversion curves for the polymerization of fluorinated vinyl ethers ($[monomer]_0 = 0.80$ M, $[IBEA]_0 = 4$ mM, $[Et_{1.5}AlCl_{1.5}]_0 = 20$ mM, [1,4-dioxane] = 1.2 M, in HCFC at 0 °C).

The limited solubility of fluorinated polymers toward common organic solvents makes one utilize fluorinated solvents for polymer characterization. In this study, the MWD of the obtained polymers was measured by SEC with fluorine-containing solvents [HCFC/1,1,1,3,3,3-hexafluoro-2-propanol (HFIP)] as eluents (*21*), since the product polymers are insoluble in chloroform and tetrahydrofuran (THF), which are common eluents for MWD measurement. The MWD analysis with HCFC/HFIP provided legitimate molecular weight data. Figure 4 shows the M_n, M_w/M_n, and SEC curves of the resulting polymers in the polymerization of 13FVE. The M_n of the polymers increased in direct proportion to monomer conversion and the product polymers had narrow MWDs. Furthermore, well-controlled diblock and triblock copolymers with various combinations of fluorinated and non-fluorinated segments as well as other homopolymers were synthesized (Table II) (*22*).

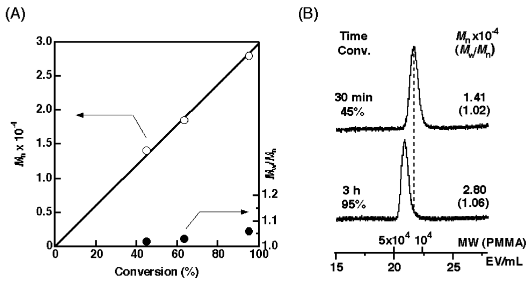

Figure 4. (A) M_n and M_w/M_n for the polymerization of 13FVE and (B) SEC curves of poly(13FVE)s ($[13FVE]_0 = 0.80$ M, $[IBEA]_0 = 4.0$ mM, $[Et_{1.5}AlCl_{1.5}]_0 = 20$ mM, [1,4-dioxane] = 1.2 M, in HCFC at 0 ºC).

Downloaded by PENNSYLVANIA STATE UNIV on August 28, 2012 | http://pubs.acs.org
Publication Date (Web): August 16, 2012 | doi: 10.1021/bk-2012-1106.ch005

Table II. Synthesis of fluorinated homopolymers and block copolymers by living cationic polymerization

type	*polymer*[a]	$M_n \times 10^{-4b}$	$M_w/M_n{}^b$
homopolymer	$5FVE_{170}$	1.93	1.07
	$9FVE_{150}$	2.04	1.08
	$12FVE_{190}$	2.29	1.14
	$13FVE_{190}$	2.80	1.06
	$17FVE_{100}$	1.63	1.05
AB diblock	$IBVE_{190}$-*b*-$9FVE_{190}$	3.40	1.15
	$13FVE_{130}$-*b*-$9FVE_{110}$	2.86	1.15
ABA triblock	$9FVE_{80}$-*b*-$IBVE_{190}$-*b*-$9FVE_{80}$	3.07	1.24
	$9FVE_{90}$-*b*-$13FVE_{200}$-*b*-$9FVE_{90}$	4.65	1.23
ABC triblock	$9FVE_{110}$-*b*-$IBVE_{200}$-*b*-$12FVE_{70}$	3.85	1.09
	$9FVE_{110}$-*b*-$13FVE_{150}$-*b*-$12FVE_{80}$	3.55	1.15

[a] The degree of polymerization was determined by ^{1}H NMR and gravimetry. [b] by SEC (HCFC/HFIP as eluents, poly(methyl methacrylate) standards).

Various Types of Fluorine-Containing Star-Shaped Polymers

Fluorine-containing star-shaped poly(vinyl ether)s with various sequences were synthesized via arm-linking reactions in living cationic polymerization (Scheme 1) (*23*). Simple reaction of living polymers with a bifunctional vinyl ether produced well-defined star block, heteroarm (or miktarm), and end-functionalized star polymers in extremely high yield, as well as homopolymer arm versions. First, the synthesis of fluorine-containing star-shaped polymers was examined under several reaction conditions, especially with various concentrations of living polymers ([P*]) and the molar feed ratio of DVE to living polymers (r = $[DVE]_{add}/[P^*]$) in a fluorinated solvent. Effective formation of star polymers was achieved under the optimum conditions. Figure 5 shows the SEC curve of the star polymer obtained from 9FVE ([P*] = 7.4 mM, r = 10). The polymerization of 9FVE in HCFC reached about 90% conversion in 2 h, producing a linear living polymer with low polydispersity (Figure 5, upper row). To this reaction mixture, was added a HCFC solution of DVE for the linking reaction. In 80 min, a star polymer of 9FVE with a narrow MWD (M_w/M_n = 1.28; Figure 5, bottom row) was obtained in almost quantitative yield (~98%). The average arm numbers per polymer (N_{arm}) calculated from the absolute weight-average molecular weight ($M_{w,LS}$) was 18.5.

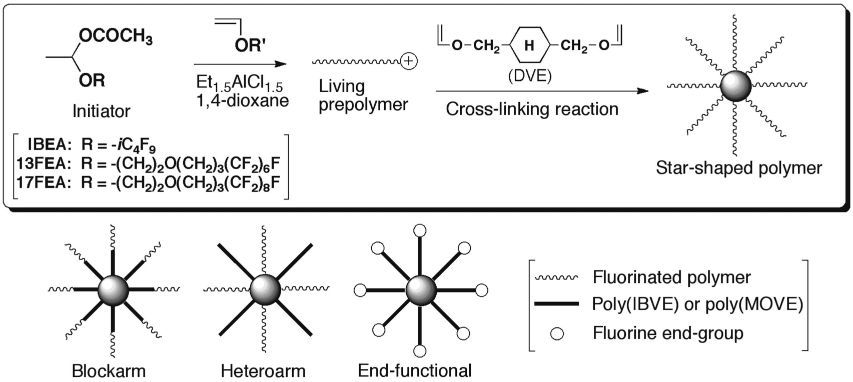
OCOCH3
OR
Initiator
OR'
Et1.5AlCl1.5
1,4-dioxane
Living prepolymer
(DVE)
Cross-linking reaction
Star-shaped polymer
IBEA: R = -iC4F9
13FEA: R = -(CH2)2O(CH2)3(CF2)6F
17FEA: R = -(CH2)2O(CH2)3(CF2)8F
Blockarm
Heteroarm
End-functional
Fluorinated polymer
Poly(IBVE) or poly(MOVE)
Fluorine end-group

Scheme 1. Synthesis of various types of fluorine-containing star-shaped polymers.

A similar strategy was applied to the synthesis of star block copolymers. For example, star polymers with 9FVE-IBVE block copolymer arms were synthesized by a linking reaction of a living diblock copolymer, obtained from the sequential living cationic polymerization of 9FVE and IBVE, with DVE (Figure 6A). The polymerization of 9FVE using $Et_{1.5}AlCl_{1.5}$ with 1,4-dioxane in HCFC at 0 °C reached 90% conversion in 2 h, yielding living poly(9FVE) with a narrow MWD. A living 9FVE-IBVE block copolymer was obtained from the polymerization of a fresh feed of IBVE, two equimolar to that of 9FVE, added to the solution at the end of the reaction of 9FVE. Finally, the living diblock copolymer was treated with a HCFC solution of DVE to give the star polymer [formulated as poly(9FVE-*b*-IBVE)-star] with a narrow MWD in almost quantitative yield.

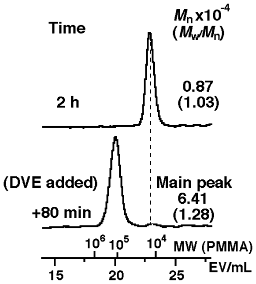

Figure 5. SEC curves of star-shaped poly(9FVE) and the corresponding prepolymer ($[9FVE]_0 = 0.40$ M, $[IBEA]_0 = 8.0$ mM, $[Et_{1.5}AlCl_{1.5}]_0 = 20$ mM, [1,4-dioxane] = 1.2 M, in HCFC at 0 ºC; for the linking reaction: [P] = 7.4 mM, r = 10).*

Downloaded by PENNSYLVANIA STATE UNIV on August 28, 2012 | http://pubs.acs.org
Publication Date (Web): August 16, 2012 | doi: 10.1021/bk-2012-1106.ch005

Downloaded by PENNSYLVANIA STATE UNIV on August 28, 2012 | http://pubs.acs.org
Publication Date (Web): August 16, 2012 | doi: 10.1021/bk-2012-1106.ch005

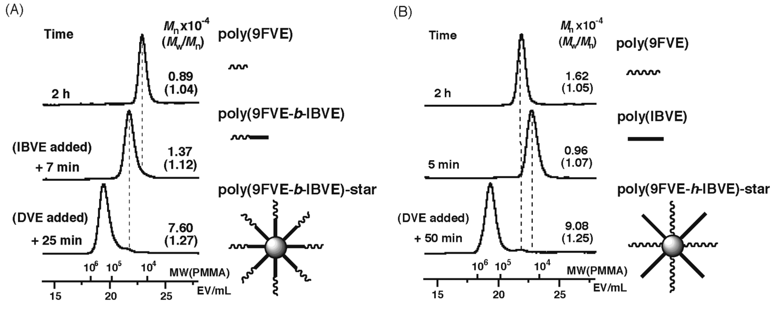

Figure 6. SEC curves for the synthesis of (A) poly(9FVE-b-IBVE)-star and (B) poly(9FVE-h-IBVE)-star {poly(9FVE-b-IBVE)-star: $[9FVE]_0$ = 0.20 M, $[IBEA]_0$ = 4.0 mM, $[Et_{1.5}AlCl_{1.5}]_0$ = 20 mM, [1,4-dioxane] = 1.2 M, $[9FVE]_0/[IBVE]_{add}$ = 1/2 (molar ratio), in HCFC at 0 ºC, [P] = 3.7 mM, r = 10, poly(9FVE-h-IBVE)-star: $[9FVE]_0$ = $[IBVE]_0$ = 0.80 M, $[IBEA]_0$ = 8.0 mM, $[Et_{1.5}AlCl_{1.5}]_0$ = 20 mM, [1,4-dioxane] = 1.2 M, in HCFC at 0 ºC, [poly(9FVE)]/[poly(IBVE)] = 1/1 (molar ratio), [P*] = 7.4 mM, r = 10}.*

Heteroarm star polymers containing two arm species including fluorinated segments were synthesized by polymer-linking reaction of a mixture of different living polymer species with DVE. First, living polymers of 9FVE and IBVE were prepared in different glass tubes in HCFC. Then, the obtained living polymers were mixed in another glass tube, and this mixture of the unquenched living polymers was treated with DVE (*r* = 10). Figure 6B shows the SEC curves of a heteroarm star-shaped polymer containing 9FVE and IBVE arms [formulated as poly(9FVE-*h*-IBVE)-star] and the corresponding linear prepolymers. The SEC curve of the product, obtained in 50 min after the addition of DVE, appeared in the much higher molecular weight region, compared to the two prepolymers, and almost no prepolymer was observed, supporting successful star polymer formation from two different living polymers. The obtained heteroarm star polymer, ($9FVE_{100}$-*h*-$IBVE_{100}$)-star, was soluble in THF and chloroform, but insoluble in acetone and toluene. The solvents mentioned above dissolve poly(IBVE)-star readily without any precipitation (*24*), whereas those are nonsolvent for poly(9FVE)-star. The mixed solubility characteristics of ($9FVE_{100}$-*h*-$IBVE_{100}$)-star reflect independent mobility both of poly(IBVE) and poly(9FVE) arm chains, indicative of the heteroarm structure of ($9FVE_{100}$-*h*-$IBVE_{100}$)-star.

Downloaded by PENNSYLVANIA STATE UNIV on August 28, 2012 | http://pubs.acs.org
Publication Date (Web): August 16, 2012 | doi: 10.1021/bk-2012-1106.ch005

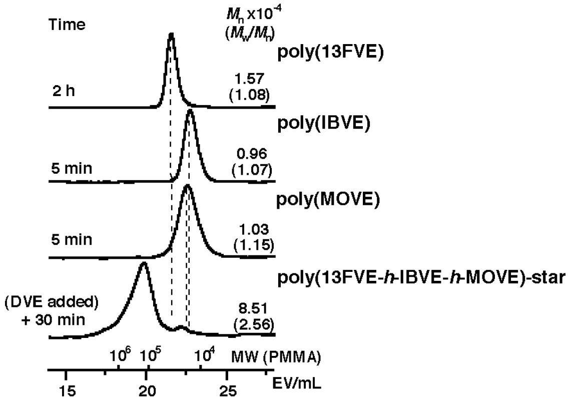

Figure 7. SEC curves for the synthesis of poly(13FVE-h-IBVE-h-MOVE)-star ($[13FVE]_0$ = $[IBVE]_0$ = $[MOVE]_0$ = 0.80 M, $[IBEA]_0$ = 8.0 mM, $[Et_{1.5}AlCl_{1.5}]_0$ = 20 mM, [1,4-dioxane] = 1.2 M, in HCFC at 0 ºC, [poly(13FVE)]/ [poly(IBVE)]/[poly(MOVE)] = 1/1/1 (molar ratio), [P] = 7.4 mM, r = 10).*

Heteroarm star polymers with more arm sets can be prepared in a similar way. Figure 7 shows the SEC curves of a heteroarm star polymer containing three kinds of arms, poly(13FVE), poly(IBVE), and poly(MOVE). Living polymerization of 13FVE, IBVE, and MOVE were carried out in different glass tubes, yielding each living polymer. These polymers, mixed together in equimolar amounts, were crosslinked using DVE. The mixture was homogeneous during the reaction for 30 min, which produced a star polymer containing fluorophilic (hydrophobic and lipophobic) poly(13FVE), lipophilic (hydrophobic) poly(IBVE), and thermosensitive (water-soluble at ambient temperature) poly(MOVE). This method is facile but highly effective for synthesizing various types of star polymers with multiple arm numbers and variable arm compositions.

End-functionalized star polymers were also prepared using a fluorinated initiator for living polymerization of vinyl ethers. The α-end modification of a prepolymer for arm chain leads to a surface-modified star polymer, which has fluorine groups at the free chain ends of the polymer arms. Thus, MOVE (see Chart 1 for its structure) was polymerized with the adduct of 13FVE with acetic acid (13FEA) as a fluorinated initiator in conjunction with $Et_{1.5}AlCl_{1.5}$ and 1,4-dioxane in toluene at 0 ºC. This reaction produced living poly(MOVE) with C_6F_{13} groups at the α-end (Figure 8). Treatment of DVE with the resulting end-functionalized living polymer induced a linking reaction smoothly. The linear prepolymer was consumed almost quantitatively (> 99%) in 8 h, and a star polymer with a relatively narrow MWD was obtained ($M_{w,\,LS}$ = 90.9 × 10^4, N_{arm} = 40.7). A star-shaped polymer with a longer perfluoro end groups (C_8F_{17}) was also prepared in a similar manner ($M_{w,\,LS}$ = 70.5 × 10^4, N_{arm} = 30.8).

Downloaded by PENNSYLVANIA STATE UNIV on August 28, 2012 | http://pubs.acs.org
Publication Date (Web): August 16, 2012 | doi: 10.1021/bk-2012-1106.ch005

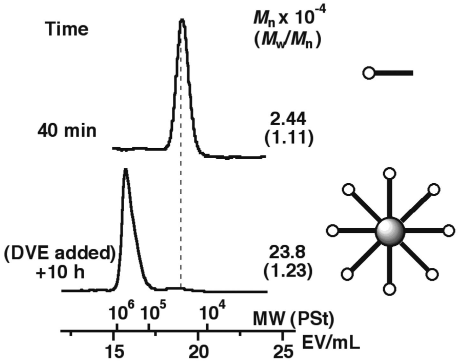

Figure 8. SEC curves of end-fluorinated linear and star-shaped poly(MOVE)s ([MOVE]$_0$ = 2.0 M, [13FEA]$_0$ = 10 mM, [Et$_{1.5}$AlCl$_{1.5}$]$_0$ = 20 mM, [1,4-dioxane] = 1.2 M, in toluene at 0 ºC; for the linking reaction: [P] = 9.1 mM, r = 10).*

Linear vs. Star Polymers

It was reported that poly(acrylate)s or poly(methacrylate)s with a C_8F_{17} group in the side chain have a high tendency to crystallize in a smectic phase (*25*, *26*). In this study, therefore, the crystalline properties were compared between the star-shaped poly(17FVE) and the linear counterpart corresponding to the arm chain based on differential scanning calorimetry (DSC) analysis. For linear polymers, the melting temperature (T_m) was almost constant irrespective of the molecular weight, while the melting enthalpy (ΔT) decreased gradually with increasing the molecular weight (Table III). On the other hand, the T_m (8.2 ºC) of the star polymer was lower than that of the corresponding linear polymer (16.7 ºC). In addition, the ΔT was clearly smaller than the linear counterparts. These observations suggest that association of the pendant fluorinated chains was drastically hampered due to the limitation of accessible conformations induced by the cross-linking core (*27*).

Table III. DSC experiments results for linear and star-shaped poly(17FVE)s

	T_m (ºC)	ΔH (J/g)
17FVE$_{50}$	16.7	14.0
17FVE$_{100}$	16.7	13.2
17FVE$_{200}$	16.7	11.1
17FVE$_{100}$-star	8.2	4.9

Downloaded by PENNSYLVANIA STATE UNIV on August 28, 2012 | http://pubs.acs.org
Publication Date (Web): August 16, 2012 | doi: 10.1021/bk-2012-1106.ch005

Solubility Characteristics of Fluorinated Polymers in Various Organic Solvents

Table IV summarizes the solubility characteristics of a series of fluorinated homopolymers with a degree of polymerization of 50 in various organic solvents including perfluoro solvents, monitored from 0 °C to the solvent boiling point. Neither the lower nor the higher fluorine content was suitable for achieving thermoresponsiveness. Poly(5FVE) was soluble in almost all common organic solvents, and poly(13FVE) was insoluble in non-fluorinated solvents but soluble in fluorine-containing solvents such as perfluorohexanes. In contrast, excellent thermosensitivity was observed with the moderately-fluorinated polymer [poly(9FVE)], which underwent UCST-type phase separation in multiple organic solvents with differing polarities (Table IV). The lipophobicity of relatively long perfluoroalkyl pendants is a key to realizing the UCST-type phase separation in wide-ranging solvents. Another interesting observation was the differences in solubility between poly(12FVE) and poly(13FVE), which have similar fluorine contents. This unexpected difference would arise from the significant dipole moment of the H-substituted side chain of 12FVE, as is the case with low molecular fluorinated surfactants (*28*).

Table IV. Solubility characteristics of fluorinated vinyl ether polymers in various organic solvents

type	*solvent*	$5FVE_{50}$	$9FVE_{50}$	$12FVE_{50}$	$13FVE_{50}$
non-fluorinated	toluene	S	T	T	I
	chloroform	S	T	T	I
	THF	S	T	S	I
	acetone	S	T	S	I
	methanol	I	I	S	I
hybrid	HCFC	S	S	S	S
perfluoro	perfluorohexanes	I	I	I	S
	perfluoro(methylcyclohexane)	I	T	I	S
	perfluorodecalin	I	T	I	S

S: soluble, I: insoluble, T: solubility transition of depending on the temperature (1 wt% solutions, from 0 ºC to solvent boiling point).

Figure 9 shows an example of the results of turbidity measurements for poly(9FVE) with a narrow MWD. A chloroform solution was transparent at high temperature, but became opaque rapidly at around 20 ºC. The phase separation was reversible; the once phase-separated mixture became transparent again with some hysteresis on increasing temperature. The cloud points of a series of poly(9FVE)s with a degree of polymerization of 50 to 200 and narrow MWDs were determined to investigate the effect of chain length on phase separation behavior. The cloud points of the solutions increased with the increasing degree of polymerization (Figure 10).

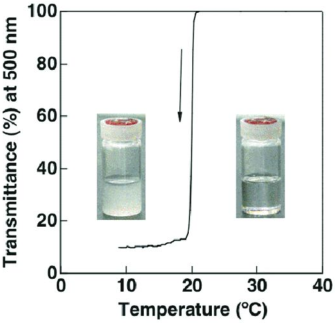

Figure 9. Temperature dependence of transmittance at 500 nm for 9FVE$_{50}$ (M_n = 9000, M_w/M_n = 1.04) in chloroform (1 wt% solution, cooling rate: 1 °C/min).

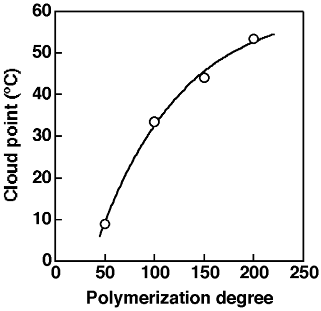

Figure 10. Dependence of the cloud points on the degree of polymerization for 1 wt% poly(9FVE) THF solutions (9FVE$_{50}$: M_n = 9000, M_w/M_n = 1.04, 9FVE$_{100}$: M_n = 15100, M_w/M_n = 1.06, 9FVE$_{150}$: M_n = 20400, M_w/M_n = 1.08, 9FVE$_{200}$: M_n = 26200, M_w/M_n = 1.14).

Table V. Solubility of star-shaped poly(9FVE-*b*-IBVE) and poly(9FVE-*h*-IBVE)

	toluene	*chloroform*	*THF*	*acetone*
(9FVE$_{50}$-*b*-IBVE$_{100}$)-star	T	S	S	T
(9FVE$_{100}$-*b*-IBVE$_{100}$)-star	T	T	S	T
(9FVE$_{100}$-*h*-IBVE$_{100}$)-star	I	S	S	I

S: soluble, I: insoluble, T: solubility transition of depending on the temperature (1 wt% solutions, from 0 ºC to solvent boiling point).

Downloaded by PENNSYLVANIA STATE UNIV on August 28, 2012 | http://pubs.acs.org
Publication Date (Web): August 16, 2012 | doi: 10.1021/bk-2012-1106.ch005

Downloaded by PENNSYLVANIA STATE UNIV on August 28, 2012 | http://pubs.acs.org
Publication Date (Web): August 16, 2012 | doi: 10.1021/bk-2012-1106.ch005

Temperature-Induced Solubility Transitions and Physical Gelation

The obtained star block and heteroarm star polymers showed solubility transitions in organic solvents characteristic to their sequence and branched structures (Table V). The clear solutions of ($9FVE_{50}$-*b*-$IBVE_{100}$)-star sharply became opaque at around 30 ºC for acetone and 55 ºC for toluene on decreasing temperature. On the other hand, no phase separation was observed in chloroform and THF, although linear poly(9FVE) underwent UCST-type phase separation in those solvents. The good solubility of the inner but long IBVE segments to chloroform and THF rendered the whole star molecule soluble. In fact, a longer 9FVE segment caused ($9FVE_{100}$-*b*-$IBVE_{100}$)-star to undergo solubility transition in chloroform (~25 ºC) as well as acetone (~40 ºC) and toluene (~80 ºC). No transition was still induced in THF from 0 ºC to the solvent boiling point. The heteroarm star polymers exhibited solubility characteristics that differ from those of the star block counterparts. For example, ($9FVE_{100}$-*h*-$IBVE_{100}$)-star, which has the same 9FVE/IBVE composition ratio as ($9FVE_{100}$-*b*-$IBVE_{100}$)-star but different sequence, is soluble in THF and chloroform, insoluble in acetone and toluene. In addition, no temperature-responsive solubility transition was observed.

Their concentrated solutions exhibited a sol-gel transition in response to temperature. For example, ($9FVE_{50}$-*b*-$IBVE_{100}$)-star was soluble in acetone or toluene at ambient temperature even at 30 wt%. These solutions became physical gels upon cooling to 0 ºC (Figure 11A for toluene). On the other hand, no gelation occurred with the corresponding arm polymer ($9FVE_{50}$-*b*-$IBVE_{100}$). Intermolecular aggregation of the outer segments of the star-shaped polymer, induced upon cooling, led to the formation of a three-dimensional physical network.

Even a slight amount of fluorine groups significantly influenced polymer's solubility characteristics. A concentrated aqueous solution of a star-shaped polymer with C_8F_{17} end groups formed a physical gel at ambient temperature (Figure 11B), whereas only a viscous solution was obtained with a star polymer with non-fluorinated end groups (Figure 11C).

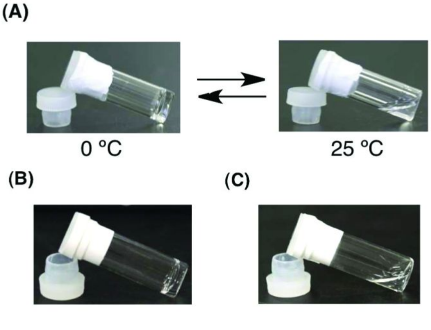

Figure 11. (A) Photographs of a 30 wt% toluene solution of ($9FVE_{50}$-b-$IBVE_{100}$)-star, (B) photograph of a 15 wt% aqueous solution of star-shaped poly(MOVE) obtained with 17FEA, and (C) photograph of a 15 wt% aqueous solution of star-shaped poly(MOVE) obtained with IBEA.

Downloaded by PENNSYLVANIA STATE UNIV on August 28, 2012 | http://pubs.acs.org
Publication Date (Web): August 16, 2012 | doi: 10.1021/bk-2012-1106.ch005

Conclusions

A new series of fluorine-containing polymers with well-defined structures were synthesized in a fluorinated solvent by base-assisting living cationic polymerization. This successful systematic synthesis shed light on unique solubility characteristics of well-defined fluorine-modified polymers. Moderately fluorinated polymers with narrow MWDs exhibited highly sensitive solubility transition (UCST-type phase separation) in various organic solvents with wide-ranging polarities including perfluoro solvents. Di- and triblock copolymers with various combinations of fluorinated segments and non-fluorinated segments were also successfully synthesized. In addition, various types of star-shaped polymers (star block, heteroarm, and end-functionalized star polymers) were synthesized. The compact structure and large numbers of fluorinated groups on their surface were responsible for their unique properties, especially in terms of solubility and association behavior, differing from the corresponding linear polymers.

Acknowledgments

This research was partially supported by a Grant-in-Aid for Scientific Research (No. 22107006) on Innovative Areas of "Fusion Materials: Creative Development of Materials and Exploration of Their Function through Molecular Control" (No. 2206) from the Ministry of Education, Culture, Sports, Science and Technology, Japan (MEXT).

References

1. *Fluoropolymers*; Wall, L. A., Ed.; Wiley: New York, 1972.
2. *Modern Fluoropolymers*; Scheirs, J., Ed.; Wiley: New York, 1997.
3. Ameduli, B.; Boutevin, B. *Well-Architectured Fluoropolymers: Synthesis, Properties and Applications*; Elsevier: Amsterdam, 2004.
4. Matsumoto, K.; Mazaki, H.; Nishimura, R.; Matsuoka, H.; Yamaoka, H. *Macromolecules* **2000**, *33*, 8295–8300.
5. Matsumoto, K.; Nishimura, R.; Mazaki, H.; Matsuoka, H.; Yamaoka, H. *J. Polym. Sci., Part A: Polym. Chem.* **2001**, *39*, 3751–3760.
6. Reisinger, J. J.; Hillmyer, M. A. *Prog. Polym. Sci.* **2002**, *27*, 971–1005.
7. Hansen, N. M. L.; Jankova, K.; Hvilsted, S. *Eur. Polym. J.* **2007**, *43*, 255–293.
8. Hirao, A.; Sugiyama, K.; Yokoyama, H. *Prog. Polym. Sci.* **2007**, *32*, 1393–1438.
9. Aoshima, S.; Kanaoka, S. *Chem. Rev.* **2009**, *109*, 5245–5287.
10. Seno, K.; Date, A.; Kanaoka, S.; Aoshima, S. *J. Polym. Sci., Part A: Polym. Chem.* **2008**, *46*, 4392–4406.
11. Hildebrand, J. H.; Fisher, B. B.; Benesi, H. A. *J. Am. Chem. Soc.* **1950**, *72*, 4348–4351.
12. Lo Nostro, P. *Adv. Colloid Interface Sci.* **1995**, *56*, 245–287.
13. Choi, W. O.; Sawamoto, M.; Higashimura, T. *Polym. J.* **1988**, *3*, 201–206.

14. Vandooren, C.; Jérôme, R.; Teyssié, Ph. *Polym. Bull.* **1994**, *32*, 387–393.
15. Höpken, J.; Möller, M.; Lee, M.; Percec, V. *Makromol. Chem.* **1992**, *193*, 275–284.
16. Bauer, B. J.; Fetters, L. J. *Rubber Chem. Technol.* **1978**, *51*, 406–436.
17. Bywater, S. *Adv. Polym. Sci.* **1979**, *30*, 90–116.
18. Sawamoto, M.; Kanaoka, S.; Higashimura, T. In *Hyper-Structured Molecules I: Chemistry, Physics and Applications*; Sasabe, H., Ed.; Gordon and Breach Science Publisher: Amsterdam, 1999; pp 43−61.
19. Shimomoto, H.; Fukami, D.; Kanaoka, S.; Aoshima, S. *J. Polym. Sci., Part A: Polym. Chem.* **2011**, *49*, 1174–1182.
20. Henne, A. L.; Newman, M. S. *J. Am. Chem. Soc.* **1938**, *60*, 1697–1698.
21. Isemura, T.; Kakita, R.; Kawahara, K. *J. Chromatogr., A* **2004**, *1026*, 109–116.
22. Shimomoto, H.; Fukami, D.; Kanaoka, S.; Aoshima, S. *J. Polym. Sci., Part A: Polym. Chem.* **2011**, *49*, 2051–2058.
23. Shimomoto, H.; Fukami, D.; Irita, T.; Katsukawa, K.; Nagai, T.; Kanaoka, S.; Aoshima, S. *J. Polym. Sci., Part A: Polym. Chem.* **2012**, *50*, 1547–1555.
24. Shibata, T.; Kanaoka, S.; Aoshima, S. *J. Am. Chem. Soc.* **2006**, *128*, 7497–7504.
25. Fujimori, A.; Masuya, R.; Masuko, T.; Ito, E.; Hara, M.; Kanai, K.; Ouchi, Y.; Seki, K.; Nakahara, H. *Polym. Adv. Technol.* **2006**, *17*, 653–663.
26. De Crevoisier, G.; Fabre, P.; Leibler, L.; Tenc-Girault, S.; Corpart, J. M. *Macromolecules* **2002**, *35*, 3880–3888.
27. Poly, J.; Ibarboure, E.; Rodriguez-Hernandez, J.; Taton, D.; Papon, E. *Maclomolecules* **2010**, *43*, 1299–1308.
28. Downer, A.; Eastoe, J.; Pitt, A. R.; Simister, E. A.; Penfold, J. *Langmuir* **1999**, *15*, 7591–7599.

Downloaded by PENNSYLVANIA STATE UNIV on August 28, 2012 | http://pubs.acs.org
Publication Date (Web): August 16, 2012 | doi: 10.1021/bk-2012-1106.ch005

Downloaded by NORTH CAROLINA STATE UNIV on August 28, 2012 | http://pubs.acs.org
Publication Date (Web): August 16, 2012 | doi: 10.1021/bk-2012-1106.ch006

Chapter 6

Semi-Fluorinated Polymer/POSS Thin Films Nanocomposites: Response to Water

**Dvora Perahia,*,[1] Dilru R. Ratnaweera,[1] Umesh M. Shrestha,[1]
Scott T. Iacono,[1,3] Dennis W. Smith,[1,2] Joseph Mabry,[4]
and Jaroslaw Majewski[5]**

**[1]Department of Chemistry, Clemson University,
Clemson, South Carolina 29634
[2]Department of Chemistry, University of Texas at Dallas,
Richardson, Texas 75080
[3]Department of Chemistry, United States Air Force Academy,
USAF Academy, Colorado 80840
[4]Air Force Research Laboratory, Space & Missile Propulsion Division,
Edwards AFB, California 93524
[5]Lujan Neutron Scattering Center, Los Alamos National Laboratory,
Los Alamos, New Mexica 87545
*E-mail: dperahi@clemson.edu**

The potential of semifluorinated polymers thin nanocomposite films to form responsive interfaces is demonstrated. The changes that take place in a random copolymer Biphenyl Perfluorocyclobutane (BPh-PFCB) impregnated with Polyhedral Oligomeric Silsesquioxane (POSS) nanoparticles (NPs) exposed to humidity were followed by neutron reflectometery. The response to water is affected by the dispersion of the NPs which is strongly influenced by the semifluorinated nature of the polymer. Thin films of the pristine polymer consist of layered structures with the air interface rich with the fluorinated block. Pristine BPh-PFCB polymer films were surprisingly fully wetted by water, with distinct accumulation of liquid at the air/polymer and substrate/polymer interface. Upon exposure of the nanocomposite thin films to

In Advances in Fluorine-Containing Polymers; Smith, D., et al.;
ACS Symposium Series; American Chemical Society: Washington, DC, 2012.

water vapor, compositional changes took place at the interfaces, which demonstrate the ability of the hybrid film to respond. The response mechanism encompasses the effect of fluorination that controls the interactions of the NPs within the polymer, coupled with entropic driving forces.

Downloaded by NORTH CAROLINA STATE UNIV on August 28, 2012 | http://pubs.acs.org
Publication Date (Web): August 16, 2012 | doi: 10.1021/bk-2012-1106.ch006

Introduction

In biological manifolds, response is often mediated by co-factors and messenger molecules that control motion at membrane interfaces (*1*). In soft synthetic materials response takes place at the interfaces and grain boundaries. The ability to respond requires a driving force for a change and sufficient mobility to respond. The response may be reversible or result in permanent changes in the manifold. Structured polymers with highly incompatible blocks are potentially effective responsive manifolds where complimentary functions are tailored into one molecule. Triggered by stimuli, such as changes of temperature, pressure, pH, electrical signals and presence of specific substances, polymers would either rearrange or react chemically to alter their properties. The response may result in perpetual or reversible transformations (*1*, *2*). The ultimate, practical responsive polymeric interface would be a durable, scratch resistance, self-cleaning, and adhesion tunable surface, with selective permeability. For any practical surface, an effective manufacturing process is also required along with a simple recyclable mechanism for damage repair (*1*, *2*). Semifluorinated polymers and their nanocomposites exhibit several characteristics that make them potentially responsive systems. They form structured interfaces with components that differ from each other in surface energies and motilities, offering a multitude of potential rearrangements as a response to changes in the chemical composition of their surroundings, changes that serve as stimuli (*3–5*). Fluorinated and partially fluorinated polymers tend to have a high degree of chemical and thermal resistance as well as hydrophobic and oleophobic characteristics. Their unique chemical stability and interfacial characteristics makes them potential responsive materials in industrial applications.

Semifluorinated polymers have been used in variety of applications. For example, they are used for retinal unfolding and permanent retinal tamponade in ophthalmology. Some of these polymers are biologically compatible and physiologically inert and can therefore serve as temporary blood substitutes and burn treatment media (*6–8*). Tuning the degree of fluorination offers a means to tune the refractive indices and the dielectric constant of the films and the incompatibility between fluorinated and protonated segments drive nano structure formations in bulk and thin films. In comparison with fully fluorinated systems, semifluorinated polymers are either partially or completely miscible in a number of solvents, including a wide range of protonated and perfluorinated alkanes (*9*, *10*).

Incorporation of small amount of nanoparticles enhances the complexity of the polymers and their responsiveness. In this work we have shown that a semifluorinated polymer impregnated with a small nanoparticle, whose size is

Downloaded by NORTH CAROLINA STATE UNIV on August 28, 2012 | http://pubs.acs.org
Publication Date (Web): August 16, 2012 | doi: 10.1021/bk-2012-1106.ch006

similar to that of the monomer, changes the response of the polymer to water vapor, one of the most prevalent natural stimuli. The response desired for industrial applications varies broadly. For some, stable membranes that change their permeability to water as a response are required where for others, formation of simultaneously hydrophobic and oleophobic layers is the goal (*11–13*).

The present study follows the response of nanocomposite thin films of Biphenyl Perfluorocyclobutyl and Polyhedral Oligomeric Silsesquioxanes NPs to water vapor. The basic premise that underlines the potential responsiveness of such a composite is a balance between the inherent tendency of fluorinated segments to migrate towards the low surface energy environment, coupled with the interactions of decorated POSS NPs and their translational and configurational entropy. The polymers and NPs studied are shown in Figure 1.

The structure of BPh-PFCB thin films impregnated with POSS has been recently investigated using neutron reflectometry (*15*, *16*). We have shown that the pristine polymer thin films consist of interfacial induced layers, which are retained as POSS NPs were incorporated into the films (*14–16*). In these studies, the NPs were decorated with, either fluorinated or protonated alkanes and some were also decorated on one site with matrix polymer. These studies have also shown that in contrast to most nanoparticles as small as POSS, the NPs migrate to the internal boundaries between protonated and fluorinated regions rather than accumulate at external interfaces, as observed on other polymeric systems. This unique behavior has been attributed to several factors including the semifluorinated nature of the polymer, the interactions of the NP with the matrix polymer, either via a polymer tether or by introduction of fluorinated groups, as well as entropy.

Herein we report the response nanocomposites to water stimuli for four nanocomposites varying the decoration of the POSS. With the expectation that the internal distribution of the NPs will alter the response we investigated four systems presented in Figure 1. The study has shown significant differences between the response of films of the pristine polymers and that of the nanocomposites.

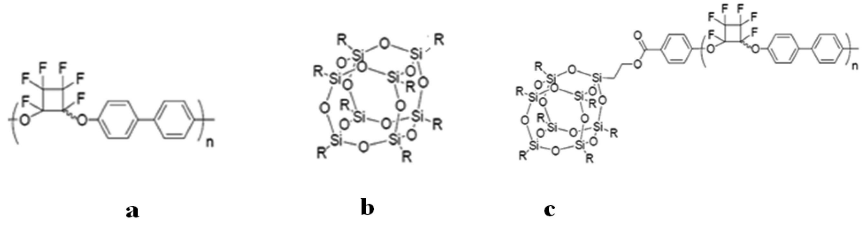

Figure 1. The chemical structures of ***a)*** *random copolymer of Biphenyl Perfluorocyclobutyl,* ***b)*** *POSS cages modified with R groups $R=CH_2CH_2CF_3$ or $R=CH_2CH(CH_3)_2$, and* ***c)*** *POSS tethered to BPh-PFCB polymer with N ~20, and R similar to b.*

Following an introduction of the methodology, the paper will discuss the response of pristine polymer to water vapor, followed by that of various nanocomposites. We will then compare the different systems studied.

Downloaded by NORTH CAROLINA STATE UNIV on August 28, 2012 | http://pubs.acs.org
Publication Date (Web): August 16, 2012 | doi: 10.1021/bk-2012-1106.ch006

Experimental Section

Materials and Thin Film Preparation

The BPh-PFCB polymers are synthesized by thermal [2+2] cyclopolymerization of trifluorovinyl biphenyl ethers and are commercially available through Tetramer Technologies, L.L.C. and distributed by Oakwood Chemical. The POSS was synthesized via condensation of commercially available isobutyl POSS triols with acetoxyethyltrichlorosilane and detailed characterization was previously reported (*17*). Octaisobutyl POSS was donated and is commercially available from Hybrid Plastics. Polydispersity of BPh-PFCB is ca. 2.1 and that of the tethered (t-POSS) nanocomposite is ca. 3. The glass transition temperature T_g of the polymer is approximately 140°C. Solutions were made by dissolving 1wt% of the polymer and the different POSS in hexafluorobenzene, obtained from Sigma-Aldrich and used as received.

In order to distinguish the systems POSS tethered to a BPh-PFCB chain is marked as t-POSS where POSS decorated with short alkanes will be referred to as POSS. The two short alkanes used are either hydrogen or fluorine terminated and are marked as (H) or (F). The nomenclature is summarized in Table I.

Table I. Nomenclature of the POSS cages used. R represents substituents as marked in Figure 1. Two of the NPs are substituted on one site by an oligomer of the polymeric matrix, while the rest of the sites by R.

Sample Name	***R***	***Oligomer***
t-POSS (H)	$-CH_2CH(CH_3)_2$	BPh-PFCB n=20
t-POSS (F)	$-CH_2CH_2CF_3$	BPh-PFCB n=20
POSS (H)	$-CH_2CH(CH_3)_2$	------
POSS (F)	$-CH_2CH_2CF_3$	------

The BPh-PFCB:POSS mole ratio was maintained at 1:1 in both POSS and t-POSS precursor solutions. Films were spin-cast on oxidized silicon wafers and kept under house vacuum at 25°C for two days to evaporate any remaining solvent. For temperature measurements, films were annealed for 12 hours under an N_2 environment and cooled to the room temperature.

Neutron reflectivity (NR) measurements were performed at Lujan Neutron Scattering Center at Los Alamos National Laboratory on the surface profile analysis reflectometer (SPEAR). SPEAR is a time-of-flight instrument, covering wavelength λ from 1.5 to 16Å. The reflectivity patterns were collected perpendicular to the sample surface as a function of momentum transfer q, where $q=4\pi\sin\theta/\lambda$ and θ is the incident angle of the incoming neutron beam. The data were normalized to the incident beam intensity (I_o) to obtain reflectivity (R), where $R = I/I_o$.

Downloaded by NORTH CAROLINA STATE UNIV on August 28, 2012 | http://pubs.acs.org
Publication Date (Web): August 16, 2012 | doi: 10.1021/bk-2012-1106.ch006

The reflectometry patterns of dry films were recorded over a large q range over ca. 4h. In order to capture changes that take place as samples are exposed to vapor, only a limited q range was recorded, sufficient however to analyze the data. This limited q range is accessible in 2-4min. The in-situ data were analyzed using the structural information obtained from the dry samples, as starting states.

Multilayer recursive Parratt formalism (*18*) was used to model the data, which is available in the Motofit software (*19*) with generic optimization to obtain the best least square fit. Data were fit to the minimum number of layers that provide a physical fit with an accuracy of $\chi^2 < 0.09$. Scattering length densities (SLDs) of BPh (1.96×10^{-6} Å^{-2}), PFCB (4.59×10^{-6} Å^{-2}) and POSS (5.92×10^{-7} Å^{-2}) were used as starting values. D_2O vapors were used to trigger stimuli. For these experiments protonated water has sufficient contrast as well; however the large inelastic cross section of the hydrogen atoms would have resulted in a high background, which would have prohibited fast measurements. The SLD of D_2O_l =6.33 x10^{-6} Å^{-1}.

Results and Discussion

The response of pristine polymer to water vapor was followed as a function of exposure time to saturated vapors of D_2O. The activity of saturated vapor equals one and therefore the vapor has the same chemical potential as the liquid phase. Representative neutron reflectivity data of pristine dry polymer layers and those of films exposed to vapor are shown along with the best fitting models in Figure 2a and 2b. The patterns of the dry polymer films are discussed first in detail, followed by introducing the changes that take place upon exposure to water vapor. The scattering pattern of the pristine polymer consists of a critical angle at low q, below which all the neutrons are reflected. The critical angle depends in part on the interfacial composition of the polymer. Following I(q), the intensity of the reflected neutrons as a function of the momentum transfer vector q, to higher q values, the patterns consist of *Kissing* fringes that correspond to the interference between neutron waves reflected from the interfaces perpendicular to the polymer surface, including the silicon, silicon oxide and the polymer. Qualitatively, with exposure to vapor, hardly any changes are observes in the critical angles. However, Δq, the distance between consecutive minima, which is inversely proportional to the overall film thickness, decreases. The decrease in Δq is a measure for an overall increase of the film thickness. In the PFCB polymers, it could originate from rearrangements in the film, as the H and F segments phase segregate, swelling of the film, or from both. Further quantitative analysis is carried out to resolve this issue. The fringes became more defined indicating enhanced contrast for neutrons. These changes clearly visible in the $R(q)q^4$ representation in Figure 2b, a format of data presentation that offers an enhanced visibility of the interference fringes.

The data were analyzed with a multi layer model that does not impose any constraints on possible outcomes, or structures, normal to the surface. The films are constructed of thin theoretical layers; each assigned a width, a scattering length density and an interfacial roughness. The reflectivity is then calculated allowing interference from all theoretical layers. All three variables are allowed to vary to best fit the experimental reseats. The SLD profile of the best fit provides the profile of the polymer. This is a common way to analyze reflectometry data, when no theory is available to describe the profiles of the layers normal to the surface (*18*). The polymer profiles in unites of SLD are shown in Figure 2c.

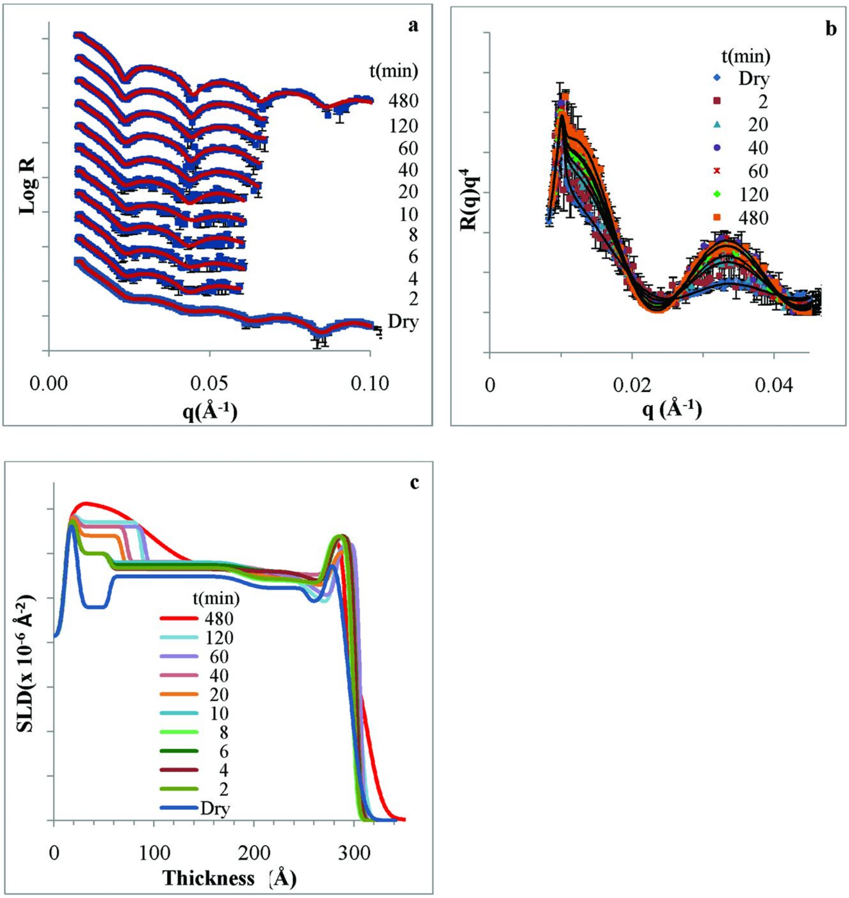

Figure 2. ***a)*** *Neutron reflectivity data of the thin film of BPh-PFCB as a function of* D_2O *exposure time. The symbols correspond to the experimental data and the solid lines correspond to the results a six layers model.* ***b)*** *R(q)*q^4 *vs. q representation and the corresponding fitting.* ***c)*** *SLD profiles of BPh-PFCB normal to the thin film surface as a function of* D_2O *exposure time.*

Pristine dry polymer thin films exhibit interfacial layering, with the air interface is fluorine-rich and the solid interface is BPh-rich. Note however that the values of SLDs extracted from the analysis show that the interfaces, though rich in one of the components consists of both. This compounded nature has been observed for semifluorinated alkanes (*3*, *4*) and is demonstrated in Figure 3.

Downloaded by NORTH CAROLINA STATE UNIV on August 28, 2012 | http://pubs.acs.org
Publication Date (Web): August 16, 2012 | doi: 10.1021/bk-2012-1106.ch006

Downloaded by NORTH CAROLINA STATE UNIV on August 28, 2012 | http://pubs.acs.org
Publication Date (Web): August 16, 2012 | doi: 10.1021/bk-2012-1106.ch006

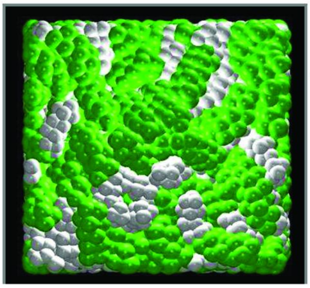

Figure 3. Top view of the interface of $CH_3(CH_2)_7(CF_2)_7CF_3$ Results from a fully atomistic MD simulation for 200 chains at T=375K. Cross-sectional area is 4.6nm x 4.6nm. Green corresponds to fluorine atoms and white to hydrogen atoms (3, 4).

While the computational studies were carried out on model systems, the compounded nature of the air interface found in our molecular dynamic simulations was rather surprising and diverged from the common agreement that one would expect the fluorine to dominate the air interface. In the PFCB polymers, the connectivity of the H and F segments forces a compounded interface. The surface energy of these interface depend on the fraction of the fluorinated component, with a minimum when the fluorine occupies half of the surface sites. Experimentally it remains a challenge to determine the surface energy of surfaces that consists of nano-domains with significantly different affinities to most solvents.

Another structural feature that results from the semifluorinated nature of the polymer is interfacial induced layering. The segregation of the H and F segments is attributed to the differences in surface energies of the fluorinated and hydrogenated segments, where lower surface energy of the fluorinated segments drives PFCB to the air/polymer interface. In addition to the differences in surface energies, incompatibility between PFCB and BPh enhances segregation driving further layering. Layering is more pronounced at the air/polymer and SiO_2/polymer interfaces. The layers become less defined away from the interfaces (*14–16*). Layering as well as surface enrichment with fluorine has been previously observed for other PFCB polymers (*5*, *14*).

The pristine polymer films were then exposed to vapors of D_2O and the reflectometry patterns were recorded initially at intervals of two seconds and the intervals were then increased. The overall shape of the polymer profiles is retained including the layered structure. The films remain overall smooth. The polymer profiles in units of SLD increase in intensity across the film with time of exposure to the vapors. To understand this enhancement a careful examination of the scattering length density is required. SLD of D_2O in its liquid form (6.33×10^{-6} Å^{-1}), is higher than that of both the protonated and fluorinated segments. Therefore the enhanced SLD shows that water penetrated the film and resides across the film with significant access at the air and solid interfaces.

Downloaded by NORTH CAROLINA STATE UNIV on August 28, 2012 | http://pubs.acs.org
Publication Date (Web): August 16, 2012 | doi: 10.1021/bk-2012-1106.ch006

The accumulation at the air interface was rather surprising since one would expect that the fluorinated interface to be hydrophobic. It could be interpreted in terms of rearrangements that occurred at the interfacial zone with exposure to water, as have been seen in computer simulations on model semifluorinated polymers that have shown in presence of water the hydrogenated segments reside longer at the interfaces than the fluorinated ones. The complex nature where both fluorinated and protonated segments reside at the interfaces allow wetting of the polymer-vapor interface.

The complexity of the semifluorinated films was then increased by incorporating POSS NPs, and the response of the nanocomposite to water vapor was explored. Our recent studies have shown that tailoring the interactions between the NP and the polymer matrix using the substituents on the NPs as described in Figure 1, results in different NP distributions (*16*, *17*). We POSS decorated with protonated and fluorinated short chains segregated to the internal interfaces whereas NPs tethered to the matrix polymer chain are more dispersed across the entire film, with some excess at the air interface..

The response of the nanocomposite in which NPs are tethered to a single polymer chain with the other substituents are either protonated (t-POSS(H)) or fluorinated (t-POSS(F)) short chains to water vapor is shown in Figure 4 The films that consist with t-POSS(H), shown in panels a and b of Figure 4, qualitatively, follow the behavior of the pristine polymer, i.e. the amplitude of the fringes increases with increasing time. For the fluorinated NP t-POSS(F) the changes are significantly smaller.

The corresponding SLD profiles derived for the pure polymer and the nanocomposite are shown in Figure 5. The center of the film has negligible solvent accumulation, therefore the figure depicts the interfacial regions. Figure 5a introduces the SLD profiles for t-POSS(H) in comparison with the matrix polymer. Upon exposure to vapor, changes take place at both air/polymer and substrate/polymer interfaces of t-POSS (H). The presence of solvent drives the NPs to the air interface, as indicated by the lower SLD values, whereas water resides close to the interface. At the polymer solid interface hardly any water is observed even after 8 hours. While the polymer itself is permeable, the presence of t-POSS(H) is sufficient to form a barrier for water vapor.

Figure 5b compares the SLD profiles t-POSS(F) with the pristine polymer. No layering is observed at the air interface. While small amounts of vapor penetrated the film, the overall SLD suggest that the surface composition has changed as response to water. Though slightly delayed in time, a similar behavior is observed at the solid interface. With both the NPs and the fluorinated POSS driven to the interface, t-POSS (F) nanocomposites hardly any water penetrate into the film. POSS is a small NP often on the order of the size of the rigid segment of the polymer. As was previously shown it tends to migrate to the interface (*20–23*) forming water barriers. In presence of water, the POSS trapped at internal interfaces is released and migrate to the interface, serving as water barrier.

Downloaded by NORTH CAROLINA STATE UNIV on August 28, 2012 | http://pubs.acs.org
Publication Date (Web): August 16, 2012 | doi: 10.1021/bk-2012-1106.ch006

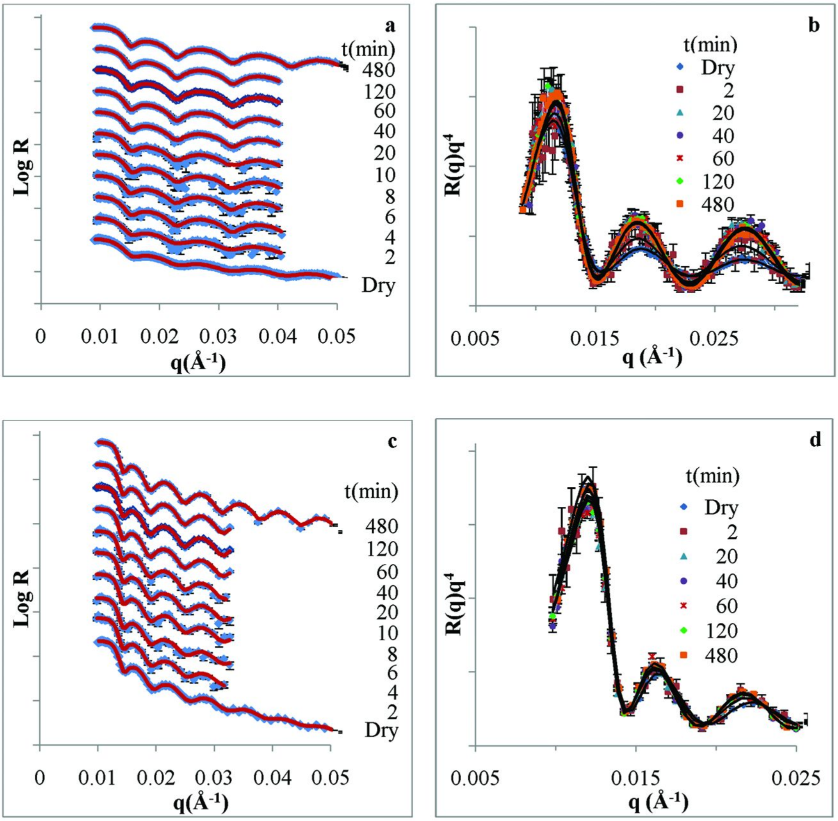

Figure 4. ***a)*** *Neutron reflectivity patterns of the thin film of t-POSS(H) and* ***c)*** *t-POSS(F) as a function of exposure time to D_2O. The symbols correspond to the experimental data and the solid lines are the best fits for 6 layer model. $R(q)q^4$ representation of data for t-POSS(H) and t-POSS(F) is given in* ***b*** *and* ***d*** *respectively.*

In order to separate the effects of the polymer tail tethered to the POSS from that of the F and H decoration on the POSS, measurements were carried out with POSS cages modified with short protonated chains (Poly-POSS(H)) and POSS grafted with short fluorinated chains (Poly-POSS(F)), blended in the polymer. The profiles obtained for these two blends are shown in Figure 6 a,b. Interestingly, while only small quantities of D_2O penetrate, those that do diffuse in mask interactions so that no well-defined layering is observed. The fact that very little water penetrate is a clear indication of POSS migrating to the air interface.

Downloaded by NORTH CAROLINA STATE UNIV on August 28, 2012 | http://pubs.acs.org
Publication Date (Web): August 16, 2012 | doi: 10.1021/bk-2012-1106.ch006

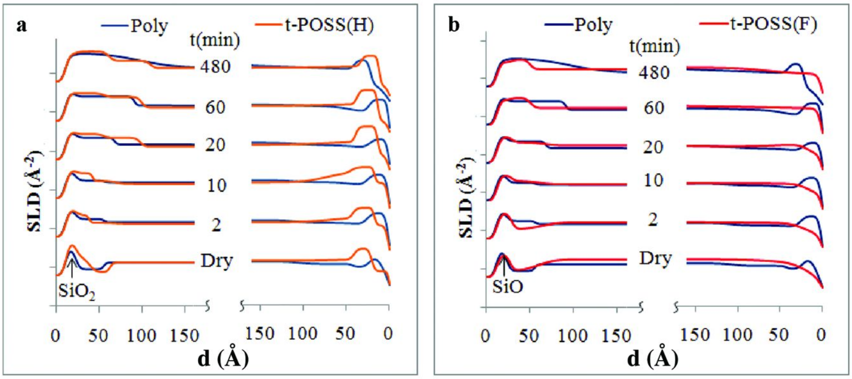

*Figure 5. The interfacial region of the SLD profiles of the pure polymer and **a)** t-POSS(H) and **b)** t-POSS(F) as a function of D_2O exposure time. The SLD profiles are shifted vertically for clarity. The x-axes are presented in absolute value from the interfaces.*

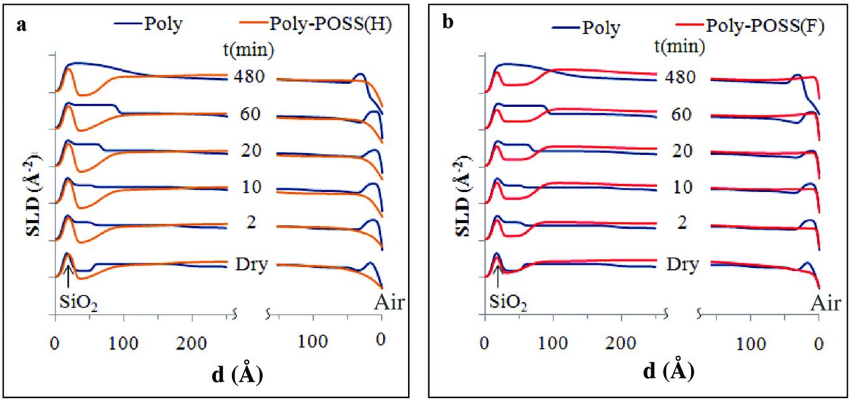

*Figure 6. The interfacial region of the SLD profiles of the pure polymer and **a)** Poly-POSS(H) and **b)** Poly-POSS(F) as a function exposure time to D_2O vapor. The SLD profiles are shifted vertically for clarity. The x-axes are presented in absolute value from the interfaces.*

The overall uptake of D_2O inside the thin films and the relative changes in film thickness for the pristine polymer and the thin nanocomposites are given in Figure 7. The thickness of the thin film defined as the distance from substrate/polymer interface to the air/polymer interface. The substrate/polymer interface is taken as the center of the roughness at the interface, which is the region of the SLD gradient from SiO_2 to the polymer. The air/polymer interface is defined as the center of the region that corresponds to the roughness at the air/polymer boundary. Figure 7a shows the changes in film thickness normalized to the thickness of the dry film as a function of exposure time. Initial rate of relative change in thickness, which is given by the slope at the onset of curves, is the highest in thin films of Poly-POSS(F) and the rate of swelling at the onset decrease in the order of polymer, t-POSS(H), t-POSS(F) and Poly-POSS(H). All the thin films reached a steady state after the initial swelling except for the pure polymer, where swelling progressed at a slower rate.

Total D_2O uptake was calculated by integrating the area of the SLD profiles between the air/polymer and substrate/polymer interfaces and subtracting the areas at a given exposure time with that of the dry film. These calculations assumed for a first approximation that SLD increments occur only due to penetration of D_2O molecules. Rates of solvent absorption at the onset of diffusion is similar for both polymer and Poly-POSS(F) films and are the highest. This is consistent with initial low packing densities of the polymer at the interfaces. Both tethered POSS films have the intermediate rates and Poly-POSS(H) the lowest.

Downloaded by NORTH CAROLINA STATE UNIV on August 28, 2012 | http://pubs.acs.org
Publication Date (Web): August 16, 2012 | doi: 10.1021/bk-2012-1106.ch006

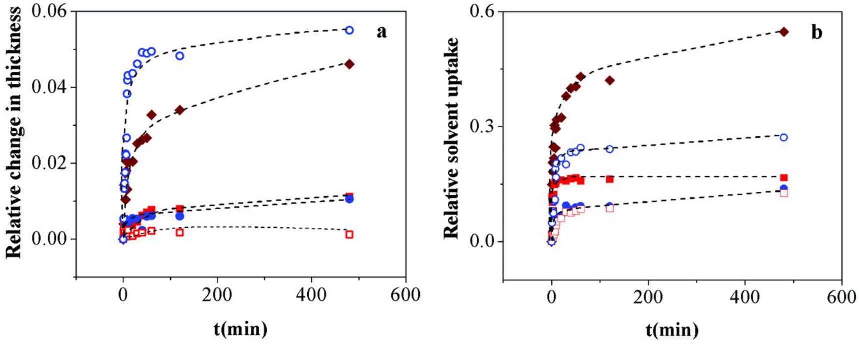

Figure 7. Film thickness as a function of s exposure time for pure polymer (Poly) (♦), t-POSS(H) (■), Poly-POSS(H) (□), t-POSS(F) (●) and Poly-POSS(F) (○) films. Lines are drawn as a guide to the eye.

Conclusions

This work explored the response to water vapor of ultrathin films of semifluorinated polymers and their nanocomposites. In thin films of several radii of gyration of the polymers, the overall structure and dynamics of polymeric films are strongly affected by interfacial forces. In pristine semifluorinated polymer films, the properties of the films are also affected by the segregation of the fluorinated segments from that of the protonated one as well as by their incompatibility. We found that when the pristine polymer films are exposed to water vapor, despite the semifluorinated nature of the interface of the pristine polymers, water vapor accumulated at the air and solid polymer interfaces. However, very limited quantities of water reside in the center of the film. The accumulation at the interfaces was attributed to interfacial rearrangements of the polymer as a response to the presence of water, which in turn allowed water penetration.

Incorporating POSS NPs into the semifluorinated polymers resulted in competition between the small NPs and the fluorinated segments for the interfacial sites, modifying the air and solid interfaces of the films, as well as the internal boundaries between fluorinated and protonated segments. The response of the thin films impregnated with POSS NPs to water vapor differs from that of the pristine polymer, where the presence of NPs inhibiting water penetration to different degrees. All films slightly swell with the degree of swelling and the rates of swelling dependent on the nature of the substituents. Correlating the degree of water uptake with the NP distribution show that in presence of water, the interactions of the NPs with the polymers were reduced to the extent that entropic forces that drive the NPs to the interfaces become dominant, driving the NPs to the macroscopic interfaces. As a result, the semifluorinated polymers become less penetrable to water.

Downloaded by NORTH CAROLINA STATE UNIV on August 28, 2012 | http://pubs.acs.org
Publication Date (Web): August 16, 2012 | doi: 10.1021/bk-2012-1106.ch006

References

1. Aragon, A. M.; Wayer, J. K.; Geubelle, P. H.; Goldberg, D. E.; White, S. R. *MRS Bull.* **2008**, *33* (8), 732–775.
2. Stuart, M. A. C.; Huck, W. T. S.; Genzer, J.; Müller, M.; Ober, C.; Stamm, M.; Sukhorukov, G. B.; Szleifer, I.; Tsukruk, V. V.; Urban, M.; Winnik, F.; Zauscher, S.; Luzinov, I.; Minko, S. *Nat. Mater.* **2010**, *9*, 101.
3. Pierce, F.; Tsige, M.; Perahia, D.; Grest, G. S. *J. Phys. Chem. B* **2008**, *112*, 16012–16020.
4. Pierce, F.; Tsige, M.; Borodin, O.; Perahia, D.; Grest, G. S. *J. Chem. Phys.* **2008**, *128*, 214903/1–214903/14.
5. Perahia, D. In *ACS Series Fluoropolymer 2003, Current Frontiers and Future Trends*; Smith, D. W, Ed.; 2003.
6. Edwards, C. M.; Lowe, K. C.; Rohlke, W.; Geister, U.; Reuter, P.; Meinert, H. *Artific. Cells, Blood Substitutes, Immobilization Biotechnol.* **1997**, *25* (3), 255–260.
7. Meinert, H; Roy, T *Eur. J. Ophthalmol.* **2000**, *10* (3), 189–97.
8. Reiss, G. *Fluorine Chemistry at the New Millenium-Fascinated by Fluorine*; Elsevier Science: Amsterdam, 2000.
9. Morgado, P.; Lewis, J. B.; Laginhas, C. M. C.; Martins, L. F. G.; McCabe, C.; Blas, F. J.; Filipe, E. J. M. *J. Phys. Chem. B* **2011**, *115* (50), 15013–15023.
10. Rabolt, J. F.; Russell, T. P.; Twieg, R. J. *Macromolecules* **1984**, *17*, 2786–94.
11. Kannan, A. G.; Choudhury, N. R.; Dutta, N. *Appl. Mater. Interfaces* **2009**, *1*, 336–347.
12. Tuteja, A.; Choi, W.; Ma, M.; Mabry, J. M.; Mazzella, S. A.; Rutledge, G. C.; McKinley, G. H.; Cohen, R. E. Designing superoleophobic surface. *Science* **2007**, *318*, 1618–1622.
13. Merkel, T. C.; Freeman, B. D.; Spontak, R. J.; He, Z.; Pinnau, I.; Meakin, P.; Hill, A. J. Ultrapermiable, reverse-selective nanocomposite membranes. *Science* **2002**, *296*, 519–52.
14. Traiphol, R.; Smith, D. W., Jr.; Perahia, D. *J. Polym. Sci., Part B* **2002**, *40*, 2817–2824.

15. Ratnaweera, D.; Shrestha, U; Smith, D. W., Jr.; Iacono, S. T.; Mabry, J.; Perahia, D *Macromolecules*, submitted.
16. Ratnaweera, D.; Iacono, S. T.; Mabry, J.; Smith, D. W., Jr.; Perahia, D *Langmuir*, submitted.
17. Iacono, S.; Budy, S. M.; Mabry, J. M.; Smith, D. W., Jr. *Polymer* **2007**, *48*, 4637–4645.
18. Parratt, L. G. Surface studies of solids by total reflection of X-rays. *Phys. Rev.* **1954**, *95*, 359–369.
19. Nelson, A. *J. Appl. Crystallogr.* **2006**, *39*, 273–276.
20. Okada, A.; Usuki, A. *Macromol. Mater. Eng.* **2006**, *291* (12), 1449–1476.
21. Hosaka, N.; Otsuka, H.; Hino, M.; Takahara, A. *Langmuir* **2008**, *24*, 5766–5772.
22. Miyamoto, K.; Hosaka, N.; Otsuka, H.; Takahara, A. *Chem. Lett.* **2006**, *35*, 1098–1099.
23. Chena, X. C.; Green, P. F. *Soft Mater* **2011**, *7*, 1192–1198.

Downloaded by NORTH CAROLINA STATE UNIV on August 28, 2012 | http://pubs.acs.org
Publication Date (Web): August 16, 2012 | doi: 10.1021/bk-2012-1106.ch006

Downloaded by STANFORD UNIV GREEN LIBR on August 28, 2012 | http://pubs.acs.org
Publication Date (Web): August 16, 2012 | doi: 10.1021/bk-2012-1106.ch007

Chapter 7

Functionalization of Fluoroalkyl Polyhedral Oligomeric Silsesquioxanes (F-POSS)

Sean M. Ramirez,*,[1] Yvonne J. Diaz,[1] Raymond Campos,[1] Timothy S. Haddad,[1] and Joseph M. Mabry[2]

[1]ERC Inc., Air Force Research Laboratory, Space & Missile Propulsion Division, Edwards Air Force Base, California 93524-7680
[2]Air Force Research Laboratory, Space & Missile Propulsion Division, Edwards Air Force Base, California 93524-7680
***E-mail: Sean.Ramirez.ctr@edwards.af.mil**

Incompletely-condensed fluoroalkyl-functional Polyhedral Oligomeric SilSesquioxanes (F-POSS) have been synthesized *via* a scaleable three-step synthetic process with an overall yield of 52%. The primary byproduct of each step in the synthesis is the completely-condensed F-POSS starting material, which enables the recycling of the starting materials. The incompletely condensed structures were readily reacted with a variety of functional dichlorosilanes to introduce reactive or unreactive functionality and produce unsymmetrical F-POSS structures. Chemical structures were confirmed by elemental analysis, multinuclear NMR (^{1}H, ^{13}C, ^{19}F, and ^{29}Si), and FT-IR methods. Single crystal X-ray diffraction was used to elucidate the crystal structure of the precursor F-POSS disilanol. The functionalized F-POSS structures were found to possess variable solubility properties, generally superior to those of the closed-cage F-POSS starting material. Dynamic contact angle measurements of these compounds were examined using water and hexadecane as the wetting liquids. Copolymers of poly(methyl methacrylate) containing F-POSS were synthesized from methacrylate F-POSS macromers. These novel structures can be used as building blocks for the development of low surface energy materials.

In Advances in Fluorine-Containing Polymers; Smith, D., et al.;
ACS Symposium Series; American Chemical Society: Washington, DC, 2012.

Downloaded by STANFORD UNIV GREEN LIBR on August 28, 2012 | http://pubs.acs.org
Publication Date (Web): August 16, 2012 | doi: 10.1021/bk-2012-1106.ch007

Introduction

Designing materials with low surface energy and mechanical robustness has become a major objective in the scientific community. Various nano-fillers have been blended into polymers in order to improve overall system performance as non-wetting surfaces. Of these fillers, a sub-class of particles possessing long-chain fluoroalkyl groups, Fluoroalkyl Polyhedral Oligomeric SilSesquioxanes (F-POSS), has recently been developed and observed to be an excellent nano-filler for low surface energy applications (*1–4*). These compounds possess an inorganic silicon-oxygen core [$SiO_{1.5}$] with a periphery of long-chain fluorinated alkyl groups. These groups impact the surface morphology, crystallinity, and overall surface energy, which bestow F-POSS with several useful properties (*3–6*). A variety of chain lengths have been investigated to determine the optimal chain length for the lowest surface energy (Figure 1). Of these peripheral chain lengths, the fluorodecyl POSS compound possesses one of the lowest surface energy values known (γ_{sv} = 9.3 mN/m) for any crystalline solid (*7*). F-POSS compounds have been blended in polymer matrices and cast neat to produce superhydrophobic and superoleophobic surfaces (*7–10*). Dramatic improvements in water and oil repellency were observed when F-POSS was blended with perfluorocyclobutyl (PFCB) aryl ether polymers (*11*).

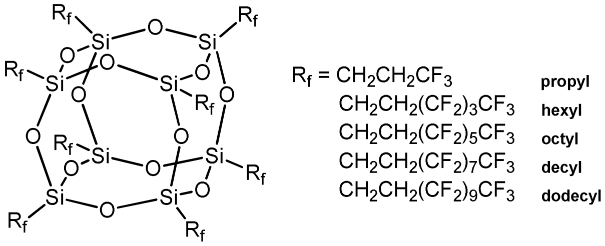
$R_f = CH_2CH_2CF_3$ **propyl**
$CH_2CH_2(CF_2)_3CF_3$ **hexyl**
$CH_2CH_2(CF_2)_5CF_3$ **octyl**
$CH_2CH_2(CF_2)_7CF_3$ **decyl**
$CH_2CH_2(CF_2)_9CF_3$ **dodecyl**

Figure 1. F-POSS peripheral chain lengths synthesized.

Neat films of F-POSS surfaces possess poor surface robustness and are susceptible to surface abrasion. To circumvent these issues, F-POSS have been physically blended with a variety of polymers (*4*, *5*). However, the physical blending has illuminated certain issues in the incorporation of F-POSS in polymer matrices. For example, these composites are still prone to surface abrasion, mechanical robustness, and phase separation of the POSS domain. To date, there is no viable methodology to covalently attach F-POSS to a host polymer matrix, whereas non-fluorinated POSS structures have been chemically bound to polymer matrices (*1*, *11–15*). An additional issue plaguing the long-chain fluoroalkyl POSS compounds is the limited range of solvents in which they are soluble. Previously, the selection has been limited to fluorinated solvents. To overcome these limitations, the development of a silanol functionalized incompletely-condensed (open-cage) F-POSS has been desired to enable new, robust, low surface energy hybrid materials. Incompletely-condensed silsesquioxane structures are used as models for silica (*16*), catalyst support (*17*), and precursors for silsesquioxane containing polymers (*11*). To date, a

Downloaded by STANFORD UNIV GREEN LIBR on August 28, 2012 | http://pubs.acs.org
Publication Date (Web): August 16, 2012 | doi: 10.1021/bk-2012-1106.ch007

viable synthetic strategy to produce long-chain F-POSS compounds possessing additional reactive or non-reactive functionality does not exist. There are few examples in the literature of short-chain incompletely condensed silsesquioxanes with functionality. For example, (3,3,3-trifluoropropyl)$_7$Si$_7$O$_9$(ONa)$_3$, has been derivatized with long-chain fluorinated trichlorosilanes to produce low surface energy materials (*8*). However, these shorter propyl chains do not possess the same magnitude of liquid repellency as longer fluoroalkyl chains (*4*). Also, the added functionality was a fluoroalkyl group and not an organic moiety with a reactive segment.

Herein, we report a simple approach to converted closed cage F-POSS into an incompletely condensed silsesquioxanes (*18*). This method follows the synthetic strategies developed by Feher and coworkers. Feher's work consisted of opening completely-condensed POSS cage edges through multistep syntheses to create silanols in varying degree *via* an acidic (*19*) or basic route (*20*). The acidic route was applied to F-POSS cages because it has proven successful for alkyl POSS cages.

Experimental

Materials

F-POSS (**1**) was synthesized according to literature procedure (*4*). Compounds **2-7** were synthesized according to previously described procedure (*18*). (3-Acryloxypropyl) methyldichlorosilane (Gelest), vinylmethyldicholorosilane (Gelest), hexafluorobenzene (C_6F_6, Synquest), 1,3-dichloro-1,2,2,3,3-pentafluoropropane (AK-225G, AGC Chemicals Americas), and hexadecane (Aldrich) were used without further purification, unless otherwise stated. All reactions were performed under a nitrogen atmosphere unless stated otherwise.

Characterization

Combustion analysis was performed by Atlantic Microlab, Inc. ^{1}H, ^{13}C, ^{19}F, and ^{29}Si NMR spectra were obtained on Bruker 300-MHz and 400-MHz spectrometers. An inverse gated 30° pulse with a 12 sec delay was used to acquire ^{29}Si NMR spectra. FT-IR spectra were taken on a Perkin Elmer Spectrum BX. Surface roughness was determined using a Digital Instruments Nanoscope IV (AFM) and a Vecco WykoNT930 optical profilometer. Size exclusion chromatography (SEC) was performed with a high-pressure liquid chromatography (HPLC, Agilent) system at a flow rate of 1.00 mL/min through two columns (Mixed pGel C and E) using THF as the carrier solvent. This was equipped with multi-angle light scatter (MALS, Dawn Helios Wyatt), viscometer (ViscoStar, Wyatt) and refractive index (RI, Optilab-rex, Wyatt) detectors. The RI detector was used to determine dn/dc values for the determination of absolute MW with the MALS detector. Surface measurements were followed according to literature procedure.

Downloaded by STANFORD UNIV GREEN LIBR on August 28, 2012 | http://pubs.acs.org
Publication Date (Web): August 16, 2012 | doi: 10.1021/bk-2012-1106.ch007

X-Ray Crystallography Data

Single crystals of compound **2** were grown from the slow evaporation of **2** in C_6F_6, resulting in clear platelets. Crystal data for **2** was collected at T=100.0 K using Kusing Bruker 3-circle, SMARTAPEX CCD with c-axis fixed at 54.748, running on SMART V 5.625 program (Bruker AXS: Madison,2001). Graphite monochromated $Cu_{K\alpha}$ (λ= 1.54179 Å) radiation was employed for data collection and corrected for Lorentz and polarization effects using SAINT V 6.22 program (Bruker AXS: Madison, 2001), and reflection scaling (SADABS program, Bruker AXS: Madison, WI, 2001). Structure was solved by direct methods (SHELXL-97, Bruker AXS: Madison, 2000) and all non-hydrogen atoms refined anisotropically using full-matrix least-squares refinement on F^2. Hydrogen atoms were added at calculated positions. For **2**, M_r=,monoclinic, space group P2(1)/c , a=11.833(2) Å, b=57.141(11) Å, c=19.069(4) Å, α=90.00°, β=92.20(3)°, γ=90.00°, V= 12884(4) $Å^3$, $F(000)$=7816, $p_{calcd}(Z=2)$= 2.068 gcm^{-3}, μ= 3.183 mm^{-1}, approximate crystal dimensions 0.60 x 0.35 x 0.20 mm^3, θ range = 0.71 to 24.74°, 122186 measured data of which 21422 (R_{int}=0.0608, R_σ = 0.0379) unique with 3715 refined parameters, 14705 restraints were applied, final R indices [I>2σ(I)]: R1=0.0915, *w*R2=0.1918, R1=0.0857, *w*R2=0.1893 (all data), GOF on F^2=1.230. CCDC 843485 contains the supplementary crystallographic data for this paper. This data can be obtained free of charge from The Cambridge Crystallographic Data Centre via www.ccdc.cam.ac.uk/data_request/cif.

General Synthesis of F-POSS Monomers

A solution of **2** (4.00 g, 0.99 mmol), 3-acryloxypropylmethyldichlorosilane (0.226 g, 0.99 mmol), and Et_3N (0.200 g, 1.95 mmol) were stirred together for 12 hr. During this time a white precipitate formed. The solution was then filtered and poured into ethyl acetate, at which time, a white solid precipitated (F-POSS). This solid was removed *via* filtration and the filtrate was concentrated, then dissolved in diethyl ether and filtered. The filtrate was collected and cooled to 0 °C affording a white precipitate. The precipitate was collected and dried under vacuum to afford a white powder (**7**) (1.9 g, 48%). ^{1}H NMR (300 MHz, $(CD_3CD_2)_2O$, ppm) δ 6.01 (s, 1H), 5.56 (s, 1H), 4.16 (t, 2H) 2.25 (m, 16H), 1.92 (s, 3H), 1.84 (m, 2H), 1.09 (m, 16H), 0.76 (t, 2H), 0.26 (s, 3H). ^{29}Si{^{1}H} NMR δ -18.1, -66.08, -68.64, -69.2 (1:2:4:2). ^{19}F NMR -82.3 (3F), -116.9 (2F), -122.6 (6F), -123.7 (2F), -124.3 (2F), -127.3 (2F).

General Polymerization of F-POSS Monomers

Methyl methacrylate (MMA, 1.31 g, 13.1 mmol), **3** (0.36 g, 0.09 mmol), azobisisobutyronitrile (AIBN, 5 mg, 0.001 mmol) were dissolved in a C_6F_6:THF mixture (4:1). This solution was purged with nitrogen for 25 minutes to remove any oxygen and was immediately submerged in a 60°C oil bath for 18 hrs. The resulting solution was precipitated in hexanes, filtered and dried to yield a fluffy white powder (0.93 g, 71%).

Results and Discussion

In order to successfully open the chemically resistant F-POSS, a three-step synthetic procedure was developed following a similar method first employed by Feher *et al* (*18*, *21*, *22*). The first step involved opening the F-POSS (**1**) cage with a trifluoromethane sulfonic acid (HOTf) to form the triflate intermediate compound **1a** (Figure 2). This reaction involves equilibrium between the open and closed-cage silsesquioxane frameworks, making the ^{29}Si NMR spectra complex. Compound 1a can be observed with ^{29}Si resonances at -62.6, -65.0, and -66.7 ppm (Si ratio 2:2:4). Starting material is also observed with a strong peak at -66.3 ppm. To obtain the maximum amount of the desired ditrifilate, this reaction was stopped at 75 minutes. If reaction time is extended, the HOTf will continue to attack the POSS cage framework, resulting in a complex mixture of triflate cages. This mixture of cages can be observed in ^{29}Si NMR (Figure 3). Attempts to isolate these additional cages have resulted in a reversion of this mixture to compound **1**. Unfortunately, the ditriflate is highly unstable and each attempt to isolate **1a** also resulted in a complete reversion to compound **1**. This has been attributed to the strong electron withdrawing effect of fluorodecyl chains and difficulty in finding a suitable solvent for compound **1a** besides C_6F_6.

As a result of the instability of the ditriflate compound, $NBut_4HSO_4$ was immediately added to the reaction mixture to bridge any disilanol functionality with a sulfate group (Figure 4). This results in the reaction mixture separating into two liquid layers; a yellow aqueous layer and a clear, colorless fluorinated solvent layer containing both **1b** and **1**. The bridging sulfate moiety appears to stabilize the electron-withdrawing F-POSS cage framework, leading to another NMR observed intermediate with ^{29}Si resonances at -64.5, -65.7, and -67.3 ppm (Si ratio 2:2:4) (Figure 5). A viable isolation procedure for intermediate **1b** has not been attained and isolation attempts have resulted in complete reversion to compound **1**. Similar to the previous reaction, the higher density clear fluorinated solvent layer from the reaction mixture is used "as is" for the next reaction step.

Downloaded by STANFORD UNIV GREEN LIBR on August 28, 2012 | http://pubs.acs.org
Publication Date (Web): August 16, 2012 | doi: 10.1021/bk-2012-1106.ch007

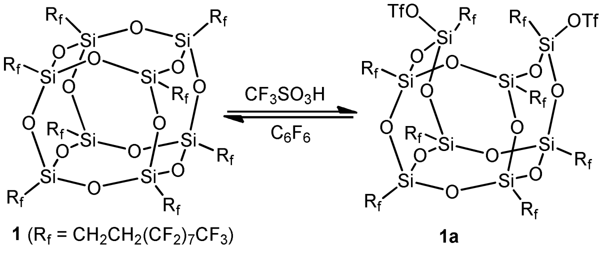

1 ($R_f = CH_2CH_2(CF_2)_7CF_3$)

1a

Figure 2. Cage opening reaction with HOTf.

Downloaded by STANFORD UNIV GREEN LIBR on August 28, 2012 | http://pubs.acs.org
Publication Date (Web): August 16, 2012 | doi: 10.1021/bk-2012-1106.ch007

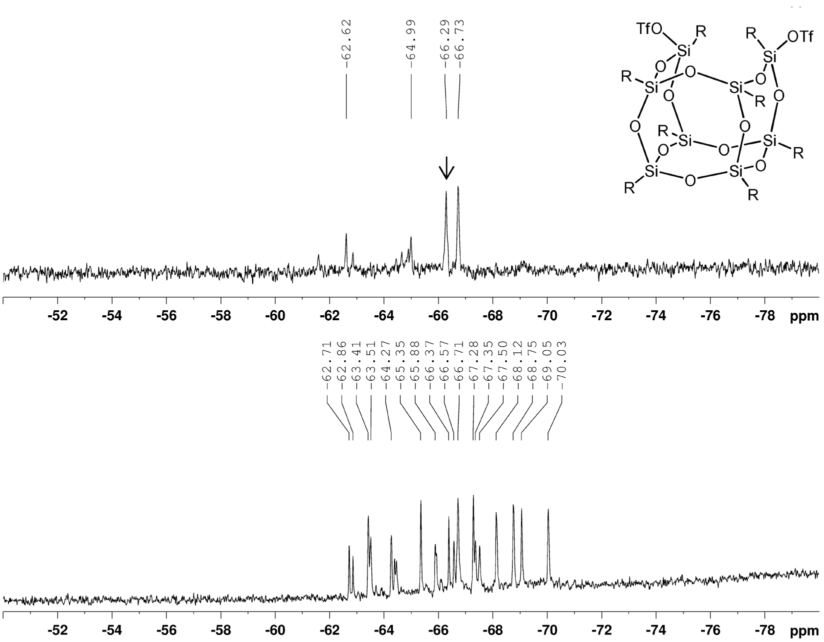

*Figure 3. ^{29}Si NMR of **1a** and **1** in C_6F_6 (top). Open cage mixture of unidentified POSS structures and open cages if reaction proceeds for extended periods of time (bottom). Arrow points to unreacted compound **1**.*

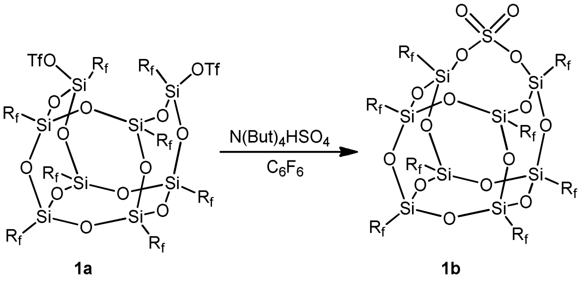

*Figure 4. Bridged sulfate reaction of reaction intermediates **1a** and **1b**.*

The bridged sulfate reaction mixture is subsequently added to a polar fluorinated solvent/water mixture to convert **1b** to disilanol F-POSS (**2**) in good overall yield (*ca. 53%*) (Figure 6). The use of a polar fluorinated solvent is vital for this reaction to proceed. This solvent allows for the introduction of water in a highly fluorinated environment. The disilanol compound **2** is purified away from any residual compound **1** through the solubility differences between the open and closed structures in C_6F_6 and ethyl acetate mixtures. Compound **1** precipitates from this solution mixture and the soluble compound **2** is precipitated from a $CHCl_3$ solution. This step also helps remove any residual resinous products that

Downloaded by STANFORD UNIV GREEN LIBR on August 28, 2012 | http://pubs.acs.org
Publication Date (Web): August 16, 2012 | doi: 10.1021/bk-2012-1106.ch007

might have formed during the reaction. The main side product produced during each step was compound **1** and this was subsequently recycled. Combustion analysis and multinuclear NMR (^{1}H, ^{13}C, ^{19}F, and ^{29}Si) were used to confirm the structure of **2**. The ^{29}Si NMR spectrum of **2** displayed peaks at -58.8, -65.6, -68.0 ppm, with an integration ratio of 2:2:4, due to the C_{2v} symmetry of the silsesquioxane (Figure 7). The peak at -59 ppm was attributed to the silanol group on the POSS structure.

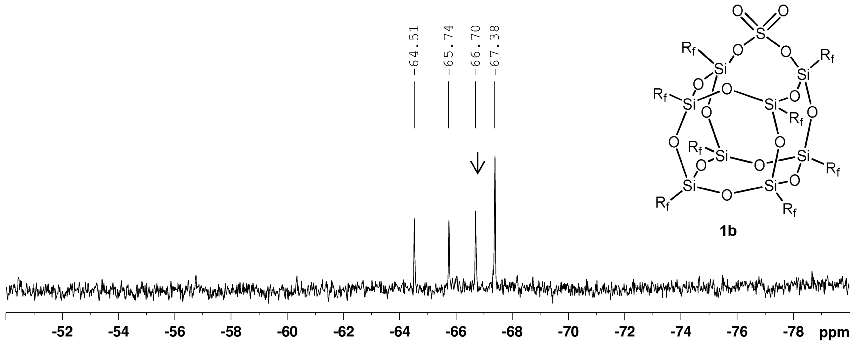

*Figure 5. ^{29}Si NMR of **1b** and **1**. Arrow points to unreacted compound **1** in C_6F_6.*

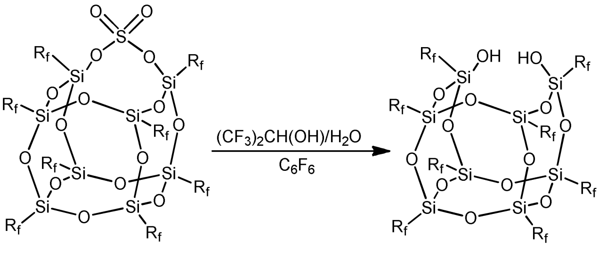

1b **2**

Figure 6. Final reaction of bridged sulfate to disilanol.

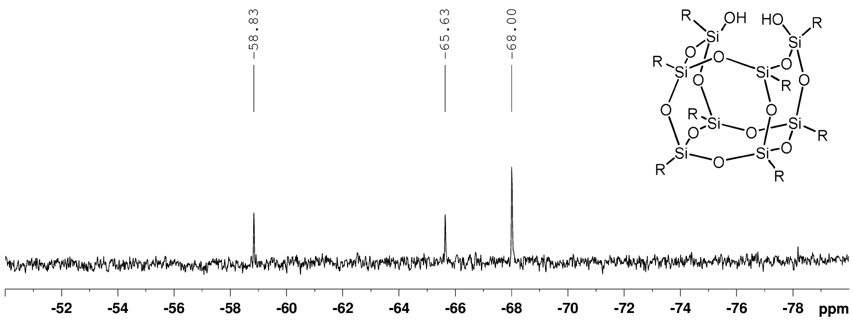

*Figure 7. ^{29}Si NMR of compound **2** in C_6F_6.*

Single crystal X-ray diffraction was used to confirm the structure and absolute stereochemistry of compound **2** (Figure 8). The crystal structure for compound **2** was obtained from crystals grown by the slow evaporation of a C_6F_6 solution. This yielded long clear, colorless, plate-like crystals. The structure was determined to be Monoclinic P2(1)/c with a lattice volume of 12884 Å^3. The structure contains rigid, helical-like fluoroalkyl chains, similar to compound **1**, which are attached to the open Si-O frame-work via methylene groups. The structure confirms the Si integration values established by ^{29}Si NMR spectra with a Si ratio of 2:2:4. This crystal structure contains substantial disorder along the fluorinated chains, due to the mobility of the fluoroalkyl groups.

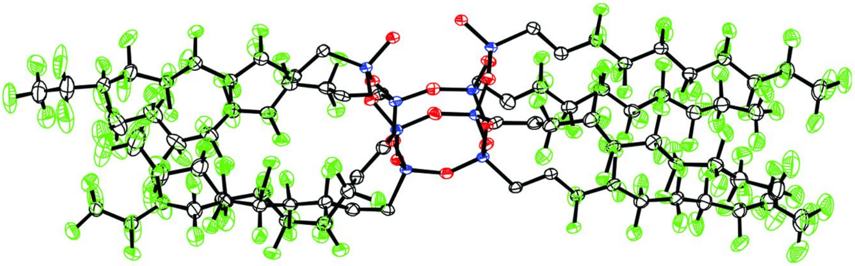

Figure 8. ORTEP representation of compound ***2*** *at 100 K. The fluorinated chains contain substantial disorder. Thermal ellipsoids at 50%. Green F, Black C, Red O, Blue Si. (Hydrogen atoms and disordered segments are omitted for clarity).*

The crystal packing of compound **2** reveals a dimeric structure with two F-POSS cages forming intermolecular hydrogen bonds between silanol groups on adjacent cages (Figure 9). A dimeric contact is established from the intermolecular silanols at a distance of 2.798 Å. These intermolecular silanols are slightly closer than intramolecular silanols at a distance of 2.810 Å. Interestingly, this observed hydrogen bonding forms an eight-membered ring from the O-H···O interaction. Additional groups have observed intermolecular hydrogen bonding between silanols on incompletely-condensed silsesquioxanes for POSS silanols (*12*). This interaction is believed to help stabilize this disilanol structure in solution as well. The disilanol F-POSS structure has a limited stability in solvents other than C_6F_6. For example, hydrochlorofluorocarbon solvent, Asahiklin-225®, is an excellent solvent for closed cage F-POSS compounds, but compound **2** will rapidly reverts to compound **1** when dissolved. The reversion of compound **2** to **1** is attributed to a dehydration of adjacent silanols (Figure 10). Compound **2** is stable in hexafluorobenzene possibly due to the dimerization of the cage in solution.

The endo, endo disilanols on the open POSS framework were found to be reactive to several dichlorosilanes (Figure 11). A variety of functional dichlorosilanes were added to compound **2** to produce a small library of compounds **3-7** (Figure 12). For example, the condensation of **2** with (3-acryloxypropyl) methyldichlorosilane in the presence of triethylamine

Downloaded by STANFORD UNIV GREEN LIBR on August 28, 2012 | http://pubs.acs.org
Publication Date (Web): August 16, 2012 | doi: 10.1021/bk-2012-1106.ch007

Downloaded by STANFORD UNIV GREEN LIBR on August 28, 2012 | http://pubs.acs.org
Publication Date (Web): August 16, 2012 | doi: 10.1021/bk-2012-1106.ch007

produced compound **6** (ca. 67% yield) with the loss of HCl. The primary side product isolated during the reaction was the initial starting material, compound **1**. Multinuclear NMR (^{1}H, ^{13}C, ^{19}F, and ^{29}Si), FT-IR, and combustion analysis were used to confirm the structure of **6**. The ^{29}Si resonances were -17.8, -65.7, -68.2, and -68.9 ppm, with a ratio of 1:2:4:2 (Figure 12). The resonance at -17.8 ppm is attributed the new Si atom in the POSS framework. A new Si resonance was observed in all the ^{29}Si NMRs of the synthesized F-POSS structures. Interestingly, the functionalization of the POSS cage influences the immediate Si-$\underline{C}H_2$ group as observed in ^{13}C NMR (Figure 13). A ratio of 2:4:2 from the symmetry of the POSS cage framework (Figure 14). Strong C-H stretches observed around 2950 and 2860 cm^{-1} in the FT-IR spectrum also confirmed the presence of the added hydrocarbon chains.

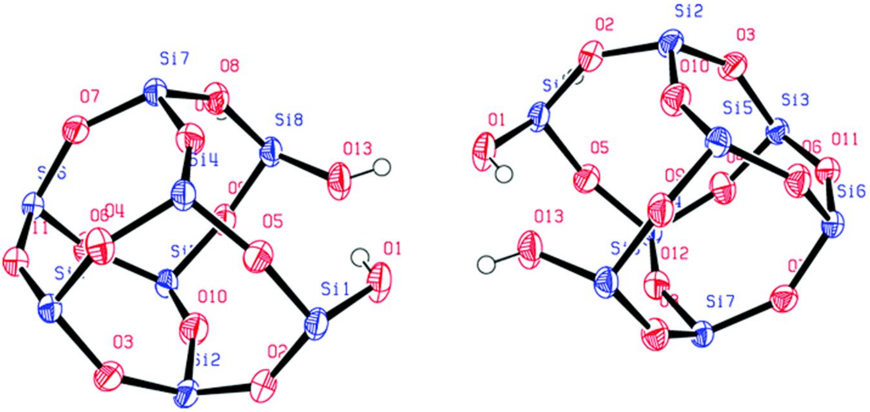

*Figure 9. ORTEP representation of compound **2** in crystal form at 100 K showing the close proximity of disilanols. Thermal ellipsoids at 50%. Green F, Black C, Red O, Blue Si. (Hydrogen atoms and fluorinated chains are omitted for clarity).*

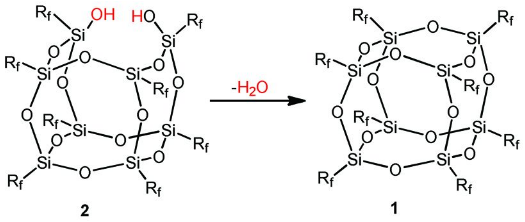

*Figure 10. Representation of reversion of compound **2** to **1** via dehydration.*

Once functionalized, the stability of the F-POSS cage improves substantially. These structures no longer revert to their parent compound **1** and their solubility properties change dramatically dependent on functional moiety. For example, the long hydrocarbon chains present in compound **3** expanded F-POSS solubility to include non-fluorinated solvents, such as Et_2O and $CHCl_3$. Additional modifications, such as the acrylate and methacrylate moieties on structures **6** and **7**, were sufficient enough to expand the solubility of F-POSS to non-fluorinated solvents, such as Et_2O. However, phenyl (**4**) and vinyl (**5**) groups did not improve the solubility of F-POSS in non-fluorinated solvents. This was attributed to rigidity and size of the groups. Solubility increases were improved overall with the addition of an aliphatic chain to the F-POSS structure. Neither asymmetric nor symmetric functionality seem to have a preferential influence on the solubility of these structures (Figure 15).

Downloaded by STANFORD UNIV GREEN LIBR on August 28, 2012 | http://pubs.acs.org
Publication Date (Web): August 16, 2012 | doi: 10.1021/bk-2012-1106.ch007

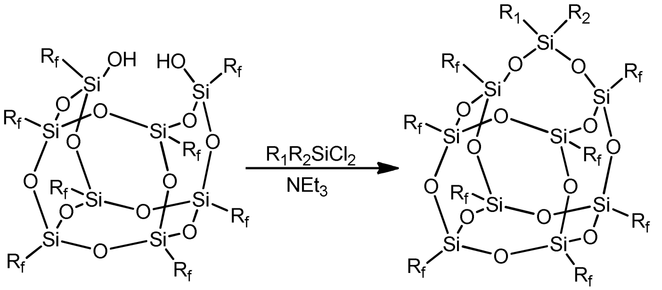

2 **3-7**

Figure 11. Reaction of disilanol F-POSS with dichlorosilanes to produce functional F-POSS compounds.

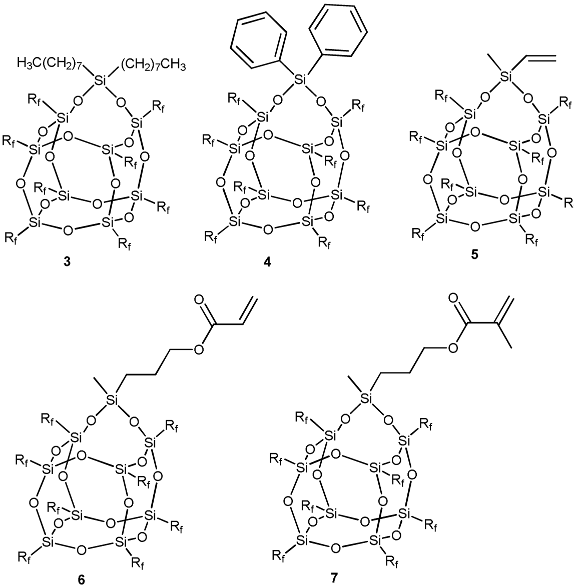

3 **4** **5** **6** **7**

Figure 12. Compounds synthesized from reaction disilanol F-POSS and dichlorosilanes.

Downloaded by STANFORD UNIV GREEN LIBR on August 28, 2012 | http://pubs.acs.org
Publication Date (Web): August 16, 2012 | doi: 10.1021/bk-2012-1106.ch007

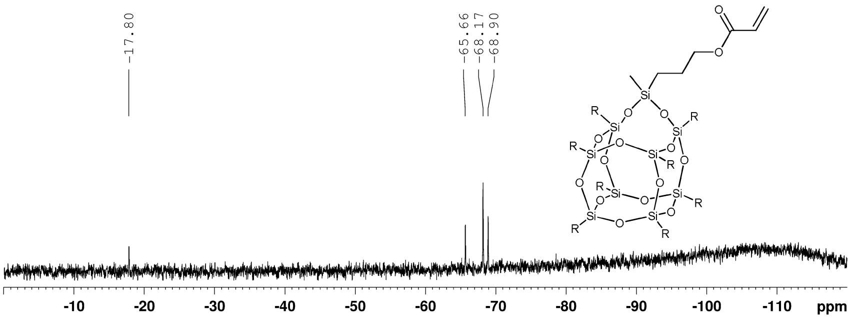

*Figure 13. ^{29}Si NMR of compound **6** in C_6F_6.*

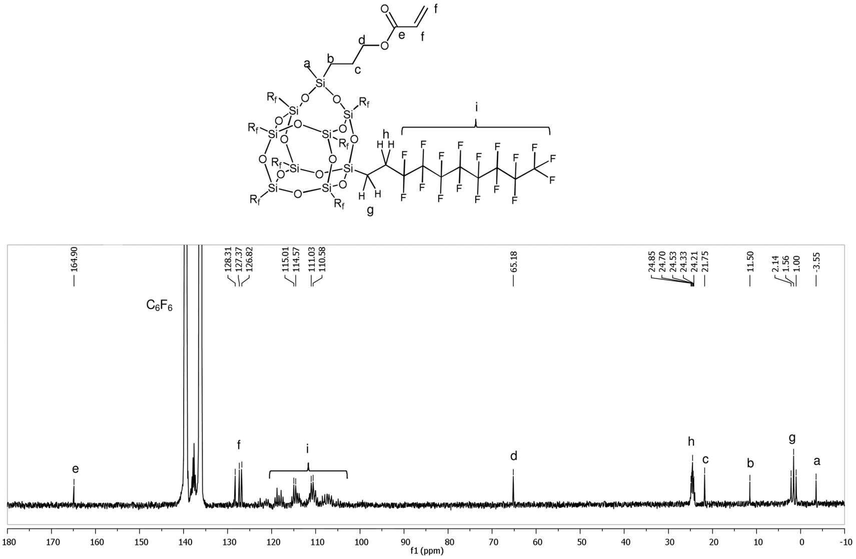

*Figure 14. ^{13}C NMR of compound **6** in C_6F_6. Peak at 128.3 ppm is residual C_6H_6 present in C_6F_6.*

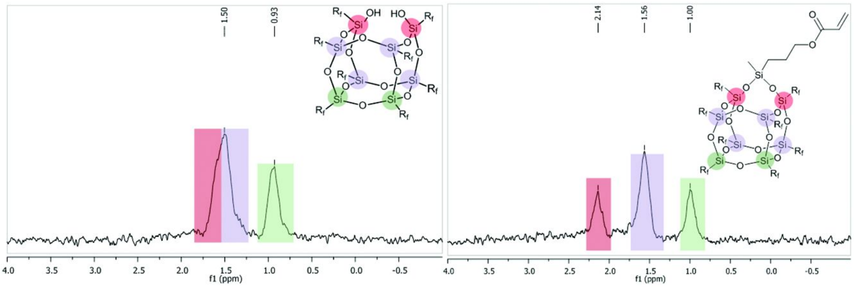

*Figure 15. Zoom in of ^{13}C NMR of compound **1** (left) and compound **6** (right) in C_6F_6. Highlights show the symmetry of the Si cage framework and how functionalization can influence the chemical shifts for Si-$\underline{\mathbf{C}}H_2$-.*

Downloaded by STANFORD UNIV GREEN LIBR on August 28, 2012 | http://pubs.acs.org
Publication Date (Web): August 16, 2012 | doi: 10.1021/bk-2012-1106.ch007

The desirable low surface energy characteristics of F-POSS are partially due to the long chain fluoroalkyl peripheral on the POSS cage framework. To study the influence of functionality on the F-POSS, both static and dynamic contact angle measurements of water and hexadecane were taken of neat films spun cast on SiO_2 wafers (Table 1) (*18*). Water was used to determine the hydrophobicity and hexadecane for oleophobicity. Samples were cast as smooth films to minimize any influence of surface roughness and topology. Surface roughness was measured (< 5 nm rms) with atomic force microscopy and optical profilometry. Dynamic contact angle measurements were used to help determine the effect of functionality on F-POSS. There were no observable adverse effects from the open cage F-POSS framework of compound **2** on non-wetting behavior. This was attributed to the dimeric structure of **2** and the shielding of the silanols from water and hexadecane. A slight increase in contact angle hysteresis, θ_{rec}-θ_{adv}, for the modified compounds (**3**, **5-7**) was observed when wetted with water. This slight increase was not observed for compounds wetted with hexadecane except for compound **3**. Compound **3** contains two long aliphatic (octyl) chains that potentially favor interaction with a long-chain organic solvent, such as hexadecane. Compounds **2** and **4** displayed the lowest hexadecane contact angle hysteresis values of all compounds and compound **4** possessed a sliding angles of ~7° with hexadecane (Figure 16e). These initial measurements provide the platform for further study of these systems with additional solvents.

Table 1. Dynamic contact angle measurements

Compound	***Water***		***Hexadecane***	
	(θ_{adv})	(θ_{rec})	(θ_{adv})	(θ_{rec})
F-POSS	124 ± 0.5°	109.6 ± 0.7°	79.1 ± 0.4°	65.1 ± 0.5°
2	116.8 ± 0.4°	111 ± 0.6°	77.4 ± 0.4°	74.4 ± 0.8°
3	117.9 ± 0.5°	95.5 ± 0.4°	69.1 ± 1.2°	23.1 ± 1.2°
4	116.2 ± 0.4°	110.5 ± 0.5°	76.0 ± 0.8°	73.2 ± 0.4°
5	116.2 ± 0.4°	100.6 ± 0.8°	78.4 ± 0.3°	70.6 ± 2.3°
6	118.2 ± 1.0°	90.6 ± 1.0°	76.8 ± 0.3°	64.8 ± 1.0°
7	117.1 ± 0.6°	93.8 ± 1.5°	78.1 ± 0.4°	63.0 ± 1.2°

After determining the influence of functionality on the F-POSS surface properties, the next step was to investigate the reactivity of the functional group on the F-POSS framework. The methacrylate based F-POSS compound **7** was examined using copolymerization with methyl methacrylate (MMA) *via* free radical polymerization. Unfortunately, any attempts at homopolymerization resulted in the starting macromer with no sign of polymerization. This was attributed to the steric hindrance of the MMA moiety on the F-POSS frame to polymerize with another bulky macromer. To circumvent this problem, copolymerizations with MMA were explored at varying weight ratio percentages of F-POSS to MMA (Figure 17). These initial polymerizations were performed at a low molar ratio of **7**:MMA (1:144) due to the large molecular weight of compound **7** (4,178 g/mol). Multinuclear NMR and size exclusion chromatography (SEC)

Downloaded by STANFORD UNIV GREEN LIBR on August 28, 2012 | http://pubs.acs.org
Publication Date (Web): August 16, 2012 | doi: 10.1021/bk-2012-1106.ch007

was used to characterize (^{1}H, ^{19}F) the polymer. ^{1}H NMR revealed resonance signals at 0.5 – 2 ppm and 3.6 ppm which were attributed to PMMA. The resonances observed in the ^{19}F NMR spectra (-81.1, -109.9, -116.5, -122.3, -123.1, -124.2, -126.9 ppm) were attributed to the fluorinated chains on F-POSS (Figure 1). Molecular weight of the polymers obtained range from 35,000 to 45,000 g/mol with polydispersity indices ~1.4. These polymers were found to be soluble in organic solvents such as tetrahydrofuran and chloroform. Currently a more in-depth analysis of these polymerizations is being undertaken.

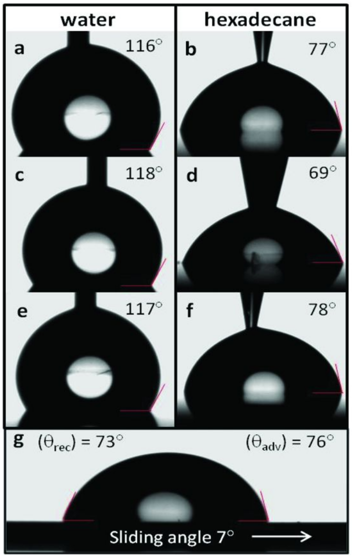

*Figure 16. Static contact angles of smooth surfaces of compounds **2** (a) and (b), **3** (c) and (d), and **4** (e) and (f). Image of hexadecane droplet (10μL) rolling off surface coated with compound **4** (e).*

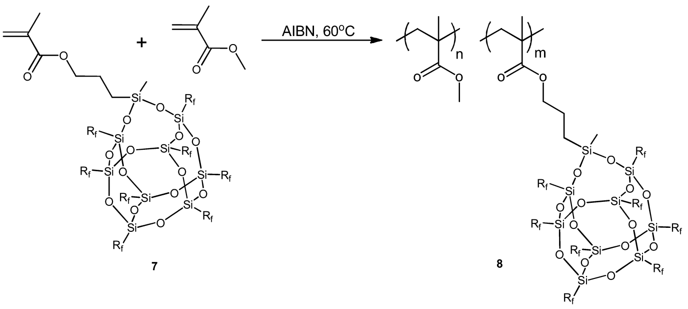

Figure 17. Free radical copolymerization of compound 7 with MMA.

Conclusion

Disilanol F-POSS was synthesized from the fully condensed F-POSS in a three-step reaction process. The disilanol F-POSS crystal structure indicates the silanol groups are hydrogen bonded *via* intra- and intermolecular interactions. The disilanol structure was demonstrated to be reactive toward dichlorosilanes, enabling the production of a variety of functional F-POSS structures, which were found to display similar wetting properties to unmodified F-POSS. Copolymers of MMA and methacylate F-POSS were prepared, demonstrating that functional groups tethered to F-POSS are still reactive. Thus, a novel tunable structure now provides unprecedented access to fluorinated building blocks for low surface energy materials. The methacrylate and acrylate monomers are currently being investigated in a variety of copolymers and are expected to deliver new robust, abrasion resistant, superhydrophobic, and oleophobic material properties.

Acknowledgments

We gratefully acknowledge the Air Force Office of Scientific Research and the Air Force Research Laboratory, Propulsion Directorate for financial support. We thank Peter Müller at the Massachusetts Institute of Technology (MIT) and the American Crystallography Association (ACA) summer course for their assistance with small molecule X-ray crystal structure determination and refinement.

References

1. Cordes, D. B.; Lickiss, P. D.; Rataboul, F. *Chem. Rev.* **2010**, *110* (4), 2081–2173.
2. Lickiss, P. D.; Rataboul, F. *Adv. Organomet. Chem.* **2008**, *57*, 1.
3. Mabry, J. M.; Vij, A.; Iacono, S. T.; Viers, b. D. *Angew. Chem., Int. Ed.* **2008**, *47*, 4137–4140.
4. Iacono, S. T.; Budy, S. M.; Mabry, J. M.; Smith, D. W., Jr. *Macromolecules* **2007**, *40*, 9517–9522.
5. Tuteja, A.; Choi, W.; Mabry, J. M.; McKinely, G. H.; Cohen, R. E. *Proc. Natl. Acad. Sci. U.S.A.* **2008**, *105*, 18200–18205S18200/1-S18200-29.
6. Tuteja, A.; Choi, W.; Ma, M.; Mabry, J. M.; Mazzella, S. A.; Rutledge, G. C.; McKinley, G. H.; Cohen, R. E. *Science* **2007**, *318*, 1618–1622.
7. Chhatre, S. S.; Guardado, J. O.; Moore, B. M.; Haddad, T. S.; Mabry, J. M.; McKinley, G. H.; Cohen, R. E. *ACS Appl. Mater. Interfaces* **2010**, *2*, 3544–3554.
8. Iacono, S. T.; Vij, A.; Grabow, W.; Smith, D. W., Jr.; Mabry, J. M. *Chem. Commun.* **2007**, 4992–4994.
9. Choi, W.; Tuteja, A.; Chhatre, S.; Mabry, J. M.; Cohen, R. E.; McKinley, G. H. *Adv. Mater.* **2009**, *21*, 2190–2195.
10. Iacono, S. T.; Budy, S. M.; Smith, D. W., Jr.; Mabry, J. M. *J. Mater. Chem.* **2010**, *20*, 2979–2984.
11. Haddad, T. S.; Lichtenhan, J. D. *Macromolecules* **1996**, *29* (22), 7302–7304.

Downloaded by STANFORD UNIV GREEN LIBR on August 28, 2012 | http://pubs.acs.org
Publication Date (Web): August 16, 2012 | doi: 10.1021/bk-2012-1106.ch007

12. Haddad, T. S.; Viers, B. D.; Phillips, S. H. *J. Inorg. Organomet. Polym. Mater.* **2001**, *11* (3), 155–164.
13. Pielichowski, K. N.; Njuguna, J.; Janowski, B.; Pielichowski, J. *Adv. Polym. Sci.* **2006**, *201*, 225–296.
14. Phillips, S. H.; Haddad, T. S.; Tomczak, S. J. *Curr. Opin. Solid State Mater. Sci.* **2004**, *8*, 21–29.
15. Koh, K.; Sugiyama, S.; Morinaga, T.; Ohno, K.; Tsujii, Y.; Fukuda, T.; Yamahiro, M.; Iijima, T.; Oikawa, H.; Watanabe, K.; Miyashita, T. *Macromolecules* **2005**, *38*, 1264–1270.
16. Feher, F. J.; Newman, D. A.; Walzer, J. F. *J. Am. Chem. Soc.* **1989**, *111* (5), 1741–1748.
17. Feher, F. J.; Tajima, T. L. *J. Am. Chem. Soc.* **1994**, *116* (5), 2145–2146.
18. Ramirez, S. M.; Diaz, Y. J.; Campos, R.; Stone, R. L.; Haddad, T. S.; Mabry, J. M. *J. Am. Chem. Soc.* **2011**, *133* (50), 20084–20087.
19. Feher, F. J.; Nguyen, F.; Soulivong, D.; Ziller, J. W. *Chem. Commun.* **1999**, 1705–1706.
20. Feher, F. J.; Terroba, R.; Ziller, J. W. *Chem. Commun.* **1999**, 2309–2310.
21. Feher, F. J.; Soulivong, D.; Nguyen, F.; Ziller, J. W. *Angew. Chem., Int. Ed.* **1998**, *37* (19), 2663–2667.
22. Feher, F. J.; Soulivong, D.; Nguyen, F. *Chem. Commun.* **1998**, 1279–1280.
23. Liu, H.; Kondo, S.; Tanaka, R.; Oku, H.; Unno, M. *J. Organomet. Chem.* **2008**, *693*, 1301–1308.

Downloaded by STANFORD UNIV GREEN LIBR on August 28, 2012 | http://pubs.acs.org
Publication Date (Web): August 16, 2012 | doi: 10.1021/bk-2012-1106.ch007

Downloaded by PENNSYLVANIA STATE UNIV on August 28, 2012 | http://pubs.acs.org
Publication Date (Web): August 16, 2012 | doi: 10.1021/bk-2012-1106.ch008

Chapter 8

The Power of Perfluorinated Amphiphilic Polymers at Interfaces

F. E. Golling, T. Schuster, C. Geidel, L. Mammen, D. Vollmer, K. Müllen, and M. Klapper[*]

**Max Planck Institute for Polymer Research, Ackermannweg 10,
55128 Mainz, Germany**
[*]E-mail: klapper@mpip-mainz.mpg.de

In three different examples, it is demonstrated that optimized polymeric perfluorinated amphiphiles are very powerful surface active compounds. Their synthesis and application is highlighted and described in regard to adjusting liquid-liquid and solid-liquid interactions: In particular, (i) fluorous amphiphilic block copolymers were designed to stabilize nonaqueous emulsions, (ii) statistical copolymers were utilized to functionalize and compatibilize the surface of inorganic nanoparticles, and finally (iii) terpolymers were applied to obtain superhydrophobic properties. As perfluorinated copolymers are synthetically easily accessible by free or controlled radical polymerization, they can be readily tailored to the desired needs such as the polarity, stability, and interactions at interfaces. In comparison to low molecular weight compounds, polymers can be easily optimized by altering the composition and therefore the amphiphilicity, the molecular weight influencing the compatibilisation and the type of the hydrophilic monomer for tuning the interaction with polar interfaces.

In Advances in Fluorine-Containing Polymers; Smith, D., et al.;
ACS Symposium Series; American Chemical Society: Washington, DC, 2012.

Downloaded by PENNSYLVANIA STATE UNIV on August 28, 2012 | http://pubs.acs.org
Publication Date (Web): August 16, 2012 | doi: 10.1021/bk-2012-1106.ch008

Introduction

Surface active materials play a decisive role for various applications, such as emulsions (*1*), polymer dispersions (*2*) and coatings (*3*). They are utilized to stabilize interfaces by reducing the interfacial tension. Surfactants are generally divided into two different classes: low and high molecular weight (*M.W.*) amphiphiles as shown in Table I.

Table I. Properties of interface-active substances

Application	*Architecture*	*Role of action*	*Aggregation behavior*
Surfactant	Low *M.W.* "block copolymer"/ molecule	Occupy solvent–air interface	Instable aggregates, fast exchange and decay rates
Emulsifier	High *M.W.* block copolymer	Stabilization of interface between solvents by micelle formation	Stable, kinetically frozen aggregates, slow exchange and decay rates
Surface modifier	Statistical copolymer	Multiple, effective anchoring to particle surface	Instable aggregates, fast exchange and decay rates

Depending on the molecular weight and the composition, they show a different aggregation behaviour and surface active properties (Figure 1). Low *M.W.* amphiphiles have found a wide range of applications especially in the field of emulsion polymerization (*4*), where they are used to stabilize water-oil interfaces. Above the critical micelle concentration (*cmc*), these surface-active molecules form micelles rapidly due to their high diffusion coefficients. In contrast, high molecular weight amphiphiles, generally having a lower *cmc* than small molecules, exhibit a much lower mobility which results in prolonged times until micelle formation reaches an equilibrium state. As amphiphi-lic block copolymers entangle and form kinetically frozen aggre-gates, they disintegrate much slower than small molecules (*5*). Hence, block copolymer emulsifiers provide a higher micelle stability; they can be used for heterophase reactions, even oil-in-oil emulsions (*6*, *7*).

The previously mentioned amphiphiles, though, show either a high mobility or provide good micelle stabilization. For applications such as surface modifications of inorganic nanoparticles, kinetically frozen amphiphiles are often not favourable, since they form non-uniform aggregates which are not in thermodynamic equilibrium and, furthermore, diffuse too slowly onto surfaces of particles. The aggregation of the inorganic particles proceeds faster than the occurrence of stabilization and precipitation. Small molecules, on the other hand, possess the desired mobility and dynamics. However, due to their small size, they may not provide enough steric and electrostatic repulsion to prevent agglomeration. Therefore, statistical amphiphilic copolymers are often used to circumvent drawbacks of the above discussed amphiphiles: They provide both, high mobility and sufficient stabilization, to obtain non-aggregated inorganic nanoparticles (*8*).

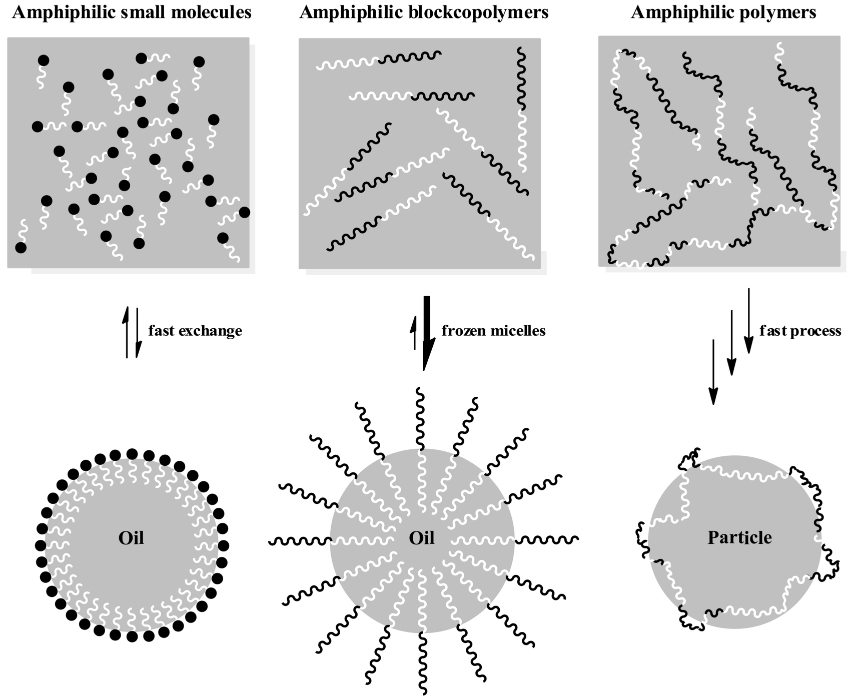

Figure 1. Difference in rate and exchange processes of small molecules, block copolymers and statistical polymers (oil = unpolar organic solvent). (see color insert)

Introducing fluorine to a molecule or polymer will alter its properties, especially its amphiphilicity and solubility (*9*) while also benefiting from its thermal, chemical and biological degradation stability (*10*). Therefore, when choosing molecular architectures comprised of fluorinated and non-fluorinated groups, either lipophilic or hydrophilic, the combined solvophilic and solvophobic behaviour can be utilized to promote amphiphilicity and phase separation. Like their hydrophilic-hydrophobic equivalents (*3*), fluorinated amphiphiles tend to self-aggregate, form supramolecular structures and show a high surface activity depending on architecture and conditions (*9*). Generally, such amphiphiles are known to be more surface active due to a higher hydrophobicity than their corresponding hydrocarbon analogues. As a consequence, not only reduced *cmc* but also lower interfacial tensions can be achieved (*11*). Furthermore, fluorinated amphiphiles form structures with less surface curvature in aqueous solutions than hydrocarbon-based surfactants. This leads to larger molecular volumes of the formed aggregates (*12*). In literature, numerous example have been reported on the use of fluorinated amphiphiles. For instance, to aid the

Downloaded by PENNSYLVANIA STATE UNIV on August 28, 2012 | http://pubs.acs.org
Publication Date (Web): August 16, 2012 | doi: 10.1021/bk-2012-1106.ch008

solubilisation of water in carbon dioxide (CO_2) solvents (*13*), to modify surfaces with fluorous compounds (*14*), e.g. fluorosilanation of SiO_2-particles for water and oil repellence (*15*) and to obtain antifouling coatings (*16*). The strong amphiphilic properties of the fluoropolymers are utilized to weaken interactions with biological adhesives.

In this treatise, we discuss the unique properties of fluorinated and perfluorinated materials (*17*) which have been explored and specially designed for the stabilisation of various interface interactions. Three different approaches are presented where fluorinated polymeric amphiphiles are used. In particular, we consider the stabilization of a nonaqueous fluorous emulsion by a lipophilic-fluorophilic block copolymer. The obtained emulsions are then utilized for heterophase polymerization of α-olefins applying water-sensitive early-transition metal catalysts. Second, *in situ* generated inorganic nanoparticles are stabilized and functionalized by a fluorous amphiphilic statistical terpolymer. The surface modified particles are compatible with perfluorinated matrices and show antibacterial properties. Lastly, the surface of polystyrene-based (*PS*-based), silica-decorated raspberry particles is tuned by a hydrophilic fluorous statistical copolymer achieving super-hydrophobic properties.

Downloaded by PENNSYLVANIA STATE UNIV on August 28, 2012 | http://pubs.acs.org
Publication Date (Web): August 16, 2012 | doi: 10.1021/bk-2012-1106.ch008

Polymeric Particles via Fluorous Emulsions

Heterophase polymerization is a widely applied technique for the synthesis of polymer particles and dispersions ranging from nano-sized up to micrometer-sized particles (*18*). In comparison to homogenous polymerizations, the non-homogenous reaction conditions give rise to good morphology control. Moreover, they enable not only an efficient heat dissipation due to the high surface area of the dispersed droplets, so called “nanoreactors”, but also prevent local overheating and thus suppressing reactor fouling, being especially important for polyolefin synthesis (*19*). Such advantageous properties are also mirrored by its industrial importance: More than 10 million tons of polymer latices are produced annually via heterophase polymerization (*20*). However, as emulsion polymerizations are generally limited to waterborne systems, water-sensitive monomers and catalysts cannot or poorly be applied for heterophase polymerization.

Alternatively, nonaqueous emulsions (*21*) can circumvent this obstacle, resulting in novel and previously inaccessible polymer particles. In literature, a number of different examples have been reported about nonaqueous systems, such as polyaddition reactions of isocyanates and diols (*22*, *23*), polycondensation of acid chlorides and diols (*24*), ring opening polymerization of lactams (*25*), and norbornene derivatives (*26*). All these nonaqueous systems have in common that they are based on an unpolar solvent (e.g. cyclohexane) as the continuous phase, and a polar solvent (e.g. DMF, DMSO, MeCN) as the dispersed phase. These intrinsic properties limit the applicability, making it necessary that one component is exclusively soluble in the dispersed phase, otherwise the polymerization would also take place in the continuous phase and render heterophase polymerizations obsolete. Besides, early transition metal catalysts such as metallocenes do not or poorly tolerate nitrile or carbonyl groups which are present in the above described nonaqueous emulsions. To overcome these short-comings, we developed a nonaqueous fluorous emulsion based on a perfluorinated solvent, the continuous phase, and an unpolar solvent (toluene), the dispersed *phase* (*27*). This heterophase system enables the use of two components that are soluble in unpolar solvents as well as polymerization catalysts that are prone to decompose in polar solvents, such as early transition metal catalysts, e.g. metallocenes (Figure 2).

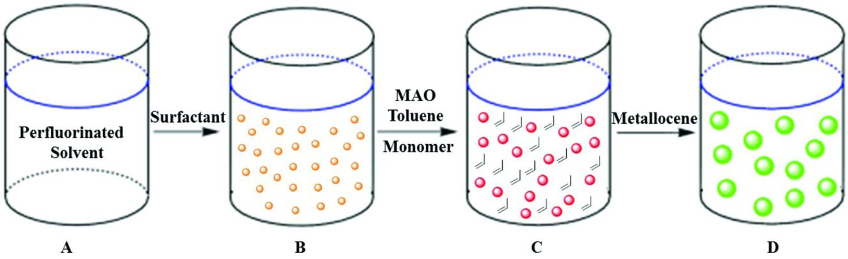

Figure 2. Polymerization procedure for the synthesis of polyolefin nanoparticles. (see color insert)

As shown in Figure 2, perfluormethylcyclohexane (*PFMCH*) was used as the continuous phase and toluene as the dispersed phase. To stabilize the biphasic mixture, we opted for a fluorophilic-lipophilic block copolymer which provides higher micelle stabilization than small molecules. A high-molecular-weight emulsifier was synthesized by nitroxide mediated polymerization (*NMP*) consisting of *PS* and a poly(pentafluorostyrene) (*PFS*) block, having a molecular weight M_n of about 49.000 g/mol (Scheme 1). The ratio of the two blocks, *PS* vs. *PFS*, was approximately 1:1. To increase the fluorophilicity of the pentalfluorophenyl rings, a perfluoroalkoxy chain was introduced at the *para*-position of the pentafluorophenyls via a nucleophilic aromatic substitution; a degree of perfluoroalkoxylation between 40-50% was achieved. The copolymer **I** was then used to successfully stabilize the nonaqueous fluorous emulsion described above. Light scattering measurements indicated the formation of stable droplets without change of size over a broad range of temperature (25 °C – 70 °C); furthermore, with increasing emulsifier concentration, a decrease of micelle radius was observed from 105 nm (1 wt.-% emulsifier) to 45 nm (10 wt.-% emulsifier) (*28*). Such trends are in agreement with expectations, as they were also found for aqueous emulsions.

To synthesize polyolefine nanoparticles via nonaqueous fluorous emulsion, the lipophilic-fluorophlic block copolymer **I** was dissolved in *PFMCH* (continuous phase) forming micelles after short ultrasonification. Subsequent addition of the monomer, such as ethylene or propylene, the methylaluminoxane (*MAO*) cocatalyst and toluene (dispersed phase) yielded the emulsion described above. In the last step, an *ansa*-metallocene was added, which efficiently catalyzes the polymerization of α-olefins. As shown in the SEM-micrographs (Figure 3), heterophase polymerization of ethylene and propylene afforded polyethylene (*PE*) and polypropylene (*PP*) with particle sizes ranging from 30 nm up to 20 µm. M_n up to 450.000 g/mol were achieved.

Downloaded by PENNSYLVANIA STATE UNIV on August 28, 2012 | http://pubs.acs.org
Publication Date (Web): August 16, 2012 | doi: 10.1021/bk-2012-1106.ch008

Downloaded by PENNSYLVANIA STATE UNIV on August 28, 2012 | http://pubs.acs.org
Publication Date (Web): August 16, 2012 | doi: 10.1021/bk-2012-1106.ch008

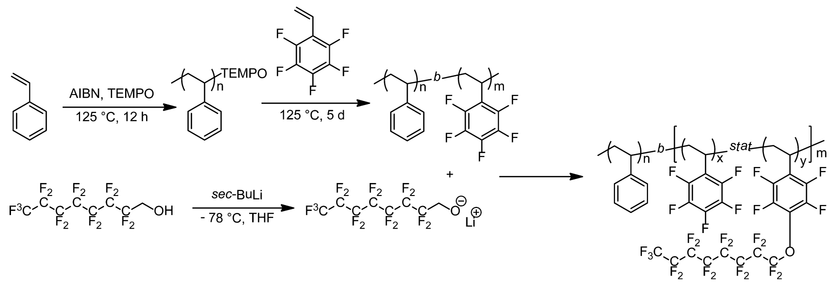

I

*Scheme 1. Synthesis of fluorophilic-lipophilic block copolymer emulsifier **I**; PS-b-PFS; M_n= 49.000 g/mol; degree of perfluoroalkoxylation: 40-50%; block ratio of polymer 1:1,2.*

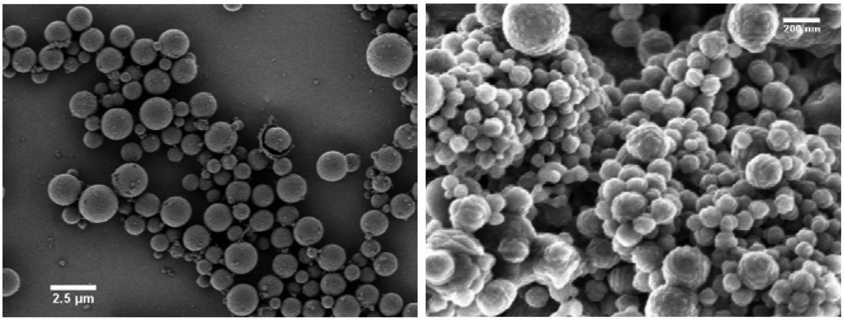

Figure 3. SEM micrographs of polyethylene (PE) particles (left) and polypropylene (PP) particles (right) obtained via fluorous nonaqueous emulsion. (see color insert)

However, as the reaction is diffusion-limited, relatively low polymerization rates (400 kg *PP*·(mol Zr·h)$^{-1}$) were observed. To overcome this drawback, the polymerization was performed under miniemulsion conditions. This is a heterophase technique where the monomer is exclusively dissolved in the dispersed droplets (*29*). As no solvent reservoirs are formed in the continuous phase, the monomer is entirely present at the locus of polymerization. To achieve such conditions, we used liquified propylene under increased pressure instead of gaseous α-olephins. As diffusion is less important, a nearly tenfold increase of polymerization rate was observed (*28*).

In conclusion, we designed a tailor-made fluorophilic-lipophilic block copolymer which gave rise to stable fluorous-organic emulsions. The dispersed organic droplets were used as nanoreactors for the heterophase polymerization of ethylene and propylene. With the synthesis of polyolefin particles, we could demonstrate the feasibility of nonaqueous fluorous emulsions as a novel and additional tool for heterophase polymerization, especially regarding water-sensitive catalysts.

Downloaded by PENNSYLVANIA STATE UNIV on August 28, 2012 | http://pubs.acs.org
Publication Date (Web): August 16, 2012 | doi: 10.1021/bk-2012-1106.ch008

Surface Modification via Fluorinated Copolymers

In the first part, we considered liquid-liquid interfaces by using block copolymers, whereas now we will focus on the stabilisation and compatibilisation of inorganic nanoparticles into fluorinated bulk materials, applying statistical terpolymers. Organic–inorganic hybrid materials have attracted substantial interest in polymer and material science and significantly improved or even led to novel properties by the incorporation of inorganic particles in polymer matrices (*30*) For instance, the mechanical enhancement of polymers (*31*), antibacterial materials (*32*), materials for sensors (*33*), etc. are accessible.

Among polymeric materials, fluoropolymers, especially polytetrafluoroethylene (*PTFE*), were investigated owing to the high thermal, biological and mechanical stability and were implemented in microelectronic devices (*34*), as antifouling or antifogging agents (*35*), coatings and medical applications (*36*), e.g. contact lenses or implants. Especially the fabrication of antibacterial composites based on a perfluorinated polymeric matrix and e.g. incorporation of silver particles is still a challenge for the fabrication of antibacterial vascular prostheses (*37*); insufficient surface modification leads to aggregation or separation from the fluorinated phase. Hence, particles require specific surface modification by suitable agents to be compatible with, in this case, the fluorinated matrix (*38*). Block copolymers and statistical copolymers have demonstrated good performance for surface modification in this context (*39*). Commonly applied routes for appropriate surface functionalization of inorganic nanoparticles are based on emulsion techniques, transfer and grafting processes and deal with oxides, sulfides, phosphonates, sulfates, carbonates (*40*). In particular, we studied the formation of Cu and Ag particles which were generated by laser ablation, i.e. a method allowing the synthesis of spherical particles by means of a laser beam from bulk metal without much preparative effort, unlike conventional methods (*41*).

As shown in Figure 4, metal nanoparticles were synthesized by using laser ablation and a dispersing solvent. In order to stabilize *in situ* formed particles fast enough avoiding self-aggregation, appropriate emulsifiers were developed using easily accessible statistical copolymers based on poly(p-hydroxystyrene) and poly(methacrylate) (Scheme 2) (*42*).

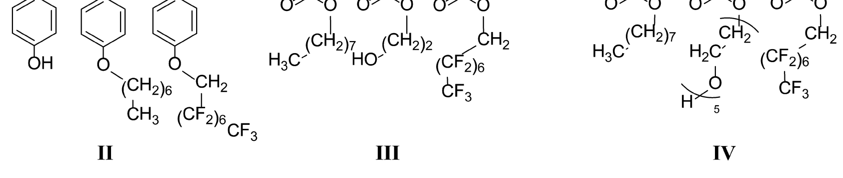

Scheme 2. Structures of amphiphilic polymers used for stabilization of metal particles.

In general, stabilization of the particles was achieved by a terpolymer with a) anchor groups which efficiently adsorb on the surface of particles avoiding aggregation, b) solvophilic groups providing solubility in the organic solvent used during the laser ablation process to form a stable dispersion, and c) fluorophilic groups making the hybrid material compatible with the fluorinated matrix.

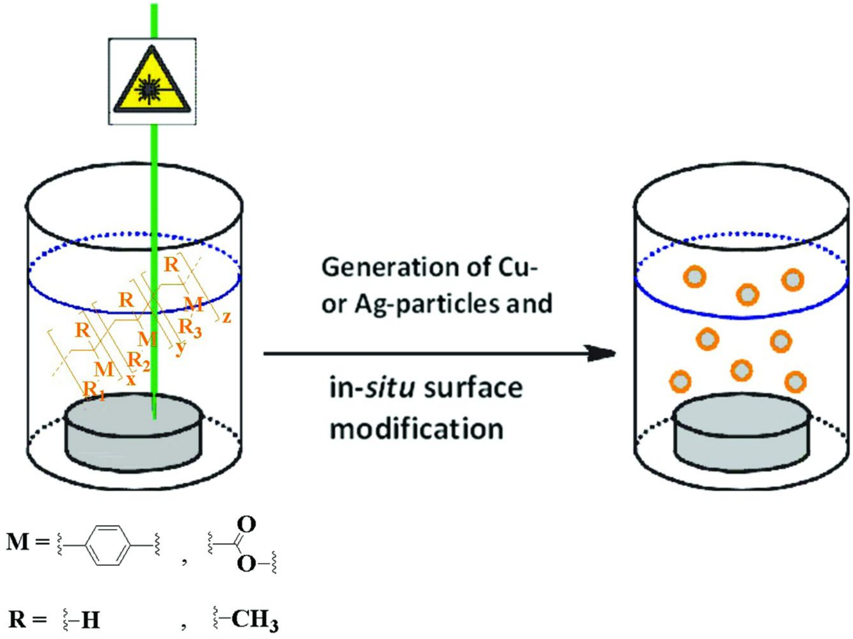
R
R
R
M
M
M
z
R_3
y
R_2
x
R_1
Generation of Cu- or Ag-particles and
in-*situ* surface modification
M =
,
O
O
R = -H
, -CH_3

Figure 4. In situ preparation of polymer stabilized metal particles via laser ablation in a copolymer solution (R_1 = alkyl chain, R_2 = perfluorinated alkyl chain, and R_3 = anchor group). (see color insert)

Once the surface adsorption of polymers slows down, such particles coalesce and eventually precipitate. This confirms our decision for stastistical copolymers, as they are in solution as "unimeric" aggregates, guaranteeing a fast adsorption before aggregation becomes important. Block copolymers, on the other hand, typically form larger micelles which have very slow diffusion and therefore longer reaction times with the particles. Similarly, without the use of amphiphilic copolymers dissolved in the overlaying organic solvent, metal particles generated by laser power tend to form aggregates. Also, when applying solutions of **III** in laser ablation, a black precipitate was obtained. In contrast, no aggregation or opacity was observed in the case of **II** and **IV**. The OH-anchor groups of copolymer **III** did not provide sufficient interaction with the *Lewis*-acidic inorganic surface, and consequently, the particles precipitated from solution. In contrast, the p-hydroxyphenyl and oligo(ethylene glycol) groups of **II** and **IV**, respectively, provided sufficient stabilisation to form non-aggregated metal nanoparticle dispersions.

Downloaded by PENNSYLVANIA STATE UNIV on August 28, 2012 | http://pubs.acs.org
Publication Date (Web): August 16, 2012 | doi: 10.1021/bk-2012-1106.ch008

Downloaded by PENNSYLVANIA STATE UNIV on August 28, 2012 | http://pubs.acs.org
Publication Date (Web): August 16, 2012 | doi: 10.1021/bk-2012-1106.ch008

Characterization of particles formed in the tetrahydrofuran (*THF*) solution was conducted by dynamic light scattering (*DLS*), transmission electron microscopy (*TEM*) and energy dispersive X-ray spectroscopy (*EDX*). The average particle radius from *TEM* micrographs was 23 ± 8 nm for **II**/Ag and 19 ± 5 nm for **II**/Cu. Since *TEM* allows differentiation between organic and inorganic domains, the measured radii from *TEM* displayed more precise values than *DLS*. The radius distribution obtained from *DLS* showed, as expected, larger particles with an average radius of approx. 25 nm for silver and 15 nm for copper. A slight bimodality was observed, as well as larger particles ranging between 30–100 nm.

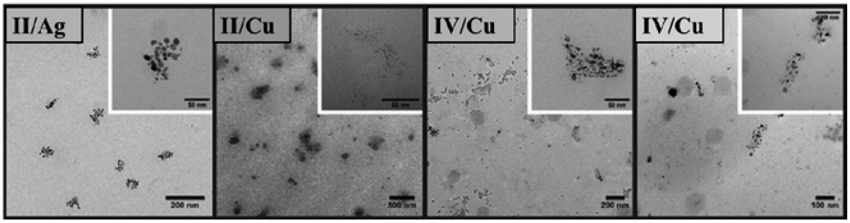

Figure 5. TEM micrographs of samples A) ***II****/Ag, B)* ***II****/Cu, C)* ***IV****/Ag and D)* ***IV****/Cu prepared by drop casting a 0.8 mg/ mL THF solution on copper or gold grids. (see color insert)*

Likewise, for **IV** 13 nm for silver and 7 nm for copper were calculated from *TEM* micrographs, providing evidence of mostly single, non-aggregated particles. Agglomerated particles, depicted in Figure 5, were referred to the sample preparation technique (drop casting) and not to the laser ablation process, since magnification revealed the presence of a polymeric layer. The hydrophobic layer provided steric hindrance, preventing particles to come in contact with each other. *EDX* measurements proved the existence of elemental silver and copper nanoparticles (*42*). In order to examine the compatibility of modified metal particles with perfluorinated polymer matrices on a laboratory scale, particles were incorporated into *PFS* and poly(1H,1H-heptafluorobutyl methacrylate) (*PFBA*). After removal of the solvent, the distribution of metal particles in the product was investigated by *TEM*. The micrographs in Figure 6 show a homogeneous distribution of the modified particles, indicating sufficient compatibility with the fluorinated matrix. As *PFS* and *PFBA* are highly fluorinated, these particles are also expected to be compatible with perfluorinated matrices, e.g. *PTFE*.

The antimicrobial properties of the final composites consisting of *PFS* or *PFBA*, respectively, and metal particles, were studied by exposure to *E. coli* from the *Gram*-negative class, being responsible for more than 80 % of the postoperative infections (*43*). No bacterial growth was observed for hybrid materials of **II**/Ag in *PFS* and **IV**/Ag in *PFS*, demonstrating the antimicrobial properties of the composites (*42*).

Downloaded by PENNSYLVANIA STATE UNIV on August 28, 2012 | http://pubs.acs.org
Publication Date (Web): August 16, 2012 | doi: 10.1021/bk-2012-1106.ch008

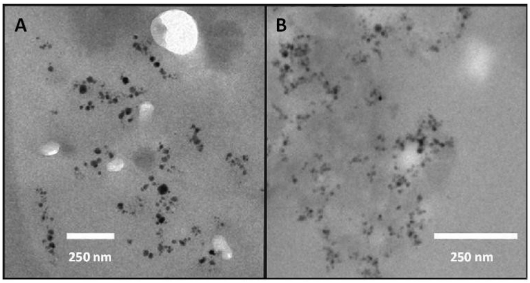

Figure 6. TEM micrographs of hybrid composites of A) ***II****/Ag and PFS and B)* ***IV****/Ag and PFS; samples were prepared by embedding the composite film into an epoxy resign and subsequent ultra microtoming. (see color insert)*

In conclusion, metal particles can be stabilized and functionalized *in situ* by the use of statistical terpolymers before aggregation occurrs. The architecture of the amphiphilic terpolymer consists of a solubilizing (lipophilic), an anchor (*Lewis*-basic) and a compatibilizing (fluorophilic) domain. By obtaining stable colloidal solutions of metal particles, the effectiveness of the anchor group in polymer **II** and **IV** as well as the solubilizing groups were shown. Additionally, the fluorophilic groups enabled incorporation into highly fluorinated matrices.

Preparation of Superhydrophobic Surfaces

In the following example also utilizing polymeric amphiphiles, we describe the use of a statistical copolymer containing fluorous, hydrophobic, and hydrophilic anchoring groups to obtain water repellent surface properties. Superhydrophobicity requires roughness on different length scales and a material with low surface tension (*49*). For the preparation of such superhydrophobic surfaces, structures derived from nature can be mimicked such as the cuticle of petals of the lotus plant (*44*). Its epidermis is exceedingly rough while additionally being covered with waxy trichomes. For industrial applications, biomimetic materials derived from the lotus leaf are promising due to their self-cleaning and anit-biofouling properties (*45*).

When a droplet of a liquid comes in contact with a superhydrophic surface, air is trapped in small cavities between the eversions, increasing the macroscopic contact angle (*CA*) observed in comparison to microscopically even geometries (*46*). Surfaces are generally defined as “superhydrophobic” if the *CA* measured for a water droplet exceeds 150°, and the drop rolls off when the surface is tilted by less than 10°. The maximum *CA* reported for water on a smooth surface is approximately 120° (fluorinated surfaces) (*47*). Raspberry-like particles (Figure 7) are promising constituents to prepare superhydrophobic surfaces (*48*), because a few tens of nm-sized particles are attached or grown on µm-sized particles, thus generating a roughness on the nano- and micrometerscale.

Downloaded by PENNSYLVANIA STATE UNIV on August 28, 2012 | http://pubs.acs.org
Publication Date (Web): August 16, 2012 | doi: 10.1021/bk-2012-1106.ch008

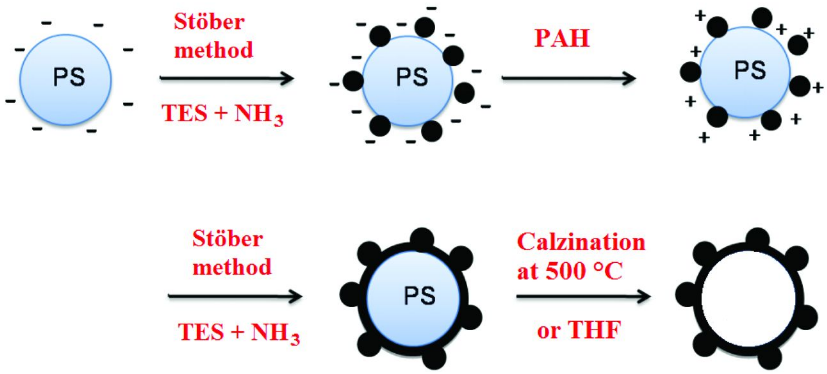

Figure 7. Schematic description of the synthesis PS based raspberry particles; PAH = polyallylamine hydrochloride, TES = tetraethoxysilane, NH_3 = ammonia. (see color insert)

The raspberry-like particles used for this work were synthesized in three steps. First, *PS* spheres with a diameter of 400 nm to 1 µm were prepared by soap-free emulsion polymerization of styrene. Small silica particles < 100 nm in size were then attached to the *PS* colloids, thus introducing surface asperities on a second length scale (Figure 7) (*49*). The number of silica particles on the *PS* core can be tuned by the amount of the comonomer, acrylic acid, added to the soap-free emulsion polymerization; its size can be adjusted by the amount of tetraethoxysilane (*TES*) used in the Stöber reaction (*50*). To prevent the silica particles from detaching of the surface of the *PS* spheres, and to improve the mechanical resistance of the raspberry-like particles, they were completely coated with a smooth silica shell of 10 nm to 40 nm thickness. To ensure growing of a smooth shell, the particles were first coated with the positively charged polyelectrolyte polyallylamine hydrochloride (*PAH*) followed by a second Stöber reaction. As the raspberry-like particles can be dispersed in water, multilayers were prepared either by drop casting or dip coating. To improve the scratch resistance, neighboring particles were chemically bound to each other and to the surface via silica bridges. They were formed during chemical vapor deposition (*CVD*) of *TES* catalyzed by ammonia suited to optimize interface interactions (*51*). After removing the *PS* core by washing with *THF*, or after calcination at 500 °C, the thin coatings turned transparent, resulting in hollow silica particles. To reduce the surface tension, on the one hand, the silica surface was functionalized by *CVD* of trichloroperfluoro-alkylsilanes, and, afterwards superhydrophobic properties were observed (*49*).

On the other hand, alternatively to coating them with semi-fluorinated silanes as described in the previous paragraph, the silica surface was also modified by amphiphilic fluoropolymers **V** – **VII** containing polar anchor groups and fluorinated groups (Scheme 3).

Downloaded by PENNSYLVANIA STATE UNIV on August 28, 2012 | http://pubs.acs.org
Publication Date (Web): August 16, 2012 | doi: 10.1021/bk-2012-1106.ch008

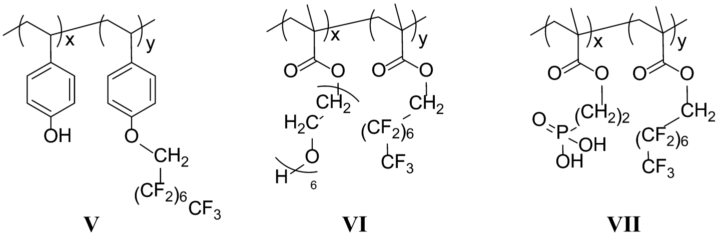

V **VI** **VII**

Scheme 3. Structures of amphiphilic polymers used for preparation of superhydrophobic surfaces.

Copolymer **V** was prepared by a *Williamson* etherification of poly(*p*-hydroxystyrene) with 1H,1H-perfluorooctylbromide (*42*). **VI** and **VII** were synthesized by a free radical polymerization with *FOMA* and *PEOMA* or (7-(methacryloyloxy)heptyl)phosphonic acid, respectively. Copolymer with varying composition, ranging from polar to unpolar (80:20 → 5:95), were synthesized and characterized by ^{1}H-NMR spectroscopy. Relative molecular weights for copolymers **V-a**, **V-b**, and **VI-a** were measured by size exclusion chromatography (*SEC*) and were in the range of 4000 to 6000 g/mol against *PS* standards.

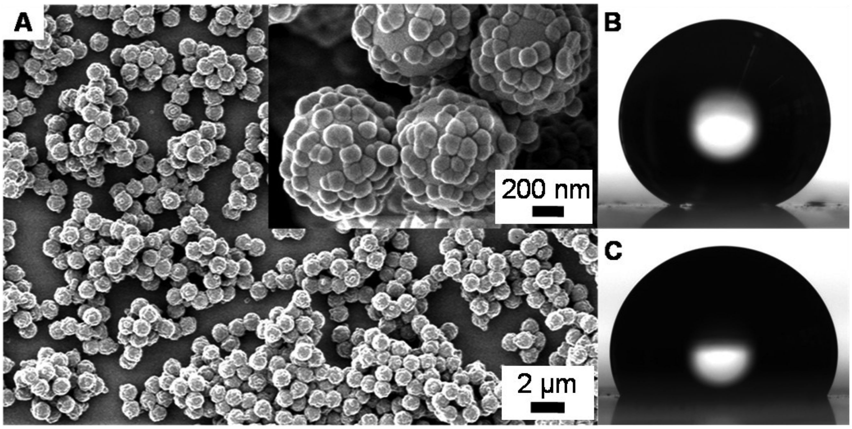

Figure 8. A) Scanning electron micrograph of a surface of irregular distributed hollow raspberry particles on a glass substrate prepared by dip coating. B) Photograph of a 3 µl water and C) tetradecane droplet deposited on the surface. The surfaces show a static contact angle for water of 153° and for tetradecane of 115°. (see color insert)

For surface modification with amphiphilic fluoropolymers, surfaces of irregularly distributed raspberry-like particles were prepared by dip coating (Figure 8). Therefore, glass substratess were dipped into a solution of *PAH* and subsequently into a dispersion of raspberry-like particles. The *PS* cores were removed by calcination and the surfaces were mechanically stabilized via silica bridges formed by *CVD* of *TES*. The mechanically stabilized “raspberry surfaces” were dipped into a solution of the fluoropolymers dissolved in a mixture of *THF* (**V-a**, **V-b**, **VI-a**, **VII-a**) and *PFMCH* (**VI-b**, **VII-b**, **VII-c**, **VII-d**), respectively. Subsequently, excess fluoropolymers were washed off and the surface was dried *in vacuo*. Results of the static *CA* measured for water and tetradecane are given in Table II.

Table II. Measured contact angles (*CAs*) for mechanically stabilized raspberry surfaces coated with copolymers of different compositions

Copolymer	*x : y*	*Static CA (water)*	*Static CA (tetradecane)*
V-a	80 : 20	137 ± 8°	< 90°
V-b	70 : 30	147 ± 2°	< 90°
VI-a	82 : 18	130 ± 10°	< 90°
VI-b	15 : 85	162 ± 3°	147 ± 1°
VII-a	20 : 80	157 ± 2°	149 ± 2°
VII-b	15 : 85	162 ± 3°	147 ± 1°
VII-c	10 : 90	161 ± 2°	149 ± 2°
VII-d	5 : 95	162 ± 2°	147 ± 3°

Raspberry surfaces coated with **V-a** and **V-b** show *CA*s with water below 150°; the same results were observed for **VI-a**. The incorporation of 20 to 30 mol% of fluorophilic groups was insufficient to achieve water or tetradecane repellence, as the high amount of hydrophilic anchoring groups counteracted the desired properties. In contrast, when copolymer **VI-b** was examined, consisting of 85 mol% fluorinated repeating units and 15 mol% polyethyleneglycol anchoring groups, superhydrophobic behaviour and high *CA*s for tetradecane of approx. 150° were obtained indicating oleophobicity. Similarly, raspberry particle surfaces coated with **VII-a**, **VII-b**, **VII-c** and **VII-d**, containing phosphonic acid groups as anchoring groups, consistently resulted in *CA*s for water > 160°.

The described statistical copolymers pave the way for an easy and efficient method to obtain water and oil repellent surfaces. After dipping the polar raspberry surfaces in a solution containing a high *M.W.* unpolar copolymer, *CA*s exceeding 160° for water and *CA*s of almost 150° for tetradecane were observed.

Conclusion

The utilization of fluorous high *M.W.* amphiphiles leads to materials having novel or enhanced interface active features, such as stabilization of a liquid-liquid-interface, surface modification and compatibilisation, and superhydrophobic properties. It is demonstrated that the properties can be optimized by free (statistical polymer) or by the more sophisticated controlled

Downloaded by PENNSYLVANIA STATE UNIV on August 28, 2012 | http://pubs.acs.org
Publication Date (Web): August 16, 2012 | doi: 10.1021/bk-2012-1106.ch008

(block copolymer) radical polymerization. The composition of the copolymers can simply be changed by varying the monomer concentration. Depending on the application, co- or terpolymers with hydrophobic and/or hydrophilic comonomers were synthesized. In the first example, the synthesis of a fluorophilic-lipophlic high *M.W.* block copolymer, to stabilize fluorous non-aqueous emulsions, was described. A hydrocarbon-perfluorocarbon mixture was utilized for the metallocene-catalyzed synthesis of unprecendented polyolefin nanoparticles. In contrast to most of the applied waterborne systems, these non-aqueous emulsions enable the feasibility of moisture sensitive catalysts. Therefore, this technique renders an additional tool for heterophase polymerization. Further, fluorous amphiphilic polymers were used to stabilize *in situ* generated inorganic particles as well as to modify the surface. The fluorous coating compatibilized the particles for the homogenous incorporation into fluorous matrices. Such materials are often applied for vascular prosthesis. Notably, it was proven that the matrix-embedded silver particles possessed antibacterial properties, rendering it an interesting synthetic approach for medical applications. Finally, the surface of hydrophilic particles could successfully be modified by a fluorous-hydrophilic statistical copolymer yielding superhydrophobic coatings. *CA*s well above 150 ° were obtained with optimized copolymers containing fluorous and *Lewis*-basic anchoring groups. The given examples demonstrate not only the efficiency, but also the straightforward synthesis, adjustment and versatile applicability of perfluorinated amphiphiles.

Downloaded by PENNSYLVANIA STATE UNIV on August 28, 2012 | http://pubs.acs.org
Publication Date (Web): August 16, 2012 | doi: 10.1021/bk-2012-1106.ch008

References

1. Garti, N.; Bisperink, C. *Curr. Opin. Colloid Interface Sci.* **1998**, *3*, 657–667.
2. Distler, D. Herstellung von Polymerdispersionen. In *Waeßrige Polymerdispersionen: Synthese, Eigenschaften, Anwendungen*; Wiley-VCH: Weinheim, Germany, 2005
3. Schramm, L. L. *Dictionary of Colloid and Interface Science*, 2nd; John Wiley & Sons: New York, 2001.
4. Urban, D.; Takamura, K. *Polymer Dispersions and Their Industrial Applications*; Wiley-VCH: Weinheim, Germany, 2002.
5. Riess, G. *Prog. Polym. Sci.* **2003**, *28*, 1107–1170.
6. Atanase, L.-I.; Riess, G. *Polym. Int.* **2011**, *60*, 1563–1573.
7. Klapper, M.; Nenov, S.; Haschick, R.; Mueller, K.; Muellen, K. *Acc. Chem. Res.* **2008**, *41*, 1190–1201.
8. Stelzig, S. H.; Klapper, M.; Muellen, K. *Adv. Mater.* **2008**, *20*, 929–932.
9. Matsuoka, K.; Moroi, Y. *Curr. Opin. Colloid Interface Sci.* **2003**, *8*, 227–235.
10. Krafft, M. P.; Riess, J. G. *Biochimie* **1998**, *80*, 489–514.
11. Krafft, M. P; Riess, J. G *Chem. Rev.* **2009**, *109*, 1714–1792.
12. Wang, K.; Karlsson, G.; Almgren, M. *J. Phys. Chem. B* **1999**, *103*, 9237–9246.
13. Keiper, J. S.; Simhan, R.; DeSimone, J. M. *J. Am. Chem. Soc.* **2002**, *124*, 1834–1835.

Downloaded by PENNSYLVANIA STATE UNIV on August 28, 2012 | http://pubs.acs.org
Publication Date (Web): August 16, 2012 | doi: 10.1021/bk-2012-1106.ch008

14. Krafft, M. P.; Goldmann, M. *Curr. Opin. Colloid Interface Sci.* **2003**, *8*, 243–250.
15. Deng, X.; Mammen, L.; Butt, H.-J.; Vollmer, D. *Science* **2012**, *335*, 67–70.
16. Wang, Y.; Pitet, L. M.; Finlay, J. A.; Brewer, L. H.; Cone, G.; Betts, D. E.; Callow, M. E.; Callow, J. A.; Wendt, D. E.; Hillmyer, M. A.; DeSimone, J. M. *Biofouling* **2011**, *27*, 1139–1150.
17. In this article, the terms "fluoro", "fluorous", or "fluorinated" are referred to organic molecules comprising a high content of C-F bonds. The prefix "perfluor" will be used in the context of molecules having replaced all C-H bounds by C-F bounds.
18. Antonietti, M.; Tauer, K. *Macromol. Chem. Phys.* **2003**, *204*, 207–219.
19. Klapper, M.; Nenov, S.; Diesing, T.; Muellen, K. *Macromol. Symp.* **2007**, *260*, 90–97.
20. Mecking, S. *Colloid Polym. Sci.* **2007**, *285*, 605–619.
21. Haschick, R.; Hoffmann, M. S.; Zhao, Y.; Klapper, M.; Muellen, K. *Macromol. Symp.* **2010**, *296*, 21–27.
22. Haschick, R.; Mueller, K.; Klapper, M.; Muellen, K. *Macromolecules* **2008**, *41*, 5077–5081.
23. Crespy, D.; Stark, D.; Hoffmann-Richter, C.; Ziener, U.; Landfester, K. *Macromolecules* **2007**, *40*, 3122–3135.
24. Mueller, K.; Klapper, M.; Muellen, K. *J. Polym. Sci., Part A: Polym. Chem.* **2007**, *45*, 1101–1108.
25. Haschick, R.; Klapper, M.; Wagener, K. B.; Muellen, K. *Macromol. Chem. Phys.* **2010**, *211*, 2547–2554.
26. Crespy, D.; Landfester, K. *Macromolecules* **2005**, *38*, 6882–6887.
27. Nenov, S.; Clark, C. G., Jr.; Klapper, M.; Muellen, K. *Macromol. Chem. Phys.* **2007**, *208*, 1362–1369.
28. Nenov, S.; Hoffmann, M. S.; Steffen, W.; Klapper, M.; Muellen, K. *J. Polym. Sci., Part A: Polym. Chem.* **2009**, *47*, 1724–1730.
29. Landfester, K. *Angew. Chem., Int. Ed.* **2009**, *48*, 4488–4507.
30. Gomez-Romero, P.; Sanchez, C. In *Functional Hybrid Materials*; Wiley-VCH: Weinheim, Germany, 2004.
31. Crosby, A. J.; Lee, J. Y. *Polym. Rev.* **2007**, *47*, 217–229.
32. Weir, E.; Lawlor, A.; Whelan, A.; Regan, F. *Analyst* **2008**, *133*, 835–845.
33. Guizard, C.; Bac, A.; Barboiu, M.; Hovnanian, N. *Sep. Purif. Technol.* **2001**, *25*, 167–180.
34. Babudri, F.; Farinola, G. M.; Naso, F.; Ragni, R. *Chem. Commun.* **2007**, 1003–1022.
35. Desimone, J. M.; Williams, M. S.; Portnow, L.; Wood, C.; Zhou, Z.; Baucom, E.; Rothrock, G. Patent WO2007/025293A2.
36. Anton, D. *Adv. Mater.* **1998**, *10*, 1197–1205.
37. Ueberrueck, T.; Zippel, R.; Tautenhahn, J.; Gastinger, I.; Lippert, H.; Wahlers, T. *J. Biomed. Mater. Res., Part B* **2005**, *74B*, 601–607.
38. Vu-Khanh, T; Sanschagrin, B.; Fisa, B. *Polym. Compos.* **1985**, *6*, 249–260.
39. Khrenov, V.; Klapper, M.; Koch, M.; Muellen, K. *Macromol. Chem. Phys.* **2005**, *206*, 95–101.
40. Landfester, K. *Annu. Rev. Mater. Res.* **2006**, *36*, 231–279.

41. Cushing, B. L; Kolesnichenko, V. L; O'Connor, C. *J. Chem. Rev.* **2004**, *104*, 3893–946.
42. Stelzig, S. H.; Menneking, C.; Hoffmann, M. S.; Eisele, K.; Barcikowski, S.; Klapper, M.; Muellen, K. *Eur. Polym. J.* **2011**, *47*, 662–667.
43. Feng, Q. L.; Kim, T. N.; Wu, J.; Park, E. S.; Kim, J. O.; Lim, D. Y. *Thin Solid Films* **1998**, *335*, 214–219.
44. Barthlott, W.; Neinhuis, C. *Planta* **1997**, *202*, 1–8.
45. Roach, P.; Shirtcliffe, N. J.; Newton, M. I. *Soft Matter* **2008**, *4*, 224–240.
46. Cassie, A. B. D.; Baxter, S. *Trans. Faraday Soc.* **1944**, *40*, 546–551.
47. Quere, D. *Annu. Rev. Mater. Res.* **2008**, *38*, 71–99.
48. Ming, W.; Wu, D.; van Benthem, R.; de With, G. *Nano Lett.* **2005**, *5*, 2298.
49. D'Acunzi, M.; Mammen, L.; Singh, M.; Deng, X.; Roth, M.; Auernhammer, G. K.; Butt, H.-J.; Vollmer, D. *Faraday Discuss.* **2010**, *146*, 35–48.
50. Stoeber, W.; Fink, A.; Bohn, E. *J. Colloid Interface Sci.* **1968**, *26*, 62–69.
51. Deng, X.; Mammen, L.; Zhao, Y.; Lellig, P.; Muellen, K.; Li, C.; Butt, H.-J.; Vollmer, D. *Adv. Mat.* **2011**, *23*, 2962–2965.

Downloaded by PENNSYLVANIA STATE UNIV on August 28, 2012 | http://pubs.acs.org
Publication Date (Web): August 16, 2012 | doi: 10.1021/bk-2012-1106.ch008

Downloaded by NORTH CAROLINA STATE UNIV on August 28, 2012 | http://pubs.acs.org
Publication Date (Web): August 16, 2012 | doi: 10.1021/bk-2012-1106.ch009

Chapter 9

Fluorinated Polymers as Oxidizers for Energetic Composites

Christopher A. Crouse*[,1,2]

[1]Air Force Research Laboratory, Materials and Manufacturing Directorate,
Wright-Patterson Air Force Base, Ohio 45433
[2]UES, Inc., Dayton, OH 45432
***E-mail: christopher.crouse.ctr@wpafb.af.mil**

Fluorinated polymers have made a significant impact on the energetic materials community over the past several decades due to the strong oxidizing nature of the fluorine atoms found within their polymeric structure. The high density of fluorine within these polymers makes them highly effective oxidizers for energetic formulations with strongly electropositive metals (Mg, B, Al, Si, etc.) serving as the fuel. Furthermore, the presence of fluoropolymers in an energetic composite also incorporates beneficial structural properties as the polymer can simultaneously serve the role of both oxidizer and binder. Energetic formulations prepared with fluoropolymers as the binder and/or oxidizer have consistently demonstrated faster flame speeds, higher flame temperatures, increased reaction pressures and higher gas output when compared to formulations prepared with more conventional oxidizers.

Introduction

The use of fluoropolymers in energetic materials (EM) is believed to have first been investigated during the 1950's shortly after polytetrafluoroethylene (PTFE) was introduced to commercial markets (*1*). Since that time fluoropolymers have actively been explored as oxidizers and/or reactive binders for a variety of energetic formulations due to the strong electronegative nature of fluorine and the high density of fluorine atoms within these polymers. Reactions of PTFE with strongly electropositive metals, such as magnesium, aluminum and

In Advances in Fluorine-Containing Polymers; Smith, D., et al.;
ACS Symposium Series; American Chemical Society: Washington, DC, 2012.

Downloaded by NORTH CAROLINA STATE UNIV on August 28, 2012 | http://pubs.acs.org
Publication Date (Web): August 16, 2012 | doi: 10.1021/bk-2012-1106.ch009

silicon, dominate the literature as examples of highly energetic fluoropolymer based EM. To date fluoropolymers have been investigated as coatings and binder materials for metal powders and/or oxidizer particles in solid rocket motors as well as primary oxidizers in several pyrolant formulations (*1–5*). Fluorocarbons and fluoropolymers offer a higher density than their hydrocarbon counterparts and substitution of fluorine for hydrogen provides an additional oxidizing capability that is not present in hydrocarbons alone. Depending on the application, fluoropolymers may also be added to an energetic formulation to manipulate the mechanical properties of the composite. Fluoropolymers are also known for their thermal stability and chemical resistance which is welcomed in a field where safety is always a concern. This chapter has been prepared to offer a brief overview regarding the utilization of fluoropolymers in EM as well as an introduction to a new method for preparing fluoropolymer/nanoparticle energetic composites.

Poly(tetrafluoroethylene) Based Energetic Materials

Magnesium-PTFE, more commonly referred to as Mg-Teflon®, was the earliest fluoropolymer based EM to be developed and investigated. Shown in Equation 1, reaction of PTFE with Mg yields the metal fluoride and carbon as the primary products. This reaction is self-sustaining and is accompanied by a highly exothermic release of energy and as such serves as the foundation for the utilization of fluoropolymers and fluorinated materials in EM.

$$2\mathrm{Mg} + (\text{-}\mathrm{C_2F_4}\text{-})_n \rightarrow 2\mathrm{MgF_2} + 2n\mathrm{C} \quad \Delta H_{rxn} = -1438.8\ \mathrm{kJ/mol} \qquad (1)$$

Commercial versions of the Mg-PTFE systems often include the copolymer poly(hexafluoropropylene-co-vinylidene fluoride) (HFP-VF), also known by the trademark name Viton®, as a binder to help hold the metal powder and PTFE together and to allow for ease of processing. These systems are commonly referred to throughout literature as Mg-Teflon®-Viton®, or simply MTV. MTV formulations are typically prepared slightly fuel rich with Mg accounting for approximately 30-33 wt% of the composite mass. Concentrations of the copolymer vary with the application but typically vary from less than 5 wt% to no more than 20 wt% with PTFE accounting for the balance (*1*, *6*). Since their introduction in the 1950's MTV composites have been employed in a variety of military and civilian pyrolant applications including, but not limited to, infrared emitters, countermeasure flares, flares, igniters and propellants (*1*).

To better understand the oxidizing nature of fluoropolymers and their highly exothermic reaction with strongly electropositive metals it is helpful to understand the decomposition mechanism of the fluoropolymer into its reactive components. The thermal degradation mechanism for PTFE, in the absence of Mg, is fairly well understood and is dependent on the atmosphere where the decomposition occurs. For example, decomposition of PTFE in air primarily leads to the formation of the monomer, tetrafluoroethylene (C_2F_4), and carbonyl difluoride

(COF_2). The monomer can further decompose into difluorocarbene (:CF_2). This process is exothermic and occurs in the temperature range of *ca.* 460-610 °C. If moisture is present during decomposition, additional products such as fluoroform (CHF_3) and hyrodofluoric acid (HF) are also produced as water reacts with the products from the initial decomposition. Decomposition of PTFE in vacuum or under inert atmospheres, however, is an endothermic event resulting in the production of monomer as well as a mixture of fluorocarbons, including cyclic fluorocarbons. Detailed discussions concerning the decomposition of PTFE under the environments described above can be found in references (*1*, *7*).

Combustion of Mg with a fluorocarbon is known to occur in both the condensed phase as well as the gas phase and involves several separate mechanisms (*2*). The total combustion process is capable of producing flame temperatures in excess of *ca.* 3000 °C; at these temperatures it is highly likely that the PTFE decomposition mechanisms and products will vary from those produced during thermal decomposition as described above. A series of papers, authored by Koch, summarize the efforts of many researchers utilizing both computational models and experimental approaches to investigate the combustion mechanism of MTV (*1*, *2*). In general, the initial reaction in the combustion of MTV, known as the pre-ignition reaction (PIR), involves a Grignard like insertion of a Mg atom into a C-F bond in the $(\text{-}CF_2\text{-})_n$ polymeric chain resulting in formation of a C-Mg-F species. This is followed by reductive elimination with an adjacent fluorine atom resulting in the formation of a double bond within the polymer chain and the elimination of MgF_2. This process occurs in the condensed phase and is highly exothermic, likely providing enough heat to accelerate the degradation of PTFE into its monomer as well as promote the melting and vaporization of Mg. Once in the gas phase the Mg vapor can react with the monomer (C_2F_4) directly, or more likely with its more reactive decomposition products such as :CF_2 and carbon tetrafluoride (CF_4) which have been calculated to the primary sources of fluorine at combustion temperatures (*6*). Additional gas phase reactions such as oxidation of residual Mg, monomer and monomer decomposition products, as well as oxidation of elemental carbon produced during the fluorination reaction also occur and contribute to the overall energy output. A general schematic diagram for the combustion of Mg with PTFE is displayed in Scheme 1.

A variety of derivations of the MTV system have been prepared throughout the past several decades, including variations in both the metal and the fluoropolymer components employed in the formulations. Aluminum-PTFE and silicon-PTFE are logical transitions from the MTV composite system, as both metals are also reactive and possess high energy densities under oxidation and fluorination as shown in Figure 1. Both systems, like MTV, result in the highly exothermic oxidation of the respective metals utilizing fluorine from PTFE as the oxidizer as shown in Equations 2 and 3, respectively. Al-PTFE has received considerable attention as an EM with several reports present in literature. Many of the more recent reports have focused on formulations prepared with the use of aluminum nanoparticles as the fuel as these powders contain the same energy density as the more traditional micrometer scale aluminum powders, however, due to their extremely high surface area the aluminum nanoparticles have a significantly higher reactivity (*8*, *9*).

Downloaded by NORTH CAROLINA STATE UNIV on August 28, 2012 | http://pubs.acs.org
Publication Date (Web): August 16, 2012 | doi: 10.1021/bk-2012-1106.ch009

Downloaded by NORTH CAROLINA STATE UNIV on August 28, 2012 | http://pubs.acs.org
Publication Date (Web): August 16, 2012 | doi: 10.1021/bk-2012-1106.ch009

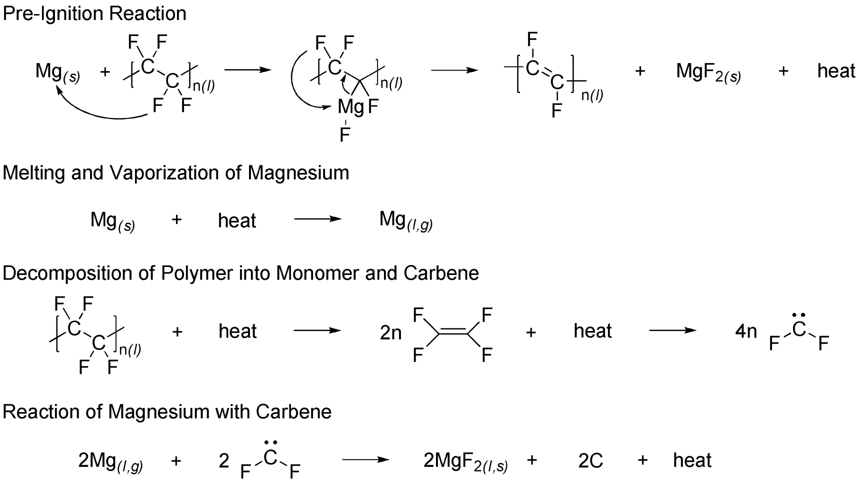
Pre-Ignition Reaction
Mg(s)
heat
MgF2(s)
Melting and Vaporization of Magnesium
Mg(s) + heat → Mg(l,g)
Decomposition of Polymer into Monomer and Carbene
2n
4n
Reaction of Magnesium with Carbene
2Mg(l,g) + 2 → 2MgF2(l,s) + 2C + heat

Scheme 1. Generalized reaction mechanism for the combustion of magnesium with PTFE.

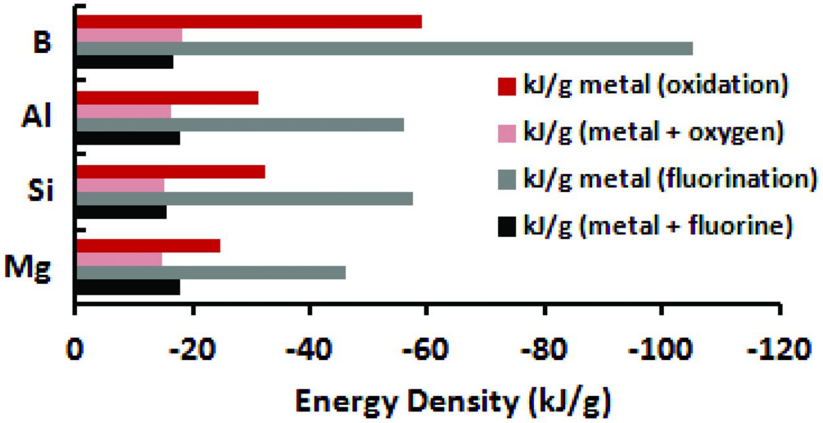

Figure 1. Calculated engery densities for the oxidation and fluorination of light metals. Energy density values have been calculated with respect to both the mass of the metal as well as the mass of the metal and the repsective oxidizer.

$$4Al + 3(-C_2F_4-)_n \rightarrow 4AlF_3 + 6nC \qquad \Delta H_{rxn} = -591.98 \text{ kJ/mol} \qquad (2)$$

$$Si + (-C_2F_4-)_n \rightarrow SiF_4 + 2nC \qquad \Delta H_{rxn} = -806.18 \text{ kJ/mol} \qquad (3)$$

Downloaded by NORTH CAROLINA STATE UNIV on August 28, 2012 | http://pubs.acs.org
Publication Date (Web): August 16, 2012 | doi: 10.1021/bk-2012-1106.ch009

When mixed with PTFE or PTFE/Viton®, aluminum and silicon are able to extract fluorine from the polymer as it decomposes, much like magnesium. These reactions are self-sustaining with the aluminum composition (Al-PTFE-Viton®, AlTV) producing aluminum trifluoride (AlF_3) and elemental carbon as the dominant products while the silicon formulations (Si-PTFE-Viton®, SiTV) yield silicon tetrafluoride (SiF_4), carbon, and silicon carbide (SiC) as the primary products. In the case of AlTV, the formation of AlF_3 as a product accelerates the reaction compared to the formation of Al_2O_3 because the combustion temperatures (>3000 °C) are sufficient to melt and sublime the AlF_3 (T_m = 1291 °C) as it is formed thereby eliminating or reducing the presence of a diffusion barrier between remaining reactant species. The formation of Al_2O_3 due to reaction of the aluminum with air or a metal oxide results in crystallization and growth of the aluminum oxide passivation layer which actually slows down the rate of the reaction as the oxide layer grows in thickness. The boiling of Al_2O_3 (T_{vap} = 2977 °C) actually limits the flame temperature since heat produced from the oxidation goes into vaporization of the product to allow for the reaction to progress. With respect to the SiTV systems, SiF_4 (T_{vap} = -86 °C) has a boiling point below room temperature so the products of combustion readily vaporize thereby allowing for the reaction to progress rapidly and allowing for combustion temperatures in excess of 4000 °C to be obtained. These temperatures are high enough to melt and vaporize Si and it has been suggested that fluorination of Si predominately occurs in the gas phase (*4*).

Aluminum nanoparticles, an increasingly common fuel used in AlTV compositions, are prepared through a variety of techniques, however, regardless of the technique all of the powders are highly pyrophoric and require the presence of an amorphous oxide passivation layer to be present to stabilize the particles resulting in a core-shell structure as shown in Figure 2. The oxide passivation layer is approximately 2-6 nm thick and can account for a considerable portion of the powder mass depending on the average particle size and particle size distribution of the powders used in the formulation. Although the presence of the oxide promotes stability of the particles the oxide layer can also serve as a barrier to the diffusion of aluminum and the oxidizer. The mechanism for oxidation of aluminum with fluorine and other oxidizers is still currently an area of intense focus within the EM community and will only be briefly discussed in this Chapter; References (*8–10*) provide a detailed discussion of the reaction pathways proposed for both the fluorination and oxidation of aluminum.

To investigate the effect of the amorphous oxide layer found on all commercial aluminum nanoparticles Pantoya et al. prepared a series of aluminum oxide/PTFE mixtures and performed differential scanning calorimetry (DSC) experiments to measure the heat flow associated with the reaction between PTFE and the aluminum oxide powder (*11*). Their investigation found that the pre-ignition reaction between PTFE and the aluminum oxide, which involves fluorination of the oxide and formation of AlF_3, is highly dependent upon the surface area of the powders with the smallest diameter powders (largest surface area) displaying the strongest exotherms. This work confirms that the oxide does indeed contribute in the combustion of the aluminum nanoparticles with PTFE and the authors also suggest that by using a higher surface area of the oxide in an aluminum nanoparticle based formulation the PIR should have a higher exothermicity and accelerate the combustion of the aluminum particles as was suggested in a previous report (*12*).

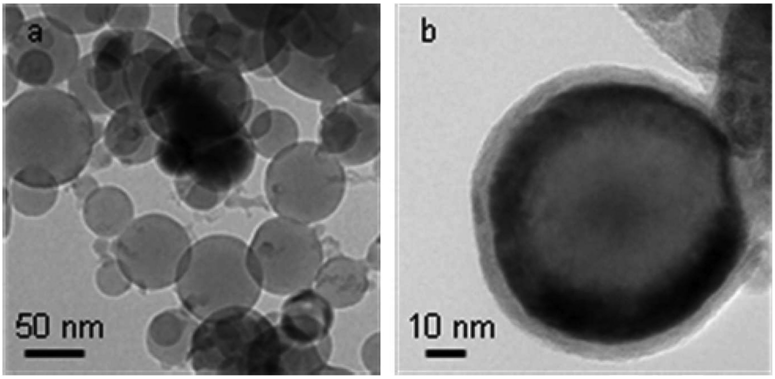

Figure 2. TEM images of (a) commercial aluminum nanoparticles and (b) a single oxide passivated aluminum nanoparticle to demonstrate the core-shell architecture of the particle. (Reprinted with permission from Crouse, C.A.; Pierce, C.J.; Spowart, J.E. ACS Appl. Mater. Interfaces ***2010,*** *2, 2560-2569. Copyright 2010 American Chemical Society.)*

Downloaded by NORTH CAROLINA STATE UNIV on August 28, 2012 | http://pubs.acs.org
Publication Date (Web): August 16, 2012 | doi: 10.1021/bk-2012-1106.ch009

Similar studies performed by the same group observed the role of PTFE as an additive to a thermite mixture comprised of aluminum particles and molybdenum trioxide (MoO_3) (*10*). Mixtures of Al/PTFE and Al/PTFE/MoO_3 (40:60 PTFE:MoO_3) were prepared with varying amounts of aluminum using both 50 nm and 1-3 micrometer sized aluminum particles as the fuel. Pressure measurements and burn velocities were obtained utilizing both open and confined burn tests. From these tests the researchers were able to demonstrate that faster flame velocities and higher pressures were obtained for the mixtures prepared with aluminum nanoparticles as the fuel regardless of the confinement. Confinement, however, proved to have a dramatic effect on the flame velocities produced in all of the Al/PTFE mixtures. Combustion of (50 nm) Al/PTFE under the open burn configuration produced peak flame speeds at a composition of 50 wt% Al that were equivalent to 4.25 m/s. Confinement led to a 200 fold increase in flame speeds with the peak speed of 837 m/s produced at a 40 wt% (50 nm) Al composition which is closer to the stoichiometric composition of 27.5 wt% Al. This reaction also produced the highest pressure out of all of the experiments performed (10.75 MPa). The use of a 40:60 PTFE:MoO_3 mixture as the oxidizer lead to faster flame velocities under both the open and confined conditions (410 m/s and 957 m/s, respectively), however, the confined condition produced flames speeds that were double those observed in the open burn. The reaction pressure also decreased

Downloaded by NORTH CAROLINA STATE UNIV on August 28, 2012 | http://pubs.acs.org
Publication Date (Web): August 16, 2012 | doi: 10.1021/bk-2012-1106.ch009

with the substitution of MoO_3 for a portion of the PTFE. The authors suggest that without confinement the gaseous decomposition products from PTFE are not able to fully react with the aluminum as the gases diffuse away from the fuel before they have had a chance to react with the metal. Confining the reactants enhances the reaction between the aluminum particles and the fluorinated decomposition products thus producing a higher flame speed and increased pressures.

Researchers at Purdue University performed a series of experiments on both loose powder and consolidated mixtures of AlTV and SiTV prepared with the respective nanometer scale metal powders (*4*). Chemical equilibrium codes were used to help identify the stoichiometric conditions for these systems as well as the dominant products, reaction temperatures and pressures. Under constant volume conditions the models predicted temperatures in excess of 4000 K for both systems with stoichiometric conditions for the AlTV system found at 28 wt% Al and the SiTV system at 24 wt% Si. Samples were prepared from powdered PTFE, HFP-VF and the respective metal nanopowders using a shock-gel method at the stoichiometric conditions predicted to produce the highest reaction temperatures. HFP-VF was held constant at 10 wt% for both systems in the loose powder samples and was increased to 15 wt% for the SiTV consolidated mixtures in order to obtain a pellet that was structurally sound. Results of the tube burn studies demonstrated that the SiTV systems performed better under fuel rich mixtures with a max flame speed of 1010 m/s observed at a mixture prepared with 34 wt% Si compared to only 367 m/s observed at the stoichiometric ratio of 24 wt% Si. AlTV systems consistently outperformed the Si systems achieving tube burn speeds of 1269 m/s at the stoichiometric condition of 28 wt% Al. Additionally, more gaseous products, and therefore higher pressures, were observed in the Al systems as well. Burning rates for the consolidated samples in pellet form were obtained under argon atmospheres at increasing pressure. These rates were generally lower for the Si systems compared to the Al systems, however, the authors comment that both systems generally display faster burning rates than consolidated MTV systems. Max flame speeds for the SiTV system were obtained at 34 wt% Si, similar to those observed during the tube burn studies. Flames speeds for the AlTV system increased with increasing Al content and optimized speeds were obtained 58 wt% Al, far beyond the stoichiometric condition of 28 wt% observed during tube burn studies. The authors provide an explanation for these observations suggesting that the Al/PTFE/Viton® systems experience both condensed phase and gas phase combustion whereas the Si/PTFE/Viton® systems are dominated primarily by gas phase combustion alone.

Non-PTFE Fluorinated Matrices for Use in Energetic Composites

Although PTFE dominates the EM literature as the most common source of fluorine for energetic formulations the use of graphite fluoride $(\text{-CF-})_n$ as an oxidizing material has also been explored with many metal systems. It has been shown that $(\text{-CF-})_n$ actually outperforms PTFE as an oxidizer in pyrolant formulations yielding higher combustion temperatures and providing improvements with respect to infrared emission (*13*). Polish researchers reported highly exothermic reactions between $(\text{-CF-})_n$ and several reductants including metallic Si and AlSi alloys (*14*). The data presented in their report demonstrated that $(\text{-CF-})_n$ is an effective oxidizer for a variety of reductant species yielding a highly exothermic and self sustaining reaction with exfoliated graphite being the dominate carbonaceous product produced regardless of the reductant used.

Researchers at the US Air Force Academy recently presented experimental results exploring the use of perfluoro-polyethers, fluorinated polyurethanes, and copolymers of the two, as fluorinated matrices for the preparation of reactive aluminum nanoparticle based composites (*15*). Although this work is still in its early phases of development, the fluorinated polymers they have studied have been shown to be viable sources of fluorine for the fluorination of aluminum nanoparticles yielding a highly energetic response upon reaction.

Downloaded by NORTH CAROLINA STATE UNIV on August 28, 2012 | http://pubs.acs.org
Publication Date (Web): August 16, 2012 | doi: 10.1021/bk-2012-1106.ch009

Fluoropolymer/Fluorocarbon Binders and Coatings

Other examples of fluorocarbons and fluoropolymers in reactive composites include the use of fluoropolymers as reactive binders in composite formulations. For example, HFP-VF has been applied as a reactive binder for a variety of EM formulations in place of hydrocarbon binders such as hydroxyl-terminated polybutadiene (HTPB). Recently, it was reported that HFP-VP was used to coat ammonium perchlorate (AP) particles in propellant formulations (*3*). It was shown that the use of HFP-VF coated AP in Al/HTPB/AP formulations for solid rocket propellants resulted in an increase in the thermal stability of the material thereby providing a safer and easier to handle product compared to control formulations prepared without the HFP-VF coated AP.

Fluoropolymer and fluorocarbons have also been utilized in the passivation of reactive particles to inhibit the formation of a nascent oxide layer that ultimately leads to the introduction of unreactive material into a energetic formulation. Jouet et al. investigated the passivation of aluminum nanoparticles, with perfluoroalkylcarboxylic acids (*16*). The perfluoroalkylcarboxylic acids were added to the unpassivated aluminum particles in a dry solvent to prevent oxidation of the particles. The perfluoroalkylcarboxylic acids were found to bind directly to the bare metal on the aluminum surface through a carboxylate bond resulting in the formation of a self-assembled monolayer on the particle surface. By use of thermogravimetric analysis (TGA) the researchers were able to demonstrate that the perfluoroalkylcarboxylic acid passivated particles were not pyrophoric and were indeed stable. The perfluoroalkylcarboxylic acid passivated aluminum particles have been used in formulations as a source for aluminum in the self-propagating high-temperature synthesis of porous Al-Ni foams (*17*). Additionally, the fluorocarbon passivated aluminum particles have also been tested under impact as a fuel for thermite mixtures prepared with metal oxides (*18*). In this work it was suggested that the fluorocarbon coating mechanically cushions the aluminum particles thereby reducing the impact sensitivity of the thermite mixtures.

Downloaded by NORTH CAROLINA STATE UNIV on August 28, 2012 | http://pubs.acs.org
Publication Date (Web): August 16, 2012 | doi: 10.1021/bk-2012-1106.ch009

New Approaches Towards Fluoropolymer/Reactive Particle Composites

As noted in the above text, fluoropolymers and fluorocarbons play a significant role in many EM formulations. These materials have been used as reactive binders and oxidizers for several decades in a variety of military and civilian pyrolant formulations. Although it was not presented in detail in the above text many of these composite formulations mentioned above are prepared by simple powder mixing followed by compaction which does not produce any direct bonding between the surfaces of the metal particles and polymer matrix. As a result the mechanical properties for fluoropolymer reactive composite materials are expected to be rather poor. To combat this issue it is common practice to add a significant percentage of a fluoroelastomer, such as HFP-VF, as a binder material to aid with processing and structural integrity of the material. As the particle size of the reactants is decreased more binder material is required to account for the increase in surface area.

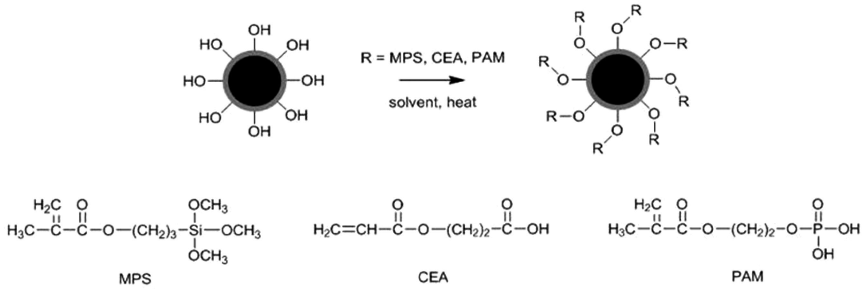

Scheme 2. Functionalization of aluminum nanoparticles with acrylic monomers.

Recently, in work done at the Air Force Research Laboratory - Materials and Manufacturing Directorate, we developed and reported on a new approach towards the preparation of fluoropolymer/aluminum nanoparticle composite materials, which we refer to as aluminized fluorinated acrylate (AlFA) composites, utilizing a direct chemical route to prepare the polymer on the particles to afford intimate contact between fuel and oxidizer (*19*, *20*). Using this approach chemical integration of the particles into the polymer matrix is shown to improve upon the mechanical properties of the final product without compromising reactivity. Experimental details and a discussion of the mechanical and reactive properties of the AlFA composites adapted from references (*19*, *20*) are provided below.

The first step applied in the formation of the AlFA composite materials involves chemical functionalization of the aluminum nanoparticles which is used to prepare a thin acrylic coating on the surface of aluminum nanoparticles (Scheme 2). Following the functionalization procedure the coated particles were mixed in a solvent along with a commercial fluorinated methacrylate and an *in situ* polymerization was initiated to prepare the composite product (Scheme 3). To ensure uniform distribution of the aluminum nanoparticles throughout the material each composite was compounded in a DACA Instruments bench top twin-screw extruder at 150 °C. The compounded material was then extruded through a circular die and into a copper clam-shell mold and was allowed to cool (Figure 3). The final product was a gray, waxy solid with variable metallic luster depending on particle content (Figure 4).

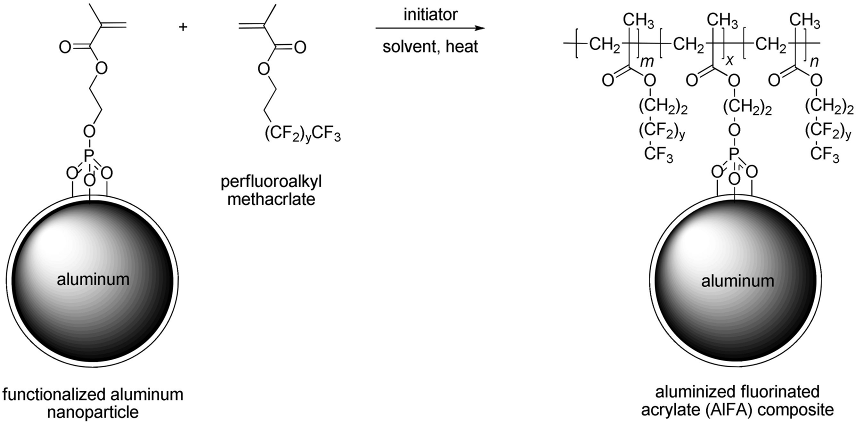
+
initiator
solvent, heat
$(CF_2)_yCF_3$
perfluoroalkyl methacrlate
aluminum
functionalized aluminum nanoparticle
CH_3
CH_2
m
x
n
$(CH_2)_2$
$(CF_2)_y$
CF_3
aluminum
aluminized fluorinated acrylate (AlFA) composite

Scheme 3. Schematic illustration for the in situ formation of AlFA composites.

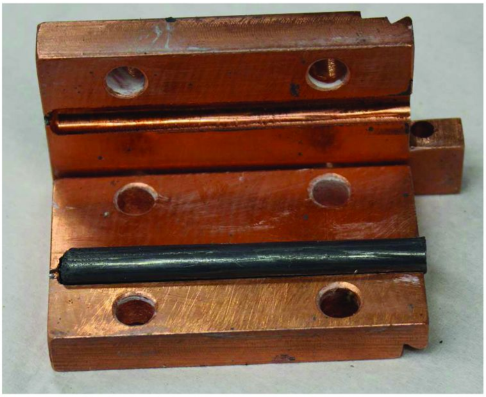

Figure 3. Image displaying a clamshell mold with an extruded aluminum nanoparticle/fluorinated polymethacrylate composite.

The initial AlFA composites prepared in our laboratory were based upon a fluorinated polymethacrylate matrix prepared from a mixture of perfluorinated alkyl methacrylates with an average molecular weight of 534 g/mol produced by DuPont under the trade name Zonyl® TM (*19*). Composites were successfully prepared with particle contents ranging from less than 20 wt% to 34.5 wt%. These materials displayed thermoplastic behavior and were easily processed using conventional polymer processing techniques such as extrusion.

Downloaded by NORTH CAROLINA STATE UNIV on August 28, 2012 | http://pubs.acs.org
Publication Date (Web): August 16, 2012 | doi: 10.1021/bk-2012-1106.ch009

Downloaded by NORTH CAROLINA STATE UNIV on August 28, 2012 | http://pubs.acs.org
Publication Date (Web): August 16, 2012 | doi: 10.1021/bk-2012-1106.ch009

More recently we have focused on the development of AlFA composites prepared with a poly(PFDMA) matrix (*20*). PFDMA is a fluorinated alkyl methacrylate monomer, MW = 532 g/mol, with a perfluorinated carbon tail that is 10 carbons long with the first two carbons adjacent to the ester being hydrogenated. Utilizing the same approach we have prepared composites with particles loadings up to 70 wt% all of which display thermoplastic behavior; composites with loadings of 60 wt% or less are capable of undergoing melt extrusion. Images of the AlFA composites prepared with PFDMA are displayed in Figure 4.

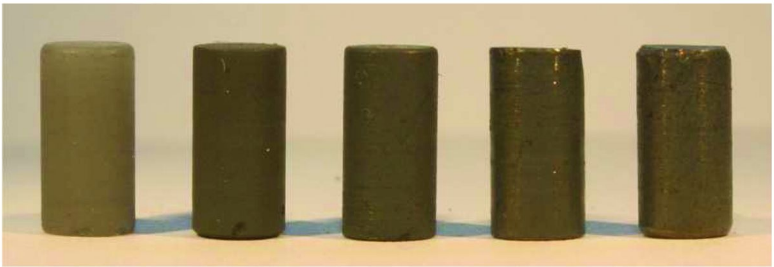

Figure 4. Picture displaying the extruded AlFA composites that have been machined into 4 mm diameter x 8 mm length cylinders with (left to right) 0, 10, 30, 50 and 60 wt% aluminum nanoparticle content in a poly(PFDMA) matrix.

Both PFDMA and the Zonyl® TM mixture possess an average fluorine content of *ca.* 60 wt%; PTFE has a fluorine content of 75% by mass. Fluorine content in the fluorinated methacrylates is lost due to the non-fluorinated methacrylate subunit of the monomer. The perfluorinated alkyl chains that are attached to the methacrylate subunit are comprised of $(\text{-CF}_2\text{-})_n$ units along with a terminal –CF_3 unit and are essentially short chain oligomers that structurally mimic PTFE; therefore it was assumed that the fluorinated polyacrylates would have similar reactivity towards metal powders.

Thermal analysis performed on the composite materials indicates that the polymer begins to degrade above 200 °C with degradation complete by 400 °C under both argon and air atmospheres regardless of whether the composite is prepared with the Zonyl® TM mixture or PFDMA. A non-fluorinated version of the AlFA material was prepared with 22.5 wt% aluminum nanoparticles in a poly(methyl methacrylate) (PMMA) matrix and compared to a 22.5 wt% AlFA composite prepared with Zonyl® TM to determine if the presence of fluorine was indeed contributing to the reactivity. Pellets were prepared from both materials, placed directly onto a firebrick and were rapidly heated with a propane/oxygen flame. A visibly more violent response (Figure 5) was observed from the fluorinated composite confirming that the fluorinated polymer matrix does indeed contribute to the reactivity of the material.

To gauge the reactivity of the AlFA composite materials with respect to the aluminum particle content a series of extruded and machined pellets were prepared with particles contents of 0, 10, 30, 50 and 60 wt% in a poly(PFDMA) matrix. Combustion of the pellets was performed in an open-air environment while the reaction progress was recorded with a high speed video camera to monitor the reaction intensity and measure the total reaction time. The results of this study are explained in detail in Ref. (*20*) and suggest that a peak in reactivity is realized at compositions prepared with 50 wt% aluminum content where the material has the ability to react through both fluorination and air oxidation mechanisms. Additionally, the reaction pathways and products, as well as the reactivity of the materials were shown to be highly dependent upon the initial composition of the pellet.

Downloaded by NORTH CAROLINA STATE UNIV on August 28, 2012 | http://pubs.acs.org
Publication Date (Web): August 16, 2012 | doi: 10.1021/bk-2012-1106.ch009

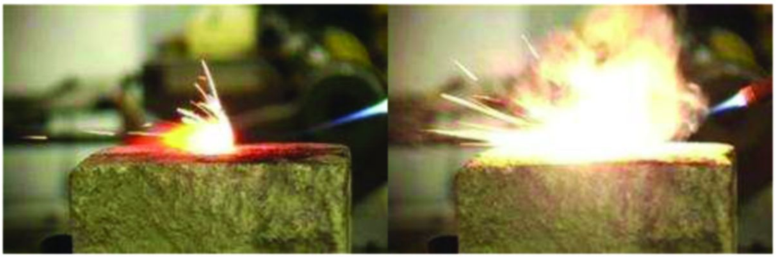

Figure 5. Combustion experiments performed on a) 22.5 wt% aluminum nanoparticle/PMMA and b) 22.5 wt% aluminum nanoparticle/Zonyl® TM AlFA composite.

Chemical functionalization of the aluminum nanoparticle surface with an acrylic monomer prior to polymerization and composite formation provides direct chemical bonding of the polymer matrix to the particles embedded within, resulting in an intimate connection between the polymer matrix and the particles. TEM microscopy has been used to probe the polymer/particle interface as shown in Figure 6. From the images it is clear that the polymer forms a direct bond to the particle surface as no separation or gaps are seen at the interface. This type of direct bonding to the particle is not achieved in any of the PTFE/Viton®/metal particle composite systems that have been currently studied and it was our hypothesis that this direct bonding could potentially increase the overall strength of the composite materials. To test this hypothesis, quasi-static compression tests were performed on a machined samples at the AlFA composites prepared with aluminum contents ranging from 0 – 60 wt%. The data from the compression tests is present in Table 1. The data demonstrates that the addition of the aluminum nanoparticles more than doubles the peak compressive strength of the neat polymer with the highest increases in strength realized at the largest particle loadings.

Downloaded by NORTH CAROLINA STATE UNIV on August 28, 2012 | http://pubs.acs.org
Publication Date (Web): August 16, 2012 | doi: 10.1021/bk-2012-1106.ch009

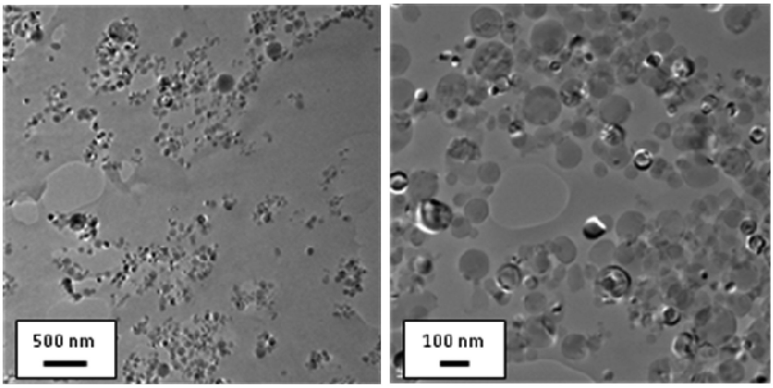

Figure 6. TEM micrographs displaying the microstructure of the 22.5 wt% AlFA composite prepared with Zonyl® TM.

Table 1. Compressive strength data for AlFA composites

poly(PFDMA) (wt%)	*Al (wt%)*	*Compressive Strength (MPa)*
100	0	11.0 +/- 2.9
90	10	13.2 +/- 0.1
70	30	14.6 +/- 1.6
50	50	25.0 +/- 2.4
40	60	28.5 +/- 0.9

Conclusions

Fluoropolymers and fluorocarbons, due to the strong oxidizing nature of the fluorine atoms found within the polymer or molecule, have found an increasing role as oxidizers and reactive binders within many modern energetic formulations. The development of MTV composites and aluminum and silicon derivatives have become large markets for the use of fluoropolymers as they serve as the sole oxidizer component for these formulations. In an effort to improve upon the structural properties of the fluoropolymer composites without compromising reactivity we have introduced a new class of aluminum nanoparticle/fluoropolymer composites prepared through a unique *in situ* polymerization approach. These AlFA composite materials display thermoplastic behavior at all particle concentrations and can be processed via melt extrusions up to 60 wt% particle content. Open air combustion tests have confirmed the reactive nature of the composites and the composites prepared with 50 wt% particle content demonstrate the highest reactivity as they are able to react simultaneously though both fluorination and oxidation mechanisms.

Downloaded by NORTH CAROLINA STATE UNIV on August 28, 2012 | http://pubs.acs.org
Publication Date (Web): August 16, 2012 | doi: 10.1021/bk-2012-1106.ch009

Acknowledgments

Funding for this work was made available by Air Force Research Laboratory, Materials and Manufacturing Directorate, from the Nanoscience and Technology STT Initiative in Nanoenergetics. Their support is gratefully acknowledged. Additionally, the author would like to acknowledge several colleagues and friends, including Dr. Jonathan Spowart, Dr. Mike Lindsay, Ms. Breanna Hardenstein, Mr. Mike Scott, Mr. Tony Houston and Ms. Pamela Lloyd, as well as others who have provided either technical support or thoughtful discussion throughout the course of this work.

References

1. Koch, E.-C. *Propellants, Explos., Pyrotech.* **2002**, *27*, 262–266.
2. Koch, E.-C. *Propellants, Explos., Pyrotech.* **2002**, *27*, 340–351.
3. Nandagopal, S.; Mehilal, M.; Tapaswi, M. A.; Jawalkar, S. N.; Radhakrishnan, K. K.; Bhattacharya, B. *Propellants, Explos., Pyrotech.* **2009**, *34*, 526–531.
4. Yarrington, C. D.; Son, S. F.; Foley, T. J. *J. Propul. Power* **2010**, *26*, 734–743.
5. Yagodnikov, D. A.; Andreev, E. A.; Vorob'ev, V. S.; Glotov, O. G. *Combust., Explos. Shock Waves* **2006**, *42*, 534–542.
6. Christo, F. C. *Thermochemistry and Kinetics Models for Magnesium/Teflon/Viton Pyrotechnic Compositions*; DSTO-TR-0938; DSTO Aeronautical and Maritime Research Laboratory: Melbourne, 1999; pp 1−31.
7. Moldoveanu, S. C. *Analytical Pyrolysis of Synthetic Organic Polymers*; Elsevier: Amsterdam, The Netherlands, 2005; pp 291−293.
8. Yetter, R. A.; Risha, G. A.; Son, S. F. *Proc. Combust. Inst.* **2009**, *32*, 1819–1838.
9. Dreizin, E. L. *Prog. Energy Combust. Sci* **2009**, *35*, 141–167.
10. Watson, K. W.; Pantoya, M. L.; Levitas, V. I. *Combust. Flame* **2008**, *115*, 619–634.
11. Pantoya, M. L.; Dean, S. W. *Thermochim. Acta* **2009**, *493*, 109–110.
12. Osborne, D. T.; Pantoya, M. L. *Combust. Sci. Technol.* **2007**, *179*, 1467–1480.
13. Koch, E.-C. *Propellants, Explos., Pyrotech.* **2004**, *29*, 9–18.
14. Cudzilo, S.; Szala, M.; Huczko, A.; Bystrzejewski, M. *Propellants, Explos., Pyrotech.* **2007**, *32*, 149–154.
15. Fantasia, R. C.; Pierson, S. N.; Hawkins, C. G.; Iacono, S. T.; Kettwich, S. C. *Polym. Prepr.* **2011**, *52*, 747.
16. Jouet, R. J.; Warren, A. D.; Rosenberg, D. M.; Belitto, V. J.; Kihong, P.; Zachariah, M. R. *Chem. Mater.* **2005**, *17*, 2987–2996.
17. Hunt, E. M.; Malcolm, S.; Pantoya, M. L.; Davis, F. *Int. J. Impact Eng.* **2009**, *36*, 842–846.
18. Hunt, E. M.; Pantoya, M. L.; Jouet, R. J. *Intermetallics* **2006**, *14*, 620–629.
19. Crouse, C. A.; Pierce, C. J.; Spowart, J. E. *Polym. Prepr.* **2011**, *52*, 742–743.
20. Crouse, C. A.; Pierce, C. J.; Spowart, J. E. *Combust. Flame* **2012**, in press.

Downloaded by COLUMBIA UNIV on August 28, 2012 | http://pubs.acs.org
Publication Date (Web): August 16, 2012 | doi: 10.1021/bk-2012-1106.ch010

Chapter 10

Recent Advances on New Fluorinated Copolymers Based on Carbonate and Oligo(ethylene oxide) by Radical Copolymerization

Ali Alaaeddine, Claire Negrell, and Bruno Ameduri*

Institut Charles Gerhardt, Ingénierie et Architectures Macromoléculaires,
UMR CNRS 5253, Ecole Nationale Supérieure de Chimie de Montpellier,
8 Rue de l'Ecole Normale, 34296 Montpellier Cedex, France
***E-mail : bruno.ameduri@enscm.fr**

The synthesis and characterizations of original poly[CTFE-*alt*-VEoligo(EO)] and poly(F-alkene-*alt*-GCVE) alternated copolymers (where CTFE, VEoligo(EO), F-alkene, and GCVE stand for chlorotrifluoroethylene, oligo(ethylene oxide) vinyl ether, hexafluoropropylene (HFP) or perfluoromethyl vinyl ether (PMVE), and glycerol carbonate vinyl ether, respectively) are presented. First, vinyl ethers bearing oligo(ethylene oxide) or carbonate side-group (i.e. 2-oxo-1,3-dioxolan-4-yl-methyl vinyl ether, GCVE) were synthesized by transetherification of ω-hydroxyl oligo(EO) (of different molecular weights (3 and 10 EO units) or glycerol carbonate with ethyl vinyl ether catalyzed by a palladium complex were obtained in 45-74% yields. Although HFP, PMVE, and vinyl ethers do not homopolymerize under radical conditions, they copolymerized readily yielding alternated poly(F-alkene-*alt*-VE) copolymers that bore carbonate group or oligo(EO) side-chains. The alternated structures of these original poly(F-alkenes-*alt*-VE) copolymers were confirmed by elemental analysis and by ^1H, ^{19}F and ^{13}C NMR spectroscopy. All copolymers were obtained in good yield (61-85 %). Their molecular weights varied depending on the [initiator]$_o$/[monomers]$_o$ intial molar ratios, reaching either 3,900-4,600 g mol^{-1} or 19,000 g.mol^{-1} with polydispersities below 2.0. While the glass transition temperatures of

In Advances in Fluorine-Containing Polymers; Smith, D., et al.;
ACS Symposium Series; American Chemical Society: Washington, DC, 2012.

poly(CTFE-*alt*-VEoligoEO) copolymers were ranging between -42 and -36 °C, those of poly(F-alkene-*alt*-GCVE) copolymers were higher (15-65 °C). Their thermogravimetric analyses under air showed decomposition temperatures at 10 % weight loss ($T_{d,10\%}$) higher than 270 °C. The HFP-based copolymer exhibited a better thermal stability than those based on CTFE and PMVE.

Downloaded by COLUMBIA UNIV on August 28, 2012 | http://pubs.acs.org
Publication Date (Web): August 16, 2012 | doi: 10.1021/bk-2012-1106.ch010

Introduction

Fluorinated polymers are remarkable niche (or low volume production) macromolecules that possess exceptional properties (*1–5*), such as chemical resistance (to acids, bases, and organic solvents), thermostability, low dielectric constants and dissipation factors, hydrophobic and oleophobic properties, excellent weathering and aging resistance, and interesting surface properties. Hence, these high added value materials have found specific applications in many fields of high technology (aerospace, aeronautics, automotive and electronic industries). However, fluoropolymers are difficulty soluble in common organic solvents and thus copolymerization of fluoroalkenes with a hydrogenated monomers can overcome such solubility issues. One interesting example deals with chlorotrifluoroethylene (CTFE) known to satisfactorily react with vinyl ethers by an acceptor-donor copolymerization that yield alternating poly(CTFE-*alt*-VE) copolymers due to the fact that fluorinated olefins have an electron-acceptor character (*6*) (*e* values for CTFE (*7*, *8*) and hexafluoropropylene (HFP) (*9*) are 1.56 and 1.50, respectively) while vinyl ethers are electron-donating ($-2.0 < e < -1.5$) (*10–12*). Moreover, vinyl ethers are known not to homopolymerize under radical initiation (*13*, *14*).

Poly(fluoroolefin-*alt*-vinyl ether) alternating copolymers (*15–28*) are endowed with interesting properties that arise directly from their composition. Thus, the 50 mol% content of fluoroolefin (*1–6*) brings film forming-properties, hydrophobicity, oleophobicity, chemical inertness, and thermostability while that of vinyl ether brings complementary properties such as solubility, adhesion, cross-linking (*29*, *30*), hydrophilicity, softness, adhesion to metal, and affinity with the lithium anions (*6*, *11*, *12*).

Recently, a quasi exhaustive review on the CTFE copolymers is on the way to be published (*31*) regarding the choice of suitable comonomers of CTFE. Their reactivity ratios have been supplied and showed that most of these comonomers are more reactive than CTFE except vinyl ethers (VE) that copolymerize readily to lead to alternated copolymers. Various vinyl ethers have been successfully used in their radical copolymerization with CTFE, nicely reported in a book chapter in 1997 (*6*) or more recently involving ethyl vinyl ether (*32*), 2-chloroethyl vinyl ether (*33*) or imidazole-containing vinyl ether (*34*).

On the other hand, aliphatic carbonate derivates are environment friendly. One of the best examples is glycerol carbonate easily achieved from CO_2 and renewable glycerol. Moreover, oligo(ethylene oxide)s are of potential interest

Downloaded by COLUMBIA UNIV on August 28, 2012 | http://pubs.acs.org
Publication Date (Web): August 16, 2012 | doi: 10.1021/bk-2012-1106.ch010

for many applications (including lithium ion batteries (*35*), cosmetics (*36*) and biomedical applications (*37*)).

Hence, preparing a copolymer bearing both a fluorinated backbone and carbonate or oligo(ethylene oxide) dangling groups is of interest due to the unique combination of complementary properties. Although the literature on the synthesis and the use of carbonate or oligo(ethylene oxide) based compounds is extensive, knowing that there is no report on fluorinated oligomers or polymers bearing such a function (*31*), these fluorinated derivatives are expected to exhibit good thermal properties, good chemical inertness, good stability at low and high electric potential, fulfilling the requirements for various applications including electrolytes and coatings.

Hence, the objective of this contribution deals with the synthesis of original fluorinated copolymers obtained by the radical copolymerization of CTFE with two types of vinyl ethers: vinyl ethers containing carbonate and bearing oligo(ethylene oxide). These vinyl ethers were synthesized from glycerol carbonate (regarded as a renewable product) or with oligo(ethylene oxide) monomethyl ether (n=3 or 10) by transetherification of ethyl vinyl ether catalyzed by a palladium(II) complex generated *in situ* (*38*). Then, these vinyl ethers were further copolymerized with chlorotrifluoroethylene (and with other fluoroalkenes).

Results and Discussion

Vinyl ethers are known to copolymerize in an alternated manner with electron-withdrawing comonomers such as fluorinated olefins (such as chlorotrifluoroethylene (*6*, *25*, *26*, *39*, *40*)). Interestingly, a wide variety of vinyl ethers have already been synthesized showing the versatility of this monomer to bear various functional groups such as ammonium (*40*), halogens (*25*, *26*), perfluorinated groups (*41*), poly(ethylene oxide) (*27*), … Thus, to obtain a fluorinated copolymer that bear carbonate or oligo(ethylene oxide), the preparation of a vinyl ether containing carbonate or oligo(ethylene oxide) and its copolymerization with fluorinated olefins is an attractive concept.

I. Synthesis and Characterization of Original Alternated Fluorinated Copolymers Bearing Carbonate Side-Groups

Glycerol carbonate (**1**) (*42*) is a bifunctional reactant arising from biomass endowed with a solvent capability towards many organic or inorganic compounds. This protic polar solvent is highly desirable in regards to its non-toxicity and high boiling point. Glycerol carbonate can also be used as an additive for the stabilization of polymers (*43*), monomers and reaction intermediates (*44*).

Two options are possible to obtain a vinyl ether bearing a carbonate: i) either from an alcohol or ii) from an epoxy group. Four main synthetic pathways have been reported for the chemical modification of an alcohol onto a functional vinyl ether: addition onto acetylene (*45*), transetherification (*46*–*52*), phase transfer catalysis (PTC) (*47*, *53*, *54*), and the modification of vinyl acetate in the presence of an iridium complex (*55*). Transetherification has been extensively studied in the presence of either mercuric acetate or palladium acetate, especially by Watanabe and Conlon (*46*), Mc Keon et al. (*56*), and Boutevin and Youssef (*47*). This last study even compared transetherification with PTC process. More recently, Pichavant et al. (*38*) reported the synthesis of a vinyl ether by transetherification catalyzed by a Palladium (II) complex in the presence of ethyl vinyl ether in dichloromethane.

The second option consists of the reaction between vinyl glycidyl ether and carbon dioxide in the presence of various catalysts (β-butyrolactone (*57*), $NaHCO_3$ (*57*), or a quaternary ammonium (*57–59*)) as described by various authors and reviewed by Webster (*60*) (Scheme 1):

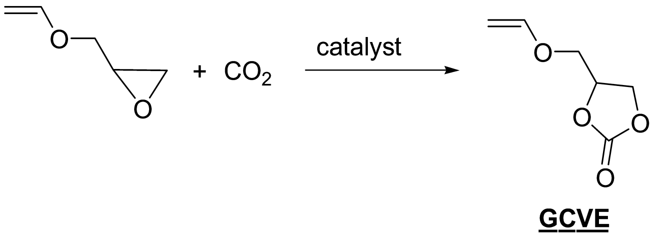

Scheme 1. Synthesis of [(2-oxo-1,3-dioxolan-4-yl)methyl vinyl ether] (GCVE) from vinyl glycidyl ether in the presence of carbon dioxide (60).

Recently, original vinyl ethers bearing lateral chloromethyl groups were synthesized by transetherification catalyzed by a palladium (II) complex generated *in situ* (*27*, *40*, *61*). Reactions were carried out in the presence of 2 mol.% of palladium (II) acetate catalyst and 1,10 phenanthroline (as ligand) at 60 °C. Using these optimized parameters, **GCVE** monomer was prepared by transetherification of ethyl vinyl ether and glycerol carbonate (Scheme 2) as a yellow liquid in 45% yield.

GCVE monomer was characterized by ^1H and ^{13}C NMR spectroscopy. The ^1H NMR spectrum (Figure 1) exhibits two non equivalent protons $C^6H_aH_b$ of the vinyl group as two doublets of doublets centered at 4.04 and 4.17 ppm. The same observation can be noted for the methylene group of the carbonate cycle (δ = 3.75 and 3.90 ppm) with a low field shift compared to that of glycerol carbonate due to the presence of the vinylic group. The signal assigned to the methyne proton (=CH-) of the vinyl ether is centered at 6.41 ppm as a doublet of doublets.

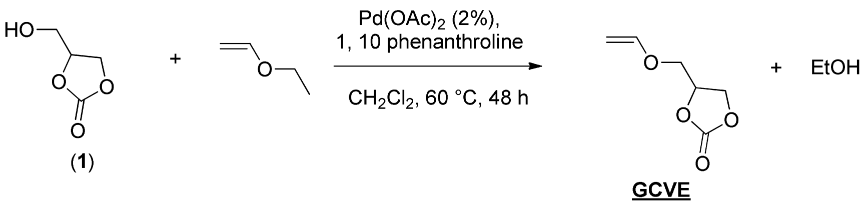

*Scheme 2. Synthesis of a vinyl ether bearing a carbonate side-group (GCVE) from glycerol carbonate (**1**).*

Downloaded by COLUMBIA UNIV on August 28, 2012 | http://pubs.acs.org
Publication Date (Web): August 16, 2012 | doi: 10.1021/bk-2012-1106.ch010

Downloaded by COLUMBIA UNIV on August 28, 2012 | http://pubs.acs.org
Publication Date (Web): August 16, 2012 | doi: 10.1021/bk-2012-1106.ch010

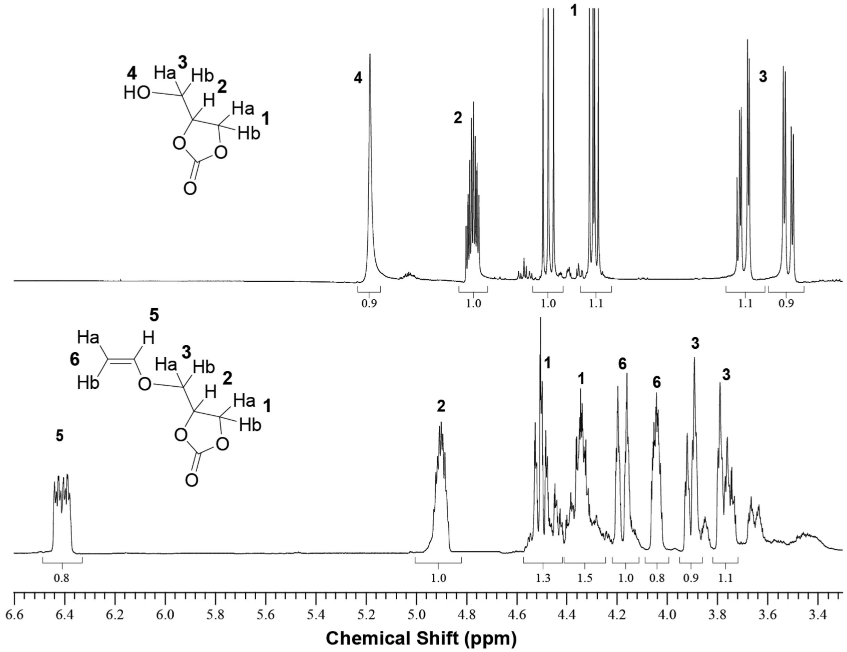

Figure 1. ^{1}H NMR spectra of (2-oxo-1,3-dioxolan-4-yl)-methyl vinyl ether, ***GCVE*** *($CDCl_3$, 20 °C, 400 MHz, lower spectrum) and glycerol carbonate (DMSO, 20 °C, 400 MHz, upper spectrum).*

Radical Copolymerization of GCVE Monomer with Fluoroolefins

Nishikubo *et al.* (*57*) reported the homopolymerization of GCVE initiated by cationic polymerization in the presence of BF_3OEt_2 that led to polyethers bearing carbonate side-groups. In addition, copolymers based on GCVE with electron-withdrawing monomers such as acrylonitrile (*62–64*), N-phenylmaleimide (*65*), methyl acrylate (*60*) or maleic anhydride (*60*) were also prepared.

Thus, the radical copolymerization of hexafluoropropylene (HFP), chlorotrifluoroethylene (CTFE), or perfluoromethyl vinyl ether (PMVE) with **GCVE** monomer, initiated by *tert*-butylperoxypivalate (TBPPi) in 1,1,1,3,3-pentafluorobutane at 74 °C, was carried out as depicted in Scheme 3. The amount of initiator (5 mol%) can be considered as high compared to usual conditions (< 1 mol.%), but for the anticipated use (polymer electrolyte for lithium batteries) low molecular weight polymers are highly desirable, and thus a high quantity of initiator was required.

A small amount of potassium carbonate (K_2CO_3) was inserted in the polymerization media to prevent from both the cationic homopolymerization (*66*) and the acetalization (*67*) of GCVE vinyl ether. The fluorinated olefin was introduced in slight excess to enable the complete consumption of the glycidyl carbonate vinyl ether and to ensure that a suitable gaseous fluoroalkenes reacted in the liquid phase.

Downloaded by COLUMBIA UNIV on August 28, 2012 | http://pubs.acs.org
Publication Date (Web): August 16, 2012 | doi: 10.1021/bk-2012-1106.ch010

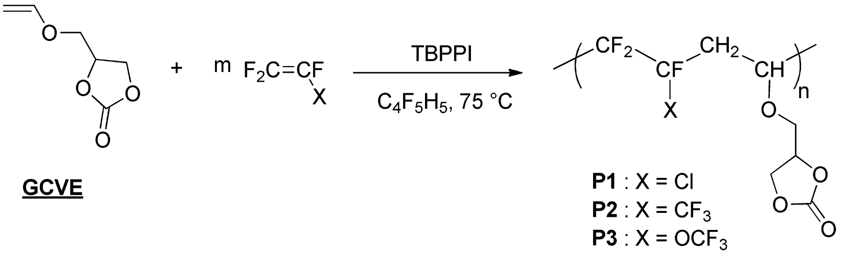

Scheme 3. Radical copolymerization of (2-oxo-1,3-dioxolan-4-yl)methyl vinyl ether (GCVE) with various fluorinated olefins [chlorotrifluoroethylene (CTFE), hexafluoropropylene (HFP) or perfluoro(methyl vinyl ether) (PMVE), and where X = Cl, CF_3, or OCF_3, respectively].

The radical copolymerization of fluoroolefins with vinyl ether is an exothermic reaction, and a rapid increase of pressure in the autoclave was observed, followed by a sharp drop of pressure linked to the consumption of the fluorinated gases. Such a copolymerization between electron withdrawing monomers is called acceptor-donor copolymerization and yields alternating copolymers (*6*). The presence of the carbonate function does not disturb the copolymerization.

The results of the radical copolymerizations of **GCVE** with these three fluorinated olefins are summarized in Table 1.

Table 1. Radical copolymerizations[a] of 2-oxo-1,3-dioxolan-4-yl)methyl vinyl ether(GCVE) with chlorotrifluoroethylene (CTFE), hexafluoropropylene (HFP), and perfluoromethyl vinyl ether (PMVE)

	Feed composition[a]					
Run #	***coM***	***(%)***	***Copolymer composition coM %[b]***	***Yield (%)***	***$M_{n,exp}$[c] [g.mol^{-1}]***	***PDI M_w/M_n[c]***
P1	CTFE	70	56	85	4,200	1.9
P2	HFP	70	46	73	4,600	1.3
P3	PMVE	70	50	77	3,900	1.8
P4	CTFE	60	55	79	5,200	1.8
P5	CTFE	80	54	71	4,500	2.1

[a] Polymerization conditions: *t*-butyl peroxypivalate (5 mol%), Solvent : 1,1,1,3,3-pentafluorobutane, potassium carbonate (3 mol%), T = 75 °C for 14 h. Products characterized after precipitation in methanol. [b] Copolymer composition was determined from elemental analyses. [c] Molar masses and polydispersity indexes assessed from SEC calibrated with PMMA standards.

Downloaded by COLUMBIA UNIV on August 28, 2012 | http://pubs.acs.org
Publication Date (Web): August 16, 2012 | doi: 10.1021/bk-2012-1106.ch010

The radical copolymerization of glycidyl carbonate vinyl ether **(GCVE)** with chlorotrifluoroethylene (CTFE), hexafluoropropylene (HFP), or perfluoromethylvinyl ether (PMVE) led to white powders in 71-85 % yield which is satisfactory compared to data from literature (yield = 47-88 %) (*6*, *11*, *12*). They were soluble in polar solvents (such as DMF, DMSO, DMAc, acetone, NMP, propylene carbonate and dimethyl carbonate, etc..) while the parent homopoly(CTFE) is not soluble in such solvents (*31*).

The ^{1}H NMR spectra of all three copolymers exhibit the absence of signals located at 6.4, 4.8, and 4.1 ppm assigned to the vinylic protons of the free vinyl ether monomer (Figure 2). In addition, the complex signals of the methylene >CF-C**H**$_2$- in the backbone (from the vinyl ether) can be found at 2.5 to 3.2, 2.5 to 3.1, and 2.6 to 3.1 ppm in the case of poly(CTFE-*alt*-GCVE), poly(HFP-*alt*-GCVE), and poly(PMVE-*alt*-GCVE) copolymers, respectively (Figure 2). The methyne groups (>C**H**-OR) in the backbone are located at 4.7 to 4.9, 4.5 and 4.6 ppm for poly(CTFE-*alt*-GCVE), poly(HFP-*alt*-GCVE), and poly(PMVE-*alt*-GCVE) copolymers, respectively. The evolution of the chemical shifts of these methylene and methyne protons results from a mixture of diastereoisomers that arises from the presence of three different asymmetric carbon atoms (two carbon atoms are located on the polymeric backbone while one in the carbonate side-group). Thus, all protons in the copolymers are chemically non equivalent and led to AB systems. A similar evolution of the chemical shifts is also observed for the protons on the side chain. For example, the protons in (-O-C**H**$_2$-carbonate) groups are anisochronous and located at 4.1 to 4.3, 3.9 to 4.2, 4.0 to 4.2 ppm in poly(CTFE-*alt*-GCVE), poly(HFP-*alt*-GCVE), and poly(PMVE-*alt*-GCVE) copolymers, respectively. The same behavior was also observed for the protons of the cyclic carbonate.

The ^{19}F NMR spectra of these original copolymers (Figure 3) display the signals of -CF$_2$- from -107.2 to -117.8 ppm, from -107.2 to -120.8 ppm, from -113.5 to -128.3 ppm, for poly(CTFE-*alt*-GCVE) (P1), poly(HFP-*alt*-GCVE) (P2), and poly(PMVE-*alt*-GCVE) (P3) copolymers, respectively (*68–71*). The CF$_2$ of P3 is slightly upfield shifted due to the presence of OCF$_3$. The spectra do not show the central CFX and CF$_2$ signals in the dyad [-CF$_2$CFX-C*F*$_2$CFX] (*25*, *72*), demonstrating the alternating structure of these copolymers, that was further confirmed by elemental analysis (Table 2). The signals of >CF- group are located at -133.6, -182.2, and -135 and -146.9 ppm for P1, P2, and P3, respectively. Other signals present at -74.9 ppm in the spectra of P2 and at -53.0 ppm (*69*) in the spectra of P3 were attributed to the CF$_3$ groups of HFP and PMVE, respectively.

P1-P3 copolymers were also characterized by ^{13}C NMR spectroscopy using a DEPT mode (Figure 4). To the best of our knowledge, only a few examples of such characterization have been reported for poly(fluoroolefin-*alt*-VE) copolymers (*12*, *26*, *32*, *33*). ^{13}C NMR spectra of P1-P3 (Figure 4) exhibit very similar signals for the carbonyl group of the GC vinyl ether at 155.6 ppm. Both carbon atoms of the OCH groups (as negative signals) of the cyclic carbonate appear closely but different in poly(PMVE-*alt*-GCVE) copolymer (P3) ($\delta_{\text{OCH-}\textit{chain}}$ = 74.0 ppm and $\delta_{\text{OCH-}\textit{carbonate}}$ = 75.80 ppm). However, both carbon atoms of OCH in poly(CTFE-*alt*-GCVE) (**P1**) and poly(HFP-*alt*-GCVE) (**P2**) copolymers are located between 74.9 and 75.8 ppm or 74.8 and 75.8 ppm, respectively. Both

OCH_2 carbon atoms in carbonate (C2) and the vinyl ether (C4) are noted at 66.5 ppm and 71.8 ppm, respectively. Furthermore, the methylene carbon atoms of the vinyl ether in the backbone (C6) are located at 38.3, 30.6, and 34.9 for P1, P2, and P3, respectively. As expected, all carbon atoms bearing fluorine atoms are observed in the 90-130 ppm range. It is interesting to note the chemical shift of the CFX group that is obviously influenced by the X side-group (Cl, CF_3 and OCF_3). The >CF- carbon atoms (C7), expected as demultipleted doublets, are located at 104.4 and 106.9 ppm for poly(CTFE-*alt*-GCVE) (P1), 116.2 and 118.7 ppm for poly(HFP-*alt*-GCVE) (P2), and 111.8 and 114.3 ppm for poly(PMVE-*alt*-GCVE) (P3). Several complex triplets are assigned to the carbon atoms in CF_2 group (C8): 112.3, 115.3 and 118.0 ppm (P1); 121.3, 124.2, 127.1 ppm (P2); 117.9, 120.3, 123.1 ppm (P3). Carbon atoms of CF_3 group are upfield shifted for poly(PMVE-*alt*-GCVE) copolymer (P3) compared to poly(HFP-*alt*-GCVE) (P2) due to the presence of the oxygen. CF_3 groups (from HFP) induce a high field shift of its CF adjacent group (δ = 93.3 and 95.4 ppm), while OCF_3 side group favors a low field shift of ca. 20 ppm (δ = 116.9, 119.5, 122.1, and 124.7 ppm, respectively) with respect to CF adjacent to CF_3.

Molecular weights and polydispersity indices (PDI) of poly(F-olefin-*alt*-VE) copolymers were assessed by size exclusion chromatography calibrated with PMMA standards. As expected from the high content of initiator, the results show that the molecular weights ranged from 3,900 to 4,600 $g.mol^{-1}$ with polydispersity below 1.9. After evaporation of methanol from the precipitation media, it was possible in the case of P2 and P3 copolymers, to isolate a low molecular weight fraction of the copolymer as a viscous liquid of M_n = 1,900 $g.mol^{-1}$ and M_w/M_n = 1.2.

Thermal Properties

Figure 5 represents the thermogravimetric thermograms (TGA) of P1-P3 copolymers, recorded under air at 10 $°C.min^{-1}$. The curves consist of a single decomposition and degradation temperatures at 5% weight loss are higher than 255 °C. At 10% weight loss, the equivalent decomposition temperatures are above 285 °C. All copolymers left no residue at 550 °C, and the main decomposition occurred between 290 and 500 °C with a thermo-oxidation at ca. 450 °C. The good thermostability of these copolymers can be explained by the presence of the fluorinated units which usually start to decompose from around 300 °C. That compensates the poor thermostability of vinyl ether units (the degradation of which occurs usually from 150 °C (*73*, *74*)). Although these thermogravimetric analyses do not enable to clearly evaluate the durability of these copolymers at a given temperature, it is possible to consider that these copolymers should be stable at temperatures from -25 to +150 °C, corresponding to the operating temperature range of lithium ion batteries.

The differential scanning calorimetry analysis of the solid fraction of P1-3 copolymers showed neat inflexion assigned to the corresponding glass transition temperatures that ranged from 16 to 66 °C (Table 2) (*25*, *75*, *76*). This difference of T_g can be explained by the size of X group since OCF_3 is more bulky than CF_3 which is bigger than a chlorine atom, and this stiffens the copolymer.

Downloaded by COLUMBIA UNIV on August 28, 2012 | http://pubs.acs.org
Publication Date (Web): August 16, 2012 | doi: 10.1021/bk-2012-1106.ch010

Downloaded by COLUMBIA UNIV on August 28, 2012 | http://pubs.acs.org
Publication Date (Web): August 16, 2012 | doi: 10.1021/bk-2012-1106.ch010

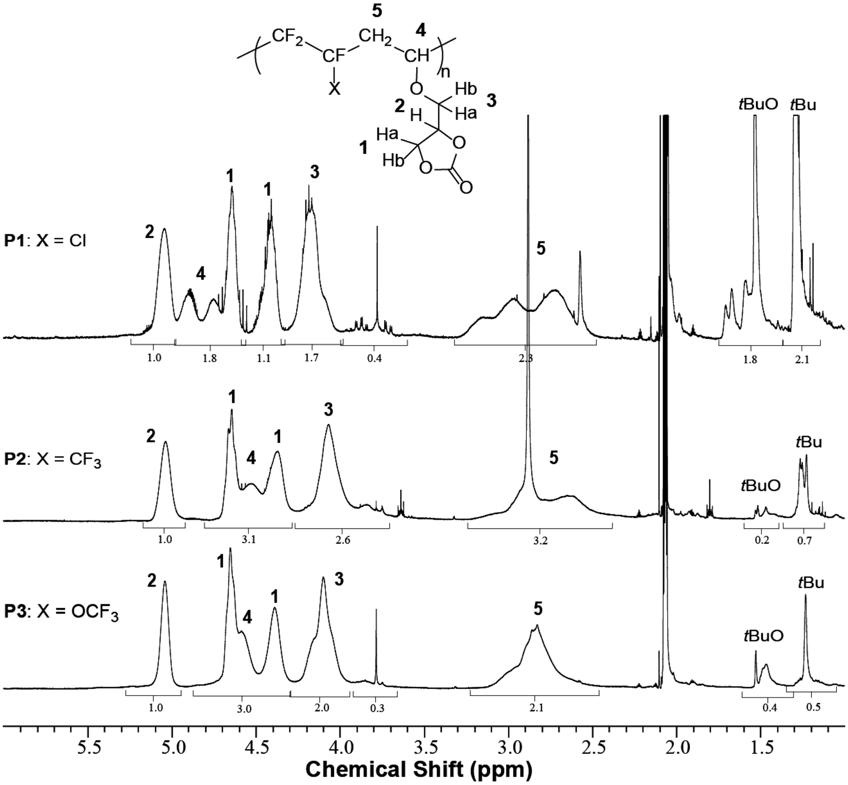

Figure 2. ^{1}H NMR spectra of poly(CTFE-alt-GCVE) (P1) (upper spectrum), poly(HFP-alt-GCVE) (P2) (middle spectrum), and poly(PMVE-alt-GCVE) (P3) (lower spectrum). (All spectra were recorded in acetone-d_6 at 20 °C). CTFE, HFP and PMVE stand for chlorotrifluoroethylene, hexafluoropropylene and perfluoromethyl vinyl ether, respectively.

Downloaded by COLUMBIA UNIV on August 28, 2012 | http://pubs.acs.org
Publication Date (Web): August 16, 2012 | doi: 10.1021/bk-2012-1106.ch010

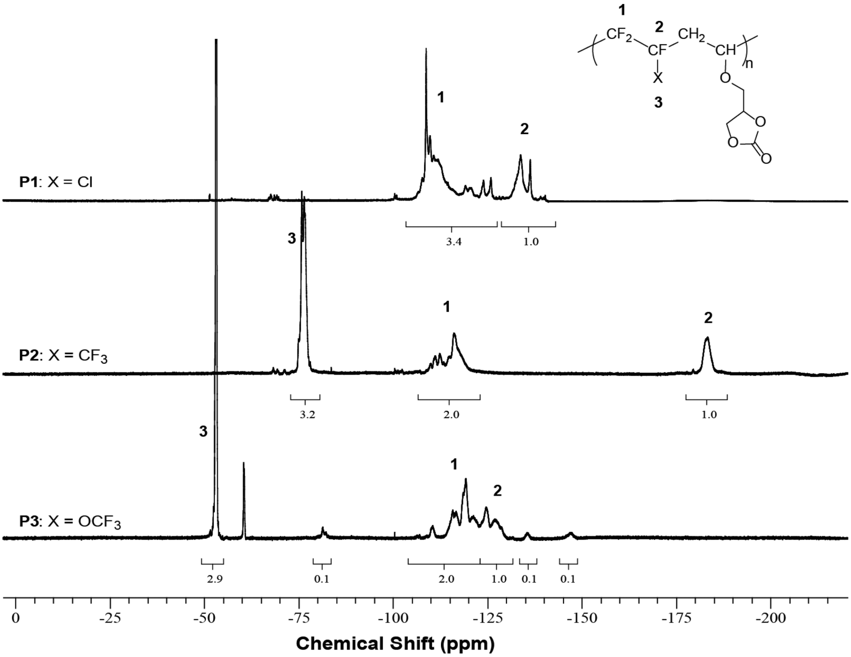

Figure 3. ^{19}F NMR spectra of poly(CTFE-alt-GCVE) (P1) (upper spectrum), poly(HFP-alt-GCVE) (P2) (middle spectrum), and poly(PMVE-alt-GCVE) (P3) (lower spectrum) copolymers (all spectra were recorded in acetone d_6 at 20 °C).

Downloaded by COLUMBIA UNIV on August 28, 2012 | http://pubs.acs.org
Publication Date (Web): August 16, 2012 | doi: 10.1021/bk-2012-1106.ch010

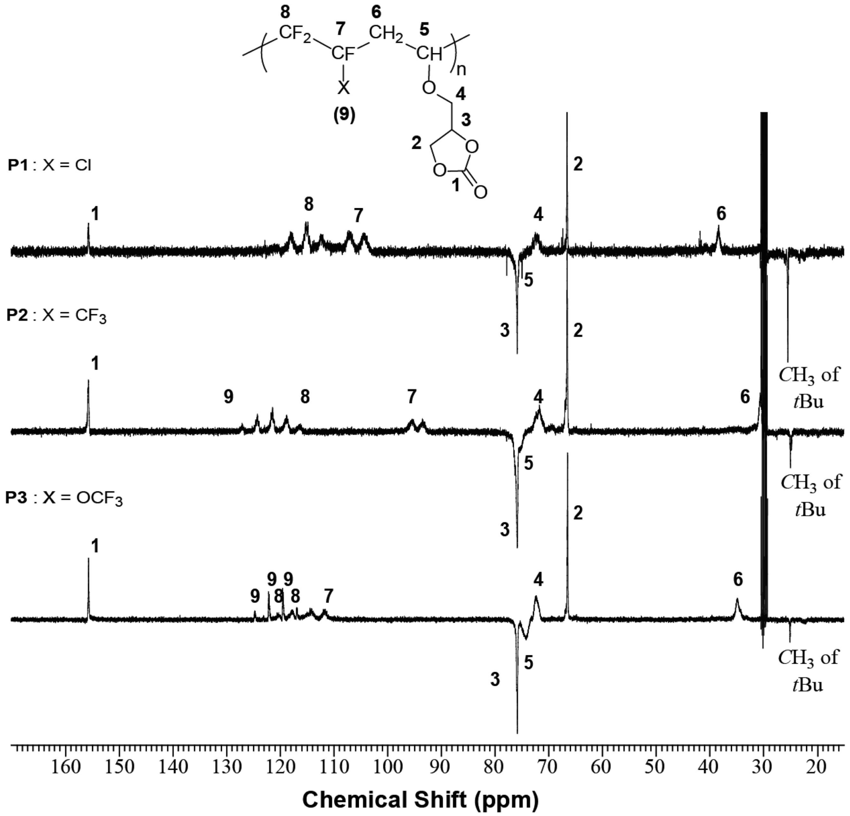

Figure 4. DEPT ^{13}C NMR spectra of poly(CTFE-alt-GCVE) (P1) (upper spectrum), poly(HFP-alt-GCVE) (P2) (middle spectrum), and poly(PMVE-alt-GCVE) (P3) (lower spectrum), (all spectra were recorded in acetone d_6 at 20 °C). CTFE, HFP and PMVE stand for chlorotrifluoroethylene, hexafluoropropylene and perfluoromethyl vinyl ether, respectively.

Downloaded by COLUMBIA UNIV on August 28, 2012 | http://pubs.acs.org
Publication Date (Web): August 16, 2012 | doi: 10.1021/bk-2012-1106.ch010

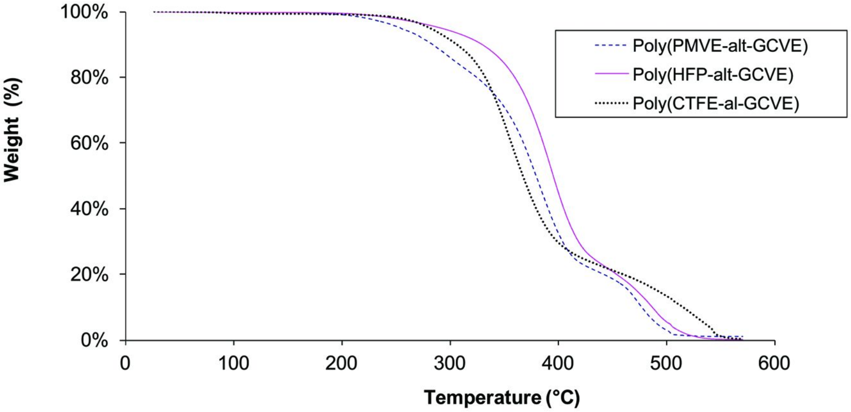

Figure 5. TGA thermograms of poly(CTFE-alt-GCVE) (P1), poly(HFP-alt-GCVE) (P2), and poly(PMVE-alt-GCVE) (P3) copolymers recorded under air at 10 °C.min^{-1}. CTFE, HFP and PMVE stand for chlorotrifluoroethylene, hexafluoropropylene and perfluoromethyl vinyl ether, respectively.

Table 2. Thermal properties of the fluorinated carbonate-bearing copolymers measured by TGA (under air) and DSC

Sample #	***Copolymers***	***%C***[a]	***%H***[a]	***%F***[a]	***$Td_{5\%}$***[b] ***(°C)***	***$Td_{10\%}$***[b] ***(°C)***	***Tg***[c] ***(°C)***
P1	poly(CTFE-*alt*-GCVE)	28.01	2.71	18.12	306	306	16
P2	poly(HFP-*alt*-GCVE)	38.33	3.14	37.08	293	330	47
P3	poly(PMVE-*alt*-GCVE)	35.35	2.82	36.91	254	284	66

[a] Percentages of carbon, fluorine and hydrogen atoms were assessed by elemental analysis (EA). [b] Assessed by thermogravimetric analysis (TGA), under air; 10 °C/min. [c] Determined by differential scanning calorimetry (DSC).

II. Synthesis and Characterization of Original Alternated Fluorinated Copolymers Bearing Oligo(ethylene oxide) Side-Chains

The development of new electrolytes endowed with a good thermostability has recently become a major challenge (*77–80*). Electrolytes based on poly(ethylene oxide) (PEO) (*36*, *37*, *80–87*) have satisfactory conducting properties for lithium batteries. PEO is capable of complexing the lithium salts, favoring the transport of Li$^+$ cations while maintaining an excellent interfacial stability.

Downloaded by COLUMBIA UNIV on August 28, 2012 | http://pubs.acs.org
Publication Date (Web): August 16, 2012 | doi: 10.1021/bk-2012-1106.ch010

Among these polymer electrolytes, fluorinated polymers based on PEO could be an attractive option since the fluorinated units bring the complementary properties required for the conduction of lithium ions (thermostability, chemical stability, mechanical properties…). Several authors have prepared blends of poly(vinylidene fluoride) (PVDF) with PEO (*88*) or PEO-*b*-PMMA (*89*) diblock copolymers (where PMMA stands for poly(methyl methacrylate) in the presence of dibutyl phthalates in 7/3/10 w/w proportions).

Cui and Xu (*90*) reported blends of PEO with other homopolymers or copolymers based on EO and propylene oxide. (Semi-) Interpenetrated polymer networks prepared by photopolymerization of blends of PVDF with di(meth)acrylates derivatives containing PEO units, have shown interesting conductivity values ($1.5x10^{-3}$ $S.cm^{-1}$) (*91*, *92*). Other authors prepared some PVDF-*g*-PEO graft copolymers from PVDF activated by ozone, γ-ray or ^{60}Co irradiation (*93*). Chen et al. (*94*) prepared original PVDF-*g*-PMMA graft copolymers that were further chemically changed by transesterification with PEO-OH leading to PVDF-*g*-PEOM (where PEOM stands for PEO-methacrylate). Furthermore, a team from MIT (*95*) achieved the same graft copolymer by atom transfer radical polymerization (ATRP) of PEOM ($M_n = 475$ g/mol) using PVDF as the macroinitiator, and CuCl complexed by *N,N,N′,N″,N″*-pentamethyldiethylene triamine. The same approach was reported by a Korean team (*96*) but from poly(VDF-*co*-CTFE) copolymer (where CTFE stands for chlorotrifluoroethylene) using a direct initiation on the C-Cl bonds to yield poly(VDF-*co*-CTFE)-*g*-PEOM graft copolymers. The major drawback of the ATRP method is the difficulty in eliminating all copper ions, which can affect the transport of lithium ions thus resulting in lower battery performances.

Although there are many articles and patents on the synthesis and use of PVDF-*g*-PEO graft copolymers, to the best of our knowledge, the literature does not mention any fluorinated oligomers or polymers based on CTFE and bearing PEO side-chains. Such PCTFE-*g*-PEO graft copolymers are of interest since they should exhibit good thermal properties and chemical inertness, and should be stable at low and high electrochemical potentials, fulfilling the requirements for Li-ion batteries electrolytes.

Several authors have reported the preparation of vinyl ethers involved in radical copolymerization that bear PEO chains (H_2C=CH-O-PEO) (*97–99*). But, none of them have been used conjointly with a fluorinated olefin to prepare either oligomers or copolymers that contain a fluorinated backbone and PEO grafts.

As above, these vinyl ethers were synthesized by transetherification of ethyl vinyl ether with oligo(ethylene glycol) monomethyl ether (n=3 or 10) catalyzed by a palladium(II) complex generated *in situ*. Such macromonomers with different molecular weights [oligo(EO) of 300 or 500 g mol^{-1}] were prepared leading to copolymers endowed with different morphologies, glass transition temperatures, and melting temperatures.

The synthesis of the oligo(EO)-bearing vinyl ether [oligo(EO)VEx where x corresponds to the number ethylene oxide units in the oligo(EO) chain] and their radical copolymerization with chlorotrifluoroethylene (CTFE) were carried out according to Scheme 4.

Downloaded by COLUMBIA UNIV on August 28, 2012 | http://pubs.acs.org
Publication Date (Web): August 16, 2012 | doi: 10.1021/bk-2012-1106.ch010

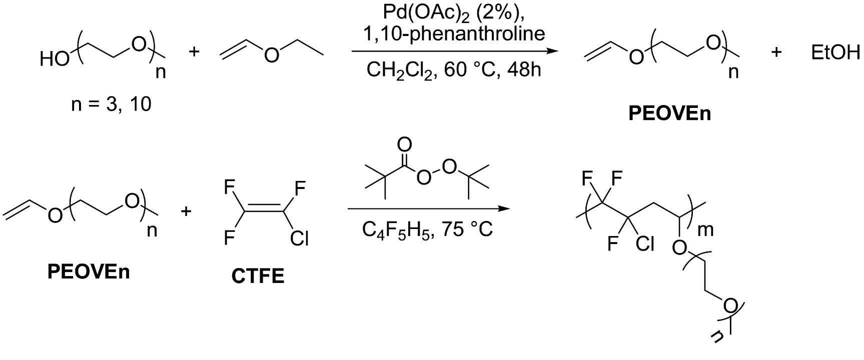

Scheme 4. Preparation of vinyl ethers bearing oligo(ethylene oxide) chains [oligo(EO)VE; n= 3 or 10)] and their radical copolymerization with chlorotrifluoroethylene (CTFE).

Original vinyl ethers that bear lateral chloromethyl (*40*) or carbonate groups (*61*) were synthesized by transetherification catalyzed by a palladium (II) complex generated *in situ*. As above, reactions were carried out in dichloromethane in the presence of 2% of palladium (II) acetate catalyst and 1,10-phenanthroline (as the ligand) at 60 °C. Using these optimized parameters (*40*, *61*), **oligo(EO)VE3** and **oligo(EO)VE10** monomers were prepared by transetherification of ethyl vinyl ether and methyl oligo(EO) (Scheme 4). The reaction was carried out yielding both macromonomers in 74 and 71 mol% yield, respectively.

Oligo(EO)VEx (x=3 or 10) vinyl ethers were characterized by ^{1}H and ^{13}C NMR spectroscopy. Both ^{1}H NMR spectra (Figure 6) in $CDCl_3$ at 20 °C display the two non-equivalent protons $C_6H_aH_b$ of the vinyl group as two doublets of doublets at 4.11 and 3.93 ppm for oligo(EO)VE3 and oligo(EO)VE10. The doublet of doublets assigned to the terminal methyne proton (=CH-) of both vinyl ethers is located at 6.41 ppm. The methylene groups in oligo (EO) can be noted as δ = 3.70 ppm. The singlet assigned to the methoxy end group is located at 3.30 ppm for oligo(EO)VE3 and oligo(EO)VE10.

The radical copolymerizations were carried out in an autoclave, in the presence of *tert*-butyl peroxypivalate (TBPPi 5 mol% initial ratio compared to monomers) and 1,1,1,3,3-pentafluorobutane at 75 °C, as the initiator and solvent, respectively (Scheme 4). As above, a high amount of initiator (5 mol.%) was intentionally used to get low molecular weight polymers for low viscosity-polymer electrolyte for lithium ion batteries.

As above, potassium carbonate (K_2CO_3) was added into the polymerization media to prevent from both the cationic homopolymerization and the formation of acetal from vinyl ether (*66*). Chlorotrifluoroethylene (CTFE) was used in slight excess to enable the complete consumption of the vinyl ether. The radical copolymerization of CTFE with vinyl ether is an exothermic reaction, and a rapid increase of pressure in the autoclave was observed (12-15 bar), followed by a sharp drop of pressure (3 bar). As above that copolymerization yielded poly(CTFE-*alt*-oligo(EO)VEx) alternating copolymers and their characteristics are listed in Table 3.

Downloaded by COLUMBIA UNIV on August 28, 2012 | http://pubs.acs.org
Publication Date (Web): August 16, 2012 | doi: 10.1021/bk-2012-1106.ch010

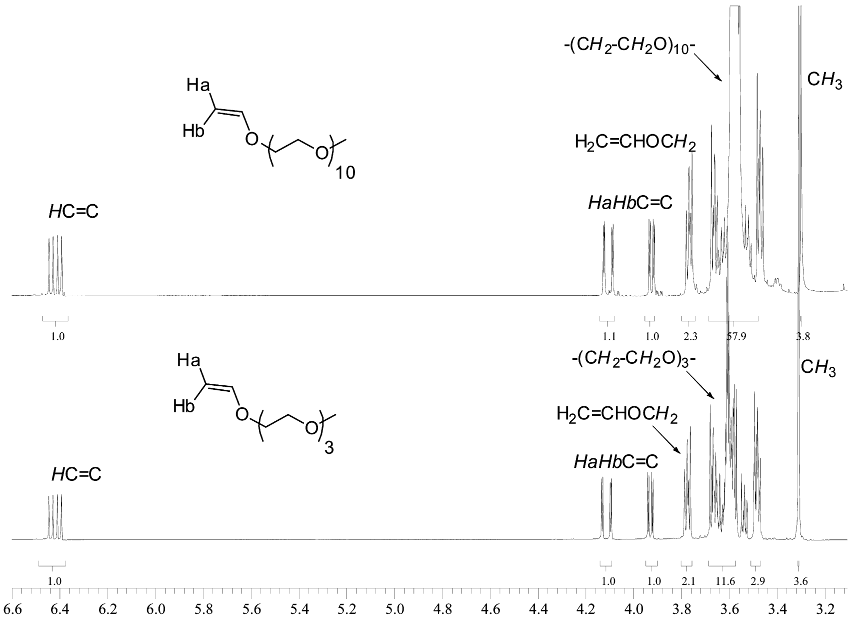

Figure 6. ^{1}H NMR spectra of vinyl ethers oligo(EO)VE3 (lower spectrum) and oligo(EO)VE10 (upper spectrum) recorded in $CDCl_3$ at room temperature.

Table 3. Radical copolymerization of oligo(EO)VE3 and oligo(EO)VE10 with chlorotrifluoroethylene (CTFE)

	Monomer feed ratio[a] (%)		*Copolymer compositon (%)[b]*				
Entry	***CTFE***	***oligo(EO)VE***	***Yield (%)***	***CTFE***	***oligo(EO)VE***	***$M_{n,exp}$[c] [g.mol^{-1}]***	***M_w/M_n[c]***
1	65	PEOVE3 (35)	61	53	47	13,700	2.4
2	65	PEOVE10 (35)	68	49	51	19,000	1.7

[a] Polymerization conditions: *t*-butyl peroxypivalate (5 mol%), Solvent : 1,1,1,3,3-pentafluorobutane, potassium carbonate (3 mol%), T = 75 °C for 14 h. Products characterized after precipitation from pentane. [b] Copolymer composition was assessed from elemental analyses. [c] Molar masses and polydispersity indices assessed from SEC calibrated with PMMA standards.

When using *t*-butyl peroxypivalate (5 mol% with respect to monomers) as the initiator at 75 °C, the yield of polymerization after precipitation ranged between 61 and 68 %. This is a satisfactory value compared to those of the literature for the radical copolymerization of CTFE with VEs in solution that

Downloaded by COLUMBIA UNIV on August 28, 2012 | http://pubs.acs.org
Publication Date (Web): August 16, 2012 | doi: 10.1021/bk-2012-1106.ch010

ranges between 47 and 88% (*6*, *11*, *12*). Both copolymers, well soluble in polar solvents (such as DMF, DMSO, DMAc, acetone, NMP, propylene carbonate and dimethyl carbonate, etc..) were characterized by ^{1}H, ^{19}F, and ^{13}C NMR spectroscopy, size exclusion chromatography (SEC) and elemental analysis. SEC showed that the molar masses of the poly(CTFE-*alt*-oligo(EO)VE) copolymers ranged from 13,700 to 19,000 g mol^{-1} and present typical polydispersity indices for such copolymerization ($1.70<M_w/M_n<2.48$). ^{1}H NMR spectra (Figure 7) of poly(CTFE-*alt*-oligo(EO)VEx) copolymer exhibit the absence of signals centered at 6.41 ppm characteristic of non-reacted VE vinylic protons. However, their polymerized equivalent –CH_2-CH[oligo(EO)Me]- can be found between 2.5 and 3.0 ppm, and between 4.5 and 5.0 ppm for the methylene and methyne protons, respectively. Both signals are complex due to the presence of two types of asymmetric carbons (in the CTFE-VE dyad) leading to two diastereoisomers, which makes these protons non equivalent (or anisochronous). Methylenic protons of the PEO chain (-OCH_2-) are similar in both polymers and located at 3.65 ppm, while that immediately adjacent to the oxygen from the vinyl ether is located at 3.93 ppm. However, as in the ^{1}H NMR spectrum of oligo(EO)VE, the methoxy protons can be found at ca. 3.30 ppm.

Furthermore, the ^{19}F NMR spectra of the poly(CTFE-*alt*-oligo(EO)VE) copolymers (Figure 8) do not exhibit the characteristic signal at -127 ppm of the CTFE-CTFE dyads i.e. the central CFCl in -CF_2CFCl-CF_2CFCl- (*25*, *72*), and evidenced that these copolymers have an alternating -[CF_2CFCl-CH_2CH(O-oligo(EO)Me)]$_x$- structure. However, these spectra showed that the chemical shifts assigned to the CTFE units are independent of the methyl oligo(EO) chain length. Signals ranging between -107.0 and -123.1 ppm (*68*), and the signal centered at -124.4 ppm were assigned to the –C**F**$_2$- and –CFCl- of both A and B diastereoisomers, respectively, as depicted in Figure 8.

Unlike other poly(fluoroalkene-*co*-vinyl ether) copolymers (*12*, *25*, *26*, *32*, *33*), these new poly[CTFE-*alt*-VEoligo(EO)] copolymers were also characterized by DEPT ^{13}C NMR spectroscopy (Figure 9). The spectra show all the signals assigned to the carbons from either CTFE or the vinyl ether and are not much affected by the oligo(EO)Me chain length (3 or 10 units). Several signals assigned to the CTFE units were observed at 121.05, 118.57, 115.94, 113.81, 111.80, and 109.97 ppm (x = 3) or, 121.04, 118.31, 115.42, 113.60, 111.40 and 109.40 (x = 10). As for the above poly(CTFE-*co*-GCVE) copolymers, the signals assigned to the methylene in -**C**H_2-CH[oligo(EO)Me]- group of vinyl ether units are located at 38.93 (x = 3) or 39.18 ppm (x = 10). The two signals either at 78.73 and 75.75 ppm (x = 3) or 78.56 and 75.75 (x = 10) resulting from both diastereoisomers were assigned to the asymmetric carbon atom in -CH_2-**C***H[oligo(EO)Me]-. These tertiary carbon atoms induced negative signals in DEPT ^{13}C NMR spectra. The –O-**C**H_2- adjacent to the backbone and the methoxy carbon (–O**C**H_3) are located at 72.41 and 58.79 ppm, or 72.81 and 58.94 ppm for copolymers having x = 3 and 10, respectively. The carbon atoms of the oligo(EO)Me chains are located between 70.41 and 74.07, or 69.90 and 73.62 ppm for x = 3 and 10, respectively.

Downloaded by COLUMBIA UNIV on August 28, 2012 | http://pubs.acs.org
Publication Date (Web): August 16, 2012 | doi: 10.1021/bk-2012-1106.ch010

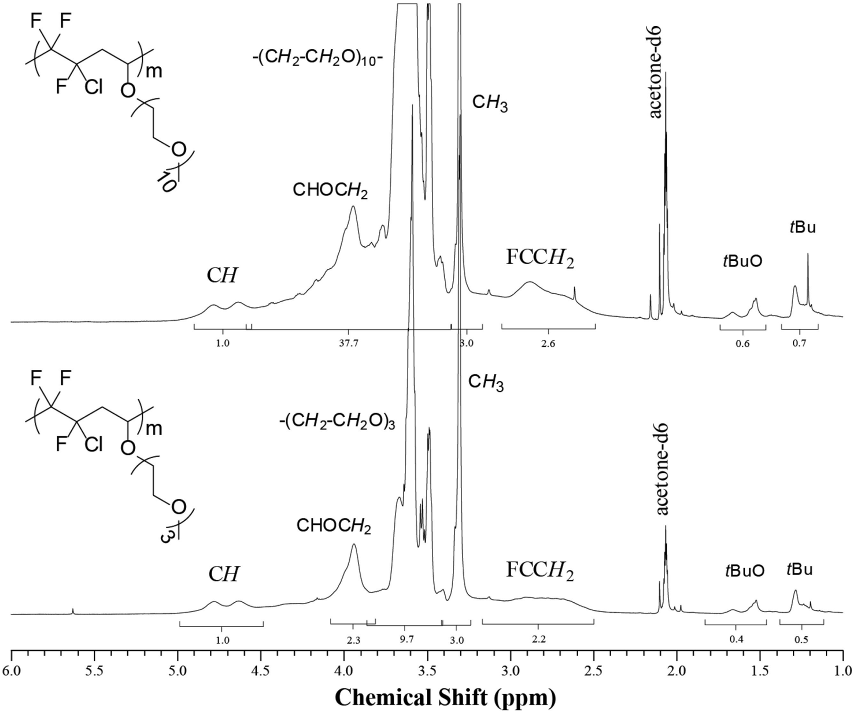

Figure 7. ^{1}H NMR spectra of poly(CTFE-alt-oligo(EO)VE3) (lower spectrum) and poly(CTFE-alt-oligo(EO)VE10) (upper spectrum) recorded in acetone-d6 at room temperature.

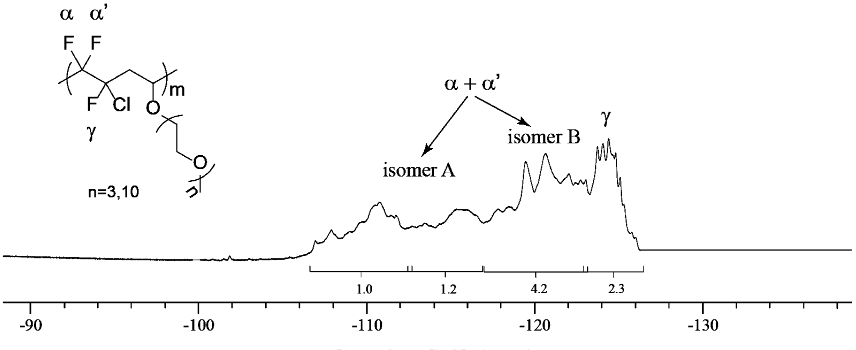

Figure 8. ^{19}F NMR spectrum of poly(CTFE-alt-oligo(EO)VE3) recorded in acetone-d6 at room temperature.

Downloaded by COLUMBIA UNIV on August 28, 2012 | http://pubs.acs.org
Publication Date (Web): August 16, 2012 | doi: 10.1021/bk-2012-1106.ch010

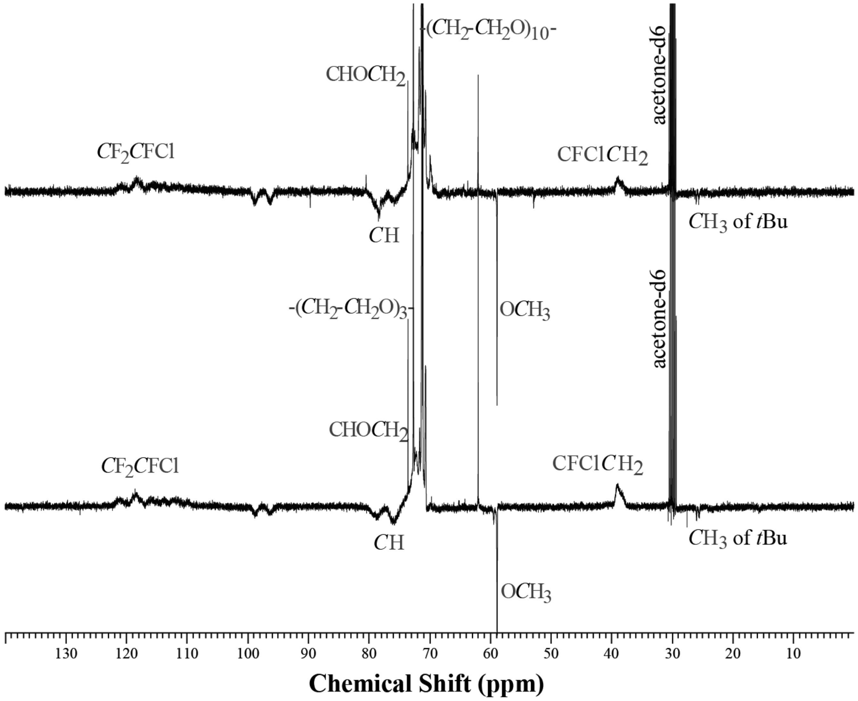

Figure 9. ^{13}C NMR spectra of poly[CTFE-alt-oligo(EO)VE3] (lower spectrum) and poly[CTFE-alt-oligo(EO)VE10] (upper spectrum) recorded in acetone-d6 at room temperature.

Thermal properties of these copolymers were assessed by thermogravimetric analysis (TGA) and differential scanning calorimetry (DSC). Figure 10 represents the TGA thermograms for both poly(CTFE-*alt*-oligo(EO)VE3) and poly[CTFE-*alt*-oligo(EO)VE10] copolymers under air. Only one main degradation was observed and the decomposition temperatures at 5 and 10 percent weight loss were different in both copolymers: poly[CTFE-*alt*-oligo(EO)VE3] degradation initiated from about 215 °C while that of poly[CTFE-*alt*-oligo(EO)VE10] copolymer started from at 267 °C and lasted up to 540 °C in both cases. This difference was attributed to the increased thermostability with increasing oligo(EO) chain length. The satisfactory thermostability of these copolymers can be explained by the good stability of the CTFE units (the degradation of which occurs from 300 °C) and compensates for the poor thermal stability of the VE units (that usually occurs as soon as 120 °C) (*73*, *74*). A more detailed analysis of the TGA thermograms enables to evidence two main decompositions: although the TGA experiments did not enable to clearly evaluate the durability of these polymers at a given temperature, we can however consider that in the operating temperature range for the lithium-ion batteries (-30 to +120 °C), these polymers should not degrade.

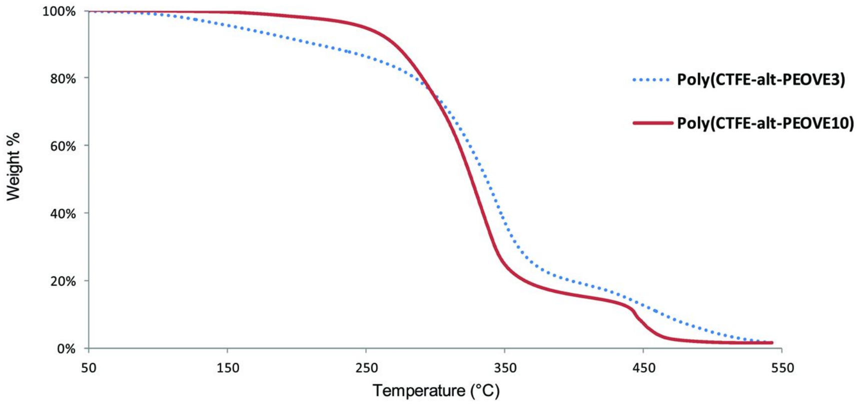

Figure 10. TGA thermograms obtained under air at 10 °C min^{-1} for both poly[CTFE-alt- oligo(EO)Vex] copolymers (x = 3 and 10).

DSC analyses (Table 4) of the poly(CTFE-*alt*-oligo(EO)VEx) copolymers enabled to evidence both the decrease of the glass transition temperature with increasing oligo(EO)VE content (i.e. chain length) and the absence of melting temperature that stems from the amorphous character of these copolymers (*25*, *75*, *76*). Actually, the presence of ether group in oligo(EO) induces a lower T_g value. This is in good agreement with the high T_g (ca 55-70 °C) and melting points (T_m = 220 °C) of PCTFE that is a semi-crystalline homopolymer in contrast to these alternating poly(CTFE-*alt*-VE) copolymers that do not contain any oligo(CTFE) sequences to enable the crystallization (*31*).

Table 4. Decomposition and glass transition temperature of poly[CTFE-*alt*-oligo(EO)VEx] copolymers obtained by TGA (under air) and DSC

Copolymers	$T_{d,5\%}$ *(°C)*	$T_{d,10\%}$ *(°C)*	T_g *(°C)*
Poly[CTFE-*alt*-oligo(EO)VE3]	160	215	-36
Poly[CTFE-*alt*-oligo(EO)VE10]	247	269	-42

These fluorinated elastomers have satisfactory (good thermostability, low glass transition temperature, amorphous character) fulfilling the requirements for polymer electrolytes for lithium-ion batteries.

Conclusions

Original fluorinated copolymers containing either carbonate groups or oligo(ethylene oxide), oligo(EO), chains were prepared by radical copolymerization of commercially available fluoroolefins with a vinyl ether bearing a carbonate group or an oligo(ethylene oxide) chain. The vinyl ethers were obtained in good yields by transetherification of ethyl vinyl ether with

Downloaded by COLUMBIA UNIV on August 28, 2012 | http://pubs.acs.org
Publication Date (Web): August 16, 2012 | doi: 10.1021/bk-2012-1106.ch010

Downloaded by COLUMBIA UNIV on August 28, 2012 | http://pubs.acs.org
Publication Date (Web): August 16, 2012 | doi: 10.1021/bk-2012-1106.ch010

the appropriate glycerol carbonate or ω-hydroxyoligo(OE) in the presence of a palladium complex generated *in situ*. Then, it was copolymerized with various fluoroalkenes (especially chlorotrifluoroethylene or with HFP and PMVE) in good yields leading to alternating structures. NMR characterization and elemental analyses enabled us to confirm the alternance of these copolymers. Molecular weights and thermal properties of these copolymers were also assessed. These copolymers could pave the way to the design of polymer electrolytes in lithium batteries and should exhibit interesting conduction of lithium ions thanks to the cyclic carbonate and oligo(ethylene oxide) chain. They also exhibit good thermal properties and good chemical inertness and stability, required for Li-ion batteries. Hence, the solid and liquid fractions of these original copolymers can be also tested [at high potential (ca. 3 - 5 V)] used as polymer electrolytes for the conduction of lithium ions, under investigation.

Experimental

Materials

Tert-butylperoxypivalate (TBPPI) was kindly provided by Akzo Nobel (Compiègne, France). Chlorotrifluoroethylene (CTFE), hexafluoropropylene (HFP), perfluoromethylvinyl ether (PMVE) and 1,1,1,3,3-pentafluorobutane were kindly provided by Honeywell (Buffalo, NY), Solvay S.A. (Tavaux, France & Bruxelles, Belgium) and DuPont Performance Elastomers (Wilmington, DE) were used as received. Ethyl vinyl ether, palladium acetate, glycerol carbonate, triethylene glycol monomethyl ether, poly(ethylene glycol) monomethyl ether (DP_n = 10), 1,10-phenanthroline, potassium carbonate, acetone (analytical grade), dichloromethane (analytical grade), methanol (analytical grade), tetrahydrofuran (THF, analytical grade) were purchased from Sigma-Aldrich (Saint Quentin-Fallavier, France). Deuterated solvents for the NMR spectroscopy were purchased from Euroiso-top (Grenoble, France) (purity>99.8%).

Characterization

Nuclear Magnetic Resonance

The nuclear magnetic resonance (NMR) spectra were recorded on a Bruker AC 400 instrument, using deuterated chloroform, d_6-N,N-dimethylsulfoxide, and d_6-acetone as the solvents and tetramethylsilane (TMS) (or $CFCl_3$) as the references for ^1H (or ^{19}F) nuclei. Coupling constants and chemical shifts are given in hertz (Hz) and part per million (ppm), respectively. The experimental conditions for recording ^1H, ^{13}C, (or ^{19}F) NMR spectra were as follows: flip angle 90° (or 30°), acquisition time 4.5 s (or 0.7 s), pulse delay 2 s (or 2 s), number of scans 128 (or 512), and a pulse width of 5 μs for ^{19}F NMR.

Downloaded by COLUMBIA UNIV on August 28, 2012 | http://pubs.acs.org
Publication Date (Web): August 16, 2012 | doi: 10.1021/bk-2012-1106.ch010

Size Exclusion Chromatography

Size exclusion chromatograms (SEC) were recorded using a GPC 50 from Polymer Labs (now Agilent) with its corresponding software (Cirrus). The system used two PL-Gel Mixed-C columns ($200<M_n<20{,}000{,}000$ g.mol^{-1}) with tetrahydrofuran as the eluent with a flow rate of 1.0 mL.min^{-1} at room temperature. Both RI and UV detectors can be used. PMMA standards were used for the calibration. Sample concentration was 1 wt%.

Thermogravimetric Analyses

Thermogravimetric analyses (TGA) were performed with a TGA Q50 apparatus from TA Instruments, under air, at the heating rate of 10 °C.min^{-1} from room temperature up to a maximum of 550 °C. The sample weight varied between 10 and 15 mg.

Differential Scanning Calorimetry

Differential scanning calorimetry (DSC) analyses were conducted on a Netzsch 200F3 DSC apparatus equipped with Proteus software under nitrogen atmosphere at a heating rate of 20 °C/min. The temperature range was between from -50 to +200 °C. DSC system was first calibrated in temperature using indium and n-hexane. The second run led to the glass transition temperature defined as the inflexion point in the heat capacity jump. The sample weight was about 10 mg.

Elemental Analyses

Weight percentages of carbon, fluorine, chlorine, and hydrogen atoms were assessed by elemental analysis (EA) at the CNRS – Service Central d'Analyse (Solaize, France) on a CH elemental analyzer equipped with a CO_2/H_2O infrared detector, from the copolymer compositions, calculated using the following equations:

Copolymer bearing carbonate groups:

$$\frac{\%H}{\%C}=\frac{8p}{(12xN)n+72p}$$

$$\frac{\%F}{\%C}=\frac{19\times F\times n}{(12xN)n+72p}$$

$$p+n=1$$

Where *F*, *N, p,* and *n* are the number of fluorine or carbon atoms in the fluorolefin, and the percentages of vinyl ether and fluoroolefin, respectively.

Example of calculation for poly(PMVE-*alt*-GCVE) copolymer P3: % C = 35.35% ; % H = 2.82% and % F = 36.91%

$$\%\,PMVE = \frac{\%F}{\%C} = \frac{19 \times F \times n}{(12xN)n + 72p} = \frac{36.91}{35.35} = 1.04$$

$$\%\,PMVE = \frac{114\ n}{36n + 72p} = 1.04$$

$$114\mathrm{n} = 1.04(36\mathrm{n} + 72 - 72\mathrm{n})\ ;\mathrm{p} = 1 - \mathrm{n}$$

$$\boldsymbol{n} = \mathbf{49.4\%}$$

$$\%\,VE = \frac{\%H}{\%C} = \frac{8p}{36n + 72p} = \frac{8\mathrm{p}}{36 + 36\mathrm{p}} = 0.08$$

$$8\mathrm{p} = 0.08(36 + 36\mathrm{p}) \quad \mathbf{p = 56\%}$$

Copolymer bearing POE groups:

$$\frac{\%H}{\%C} = \frac{(6 + 4n)q}{24p + (36 + 24n)q}$$

$$\frac{\%F}{\%C} = \frac{57p}{24p + (36 + 24n)q}$$

$$p + q = 1$$

where p, q and n are the percentages of fluoroolefin, of vinyl ether and number of ethylene oxide groups in oligo(EO) (n = 3 or 10), respectively.

Chemistry

Autoclave Operations

The radical copolymerizations were performed in a 160 mL Hastelloy Parr autoclave systems (HC 276) equipped with a manometer, a mechanical Hastelloy anchor, a rupture disk (3000 PSI), inlet and outlet valves. An electronic device regulated and controlled both the stirring and heating of the autoclave. Prior to reaction, the autoclave was pressurized with 30 bars of nitrogen to check for leaks. The autoclave was then conditioned for the reaction with vacuum (10^{-2} mbar) for 40 minutes to remove any trace of oxygen. The liquid and dissolved solid phases were introduced via a funnel and then the gases (CTFE, HFP or PMVE) were

Downloaded by COLUMBIA UNIV on August 28, 2012 | http://pubs.acs.org
Publication Date (Web): August 16, 2012 | doi: 10.1021/bk-2012-1106.ch010

introduced by double weighing (i.e. the difference of weight before and after filling the autoclave with the gas).

Synthesis of (2-Oxo-1,3-dioxolan-4-yl)methyl Vinyl Ether (GCVE)

In a Schlenk, palladium acetate (760 mg, 3.38 mmol) was dissolved in dichloromethane (10 mL). A solution of 1,10-phenanthroline (916 mg, 5.08 mmol) in dichloromethane (10 mL) was then added into the Schlenk. The reaction medium was stirred at room temperature for 30 minutes to generate the palladium catalyst *in situ*. A glycerol carbonate solution (20.00 g, 0.169 mol) and ethyl vinyl ether (73.33 g, 1.01 mol) were added to the reaction medium that was further transferred into the autoclave and heated at 60 °C for 24 hrs. After cooling, the autoclave was opened and both dichoromethane and ethyl vinyl ether were evaporated under vacuum. The remaining product was dissolved in 200 mL of deionized water. The mixture was extracted three times with 200 mL of dichloromethane. The organic phase was dried with sodium sulfate, filtered, and the dichloromethane evaporated. The final product was a yellow liquid obtained in 45% yield.

Synthesis of Methoxy-tri(ethylene oxide) Vinyl Ether Oligo(EO)VE3

The experimental procedure and purification were similar to that of **GCVE**. Palladium acetate (380 mg, 1.69 mmol), dichloromethane (10 mL), 1,10-phenanthroline (458 mg, 2.54 mmol), A triethylene glycol monomethyl ether solution (13.90 g, 0.0847 mol) and ethyl vinyl ether (36.66 g, 0.50 mol) were introduced in the autoclave. The reaction medium was then transferred into the autoclave and heated at 60 °C for 24 hrs. After cooling, the autoclave was opened and both dichoromethane and ethyl vinyl ether were evaporated under vacuum. The remaining product was dissolved in 100 mL of deionized water. The mixture was extracted three times with 100 mL of dichloromethane. The organic phase was dried with sodium sulfate, filtered, and the dichloromethane evaporated. The final product was a yellow liquid obtained in 84% yield.

Synthesis of Methoxyoligo(ethylene oxide) Vinyl Ether Oligo(EO)VE10

The experimental procedure and purification were similar to that of methoxy-tri(ethylene oxide) vinyl ether **oligo(EO)VE3**. Palladium acetate (448 mg, 2.0 mmol), dichloromethane (25 mL), 1,10-phenanthroline (540 mg, 3.0 mmol), oligo(ethylene glycol) monomethyl ether, (20.00 g, 0.04 mol) and ethyl vinyl ether (17.3 g, 0.24 mol) were introduced in the autoclave. The reaction was carried out at 60 °C for 24 hrs. The purification were similar as that used above for oligo(EO)VE3. The final product was a yellow liquid obtained in 71% yield.

Downloaded by COLUMBIA UNIV on August 28, 2012 | http://pubs.acs.org
Publication Date (Web): August 16, 2012 | doi: 10.1021/bk-2012-1106.ch010

Downloaded by COLUMBIA UNIV on August 28, 2012 | http://pubs.acs.org
Publication Date (Web): August 16, 2012 | doi: 10.1021/bk-2012-1106.ch010

Radical Copolymerization

Radical Copolymerization of GCVE with Chlorotrifluoroethylene (CTFE)

To prevent any homopolymerization of the GCVE vinyl ether by acid catalysis and the formation of the acetal from the vinyl ether (*67*), potassium carbonate K_2CO_3 (161 mg, 1.16 mmol) was inserted in the reaction prior conditioning. Vinyl ether **GCVE** (5.6 g, 0.0338 mol), *tert*-butylperoxypivalate (TBPPi) (1.80 g, 7.76 mmol), and 50 mL of 1,1,1,3,3-pentafluorobutane were transfered *via* a tight funnel. Chlorotrifluoroethylene (13.5 g, 0.116 mol) was then introduced by double weighing (i.e. difference of weight before and after transferring the gas). The copolymerization was carried out at 75 °C for 15 hrs. First, a pressure increase was noted due to the increasing temperature and exothermicity of this reaction. Then, a pressure drop (12 bar) was noticed attributed to the consumption of the CTFE during the polymerization. After the polymerization, the reactor was cooled in an ice bath for 30 min and then degased. No gas was released meaning a quantitative gas conversion (though CTFE has a good solubility in the 1,1,1,3,3-pentafluorobutane). The reaction mixture was dissolved in acetone and precipitated from unreacted methanol to eliminate any residual solvent, monomer, potassium carbonate, and initiator. The product was dried under vacuum at 50 °C until constant weight yielding 17.14 g of a white powder. The massic yield was 90%.

Radical Copolymerization of GCVE with Hexafluoropropylene (HFP)

The procedure was similar as that of the radical copolymerization of chlorotrifluoroethylene with GCVE, using potassium carbonate (138 mg, 1 mmol), GCVE (4.8 g, 0.033 mol), *tert*-butyl peroxypivalate (TBPPi) (1.54 g, 6.66 mmol), 50 mL of 1,1,1,3,3-pentafluorobutane, and hexafluoropropylene (15.00 g, 0.1 mol). The copolymerization was carried out in the same above autoclave at 75 °C for 15 hrs. Similar increase (11 bar) and drop of pressure was observed. A similar post-copolymerization procedure was also carried out. The copolymerization yielded 14.10 g of brown powder after precipitation. The massic yield was 71%. The filtrate from the precipitation was evaporated under vacuum, dissolved in acetone again and precipitated from water. The precipitate was dried at 70 °C under vacuum and 3.0 g of viscous beige liquid was obtained.

Radical Copolymerization of GCVE with Perfluoromethylvinyl Ether (PMVE)

The experimental procedure was similar to that of CTFE and HFP, using potassium carbonate (100 mg, 0.72 mmol), GCVE (3.5 g, 0.0243 mol), *tert*-butyl peroxypivalate (TBPPi) (1.41 g, 6.07 mmol), 50 mL of 1,1,1,3,3-pentafluorobutane, and perfluoromethylvinyl ether (16.00 g, 0.097 mol). The copolymerization was carried out in the autoclave at 75 °C for 15 hrs. A similar increase (9 bar) and drop of pressure were observed. The work up of the copolymer was carried out as above. The copolymerization yielded 11.60 g of brown powder after precipitation, leading to a massic yield of 60%. The filtrate

Downloaded by COLUMBIA UNIV on August 28, 2012 | http://pubs.acs.org
Publication Date (Web): August 16, 2012 | doi: 10.1021/bk-2012-1106.ch010

from the precipitation was evaporated under vacuum, dissolved in acetone again and precipitated from water. The precipitate was dried at 70 °C under vacuum and 3.4 g of viscous liquid was obtained (Mn =1,900 g/mol^{-1}).

Copolymerization of Oligo(EO)VE3 with Chlorotrifluoroethylene

The procedure was similar as that of the radical copolymerization of chlorotrifluoroethylene with GCVE, using potassium carbonate (161 mg, 1.16 mmol), **oligo(EO)VE3** (7.30 g, 0.0338 mol), *tert*-butyl peroxypivalate (TBPPi) (1.80 g, 7.76 mmol), and 50 mL of 1,1,1,3,3-pentafluorobutane were inserted via a tight funnel. Chlorotrifluoroethylene (13.5 g, 0.116 mol) was then introduced by double weighing. The copolymerization was carried out at 75 °C for 15 hrs. First, an increase of pressure was noted due to the increasing temperature and exothermicity of this reaction. Then, a pressure drop was observed correlated to the consumption of the CTFE during the polymerization. After the polymerization, the reactor was cooled in an ice bath for 30 min and then degased. No gas was released meaning a high gas conversion (though CTFE has a good solubility in the 1,1,1,3,3-pentafluorobutane). The reaction mixture was dissolved in acetone and precipitated from pentane to eliminate any residual solvent, monomer, potassium carbonate, initiator and oligomers. The product was dried under vacuum at 50 °C until constant weight yielding 12.6 g of white powder (**5**) (yield = 61%).

Copolymerization of Oligo(EO)VE10 with Chlorotrifluoroethylene

The experimental procedure was similar as that of the radical copolymerization of CTFE with vinyl ether **oligo(EO)VE10**. Potassium carbonate (138 mg, 1 mmol), **oligo(EO)VE10** (20.41 g, 0.0388 mol), *tert*-butyl peroxypivalate (TBPPi) (1.80 g, 7.76 mmol), 50 mL of 1,1,1,3,3-pentafluorobutane, and CTFE (13.5 g, 0.116 mol) were introduced in the autoclave. The copolymerization was carried out at 75 °C for 15 hrs. Similar increase and drop of pressure were observed. Similar post-copolymerization procedure work-up and purification were also carried out. The copolymerization yielded 22.8 g of a brown powder after precipitation (**6**) (yield = 68%).

Acknowledgments

The authors thank Prof. Boutevin for inspiration and Honeywell, Solvay-Solexis and DuPont Performance Elastomers for supplying free samples of CTFE, HFP and PMVE, respectively.

References

1. Feiring, A. E. In *Organofluorine Chemistry: Principles and Commercial Applications*; Banks, R. E., Smart, B. E., Tatlow, J. C., Eds.; Plenum Press: New York, 1994; Volume 15, pp 339−372.

Downloaded by COLUMBIA UNIV on August 28, 2012 | http://pubs.acs.org
Publication Date (Web): August 16, 2012 | doi: 10.1021/bk-2012-1106.ch010

2. Scheirs, J. In *Modern Fluoropolymers*; Scheirs, J., Ed.; Wiley: New York, 1997; Chapter 24, pp 435−486.
3. Hougham, G.; Cassidy, P. E.; Johns, K.; Davidson, T. *Fluoropolymers 2: Properties*; Kluwer/Plenum: New York, 1999.
4. Ameduri, B.; Boutevin, B. In *Well-Architectured Fluoropolymers: Synthesis, Properties and Applications*; Elsevier: Amsterdam, 2004; Chapter 3.
5. David, G.; Boyer, C.; Tonnar, J.; Ameduri, B.; Lacroix-Desmazes, P.; Boutevin, B. *Chem. Rev.* **2006**, *106*, 3936–3962.
6. Takakura, T. In *Modern Fluoropolymers*; Scheirs, J., Ed.; Wiley Interscience: New York, 1997; Chapter 29, pp 557−564.
7. Brown, D. W.; Wall, L. A. *J. Polym. Sci., Part A: Polym. Chem.* **1968**, *6*, 1367–1379.
8. Greenley, R. Z. In *Polymer Handbook*; Abe, A., Bloch, D. R., Immergut, E. H., Eds.; Wiley Intersciences: New York, 1999; Vol. II, pp 309−378.
9. Moggi, G.; Bonardelli, P.; Russo, S. *Conv. Ital. Sci. Macromol.* **1983**, *2*, 405–408.
10. Kojima, G.; Yamabe, M. *Yuki Gosei Kagadu Kyokaishi (J. Synth. Org. Chem. Jpn.)* **1984**, *42*, 841–849.
11. Boutevin, B.; Cersosimo, F.; Youssef, B. *Macromolecules* **1992**, *25*, 2842–2846.
12. Gaboyard, M.; Hervaud, Y.; Boutevin, B. *Polym. Int.* **2002**, *51*, 577–584.
13. Braun, D.; Elsasser, H.; Hu, F. *Eur. Polym. J.* **2001**, *37*, 1779–1784.
14. Reyntjens, W. G. S.; Goethals, E. *J. Polym. Adv. Technol.* **2001**, *12*, 107–122.
15. Ameduri, B.; Boutevin, B. *J. Fluorine Chem.* **2000**, *104*, 53–62.
16. Boutevin, B.; Ameduri, B. *Macromol. Symp.* **1994**, *82*, 1–17.
17. Tabata, Y.; Du Plessis, T. A. *J. Polym. Sci., Part A: Polym. Chem.* **1971**, *9*, 3425–3435.
18. Samuels, G. J.; Shafer, G. J.; Li, T.; Threlfall, C. A.; Iwamoto, N.; Rainal, E. J. WO-2008/079986 A1, assigned to Honeywell International, Inc.
19. Yamabe, M.; Higaki, H.; Kojima, G. *Org. Coat. Sci. Technol.* **1984**, *16*, 25–39.
20. Munekata, S. *Prog. Org. Coat.* **1988**, *16*, 113–134.
21. Scheirs, J.; Burks, S.; Locaspi, A. *Trends Polym. Sci.* **1995**, *3*, 74–82.
22. Yamauchi, M.; Hirono, T.; Kedama, S. I.; Matsuo, M. *Eur. Coat. J.* **1996**, 124–128.
23. Ichimura, M.; Miyake, H.; Kodama, S.; Hisasue, M. DE-1978/2804262, assigned to Asahi Glass Co,. Ltd., Japan.
24. Hisasue, M.; Kojima, G.; Kojima, H. Japan-1979/54163985, assigned to Asahi Glass Co., Ltd., Japan.
25. Valade, D.; Boschet, F.; Ameduri, B. *Macromolecules* **2009**, *42*, 7689–7700.
26. Tayouo, R.; David, G.; Ameduri, B.; Roualdès, S.; Rozière, J. *Macromolecules* **2010**, *43*, 5269–5276.
27. Alaaeddine, A.; Ameduri, B.; Galiano, H. French patent FR2010/1055964 CEA and CNRS, 2011.
28. Kostov, G.; Rousseau, A.; Boutevin, B.; Pascal, T. *J. Fluorine Chem.* **2005**, *126*, 231–240.
29. Taguet, A.; Boutevin, B.; Ameduri, B. *Adv. Polym. Sci.* **2005**, *184*, 127–211.

30. Tillet, G.; Ameduri, B.; Boutevin, B. *Prog. Polym. Sci.* **2011**, *36*, 191–217.
31. Boschet, F.; Ameduri, B. *Chem. Rev.* **2012**, in press.
32. Carnevale, D.; Wormald, P.; Ameduri, B.; Tayouo, R.; Ashbrook, S. E. *Macromolecules* **2009**, *42*, 5652–5659.
33. Tayouo, R.; David, G.; Ameduri, B. *Eur. Polym. J.* **2010**, *46*, 1111–1118.
34. Frutsaert, G.; Delon, L.; David, G.; Ameduri, B.; Jones, D. J.; Glipa, X.; Rozière, J. *J. Polym. Sci., Part A: Polym. Chem.* **2010**, *48*, 223–231.
35. Tarascon, J.-M.; Armand, M. *Nature* **2001**, *414*, 359.
36. Prem Kumar, T.; Anbu Kulandainathan, M.; Angu Lakshmi, N. *J. Phys. Chem. B* **2009**, 1963–1971.
37. Zhang, H.; Kulkarni, S. L.; Wunder, S. *J. Phys. Chem. B* **2007**, *11*, 3583–3590.
38. Pichavant, L.; Guillermain, C.; Coqueret, X. *Biomacromolecules* **2010**, *11*, 2415–2421.
39. Park, J.-S.; Park, S.-H.; Yim, S.-D.; Yoon, Y.-G.; Lee, W.-Y.; Kim, C.-S. *J. Power Sources* **2008**, *178*, 620–626.
40. Alaaeddine, A.; Ameduri, B.; Martinent, A.; Capron, P. French Patent, FR 2010/0404, assigned to CEA and CNRS US2011/0190404.
41. Meskini, A.; Raihane, M.; Ameduri, B. *Macromolecules* **2009**, 3532–3539.
42. Weissermel, K.; Arpe, H.-J. *Industrial Organic Chemistry*, 3rd ed.; VCH: New York, 1997.
43. Takemoto, K.; Ottenbrite, R. M.; Kamashi, M. *Functional Monomers and Polymers*; Marcel Dekker: New York, 1997.
44. Rokicki, G. *Progr. Polym. Sci.* **2000**, *25*, 259–342.
45. Weisserme, K.; Arpe, H.*J. Chimie Organique Industrielle*; Elsevier: Masson, Paris, 1981; p 217.
46. Watanabe, W. H.; Conlon, L. E. *J. Am. Chem. Soc.* **1957**, *79*, 2829.
47. Boutevin, B.; Youssef, B. *J. Fluorine Chem.* **1989**, *44*, 395.
48. Handerson, S.; Schlaf, M. *Org. Lett.* **2002**, *4*, 407–409.
49. Weintraub, P.; King, C.-H. R. *J. Org. Chem.* **1997**, *62*, 1560–1562.
50. Ohmiya, H.; Makida, Y.; Tanaka, T.; Sawamura, M. *J. Am. Chem. Soc.* **2008**, *130*, 17276–17277.
51. Bosch, M.; Schlaf, M. *J. Org, Chem.* **2003**, *68*, 525–5227.
52. Fugami, K.; Oshima, K.; Utimoto, K. *Bull. Chem. Soc. Jpn.* **1989**, *62*, 2050–2054.
53. Boutevin, B.; Malek, F. *Eur. Polym. J.* **1995**, *31*, 1279–1285.
54. Galluci, R. R.; Coing, R. C. *J. Org, Chem.* **1983**, *48*, 342.
55. Okimoto, Y.; Sakaguchi, S.; Ishii, Y. *J. Am. Chem. Soc.* **2002**, *124*, 1590.
56. Mc Keon, J.-E.; Fitton, P.; Grisvold, A.-A. *Tetrahedron* **1972**, *28*, 277.
57. Nishikubo, T.; Kameyama, A.; Sasano, M. *J. Polym. Sci., Part A : Polym. Chem.* **1994**, *32*, 301.
58. Moon, J. Y.; Yang, J. G.; Jung, S. M.; Park, D. W.; Lee, J. K. *React. Kinet. Catal. Lett.* **1997**, *61*, 315–322.
59. Moon, J. Y.; Yang, J. G.; Park, D. W.; Lee, M. H.; Lee, J. K. *Kongop Hwahak* **1995**, *6*, 1162.
60. Webster, D. C. *Prog. Org. Coat.* **2003**, *47*, 77–86.

Downloaded by COLUMBIA UNIV on August 28, 2012 | http://pubs.acs.org
Publication Date (Web): August 16, 2012 | doi: 10.1021/bk-2012-1106.ch010

61. Alaaeddine, A.; Ameduri, B.; Boutevin, B.; Galiano, H. French patent FR2010/091579, assigned to CEA and CNRS WO2012/049070.
62. Park, D. W.; Moon, J. Y; Yang, J. G.; Jung, S. M; Lee, M. K.; Ha, C. S. *Stud. Surf. Sci. Catal.* **1998**, *114*, 403.
63. Moon, J. Y.; Jang, H. J.; Kim, K. H.; Na, S. E; Park, D. W.; Lee, J. K. *Korean J. Chem. Eng.* **1999**, *16*, 721.
64. Ha, C. S.; Yoo, G.; Park, D. W.; Jo, N. J; Lee, J. K; Cho, W. *J. Polym. Inter.* **2002**, *51*, 1023–1030.
65. Moon, J. Y.; Jang, H. J.; Kim, K. H.; Park, D. W.; Ha, C. S.; Lee, J. K. *J. Appl. Polym. Sci* **2000**, *77*, 1809–1815.
66. Miyamoto, M.; Sawamoto, M.; Higashimura, T. *Macromolecules* **1984**, *17*, 265–268.
67. Rekusheva, T. *Russ. Chem. Rev.* **1968**, *37*, 1009.
68. Boutevin, B.; Cersosimo, F.; Youssef, B.; Kappler, P. *J. Fluorine Chem.* **1991**, *52*, 403–418.
69. Boyer, C.; Ameduri, B.; Hung, M. H. *Macromolecules* **2010**, *43*, 3652–3663.
70. Schmiegel, W. W. *Angew. Makromol. Chem.* **1979**, *76-7*, 39–65.
71. Gelin, M.-P.; Ameduri, B. *J. Polym. Sci., Part A: Polym. Chem.* **2002**, *41*, 160–171.
72. Tiers, G. V. D.; Bovey, B. A. *J. Polym. Sci. Part A: Gen. Papers* **1963**, *1*, 833–841.
73. Walling, C.; Mayo, F. R. *J. Polym. Sci.* **1948**, *3*, 895–897.
74. Handforth, V. *J. Oil Colour Chem. Assoc.* **1990**, *73*, 145–148.
75. Schappacher, M.; Deffieux, A. *Macromol. Chem. Rapid. Commun.* **1991**, *12*, 447–453.
76. Schappacher, M.; Deffieux, A. *Macromolecules* **1992**, *25*, 6744–6751.
77. Xing, L.; Weishan, L.; Wang, C.; Gu, F.; Xu, M.; Tan, C.; Yi, J. *J. Phys. Chem. B* **2009**, *113*, 16596–16602.
78. Zhang, X. *Electrochem. Acta* **2011**, *56*, 1246–1255.
79. Yao, W.; Zhang, Z.; Gao, J.; Li, J.; Xu, J.; Wang, Z.; Yang, Y. *Energy Environ. Sci.* **2009**, *2*, 1102–1108.
80. Zhang, Z.; Lyons, L. J.; West, R.; Amine, K.; West, R. *Silicon Chem.* **2005**, *3*, 259–266.
81. Yu, X.-Y.; Xiao, M.; Wang, S.-J.; Zhao, Q.-Q.; Meng, Y.-Z. *J. Appl. Polym. Sci.* **2010**, *115*, 2718.
82. Wen, T. C.; Chen, W. C. *J. Power Sources* **2001**, *92*, 139.
83. Ciosek, M.; Siekierski, M.; Wieczorek, W. *Electrochem. Acta* **2005**, *50*, 3922.
84. Aydin, H.; Sanel, M.; Erdemi, H.; Baykal, A.; Mertin, T.; Ata, A.; Bozkurt, A. *J. Power Sources* **2011**, *196*, 1425–1432.
85. Zhang, Z.; Lyons, L.-J.; West, R.; Amine, K.; West, R. *Silicon Chem.* **2005**, 259–266.
86. Thompson, M.-S.; Vadala, T.-P.; Lin, Y.; Riffle, J.-S. *Polymer* **2008**, *49*, 345–373.
87. Yu, X.-Y.; Xia, M.; Wang, S.-J.; Zhao, Q.-Q.; Meng, Y.-Z. *J. Appl. Polym. Sci.* **2010**, *115*, 2718–2722.

Downloaded by COLUMBIA UNIV on August 28, 2012 | http://pubs.acs.org
Publication Date (Web): August 16, 2012 | doi: 10.1021/bk-2012-1106.ch010

88. Sannier, L.; Bouchet, R.; Rosso, M.; Tarascon, J.-M. *J. Power Sources* **2006**, *185*, 564–570.
89. Xiao, Q.; Wang, X.; Li, W.; Li, Z.; Zhang, T.; Zhang, H. *J. Membr. Sci* **2009**, 334.
90. Cui, Z. Y.; Xu, Y. Y. *J. Membr. Sci* **2008**, *325*, 957–963.
91. Wang, Y. J.; Kim, D. *J. Power Sources* **2007**, *166*, 202–210.
92. Li, Z.; Su, G.; Wang, X.; Gao, D. *Solid State Ionics* **2005**, *176*, 1903–1908.
93. Xue, J.; Chen, L.; Wang, H. L.; Zhang, Z. B.; Zhu, X. L.; Kang, E.; Neoh, K. G. *Langmuir* **2008**, *24*, 14151–14158.
94. Chen, Y.; Sun, W.; Deng, Q.; Chen, L. *J. Polym. Sci., Part A: Polym. Chem* **2006**, *44*, 3071–3082.
95. Akthakul, A.; Salinaro, R. F.; Mayes, A. M. *Macromolecules* **2004**, *37*, 7663–7668.
96. Koh, J. H.; Kim, Y. W.; Park, J. T.; Kim, J. H. *J. Polym. Sci., Part B: Polym. Phys.* **2008**, *46*, 702–709.
97. Miyamoto; Ishii2, T.; Sakai, T.; Kimura, Y. *Macromol. Chem. Phys.* **1998**, *199*, 119–125.
98. Haraldsson, T.; Johansson, M.; Hult, A. *J. Polym. Sci.: Part A: Polym. Chem.* **2010**, *48*, 2810–2816.
99. Mizrahi, D.; Omer-Mizrahi, M.; Goldshtein, J.; Askinadze, N.; Margel, S. *J. Polym. Sci., Part A: Polym. Chem.* **2010**, *48*, 5468–5478.

Downloaded by COLUMBIA UNIV on August 28, 2012 | http://pubs.acs.org
Publication Date (Web): August 16, 2012 | doi: 10.1021/bk-2012-1106.ch010

Downloaded by OHIO STATE UNIV LIBRARIES on August 28, 2012 | http://pubs.acs.org
Publication Date (Web): August 16, 2012 | doi: 10.1021/bk-2012-1106.ch011

Chapter 11

Superoleophobic Surfaces

Arun K. Kota and Anish Tuteja[*]

Department of Materials Science and Engineering,
University of Michigan, Ann Arbor, Michigan 48105
[*]E-mail: atuteja@umich.edu

Surfaces that display contact angles greater than 150° along with a low contact angle hysteresis for low surface tension liquids such as oils and alcohols are known as superoleophobic surfaces. Such surfaces are of interest for a diverse array of applications including self-cleaning, stain-free clothing and drag reduction. Recently, significant advances have been made in understanding the criteria required to design superoleophobic surfaces. In this chapter, we will discuss two dimensionless design parameters that can be used for the rational design of superoleophobic surfaces. We will also summarize the recent studies on superoleophobic surfaces and emphasize the need for careful and diligent characterization. Finally, we will conclude with the major challenges and opportunities for research on superoleophobic surfaces.

Introduction

Surfaces and materials with extreme repellency to liquids are of significant interest for a wide variety of military, commercial, and specialty applications including self-cleaning (*1*), non-fouling (*2*), stain-free clothing and spill-resistant protective wear (*3*), drag reduction (*4*), locomotion of microrobots on aqueous and chemical environments (*5*, *6*) and icephobicity (*7*). The primary measure of wetting of a liquid on a non-textured (or smooth) surface is the equilibrium contact angle θ, given by Young's relation (*8*) as:

$$\cos\theta = \frac{\gamma_{SV} - \gamma_{SL}}{\gamma_{LV}} \qquad (1)$$

In Advances in Fluorine-Containing Polymers; Smith, D., et al.;
ACS Symposium Series; American Chemical Society: Washington, DC, 2012.

Downloaded by OHIO STATE UNIV LIBRARIES on August 28, 2012 | http://pubs.acs.org
Publication Date (Web): August 16, 2012 | doi: 10.1021/bk-2012-1106.ch011

Here, γ refers to the interfacial tension and S, L, and V refer to the solid, liquid, and vapor phases, respectively. The solid-vapor interfacial tension (γ_{SV}) and the liquid-vapor interfacial tension (γ_{LV}) are also commonly referred to as the solid surface energy and the liquid surface tension, respectively. Non-textured surfaces that display contact angles $\theta > 90°$ with water are considered hydrophobic, while non-textured surfaces that display contact angles $\theta < 90°$ with water are considered hydrophilic. Typically, surfaces with high γ_{SV} tend to be hydrophilic, whereas those with low γ_{SV} (such as highly fluorinated compounds) tend to be hydrophobic.

Relatively recently, a new classification, known as '*superhydrophobic*' surfaces, has emerged. Superhydrophobic surfaces display contact angles greater than 150° along with a low contact angle hysteresis (the difference between the advancing and the receding contact angles) for water (*9*, *10*). Water droplets can easily roll-off from and bounce on such surfaces. Note that all superhydrophobic surfaces are textured (or rough), as the maximum water contact angle measured thus far on a smooth surface is ≈ 130° (*11*, *12*). Superhydrophobic surfaces are pervasive in nature (see Figure 1) with various plant leaves (*13–15*), legs of the water strider (*16–18*), gecko's feet (*2*, *19*), troughs on the elytra of desert beetles (*20*), and insect wings (*21*) displaying extreme water-repellency. Inspired by the natural superhydrophobic surfaces, several researchers have also engineered artificial (or synthetic) superhydrophobic surfaces (*22*).

In a similar manner, based on their respective contact angles with oil, it is possible to classify surfaces as oleophilic ($\theta < 90°$), oleophobic ($\theta > 90°$), or superoleophobic ($\theta^* > 150°$ and low contact angle hysteresis). Here, θ^* refers to the apparent contact angle, i.e., the contact angle on a textured surface. In spite of numerous natural superhydrophobic surfaces, until recently there were no known naturally occurring oleophobic surfaces (*23*). This is because oils possess significantly lower surface tension values than water and consequently spread on most natural and synthetic surfaces. Recently, we (*24–26*) and others (*27–29*) have explained how *re-entrant surface texture*, in conjunction with surface chemistry and roughness, can be used to engineer superoleophobic surfaces, even with extremely low surface tensions liquids such as various oils and alcohols. In this chapter, we will discuss how to systematically design superoleophobic surfaces and also provide an overview of the recent studies on fabrication and characterization of superoleophobic surfaces.

Fundamentals of Wetting on Textured Surfaces

When a droplet of liquid contacts a textured substrate, it can adopt one of the following two configurations to minimize its overall free energy (*9*, *30–33*) – the Wenzel (*34*) state or the Cassie-Baxter (*35*) state. In the Wenzel state, as shown in Figure 2A, the contacting liquid droplet completely permeates the surface protrusions, forming the so-called 'fully-wetted' interface. In this state, the apparent contact angles are calculated using the Wenzel relation (*34*), given as:

$$\cos\theta^* = r\cos\theta \qquad (2)$$

Downloaded by OHIO STATE UNIV LIBRARIES on August 28, 2012 | http://pubs.acs.org
Publication Date (Web): August 16, 2012 | doi: 10.1021/bk-2012-1106.ch011

Here, r is the surface roughness, defined as the ratio of the actual surface area to the projected surface area. Since r is always greater than unity, roughness amplifies both the wetting and non-wetting behavior of materials in the Wenzel state. In other words, $\cos\theta^{*} \gg 0$ if $\cos\theta > 0$ and $\cos\theta^{*} \ll 0$ if $\cos\theta < 0$.

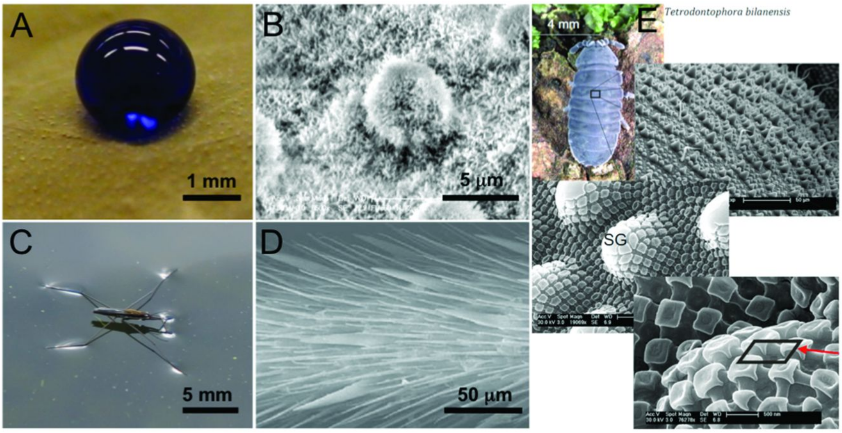

*Figure 1. **A.** A water droplet displaying very high contact angle on the surface of a lotus leaf. **B.** SEM image of the lotus leaf surface showing the rough texture with nanoscale protrusions superimposed on microbumps. **C.** A pond skater walking on the surface of water. **D.** SEM image of the pond skater leg showing the rough texture with oriented hairs. Reproduced with permission from (18). Copyright 2004. **E.** A picture and SEM images of springtail skin showing secondary granules (SG) superimposed on primary granules. Note that the secondary granules have a re-entrant curvature, which allows the springtail skin to be oleophobic. Reproduced with permission from (23). Copyright 2011.*

On the other hand, in the Cassie-Baxter state, as shown in Figure 2B, the liquid does not completely wet the surface texture. Instead, pockets of air remain trapped underneath the liquid droplet. The liquid penetrates into the surface texture until the local texture angle (ψ) becomes equal to the equilibrium contact angle θ (given by Young's relation) for the three-phase contact line (*31*, *32*). Consequently, substrates with a re-entrant surface texture (i.e., textures with $\psi < 90°$, such as the springtail skin shown in Figure 1E) can support a composite (solid-liquid-air) interface even for low surface tension liquids, such as oils and alcohols, which display Young's contact angles $\theta < 90°$ (See Figure 2B). It must be noted that the existence of points on the surface that enable the condition $\psi = \theta$ (*32*) is a necessary, but not sufficient, condition (*29*, *31*, *32*) for the formation of such a composite interface, as discussed later. The apparent contact angles in this state are typically calculated using the Cassie-Baxter relation (*35*), given as:

$$\cos\theta^{*} = f_{SL}\cos\theta + f_{SV}\cos\pi = f_{SL}\cos\theta - f_{SV} \qquad (3)$$

Downloaded by OHIO STATE UNIV LIBRARIES on August 28, 2012 | http://pubs.acs.org
Publication Date (Web): August 16, 2012 | doi: 10.1021/bk-2012-1106.ch011

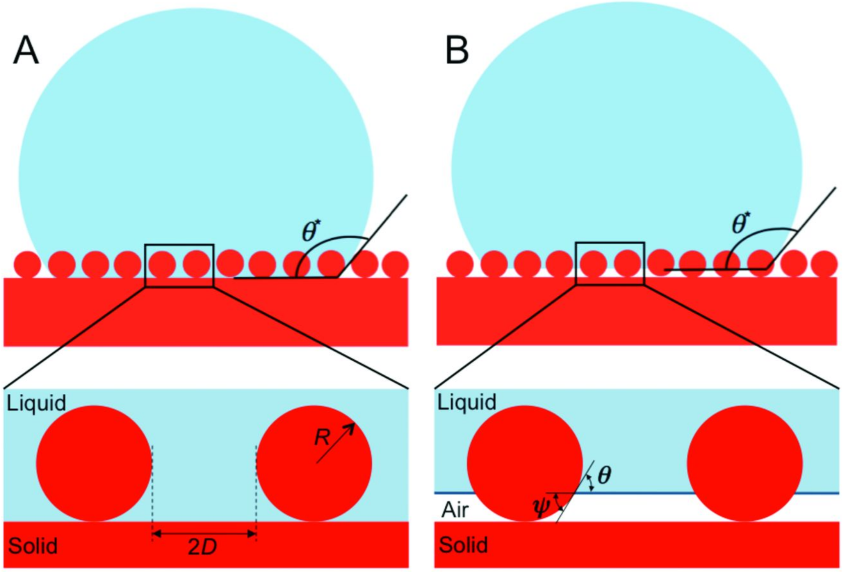

Figure 2. ***A.*** *A liquid droplet in the Wenzel state on a rough surface.* ***B.*** *A liquid droplet in the Cassie-Baxter state on a rough surface. Note that the texture angle ψ varies from 0° to 180°. Textures with a re-entrant curvature, i.e., ψ < 90°, can support a composite (solid-liquid-air) interface even for liquids which display θ < 90°.*

Here, f_{SL} is the area fraction of the solid-liquid interface and f_{SV} is the area fraction of the liquid-air interface underneath the liquid droplet. In contrast to the Wenzel state, the formation of the Cassie-Baxter state typically enhances the super-repellency by promoting high apparent contact angles (θ^*) and a low contact angle hysteresis (*10*, *36*, *37*).

Design Parameters for Superoleophobic Surfaces

Recent theoretical analyses by Nosonovsky (*32*) and Marmur (*29*) indicate that surfaces with re-entrant curvature (i.e., convex topographies) promote the formation of the Cassie-Baxter state. In designing superoleophobic surfaces, the formation of the Cassie-Baxter state can be parameterized in terms of two important physical characteristics – the magnitude of the observed apparent contact angle θ^* and the magnitude of the breakthrough pressure ($P_{breakthrough}$), i.e., the external pressure which when applied upon a contacting liquid can force a transition from the composite Cassie-Baxter state to the fully-wetted Wenzel state. In our recent work (*25*, *26*) we discussed a design parameter, the spacing ratio D^*, which provides a dimensionless measure of the surface porosity. For substrates possessing a predominantly cylindrical texture, $D^*_{cylinder} = (R+D)/R$, while for substrates possessing a predominantly spherical texture, $D^*_{sphere} = \left[(R+D)/R\right]^2$. Here, R is the radius of the cylinder (or sphere) and $2D$ is the inter-cylinder (or

Downloaded by OHIO STATE UNIV LIBRARIES on August 28, 2012 | http://pubs.acs.org
Publication Date (Web): August 16, 2012 | doi: 10.1021/bk-2012-1106.ch011

sphere) spacing (see Figure 2A). Based on this definition of the spacing ratio, the Cassie-Baxter relation (Equation (3)) may be rewritten for surfaces possessing a cylindrical (Equation (4)) or a spherical (Equation (5)) texture as (*24*, *38*):

$$\cos\theta^{*}_{cylinder} = -1 + \frac{1}{D^{*}_{cylinder}}\left[\sin\theta + \left(\pi - \theta\right)\cos\theta\right] \tag{4}$$

$$\cos\theta^{*}_{sphere} = -1 + \frac{1}{D^{*}_{sphere}}\left[\frac{\pi}{2\sqrt{3}}\left(1 + \cos\theta\right)\right]^{2} \tag{5}$$

Note that Cassie-Baxter relation may be rewritten recursively for hierarchically textured surfaces, i.e., surfaces with texture on multiple length scales (*39*). Consequently, hierarchically textured surfaces typically possess higher values of D^*.

Higher values of D^* correspond to a higher fraction of air within the composite interface. It is evident from Equations (4) and (5) that θ^* increases with increasing values of D^*. However, for large values of the inter-feature spacing D, which typically yield very high values for the spacing ratio, i.e., $D^* >> 1$, it may be intuitively expected that the surface can no longer support the contacting liquid in the Cassie-Baxter state and allows it to breakthrough. In order to parameterize the breakthrough pressure $P_{breakthrough}$ for a known surface texture, we also discussed the robustness factor A^* in our recent work (*24*, *25*). The robustness factor A^* is the ratio of the breakthrough pressure ($P_{breakthrough}$) to a reference pressure $P_{ref} = 2\gamma_{LV}/l_{cap}$. Here, $l_{cap} = \sqrt{\gamma_{LV}/\rho g}$ is the capillary length for the liquid, ρ is the fluid density and g is the acceleration due to gravity. P_{ref} is close to the minimum possible pressure differential across a millimeter sized liquid droplet or a puddle. As a consequence, substrates on which the robustness factor $A^* \leq 1$ for a given contacting liquid, cannot support a composite interface. On the other hand, values of A^* significantly greater than unity imply the formation of a robust composite interface that can withstand high breakthrough pressures. The robustness factors for surfaces possessing a cylindrical (Equation (6)) or a spherical (Equation (7)) texture are given as (*24*, *38*):

$$A^{*}_{cylinder} = \frac{P_{breakthrough}}{P_{ref}} = \frac{l_{cap}}{R\left(D^{*}_{cylinder} - 1\right)}\frac{\left(1 - \cos\theta\right)}{\left(D^{*}_{cylinder} - 1 + 2\sin\theta\right)} \tag{6}$$

$$A^{*}_{sphere} = \frac{P_{breakthrough}}{P_{ref}} = \frac{2\pi l_{cap}}{R\left(2\sqrt{3}D^{*}_{sphere} - \pi\right)}\frac{\left(1 - \cos\theta\right)}{\left(\sqrt{D^{*}_{sphere}} - 1 + 2\sin\theta\right)} \tag{7}$$

Optimal superoleophobic surfaces are expected to simultaneously display high contact angles and high breakthrough pressures with the contacting liquid. Thus, they must be designed with both $D^* >> 1$ and $A^* >> 1$.

Downloaded by OHIO STATE UNIV LIBRARIES on August 28, 2012 | http://pubs.acs.org
Publication Date (Web): August 16, 2012 | doi: 10.1021/bk-2012-1106.ch011

Recent Studies on Superoleophobic Surfaces

While there are more than a thousand published reports on superhydrophobic surfaces, there are very few reports on superoleophobic surfaces. The low surface tension of oils compared to water makes it a challenge to fabricate superoleophobic surfaces. In this regard, the two design parameters discussed above can be useful to rationally design superoleophobic surfaces.

Further, superoleophobic surfaces must be characterized carefully. In this context, we emphasize two important things that are sometimes neglected in literature. First, as mentioned before, superoleophobic surfaces are defined as surfaces that display contact angles greater than 150° with oils *and* low contact angle hysteresis ($\Delta\theta^*$). We emphasize that a static contact angle (θ^*) or an advancing contact angle (θ^*_{adv}) greater than 150° for an oil does not adequately describe superoleophobicity. The receding contact angle (θ^*_{rec}) and consequently the contact angle hysteresis must be diligently measured. Obtaining a low contact angle hysteresis (typically $\Delta\theta^* < 10°$) and consequently low roll-off angles (i.e., the minimum angle by which the substrate is tilted for the droplet to roll off from the surface) for oils is perhaps as important as the maximum achievable contact angle in qualifying a surface as superoleophobic. Second, there is some ambiguity regarding which oil is used in characterizing superoleophobicity. In literature, it is sometimes difficult to compare across different superoleophobic surfaces because many different oils ranging in surface tension from octane (γ_{LV} = 21.6 mN/m) to rapeseed oil (γ_{LV} = 35.7 mN/m) have been used for contact angle measurements. In some reports, the surface tension of the oil is not mentioned. In yet other reports, claims of superoleophobicity are based on liquids such as diiodomethane and glycerol, which are not oils. In order to allow easier comparison across literature, it is important to diligently measure and report the advancing and receding contact angles for a variety of oils, especially for those possessing a low surface tension (< 30 mN/m).

One of first reports on surfaces displaying very high static contact angles with oils dates back to the work of Tsujii et al. (*40*) in 1997. They developed an anodically oxidized aluminum surface with a fractal structure, which was modified with fluorinated low surface energy molecules (perfluorodecyl phosphate or perfluorododecyl phosphate). The resulting surface displayed a static contact angle θ^* = 150° with rapeseed oil, as shown in Figure 3A. Further, the oil droplet rolled around even if the substrate was only slightly tilted (*41*) indicating a low contact angle hysteresis. In more recent work, Fujii et al. (*42*) developed a dual scale pillared structure of aluminum-niobium alloy by combining oblique angle magnetron sputtering with anodic oxidation. Upon modification with perfluorodecyl phosphate, the surfaces displayed superoleophobicity with θ^* = 156° and 151° and $\Delta\theta^*$ = 2° and 6° for rapeseed oil and hexadecane (γ_{LV} = 27.5 mN/m), respectively (see Figure 3B). The hierarchical structure results in a high value for D^*, which in turn leads to high apparent contact angles and low contact angle hysteresis. Barring the above two reports, rendering surfaces extremely oil-repellant by modifying them with fluorinated phosphates has not been common.

Downloaded by OHIO STATE UNIV LIBRARIES on August 28, 2012 | http://pubs.acs.org
Publication Date (Web): August 16, 2012 | doi: 10.1021/bk-2012-1106.ch011

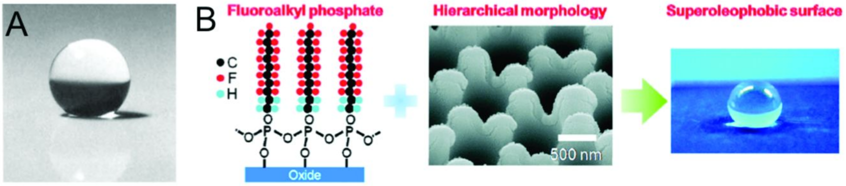

*Figure 3. **A.** A droplet of rapeseed oil displaying a very high contact angle on a fluorinated aluminum surface with a fractal structure. Reproduced with permission from (40). Copyright 1997. **B.** A scheme showing the fabrication of a fluorinated dual scale pillared structure that is superoleophobic for rapeseed oil. Reproduced with permission from (42). Copyright 2011.*

On the other hand, modifying a surface with fluorinated silanes has been one of the most common choices to imbue a surface with low surface energy because of the commercial availability of fluorinated silanes, as well as, the ease of the silanization process. Li et al. (*43*) modified the surface of aligned carbon nanotube (CNT) films with perfluorodecyl trimethoxysilane. Since the surface of CNTs is rather inert, they oxidized the CNTs with acidic treatment, followed by silanization. The resulting surfaces displayed a static contact angle $\theta^* = 161°$ with rapeseed oil, but the oil droplet remained pinned to the surface, indicating a high contact angle hysteresis. Cao et al. (*28*) fabricated porous silicon films with a hierarchical structure by a gold-assisted electroless etching process. Upon silanization with perfluorooctyl trichlorosilane, the surfaces displayed a static contact angle $\theta^* = 151°$ with hexadecane. Leng et al. (*3*) prepared hierarchically textured cotton textiles that are coated first with positively charged silica microparticles and then with negatively charged silica nanoparticles. The silica microparticles were covalently attached to the substrate by an *in situ* Stober reaction, while the silica nanoparticles adsorbed on the surface of the silica microparticles via electrostatic interaction (see Figure 4A). Upon silanization with perfluorodecyl trichlorosilane, the surfaces displayed a static contact angle as high as $\theta^* = 152°$ and a roll off angle as low as $\omega = 9°$ with hexadecane (see Figure 4B). Wu et al. (*44*) fabricated alumina nanowire forests by electrochemically etching aluminum foils to form a multi-faceted microstructure followed by anodizing the activated aluminum to the form the nanowires. Upon silanization with perfluorooctadecyl trichlorosilane, the surfaces were superoleophobic with static contact angles $\theta^* = 155°$, 153° and 150°, and roll-off angles $\omega = 5°$, 3° and 12° for rapeseed oil, hexadecane and silicone oil ($\gamma_{LV} = 22$ mN/m), respectively. The higher roll-off angles for the lower surface tension silicone oil indicates that the contact angle hysteresis is higher for silicone oil when compared to rapeseed oil and hexadecane. Saraf et al. (*45*) modified the surface of nylon non-woven fabrics with perfluorodecyl trimethoxysilane and cured it in a microwave. The

Downloaded by OHIO STATE UNIV LIBRARIES on August 28, 2012 | http://pubs.acs.org
Publication Date (Web): August 16, 2012 | doi: 10.1021/bk-2012-1106.ch011

resulting surface displayed a high static contact angle $\theta^* = 160°$ for dodecane (γ_{LV} = 25.3 mN/m), but the roll-off angle $\omega = 21°$ was also high indicating a high contact angle hysteresis. Wang et al. (*46*) constructed a hierarchical texture consisting of well-aligned titanium dioxide nanotubes on micropillars of titanium. The micropillars of titanium were fabricated by laser micromachining and the titanium dioxide nanotubes were fabricated by anodization (see Figure 4C). Upon silanization with perfluorooctyl trichlorosilane, the surfaces were superoleophobic with static contact angles θ^* = 155°, 156° and 157° and roll-off angles ω = 7°, 6° and 5° for hexadecane, colza oil and crude oil, respectively.

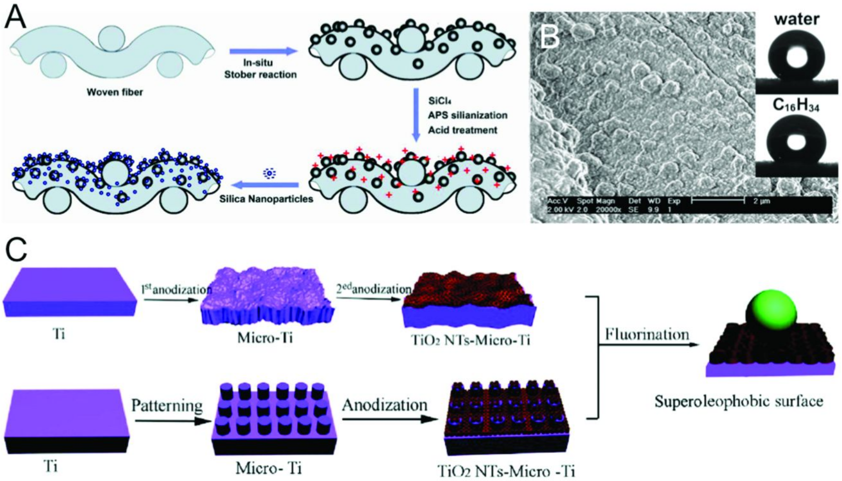
A
Woven fiber
In-situ
Stober reaction
$SiCl_4$
APS silianization
Acid treatment
Silica Nanoparticles
B
water
$C_{16}H_{34}$
Acc.V Spot Magn Det WD Exp
2.00 kV 2.0 20000x SE 9.9 1
2 μm
C
Ti
1st anodization
Micro-Ti
2ed anodization
TiO_2 NTs-Micro-Ti
Fluorination
Superoleophobic surface
Ti
Patterning
Micro- Ti
Anodization
TiO_2 NTs-Micro -Ti

*Figure 4. **A.** A schematic illustrating the procedure for preparing a surface with dual scale roughness on a woven cotton textile. **B.** An SEM image of the cotton textile with dual scale roughness. The insets show droplets of water and hexadecane displaying very high contact angles on the corresponding fluorinated surface. Reproduced with permission from (3). Copyright 2009. **C.** A schematic illustrating two alternative procedures to construct a hierarchical texture consisting of well-aligned titanium dioxide nanotubes on titanium with microscale texture. Reproduced with permission from (46). Copyright 2010.*

There have also been a few reports on developing extremely oil-repellant surfaces using polymer composites. Steele et al. (*47*) spray-casted composites of zinc oxide nanoparticles and a perfluoroalkyl methacrylic copolymer on to glass slides using mixtures of water and acetone. The resulting hierarchically structured surfaces displayed a static contact angle $\theta^* = 154°$ and a contact angle hysteresis $\Delta\theta^* = 6°$ for hexadecane.

Downloaded by OHIO STATE UNIV LIBRARIES on August 28, 2012 | http://pubs.acs.org
Publication Date (Web): August 16, 2012 | doi: 10.1021/bk-2012-1106.ch011

In our recent work (*24–26*), we reported the synthesis of perfluorodecyl polyhedral silsesquioxane (fluorodecyl POSS), which possesses one of the lowest known surface energies ($\gamma_{SV} \approx 10$ mN/m). The addition of fluorodecyl POSS molecules to different polymers leads to a rapid decrease in the overall surface energy of the synthesized blends, and also provides a facile route to systematically tune the surface energy of the produced blend over a very wide range. By spray coating, electrospinning (see Figure 5A-5C) or dip coating (see Figure 5D) the polymer-fluorodecyl POSS blends, we designed surfaces with high D^* and A^* such that they displayed superoleophobicity with a variety of oils including hexadecane ($\theta^*_{adv} = 156°$ and $\Delta\theta^* = 6°$). We also demonstrated that hexadecane droplets can actually bounce on our superoleophobic surfaces (see Figure 5E) (*26*).

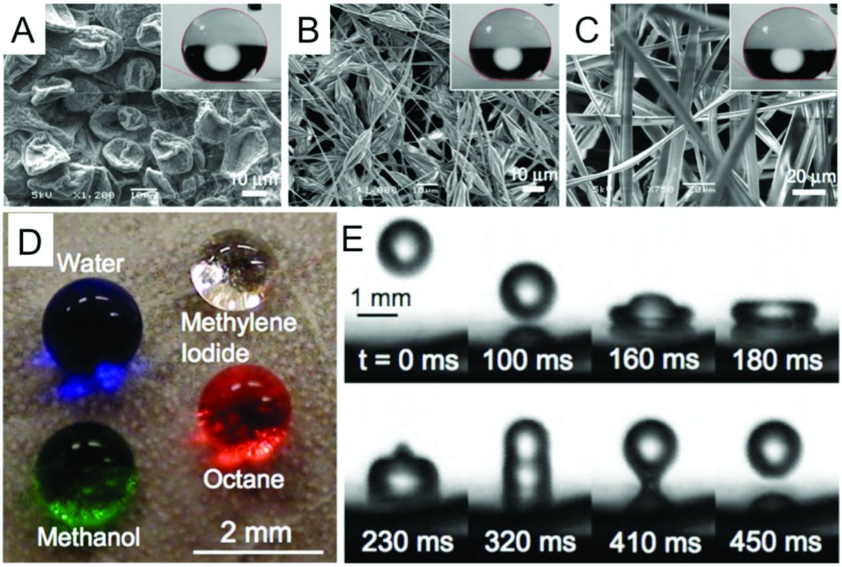

*Figure 5. **A, B** and **C.** Electrospun surfaces of polymer-fluorodecyl POSS blends showing beads only, beads on strings, and fibers only morphologies, respectively. The insets show droplets of hexadecane displaying very high contact angles on the corresponding surfaces. **D.** A lotus leaf surface that is dip-coated with polymer-fluorodecyl POSS blends results in a robust omniphobic surface that can support even low surface tension liquids in the Cassie-Baxter state. **E.** A series of images obtained using a high-speed digital video camera illustrate the bouncing of a droplet of hexadecane on the micro-hoodoo surface (26). Reproduced with permission from (25) and (26). Copyright 2008.*

Downloaded by OHIO STATE UNIV LIBRARIES on August 28, 2012 | http://pubs.acs.org
Publication Date (Web): August 16, 2012 | doi: 10.1021/bk-2012-1106.ch011

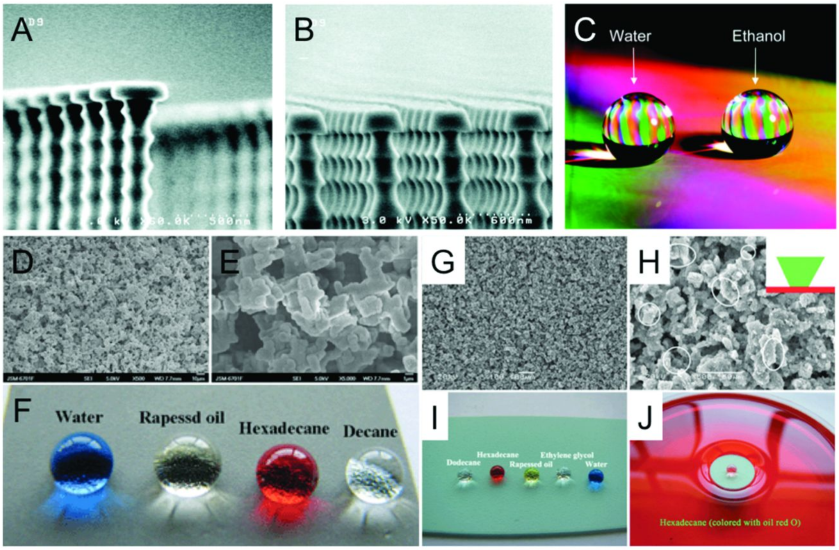

Figure 6. ***A*** *and* ***B.*** *SEM images of the nanonail structures with a pitch of 2 µm and 0.9 µm, respectively.* ***C.*** *Droplets of water and ethanol displaying very high contact angles on the fluorinated nanonail structure. Reproduced with permission from (27). Copyright 2008.* ***D*** *and* ***E.*** *SEM images showing the nanoscale flakes and the microscale protrusions, respectively, on the surface of an aluminum sheet.* ***F.*** *A variety of oils displaying very high contact angles on the corresponding fluorinated surface. Reproduced with permission from (48). Copyright 2011.* ***G*** *and* ***H.*** *SEM images of a surface spray coated with copper perfluorooctonoate at a low magnification and a high magnification, respectively.* ***I.*** *A variety of oils displaying very high contact angles on the corresponding surface.* ***J.*** *The substrate floats on a bath of hexadecane, indicating that hexadecane does not penetrate the surface texture. Reproduced with permission from (49). Copyright 2011.*

In other reports, surface modification was achieved by treating the surface with a fluorinated precursor or a monomer or a polymer. Ahuja et al. (*27*) fabricated silicon nanonail structures with re-entrant curvature using reactive ion etching (see Figures 6A and 6B). When these structures were conformally coated with plasma-assisted chemical vapor deposition using C_4F_8 as the precursor, they displayed an advancing contact angle $\theta^{*}_{adv} \approx 155°$ with a variety of alcohols (see Figure 6C) including methanol (γ_{LV} = 22.1 mN/m), ethanol (γ_{LV} = 21.8 mN/m), 1-propanol (γ_{LV} = 23.7 mN/m), 1-butanol (γ_{LV} = 26.2 mN/m), 1-octanol (γ_{LV} = 27.6 mN/m) and 1-decanol (γ_{LV} = 28.5 mN/m). Hsieh et al. (*50*) prepared silica sphere stacks with two-tier roughness by using a two-stage spin coating

Downloaded by OHIO STATE UNIV LIBRARIES on August 28, 2012 | http://pubs.acs.org
Publication Date (Web): August 16, 2012 | doi: 10.1021/bk-2012-1106.ch011

technique. When the surfaces were further spin-coated with a perfluoroalkyl methacrylic copolymer, they displayed an advancing contact angle $\theta^{*}_{adv} \approx 150°$ and contact angle hysteresis $\Delta\theta^{*} \approx 3°$ for hexadecane. They also measured the contact angle hysteresis for a wide variety of liquids with γ_{LV} = 23.4 mN/m to γ_{LV} = 72.1 mN/m and concluded that the contact angle hysteresis increases with decreasing γ_{LV}. Darmanin et al. (*51*) synthesized a highly fluorinated conductive monomer, 3,4- ethylenedioxypyrrole, and electrochemically polymerized the monomer to form spherical nanoporous films of poly(3,4- ethylenedioxypyrrole) on non-textured gold substrates. These substrates displayed an advancing contact angle θ^{*}_{adv} = 153°, a contact angle hysteresis $\Delta\theta^{*}$ = 13° and a roll-off angle ω = 6° for hexadecane. In subsequent work, Daramanin et al. (*52*) electrochemically deposited spherical nanoporous films of poly(3,4- ethylenedioxypyrrole) on textured micropillar surfaces fabricated using photolithography. These substrates displayed an advancing contact angle θ^{*}_{adv} = 153°, a contact angle hysteresis $\Delta\theta^{*}$ = 35° and a roll-off angle ω = 27° for hexadecane. The high contact angle hysteresis and high roll-off angle indicate that the textured surface is possibly unable to support a robust composite interface because of low values of A^{*}. However, the same surface is superoleophobic for sunflower oil (γ_{LV} = 31 mN/m, θ^{*}_{adv} = 155°, $\Delta\theta^{*}$ = 4° and ω = 3°). This is because the higher surface tension of sunflower oil results in higher values of A^{*} compared to hexadecane. Yang et al. (*48*) fabricated aluminum sheets with a hierarchical structure composed of distorted nanoscale flakes on microscale protrusions (see Figures 6D and 6E). While the microscale protrusions and pores were obtained by etching in hydrochloric acid, the nanoscale flakes were obtained by dipping the etched structure in boiling water. Upon modifying the surface with perfluorooctanoic acid, it displayed static contact angles θ^{*} = 158°, 156°, 155° and 152°, contact angle hysteresis $\Delta\theta^{*}$ = 5°, 8°, 18° and 45°, and roll-off angles ω = 5°, 7°, 15° and 40°, for rapeseed oil, hexadecane, dodecane and decane (γ_{LV} = 23.8 mN/m), respectively, as shown in Figure 6F. It is evident from the contact angle hysteresis and roll-off angles that the surface is superoleophobic for rapeseed oil and hexadecane, but not superoleophobic for dodecane and decane. In subsequent work, Yang et al. (*49*) fabricated hierarchical structures with re-entrant curvature by spray coating a suspension of copper perfluorooctanoate in ethanol (see Figures 6G and 6H). The copper perfluorooctanoate was rapidly synthesized by a reaction of aqueous copper acetate with a dispersion of perfluorooctanoic acid in water. The spray coated surfaces displayed static contact angles θ^{*} = 155° and 156°, and roll-off angles ω = 15° and 40°, for rapeseed oil and hexadecane (see Figure 6I). The high roll-off angles for hexadecane indicate that the surface is not superoleophobic for hexadecane. However, the surface floats on a bath of hexadecane, possibly because hexadecane cannot penetrate the texture due to high values of A^{*} (see Figure 6J). Yao et al. (*53*) prepared copper hydroxide ribbed nanoneedle arrays by a chemical base deposition method. Upon modifying the surface with perfluorodecane thiol, it displayed a static contact angle $\theta^{*} \approx 160°$ for hexadecane.

Downloaded by OHIO STATE UNIV LIBRARIES on August 28, 2012 | http://pubs.acs.org
Publication Date (Web): August 16, 2012 | doi: 10.1021/bk-2012-1106.ch011

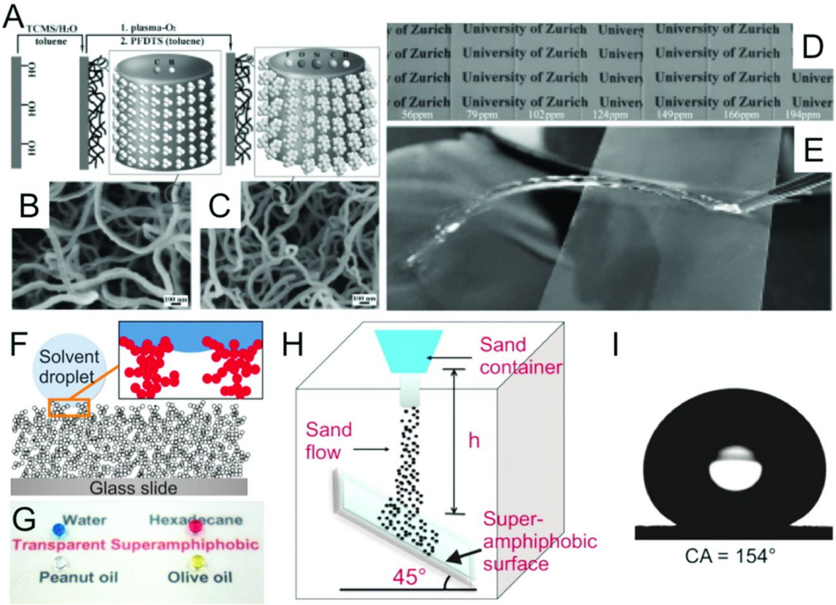
A
TCMS/H₂O toluene
1. plasma-O₂
2. PFDTS (toluene)
D
University of Zurich
56ppm
79ppm
102ppm
124ppm
149ppm
166ppm
194ppm
E
B
C
F
Solvent droplet
Glass slide
G
Water
Hexadecane
Transparent Superamphiphobic
Peanut oil
Olive oil
H
Sand container
Sand flow
h
Super-amphiphobic surface
45°
I
CA = 154°

*Figure 7. **A.** A schematic depicting the fabrication of superoleophobic surfaces with fluorinated nanofilaments of silanes. **B** and **C.** The silane nanofilaments before and after fluorination, respectively. **D.** Images of the superoleophobic glass surfaces on a paper, indicating the transparency. **E**. A jet of toluene bouncing off from the superoleophobic surface, indicating its chemical durability. Reproduced with permission from (54). Copyright 2011. F. A schematic illustrating the fractal-like structure of the candle soot morphology coated with a silica shell. G. A variety of oils displaying very high contact angles on the corresponding fluorinated glass surface. The superoleophobic glass surface is transparent. H. A schematic illustrating the sand abrasion procedure to characterize the mechanical durability. I. A droplet of hexadecane displays a high contact angle even after the sand abrasion test, indicating the mechanical durability of the superoleophobic surface. Reproduced with permission from (55). Copyright 2011.*

Practical application of superoleophobic surfaces in stain-free clothing, spill-resistant protective wear and drag reduction requires good chemical, mechanical and thermal durability. Developing durable superoleophobic surfaces has thus far been a challenge. There are very few reports that discuss the durability of superoleophobic surfaces. Zhang et al. (*54*) fabricated glass slides coated with nanofilaments of methyl trichlorosilane (see Figures 7A-7C). Upon activating the nanofilaments with oxygen plasma and silanization with perfluorodecyl trichlorosilane, the surfaces were transparent and superoleophobic (see Figure 7D) for a wide variety of liquids including mineral oil (γ_{LV} = 32 mN/m, θ^* = 172°, ω =1.2°), toluene (γ_{LV} = 28.4 mN/m, θ^* = 168°, ω = 2.5°), *p*-xylene (γ_{LV} = 28.3 mN/m, θ^* = 171°, ω = 3.0°), hexadecane (θ^* = 174°, ω = 2.0°), dodecane (θ^* = 167°, ω = 2.3°), cyclohexane (γ_{LV} = 25 mN/m, θ^* = 157°, ω =

5.7°) and decane ($\theta^* = 163°$, $\omega = 5.3°$). These surfaces were reported to be stable against outdoor conditions, ozone, deep UV, immersion in sodium hydroxide and sulfuric acid, and temperatures up to 200°C for 24 hours. While the chemical and environmental stability of the surface is good (see Figure 7E), they reported that the mechanical stability needs significant improvement. Deng et al. (*55*) developed a candle soot morphology coated with a silica shell (see Figure 7F) using chemical vapor deposition of tetraethoxysilane catalyzed by ammonia. Upon calcination and silanization with perfluorooctyl trichlorosilane, the surfaces were transparent and superoleophobic (see Figure 7G) for a wide variety of liquids including peanut oil ($\gamma_{LV} = 34.5$ mN/m, $\theta^* = 158°$, $\omega = 4°$), olive oil ($\gamma_{LV} = 32$ mN/m, $\theta^* = 157°$, $\omega = 4°$), hexadecane ($\theta^* = 156°$, $\omega = 5°$) and tetradecane ($\gamma_{LV} = 26.5$ mN/m, $\theta^* = 154°$, $\omega = 5°$). The surfaces were reported to be reasonably stable under continuous drop impact, sand abrasion (see Figure 7H) and annealing up to 400°C, but they showed damage under peel tests. Thus, efforts to develop durable superoleophobic surfaces remain an active area of research.

Downloaded by OHIO STATE UNIV LIBRARIES on August 28, 2012 | http://pubs.acs.org
Publication Date (Web): August 16, 2012 | doi: 10.1021/bk-2012-1106.ch011

Conclusion and Outlook

The development of superoleophobic surfaces is important for basic research, as well as, for numerous commercial applications. Significant strides have been taken in the past few years in understanding the design of superoleophobic surfaces. In this chapter, design parameters that aid the rational design of superoleophobic surfaces are discussed. The spacing ratio, D^*, provides a dimensionless measure of surface porosity, while the robustness factor, A^*, is a measure of a surface's resistance to liquid breakthrough. The most favorable non-wetting surface would, therefore, possess high values of both D^* and A^* simultaneously. Hierarchically structured surfaces, with surface porosity at multiple length scales, are a good choice in designing superoleophobic surfaces because they lead to high values of D^*. Modification of the surface with low surface energy materials such as heavily fluorinated phosphates, silanes, precursors, monomers and polymers, along with re-entrant curvature, leads to high values of A^*.

As briefly discussed earlier, the commercial application of superoleophobic surfaces largely relies on their mechanical durability. This aspect has been sparingly addressed in literature and there is a need and an opportunity to develop mechanically durable superoleophobic surfaces. Further, there are no known surfaces that display ultra-low contact angle hysteresis ($\Delta\theta^* < 5°$) for extremely low surface tension liquids with $\gamma_{LV} \leq 20$ mN/m. While this can be quite a challenge, we believe that rational design using the design parameters discussed here can help develop such surfaces. In addition, there are a few reports on self-repairing slippery surfaces for oils (*56*, *57*). Such surfaces may or may not be superoleophobic, but they offer pressure-stable oleophobicity with ultra-low contact angle hysteresis. Materials with switchable superoleophobic to superoleophilic wettability are also gradually emerging (*24*, *58–60*). Such surfaces can find myriad applications in the separation of low surface tension liquid mixtures and microfluidics. As an increasing number of scientists and engineers contribute to the understanding and the design of superoleophobic surfaces, we predict an exciting future for the innovation and commercialization of superoleophobic surfaces.

References

1. Sun, T. L.; Feng, L.; Gao, X. F.; Jiang, L. *Acc. Chem. Res.* **2005**, *38*, 644.
2. Genzer, J.; Efimenko, K. *Biofouling* **2006**, *22*, 339.
3. Leng, B. X.; Shao, Z. Z.; de With, G.; Ming, W. H. *Langmuir* **2009**, *25*, 2456.
4. Lee, C.; Kim, C.-J. *Phys. Rev. Lett.* **2011**, *106*.
5. Zhang, X.; Zhao, J.; Zhu, Q.; Chen, N.; Zhang, M.; Pan, Q. *ACS Appl. Mater. Interfaces* **2011**, *3*, 2630.
6. Jin, H.; Kettunen, M.; Laiho, A.; Pynnonen, H.; Paltakari, J.; Marmur, A.; Ikkala, O.; Ras, R. H. A. *Langmuir* **2011**, *27*, 1930.
7. Ma, M.; Hill, R. M. *Curr. Opin. Colloid Interface Sci.* **2006**, *11*, 193.
8. Young, T. *Philos. Trans. R. Soc. London* **1805**, *95*, 65.
9. Shuttleworth, R.; Bailey, G. L. J. *Discuss. Faraday Soc.* **1948**, *3*–16.
10. Chen, W.; Fadeev, A. Y.; Hsieh, M. C.; Oner, D.; Youngblood, J.; McCarthy, T. J. *Langmuir* **1999**, *15*, 3395.
11. Genzer, J.; Efimenko, K. *Science* **2000**, *290*, 2130.
12. Nishino, T.; Meguro, M.; Nakamae, K.; Matsushita, M.; Ueda, Y. *Langmuir* **1999**, *15*, 4321.
13. Barthlott, W.; Neinhuis, C. *Planta* **1997**, *202*, 1.
14. Herminghaus, S. *Europhys. Lett.* **2000**, *52*, 165.
15. Neinhuis, C.; Barthlott, W. *Ann. Bot. London* **1997**, *79*, 667.
16. Hu, D. L.; Chan, B.; Bush, J. W. M. *Nature* **2003**, *424*, 663.
17. Hu, D. L.; Bush, J. W. M. *Nature* **2005**, *437*, 733.
18. Gao, X.; Jiang, L. *Nature* **2004**, *432*, 36.
19. Autumn, K.; Liang, Y. A.; Hsieh, S. T.; Zesch, W.; Chan, W. P.; Kenny, T. W.; Fearing, R.; Full, R. J. *Nature* **2000**, *405*, 681.
20. Parker, A. R.; Lawrence, C. R. *Nature* **2001**, *414*, 33.
21. Wagner, T.; Neinhuis, C.; Barthlott, W. *Acta Zool. Stockholm* **1996**, *77*, 213.
22. Bhushan, B.; Jung, Y. C. *Prog. Mater. Sci.* **2011**, *56*, 1.
23. Helbig, R.; Nickerl, J.; Neinhuis, C.; Werner, C. *PLoS One* **2011**, *6*.
24. Choi, W.; Tuteja, A.; Chhatre, S.; Mabry, J. M.; Cohen, R. E.; McKinley, G. H. *Adv. Mater.* **2009**, *21*, 2190.
25. Tuteja, A.; Choi, W.; Mabry, J. M.; McKinley, G. H.; Cohen, R. E. *Proc. Natl. Acad. Sci. U.S.A.* **2008**, *105*, 18200.
26. Tuteja, A.; Choi, W.; Ma, M. L.; Mabry, J. M.; Mazzella, S. A.; Rutledge, G. C.; McKinley, G. H.; Cohen, R. E. *Science* **2007**, *318*, 1618.
27. Ahuja, A.; Taylor, J. A.; Lifton, V.; Sidorenko, A. A.; Salamon, T. R.; Lobaton, E. J.; Kolodner, P.; Krupenkin, T. N. *Langmuir* **2008**, *24*, 9.
28. Cao, L.; Price, T. P.; Weiss, M.; Gao, D. *Langmuir* **2008**, *24*, 1640.
29. Marmur, A. *Langmuir* **2008**, *24*, 7573.

Downloaded by OHIO STATE UNIV LIBRARIES on August 28, 2012 | http://pubs.acs.org
Publication Date (Web): August 16, 2012 | doi: 10.1021/bk-2012-1106.ch011

30. Johnson, R. E.; Dettre, R. H. Contact Angle Hysteresis. In *Contact Angle, Wettability, and Adhesion*; ACS Advances in Chemistry Series 43; American Chemical Society: Washington, DC, 1964.
31. Marmur, A. *Langmuir* **2003**, *19*, 8343.
32. Nosonovsky, M. *Langmuir* **2007**, *23*, 3157.
33. Patankar, N. A. *Langmuir* **2003**, *19*, 1249.
34. Wenzel, R. N. *Ind. Eng. Chem.* **1936**, *28*, 988.
35. Cassie, A. B. D.; Baxter, S. *Trans. Faraday Soc.* **1944**, *40*, 0546.
36. Lafuma, A.; Quéré, D. *Nat. Mater.* **2003**, *2*, 457.
37. Callies, M.; Quéré, D. *Soft Matter* **2005**, *1*, 55.
38. Chhatre, S. S.; Choi, W.; Tuteja, A.; Park, K. C.; Mabry, J. M.; McKinley, G. H.; Cohen, R. E. *Langmuir* **2010**, *26*, 4027.
39. Herminghaus, S. *Europhys. Lett.* **2007**, *79*.
40. Tsujii, K.; Yamamoto, T.; Onda, T.; Shibuichi, S. *Angew. Chem., Int. Ed.* **1997**, *36*, 1011.
41. Shibuichi, S.; Yamamoto, T.; Onda, T.; Tsujii, K. *J. Colloid Interface Sci.* **1998**, *208*, 287.
42. Fujii, T.; Aoki, Y.; Habazaki, H. *Langmuir* **2011**, *27*, 11752.
43. Li, H. J.; Wang, X. B.; Song, Y. L.; Liu, Y. Q.; Li, Q. S.; Jiang, L.; Zhu, D. B. *Angew. Chem., Int. Ed.* **2001**, *40*, 1743.
44. Wu, W.; Wang, X.; Wang, D.; Chen, M.; Zhou, F.; Liu, W.; Xue, Q. *Chem. Commun.* **2009**, 1043.
45. Saraf, R.; Lee, H. J.; Michielsen, S.; Owens, J.; Willis, C.; Stone, C.; Wilusz, E. *J. Mater. Sci.* **2011**, *46*, 5751.
46. Wang, D.; Wang, X.; Liu, X.; Zhou, F. *J. Phys. Chem. C* **2010**, *114*, 9938.
47. Steele, A.; Bayer, I.; Loth, E. *Nano Lett.* **2009**, *9*, 501.
48. Yang, J.; Zhang, Z.; Xu, X.; Men, X.; Zhu, X.; Zhou, X. *New J. Chem.* **2011**, *35*, 2422.
49. Yang, J.; Zhang, Z. Z.; Men, X. H.; Xu, X. H.; Zhu, X. T. *New J. Chem* **2011**, *35*, 576.
50. Hsieh, C. T.; Wu, F. L.; Chen, W. Y. *J. Phys. Chem. C* **2009**, *113*, 13683.
51. Darmanin, T.; Guittard, F. *J. Am. Chem. Soc.* **2009**, *131*, 7928.
52. Darmanin, T.; Guittard, F.; Amigoni, S.; de Givenchy, E. T.; Noblin, X.; Kofman, R.; Celestini, F. *Soft Matter* **2011**, *7*, 1053.
53. Yao, X.; Gao, J.; Song, Y.; Jiang, L. *Adv. Funct. Mater.* **2011**, *21*, 4270.
54. Zhang, J. P.; Seeger, S. *Angew. Chem., Int. Ed.* **2011**, *50*, 6652.
55. Deng, X.; Mammen, L.; Butt, H.-J. r.; Vollmer, D. *Science* **2011**.
56. Wong, T.-S.; Kang, S. H.; Tang, S. K. Y.; Smythe, E. J.; Hatton, B. D.; Grinthal, A.; Aizenberg, J. *Nature* **2011**, *477*, 443.
57. Wang, X.; Liu, X.; Zhou, F.; Liu, W. *Chem. Commun.* **2011**, *47*, 2324.
58. Yang, J.; Zhang, Z.; Men, X.; Xu, X.; Zhu, X.; Zhou, X.; Xue, Q. *J. Colloid Interface Sci.* **2012**, *366*, 191.
59. Zhang, M.; Zhang, T.; Cui, T. *Langmuir* **2011**, *27*, 9295.
60. Zimmermann, J.; Rabe, M.; Artus, G. R. J.; Seeger, S. *Soft Matter* **2008**, *4*, 450.

Downloaded by OHIO STATE UNIV LIBRARIES on August 28, 2012 | http://pubs.acs.org
Publication Date (Web): August 16, 2012 | doi: 10.1021/bk-2012-1106.ch011

Downloaded by OHIO STATE UNIV LIBRARIES on August 28, 2012 | http://pubs.acs.org
Publication Date (Web): August 16, 2012 | doi: 10.1021/bk-2012-1106.ch012

Chapter 12

2D-NMR Studies of Polyvinylidene Fluoride

**Eric B. Twum,[1] Xiaohong Li,[1] Elizabeth F. McCord,[2]
Peter A. Fox,[2] Donald F. Lyons,[2] and Peter L. Rinaldi*,[1]**

**[1]Department of Chemistry, The University of Akron,
Akron, Ohio 44325-3601
[2]E. I. du Pont de Nemours and Co, Experimental Station,
Wilmington, Delaware 19880-0402
*E-mail: peterrinaldi@uakron.edu**

This study employs a variety of solution 2D-NMR techniques to characterize the microstructure of polyvinylidene fluoride (PVDF). The microstructural characterization of PVDF is of great interest as it provides useful information to understand the polymerization process. It also provides insight into the relationship between the chemical structure of polymers and their physical and chemical properties. Through a combination of 1D-NMR experiments such as $^{19}F\{^{1}H\}$ 1D-NMR and 2D-NMR experiments such as 1) $^{19}F\{^{13}C\}$ heteronuclear single quantum coherence (HSQC) with continuous ^{1}H decoupling, 2) ^{19}F-^{19}F gradient double quantum filtered correlation spectroscopy (gDQCOSY) with continuous ^{1}H decoupling, and 3) ^{19}F-^{19}F selective correlation spectroscopy (COSY) with continuous ^{1}H decoupling, the microstructures and resonance assignments of PVDF have been identified. Very weak resonances, which have been reported in the literature but have not been previously assigned, are assigned in this work. In addition to the resonances of main chain sequences, the resonance assignments of end groups in PVDF are presented.

In Advances in Fluorine-Containing Polymers; Smith, D., et al.;
ACS Symposium Series; American Chemical Society: Washington, DC, 2012.

Downloaded by OHIO STATE UNIV LIBRARIES on August 28, 2012 | http://pubs.acs.org
Publication Date (Web): August 16, 2012 | doi: 10.1021/bk-2012-1106.ch012

Introduction

^{19}F NMR spectroscopy is an important technique for characterizing fluoropolymers. ^{19}F 1D-NMR or ^{19}F detected 2D-NMR experiments often provide more information than ^{1}H or ^{13}C detected experiments. This is in part due to the large chemical shift range in ^{19}F 1D-NMR spectra, which gives better dispersion of resonances compared to ^{1}H 1D-NMR spectra, where the resonances may overlap with one another. ^{19}F NMR, like ^{1}H NMR, is very sensitive due to the high natural abundance of ^{19}F (100%) and the large magnetogyric ratio (94 % of ^{1}H). The large chemical shift range, together with the high sensitivity of ^{19}F NMR, permits the detection and resolution of weak signals which cannot be resolved in ^{1}H or ^{13}C NMR.

The earliest ^{19}F NMR studies on fluoropolymers were carried out without ^{1}H decoupling. For fluoropolymers with a large number of protons, like polyvinylidene fluoride (PVDF), the many unresolved *J*-couplings between ^{1}H and ^{19}F resulted in very poor resolution. In earlier studies, the unavailability of high resolution instruments hindered thorough microstructural studies of most fluoropolymers. Schilling *et al.* (*1*, *2*) first demonstrated that triple resonance experiments, in the form of simultaneous ^{1}H and ^{19}F decoupling, while collecting ^{13}C 1D-NMR spectra, could simplify spectra and facilitate resolution of individual resonances in complex spectra from fluoropolymers. In recent years, with the advent of very high field NMR instruments, the ready availability of hardware for ^{1}H/^{19}F double resonance and ^{1}H/^{19}F/^{13}C triple resonance experiments, and the development of multidimensional pulse sequences specially suited for fluoropolymers, renewed interest has been generated in the microstructural characterization of these polymers.

PVDF is an extremely important fluoropolymer due to its desirable properties such as high thermal stability and low flammability. It is chemically inert, has high resistance to acids (*3*, *4*) and is therefore used for making containers for chemical storage. It also exhibits piezo- and pyroelectric properties (*3–5*). Thorough microstructural characterization of PVDF is important as this allows the polymer's microstructure to be correlated with its possession of desirable chemical and physical properties and the occurrence of the different reaction pathways during the polymerization process (*6*). Thorough structural characterization also provides information to improve the production efficiency and usefulness of the material.

PVDF is usually prepared by free radical emulsion polymerization, although its preparation by other polymerization techniques has been described in the literature. The polymerization process is not completely regiospecific (*7*). The addition of inverted monomer units can occur, resulting in formation of both head-head (H-H) and tail-tail (T-T) units in addition to the head-tail (H-T) units from normal monomer addition. The CF_2 groups from the defects (inverse addition) and those from the chain-end structures are in very low concentration compared to the bulk of the CF_2 groups in structures from normal addition. This makes the unequivocal NMR characterization of defects and chain-end structures challenging.

Earlier studies reporting the characterization of PVDF mainly used ^{19}F 1D-NMR spectroscopy. Sometimes the assignments were based on empirical schemes such as the γ effect described by Tonelli *et al.* (*8*) and other empirical calculation/prediction methods (*9*, *10*). In the mid 1990's, studies of PVDF contained spectra with better resolution of the peaks due to better instrumentation and higher field magnets. However, researchers still based their assignments partly or wholly on the same 1D-NMR studies used in the late 1970's and 1980's (*6*, *11*). Newly resolved peaks were given tentative assignments (*6*).

In recent years, with the advent of high field NMR, 2D-NMR studies have been done to confirm these assignments. In most cases additional weak peaks were clearly resolved, in some cases enabling the assignment of resonances from end groups. While some 2D-NMR studies have been done on PVDF, most of these studies were done on low molecular weight PVDF (*12*) or VDF telomers (*13*). No thorough 2D-NMR assignments of resonances from high molecular weight PVDF in-chain monomer sequences and chain-end resonances have been found in the literature. 2D-NMR studies on PVDF were performed by Katoh *et al.* (*12*); however, they were only successful in assigning relatively high intensity peaks, which resulted from a single inversion in the chain. Other peaks in their ^{19}F 1D-NMR spectrum, such as resonances from end groups, were not mentioned in their assignments. Their work was augmented by Wormald *et al.* (*14*), who studied high molecular weight PVDF using 2D-NMR. However, once again they did not assign resonances from chain-ends and other weak signals in the ^{19}F 1D-NMR spectrum.

The only study found in the literature close to the analysis presented in this paper was by Wormald *et al* (*13*). They studied a vinylidene fluoride telomer (VDFT), with an average molecular weight of about 1200 g/mol. However, their system is far more amenable to NMR compared to the system studied here. The polymer described in this paper is a high molecular weight PVDF; more peaks from a range of different sequences are expected in the spectra of PVDF compared to those found in the spectra of VDFT. Again, the high molecular weight makes it less amenable to NMR analysis. It is especially difficult to detect and assign low intensity signals from chain-ends. Despite the challenge, it has been possible to characterize weak ^{19}F and ^{1}H NMR signals which have been previously reported without assignments. In this paper, where possible, the ^{13}C NMR assignments of the resonances are also presented. Although PVDF is usually prepared with an organic peroxide initiator (*15*) for color stability (*16*), a persulfate-initiated polymer was used here to simplify end group analysis.

Experimental Section

Materials

All reagents were used as received. Acetone-d_6 (99.9 %), used as the solvent, was purchased from Cambridge Isotope Laboratories Inc. Trichlorofluoromethane ($CFCl_3$, 99.5 %), used as internal standard for ^{19}F NMR and TMS (99.9 %), used as internal standard for ^{1}H and ^{13}C NMR, were purchased from Sigma-Aldrich.

Downloaded by OHIO STATE UNIV LIBRARIES on August 28, 2012 | http://pubs.acs.org
Publication Date (Web): August 16, 2012 | doi: 10.1021/bk-2012-1106.ch012

Downloaded by OHIO STATE UNIV LIBRARIES on August 28, 2012 | http://pubs.acs.org
Publication Date (Web): August 16, 2012 | doi: 10.1021/bk-2012-1106.ch012

Synthesis of Polyvinylidene Fluoride (PVDF)

The PVDF used in this study was prepared by the following procedure. A 2 L continuous process reactor, heated to 101 °C, was charged with a water feed rate of 8 L/h. Monomer flows were set at 1600 g/h vinylidene fluoride giving an overall reactor pressure of 4.14 Mpa. Feeds of ammonium peroxydisulfate, sodium hydroxide and ammonium perfluorooctanoate were delivered at 12.8 g/h, 1.6 g/h, and 16.0 g/h, respectively. The reactor was then equilibrated for 1 h under the above conditions. After this initial equilibration, the material was collected for 15 min. Offgas was measured at ~20 L/h. The polymer was isolated as a fine white powder.

Sample Preparation for NMR Analysis

Samples for NMR analyses were prepared by dissolving 50 mg of the PVDF in about 700 µl of the acetone-d_6 solvent and heating in a sonicator to about 45-50 °C. The solution was then transferred into a 5 mm NMR tube for NMR studies. The PVDF sometimes crystallizes from solution with time; therefore the temperature is often raised to about 45-50 °C in a sonicator to redissolve all the crystals prior to NMR analyses at 30 °C.

Instrumentation

All the NMR spectra were acquired on a Varian Direct-Drive 500 MHz spectrometer equipped with five broad-band rf channels and a 5 mm ^{1}H/^{19}F/^{13}C triple resonance pulse field gradient (PFG) probe. The specially- made probe from Varian is suitable for fluoropolymers as it has a minimum of fluorine-containing materials near the detection coil to minimize interference from background signals that are common in standard probes. It has a single channel, doubly tuned to ^{1}H and ^{19}F with the capability of producing very short 90° pulse widths (5 µs). A duplexer was used to combine the signals from the ^{1}H and ^{19}F rf channels and direct them through the dual-tuned ^{1}H/^{19}F high frequency channel of the probe. The detected ^{1}H or ^{19}F signals returning from the probe are separated and the signal of interest (^{1}H or ^{19}F) is directed to the receiver.

Acquisition of 1D-NMR Spectra

The ^{19}F 1D-NMR spectra were collected with a 16.7 kHz spectral window with gated ^{1}H decoupling (to suppress NOE's) using WALTZ-16 modulation (γB_H = 2.7 kHz) (*17*, *18*). For the purpose of quantitation, a 20.0 s relaxation delay, a 1.0 s acquisition time and a 3.4 µs (30°) pulse width were used. The transmitter power was attenuated by 6db relative to the maximum power output. The data were zero-filled to 256k and the first three data points were backwards linear predicted before Fourier transformation. The linear prediction was done to eliminate roll in the baseline.

The ^1H 1D-NMR spectra were collected with a 5.0 kHz spectral window, a 30.0 s relaxation delay, a 4.68 s acquisition time, a 9.5 μs (90°) pulse width, and gated ^{19}F decoupling using CHIRP modulation (γB_F = 17.9 kHz) (*19*). The data were zero-filled to 128k and the first three data points were backwards linear predicted before Fourier transformation. Line broadening was set to 0.5 Hz for both the ^1H and ^{19}F 1D-NMR spectra.

The ^{13}C 1D-NMR spectrum was collected with a 19 kHz spectral window, 1.0 s relaxation delay, 2.0 s acquisition time, and a 10 μs (90°) pulse width, with simultaneous ^1H (WALTZ-16, γB_H = 2.7 kHz) and ^{19}F (CHIRP, γBF = 17.9 kHz) decoupling. The data were zero-filled to 256k; the first three points in the spectrum were backwards linear predicted, and exponential weighting with line broadening of 3 Hz were applied before Fourier transformation.

Downloaded by OHIO STATE UNIV LIBRARIES on August 28, 2012 | http://pubs.acs.org
Publication Date (Web): August 16, 2012 | doi: 10.1021/bk-2012-1106.ch012

Acquisition of 2D-NMR Spectra

The one-bond ($^1J_{CF}$) and two-bond ($^2J_{CF}$) $^{19}F\{^{13}C\}$ gHSQC experiments were performed with a previously described pulse sequence (*20*, *21*). The ^{19}F dimension had 16.7 kHz spectral window in both one-bond and two-bond experiments; the ^{13}C dimension had spectral windows of 9 kHz and 19 kHz in the one-bond and two-bond experiments, respectively. The following parameters were used for the one-bond experiment: 0.06 s acquisition time, 1.0 s relaxation delay, and 90° pulse widths of 9.8 μs and 12.9 μs for ^{19}F and ^{13}C, respectively. Sixteen transients were averaged for each 2 x 320 increments using the States method of phase sensitive detection (*22*). Continuous ^1H decoupling with WALTZ-16 modulation (γB_H = 2.7 kHz) was used. The following parameters were used for the two-bond experiment: 0.1 s acquisition time, 1.0 s relaxation delay, and 90° pulse widths of 9.8 μs and 12.9 μs for ^{19}F and ^{13}C, respectively. Thirty-two transients were averaged for each 2 x 384 increments using the States method of phase sensitive detection. Continuous ^1H decoupling with WALTZ-16 modulation (γB_H = 2.7 kHz) was used.

Delays were optimized depending on the couplings of interest. The delay, $\Delta=1/4J_{CF}$, was set to 0.96 ms ($^1J_{CF}$=260) for a one-bond $^{19}F\{^{13}C\}$ correlation experiment, and to 8.3 ms ($^2J_{CF}$=30) for a two-bond $^{19}F\{^{13}C\}$ correlation experiment. The data were zero-filled to a 4096 x 4096 data matrix and weighted with sinebell and shifted sinebell functions prior to Fourier transformation.

The ^{19}F-^{19}F gDQCOSY (gradient double quantum filtered COSY) experiment was performed with the standard Varian pulse sequence, using continuous ^1H WALTZ-16 decoupling (γB_H = 2.7 kHz). The data were collected with a 16.7 kHz spectral window, 1.0 s relaxation delay and 9.8 μs (90°) pulse width. Eight transients were averaged for each 2 x 512 increments using the States method of phase sensitive detection in the f_1 dimension. Processing was done with sinebell and shifted sinebell weighting functions and zero-filling to a 4096 x 4096 data matrix prior to Fourier transformation.

The $^{19}F\{^1H\}$ gHETCOR experiment was performed with an ^{19}F spectral window of 16.7 kHz, an ^1H spectral window of 4 kHz, a 1.0 s relaxation delay, a 0.15 s acquisition time with gated ^1H WALTZ-16 decoupling (γB_H = 2.7 kHz), and 90° pulse widths of 9.8 μs and 12 μs for ^{19}F and ^1H, respectively. Eight transients were averaged for each 2 x 256 increments in the f_1 dimension. The data were zero-filled to a matrix of 4096 x 2048 complex points and processed with sinebell and shifted sinebell weighting functions prior to Fourier transformation. The gHETCOR spectrum had many weak peaks hidden by the tails of strong peaks. The weighting functions were adjusted differently for each region depending on the peaks of interest, in order to suppress the signals from strong peaks and to optimally resolve the weak cross peaks of interest.

The ^{19}F-^{19}F selective COSY experiment was performed using the pulse sequence previously described (*20*), but with continuous ^{1}H WALTZ-16 decoupling (γB_H = 2.7 kHz). The following parameters were used: 1.0 s relaxation delay, 0.06 s acquisition time; four transients were averaged for each 2 x 256 increments in the f_1 dimension. The pulse widths used for the f_1 and f_2 dimensions were selective for the desired spectral windows. The FID was weighted with sinebell and shifted sinebell weighting functions in both dimensions, and zero-filled to a matrix of 2048 x 2048 complex points before Fourier transformation.

Results and Discussion

Structure and Nomenclature

The mechanism described in Scheme 1 below, illustrates the homopolymerization of VDF monomer to form PVDF using free radical polymerization. The free radical is produced from the initiator (I_2) during the initiation stage. Examples of common radicals used in the polymerization process include; di-*t*-amyl peroxide, ammonium peroxy disulfate, di-$_t$-butyl-peroxide (DTBP) and others.

The VDF monomer prefers to add to the growing chain in a head-tail fashion, hence most of the polymer is composed of head-tail VDF units. However, ca. 3-6 % of the time, the polymerization would occur to produce head-head and tail-tail structures introduced by monomer inversions in the polymer chain.

A short chain branch (SCB) can occur through intramolecular hydrogen abstraction (the so called backbiting reaction) as illustrated in Scheme 1. Long chain branching (LCB) on the other hand can occur through hydrogen transfer from the polymer backbone to an existing radical and propagation from the newly formed radical (*23*). Termination can occur through coupling of two radicals (not observed), hydrogen abstraction from another polymer chain, or by disproportionation reaction to create an unsaturated polymer chain-end from which further polymerization can occur to give a LCB. Termination by chain transfer to solvent is absent since the polymer was obtained under solventless conditions.

In this paper, CF_2 = 2, CH_2 = 0, where the number designation corresponds to the number of fluorines on a saturated (sp^3) carbon, based on common practice in the literature. The ^{19}F resonances are designated with upper case letters, the label K (which was arbitrarily chosen) designates the fluorines of CF_2 groups in

Downloaded by OHIO STATE UNIV LIBRARIES on August 28, 2012 | http://pubs.acs.org
Publication Date (Web): August 16, 2012 | doi: 10.1021/bk-2012-1106.ch012

long sequences derived from normal head-tail addition. Labels A-F designate ^{19}F resonances/atoms of CF_2 groups in sequences with a single inversion in the chain; labels with a single prime (e.g. A′, B′, C′…) designate ^{19}F atoms of CF_2 groups in sequences from a double inversion. Fluorines labeled with double primes (e.g. A″, B″, C″…) designate signals from chain-end structures, and those with triple primes (e.g. A‴, B‴, C‴…) are ^{19}F resonances suspected to arise from long-chain or short-chain branching species. ^{13}C resonances are labeled with lower case letters, where for example labels a-f designate carbons bound to fluorines, and t-z are carbons without attached fluorines (e.g. CH_2 carbons). ^1H resonances/atoms are labeled with numbers.

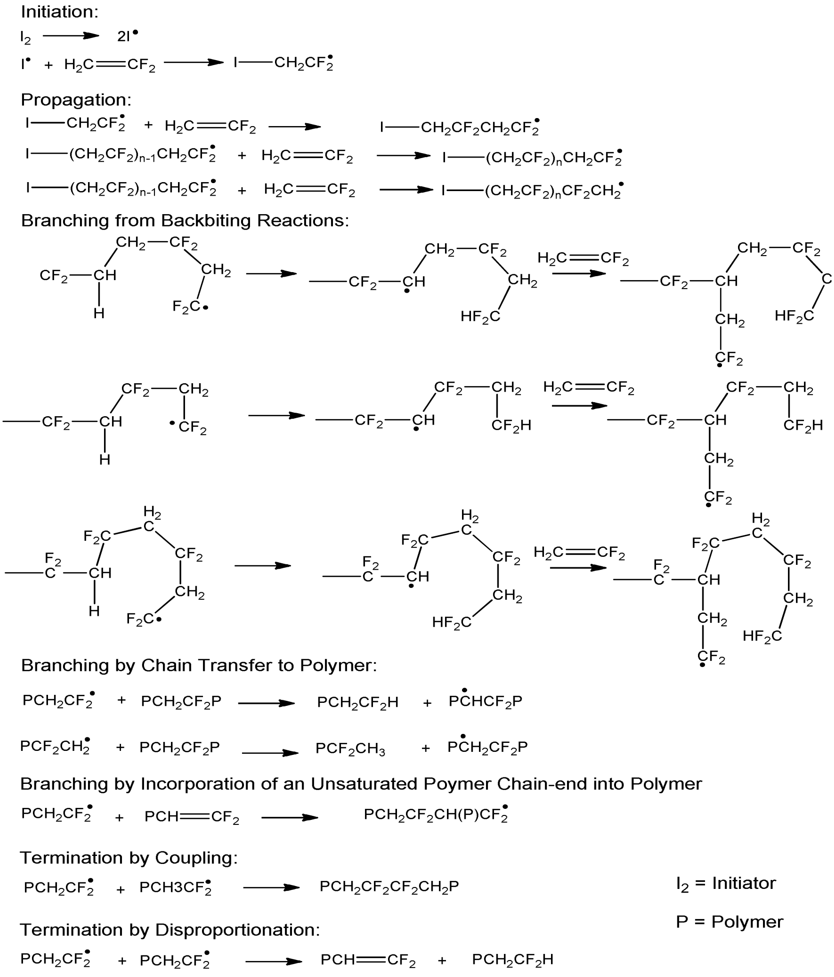
Initiation:
I2 → 2I•
I• + H2C=CF2 → I—CH2CF2•
Propagation:
I—CH2CF2• + H2C=CF2 → I—CH2CF2CH2CF2•
I—(CH2CF2)n-1CH2CF2• + H2C=CF2 → I—(CH2CF2)nCH2CF2•
I—(CH2CF2)n-1CH2CF2• + H2C=CF2 → I—(CH2CF2)nCF2CH2•
Branching from Backbiting Reactions:
H2C=CF2
Branching by Chain Transfer to Polymer:
PCH2CF2• + PCH2CF2P → PCH2CF2H + P•CHCF2P
PCF2CH2• + PCH2CF2P → PCF2CH3 + P•CH2CF2P
Branching by Incorporation of an Unsaturated Poymer Chain-end into Polymer
PCH2CF2• + PCH=CF2 → PCH2CF2CH(P)CF2•
Termination by Coupling:
PCH2CF2• + PCH3CF2• → PCH2CF2CF2CH2P
Termination by Disproportionation:
PCH2CF2• + PCH2CF2• → PCH=CF2 + PCH2CF2H
I2 = Initiator
P = Polymer

Scheme 1. Homopolymerization of VDF monomer using an initiator I_2.

In Advances in Fluorine-Containing Polymers; Smith, D., et al.;
ACS Symposium Series; American Chemical Society: Washington, DC, 2012.

Downloaded by OHIO STATE UNIV LIBRARIES on August 28, 2012 | http://pubs.acs.org
Publication Date (Web): August 16, 2012 | doi: 10.1021/bk-2012-1106.ch012

Downloaded by OHIO STATE UNIV LIBRARIES on August 28, 2012 | http://pubs.acs.org
Publication Date (Web): August 16, 2012 | doi: 10.1021/bk-2012-1106.ch012

If a triad segment of PVDF is considered, there can be eight sequences if direction is specified. However, since NMR is not able to distinguish between the different directions along a polymer chain, only four sets of triad resonances can be detected by NMR. Hypothetical structure **1** below shows a polymer backbone segment with several different triad sequences detectable by NMR. The notation 0 and 2 are used, where 0 is a CH_2 group (tail) and 2 is a CF_2 group (head). From the triad sequences in structure **1**(containing segments a, b, c and d), four unique 2-centered five-carbon sequences (see Table I) (*10*), necessary for NMR resonances assignments are seen.

$$—\underbrace{020202}_{a}—\underbrace{022002}_{b}—\underbrace{200202}_{c}—\underbrace{020220}_{d}—$$

1

By extension, if direction is not specified, from tetrad sequences of PVDF, there can be eight unique 2-centered seven-carbon sequences (Table I). For pentad sequences of PVDF, without specifying direction there are sixteen unique nine-carbon sequences of PVDF. These sets of sequences are for the resonances of the backbone units of PVDF, excluding the chemically dissimilar resonances from end groups and/or branching chains.

Table I. Possible Odd Numbered Carbon Sequences in PVDF

CF_2 Centered Sequences			
5-carbons	*7-carbons*	*9-carbons*	
20$\underline{2}$02	020$\underline{2}$020	2020$\underline{2}$0202	2020$\underline{2}$0200
20$\underline{2}$00	020$\underline{2}$022	0020$\underline{2}$0220	2020$\underline{2}$0220
02$\underline{2}$02	220$\underline{2}$002	0220$\underline{2}$0020	0220$\underline{2}$0022
02$\underline{2}$00	020$\underline{2}$002	2020$\underline{2}$0020	2020$\underline{2}$0022
	202$\underline{2}$020	0202$\underline{2}$0200	0202$\underline{2}$0202
	002$\underline{2}$020	2002$\underline{2}$0202	2002$\underline{2}$0200
	202$\underline{2}$002	0202$\underline{2}$0022	0202$\underline{2}$0020
	002$\underline{2}$002	2002$\underline{2}$0020	2002$\underline{2}$0022

While the ^{19}F resonances expected from the 2-centered seven-carbon sequences derived from tetrads of PVDF can be distinguished from one another in the ^{19}F 1D-NMR spectrum, not all the eight ^{13}C resonances are distinguishable in the ^{13}C 1D-NMR spectrum. Some of the ^{13}C resonances will not show up in the ^{13}C 1D-NMR spectrum because they are from sequences with low occurrence, and the sensitivity of detecting ^{13}C nuclei is low. Additionally, the ^{13}C chemical shift dispersion of the carbon resonances from these structures is not very large; hence, the resonances of higher n-ad sequences are not distinguishable. The ^{19}F chemical shift dispersion of the resonances from these structures is large. Hence, the complex spectra cannot be explained using only seven-carbon sequences; longer sequences (nine-carbon) are needed to explain/assign all the ^{19}F resonances.

Downloaded by OHIO STATE UNIV LIBRARIES on August 28, 2012 | http://pubs.acs.org
Publication Date (Web): August 16, 2012 | doi: 10.1021/bk-2012-1106.ch012

Assignment of Resonances Based on 1D NMR

Figure 1 shows the ^{19}F 1D-NMR spectra of PVDF without ^{1}H decoupling (Figure 1a) and with ^{1}H decoupling (Figure 1b).

These two ^{19}F 1D-NMR spectra indicate that decoupling of ^{1}H, which are in a ratio of about 1:1 with ^{19}F in PVDF, gives considerable simplification of the spectra ($^{n}J_{FH}$ couplings are eliminated in Figure 1b). Once the $^{n}J_{HF}$ couplings are removed, many $^{n}J_{FF}$ homonuclear couplings are revealed. For instance the peak near -104.5 ppm (F″) appears as a triplet in the broadband ^{1}H decoupled spectrum, with a coupling constant of ca. 10 Hz ($^{4}J_{FF}$), while in the coupled spectrum (Figure 1a), this resonance appears as a broad peak with unresolved couplings. Most of the major peaks appearing in the ^{1}H decoupled ^{19}F 1D-NMR spectrum have been reported in the literature. They have been assigned using 1D-NMR data with the help of some empirical chemical shift calculation schemes, and in some other cases with the help of 2D-NMR studies. However, other signals appear that have not been assigned because they have not been detected (too weak or overlapping with other resonances) in spectra obtained using older instruments having lower field and/or fewer advanced electronic capabilities. For instance, the resonances labeled I″ and J″ have previously been assigned as a single resonance (*6*). The resonances labeled D′ and E′ have also been assigned previously as a single resonance (*6*), while the resonance labeled F′ in the ^{19}F 1D-NMR is unassigned.

Peaks in the -90 to -96 ppm range of the ^{19}F 1D-NMR spectrum are resonances of ^{19}F atoms in $0\underline{2}0$ units, therefore ^{19}F-^{19}F COSY correlations among peaks within this region are expected to arise mainly from $^{4}J_{FF}$ correlations. For instance, the two ^{19}F resonances in **2a**, are each from $0\underline{2}0$ units, and are correlated through four-bonds. The peaks from -113 to -116 ppm are resonances of ^{19}F atoms in $2\underline{2}0$ units. ^{19}F -^{19}F correlations among peaks in this region are expected to be mainly from $^{3}J_{FF}$ correlations, although weak correlations through $^{5}J_{FF}$ are possible. The two ^{19}F resonances in **2b** are both from $2\underline{2}0$ units; they are correlated through three-bonds. Peaks from the two regions are correlated by either $^{4}J_{FF}$ or $^{5}J_{FF}$ correlations (*vide infra*).

Downloaded by OHIO STATE UNIV LIBRARIES on August 28, 2012 | http://pubs.acs.org
Publication Date (Web): August 16, 2012 | doi: 10.1021/bk-2012-1106.ch012

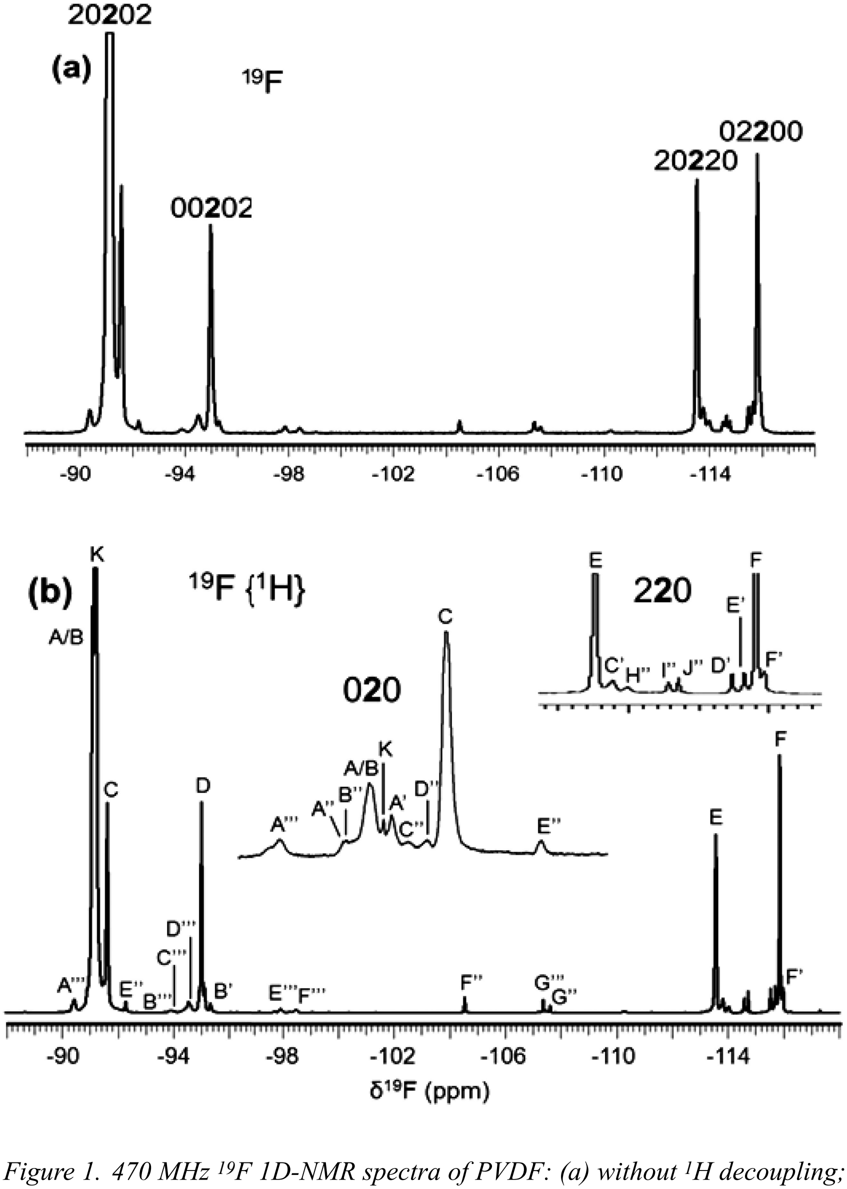

Figure 1. 470 MHz ^{19}F 1D-NMR spectra of PVDF: (a) without ^{1}H decoupling; and (b) with ^{1}H decoupling. Spectral inserts in (b) are selected regions from ^{1}H decoupled spectrum with the K peak saturated and expansion around the 220 region. The saturation reveals peaks hidden near the base of the K peak.

Downloaded by OHIO STATE UNIV LIBRARIES on August 28, 2012 | http://pubs.acs.org
Publication Date (Web): August 16, 2012 | doi: 10.1021/bk-2012-1106.ch012

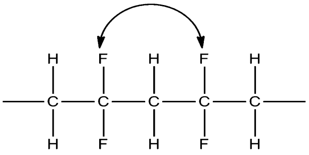

2a

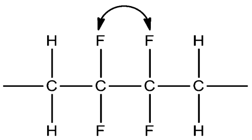

2b

Figure 2 shows the ^{13}C 1D-NMR spectrum of PVDF obtained with simultaneous ^{1}H and ^{19}F decoupling. This spectrum reveals 5 CH_2 and 6 CF_2 ^{13}C resonances. One of the CH_2 ^{13}C resonances falls under the solvent resonance, and is therefore not visible in the 1D spectrum. This signal is evident in the 2D HSQC spectra (*vide infra*).

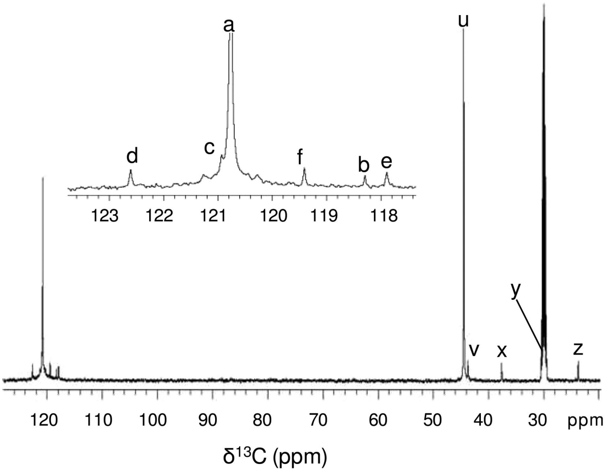

Figure 2. 125 MHz $^{13}C\{^{1}H,^{19}F\}$ 1D-NMR spectrum of PVDF; the insert is an expansion of the CF_2 region.

The ^{13}C 1D-NMR spectrum was obtained with simultaneous ^{1}H and ^{19}F broadband decoupling, hence benefitting from the NOE and spectral simplification from both decoupled ^{1}H and ^{19}F. Assuming that the CF_2 and CH_2 carbons are sensitive to variations in structures at least three-carbons away, 8 unique CF_2 and 8 unique CH_2 ^{13}C resonances would be expected for the backbone units of PVDF (Table I). This excludes the possibility of detecting ^{13}C resonances from chemically dissimilar CF_2 and CH_2 end groups. However, fewer numbers of CF_2 and CH_2 ^{13}C resonances are seen from the ^{13}C 1D-NMR spectrum than predicted. This is due to the relatively low occurrence of some of these possible structures, leading to weak signals, and also the relative insensitivity of ^{13}C chemical shifts (compared to ^{19}F) to variations in chemical structure. Some of the ^{13}C resonances from low probability sequences not seen in the ^{13}C 1D-NMR spectrum are seen in the 2D $^{19}F\{^{13}C\}$ HSQC spectra, which have the better sensitivity associated with ^{19}F detection. The end group ^{13}C resonances are also not detected in the ^{13}C 1D-NMR spectrum, as these structures also occur with much lower probability.

Downloaded by OHIO STATE UNIV LIBRARIES on August 28, 2012 | http://pubs.acs.org
Publication Date (Web): August 16, 2012 | doi: 10.1021/bk-2012-1106.ch012

The spectrum in Figure 3 is a ^{1}H 1D-NMR spectrum of PVDF. This spectrum (like the ^{19}F 1D-NMR spectrum) shows better resolution and simplification when acquired with ^{19}F decoupling. The ^{1}H resonances are identified with numbers as shown on the different structures (*vide infra*). Combining information from ^{1}H 1D-NMR spectra collected with and without ^{19}F decoupling, and ^{19}F 1D-NMR with and without ^{1}H decoupling is a key to most studies that use simple 1D-NMR for ^{1}H and ^{19}F NMR resonance assignment. Unfortunately, the resonances assignments obtained from the ^{1}H and ^{19}F 1D-NMR studies are often not definitive. In order to provide unequivocal assignment of resonances, multidimensional NMR techniques are valuable.

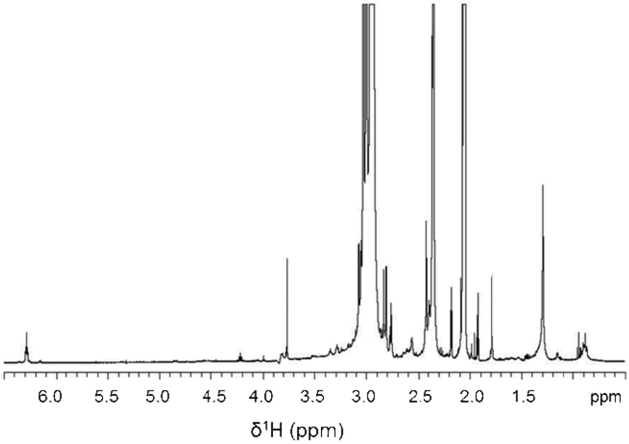

Figure 3. 500 MHz ^{1}H{^{19}F} 1D-NMR spectrum of PVDF.

2D NMR Methods

Gradient Assisted Double Quantum Filtered COSY (gDQCOSY) and Gradient Heteronuclear Correlation (gHETCOR) NMR Experiments

The ^{19}F-^{19}F gDQCOSY experiment provides much more information than the conventional ^{1}H-^{1}H gDQCOSY experiment when applied to fluoropolymers. Usually the ^{19}F-^{19}F COSY correlations "leap-frog" vicinal groups since $^3J_{FF}$ couplings are weaker compared to $^4J_{FF}$ couplings (*24*); four-bond correlations are therefore predominant in these spectra, although three-bond and five-bond correlations are possible. However, the distinction between three-, four- and five-bond correlations is not always obvious.

For relatively low molecular weight fluorochemicals, the through space NOESY (Nuclear Overhauser Enhancement Spectroscopy) experiment mainly provides correlations between vicinal fluorines, and is used together with the COSY experiment to provide unambiguous assignments (*24*). The limitation of the NOESY experiment, however, is that the cross-peaks from NOE interactions are relatively weak (about 1 % of the diagonal peak) compared to those from COSY. The NOESY experiment requires relatively high concentration samples. This requirement is difficult to meet for PVDF which has limited solubility; the NOESY experiment was therefore not used in this work.

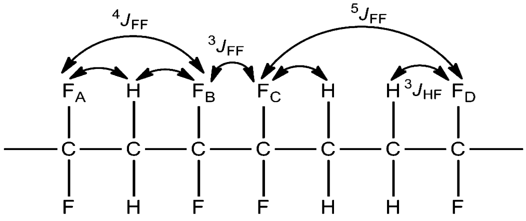

3

The $^{19}F\{^1H\}$ gHETCOR experiment is used in this study to differentiate vicinal ($^3J_{FF}$) correlations from $^4J_{FF}$ correlations. For a hypothetical PVDF backbone structure, **3** the gDQCOSY experiment will give a four-bond correlation between the resonances of FA and FB; the $^{19}F\{^1H\}$ gHETCOR will give $^3J_{FH}$ correlations from resonances F_A and F_B to the same proton. This will confirm the cross-peaks between the resonances F_A and F_B as a four-bond correlation. The gDQCOSY will give a three-bond correlation between the resonances of F_B and F_C. The correlation can be confirmed as a three-bond correlation from the $^{19}F\{^1H\}$ gHETCOR spectrum, which will show that the resonances of F_B and F_C each have single ^{19}F-^1H correlations to different protons. Lastly, a five-bond correlation between the resonances of FC and FD will occur in a gDQCOSY spectrum. The $^{19}F\{^1H\}$ gHETCOR experiment will show that ^{19}F resonances of F_C and F_D do not have correlations to a common proton. The $^{19}F\{^{13}C\}$ gHSQC experiment can also be used to distinguish the different ^{19}F-^{19}F couplings from one another (*vide infra*).

^{19}F-^{19}F Selective COSY Experiment

The ^{19}F-^{19}F selective COSY experiment like the traditional ^{19}F-^{19}F COSY experiment gives $^3J_{FF}$, $^4J_{FF}$ and $^5J_{FF}$ correlations. The large chemical shift dispersion in ^{19}F NMR spectra requires that very short pulse widths must be used for effective excitation of the entire spectral window. Applying the conventional COSY experiment to most fluoropolymers, which can have spectral dispersion in a range of about 200 ppm (100 kHz on a 500 MHz instrument), is difficult.

At present, most solution NMR probes cannot produce 3 μs 90° pulse widths needed to excite the typical 100 kHz spectral window encountered in ^{19}F NMR. To circumvent the difficulty of exciting the large spectral window, the selective COSY experiment can be used. The selective COSY excites only regions of interest, thus, there is no requirement of very short pulse widths. The selective nature of the experiment enhances digital resolution and makes the experiment shorter, as fewer t_1 increments are required to provide high digital resolution in the indirectly detected dimension. It is also possible to eliminate couplings in the f_1 dimension by incorporating selective inversion pulses in the middle of the t_1 evolution period.

Downloaded by OHIO STATE UNIV LIBRARIES on August 28, 2012 | http://pubs.acs.org
Publication Date (Web): August 16, 2012 | doi: 10.1021/bk-2012-1106.ch012

This produces spectra with much simpler cross peak patterns, leading to improved signal intensity, and making it easier to resolve and identify sets of cross-peaks patterns from the many structures present in the polymer mixture. In the traditional COSY experiment, the digital resolution is low. Complex cross-peak patterns are obtained, there is cancellation of antiphase multiplet components from overlapping cross-peaks, and there is poor resolution of the cross-peak from one another. The problem is particularly severe for 2D-NMR spectra when large spectral windows are involved.

Even though the spectral window in the ^{19}F spectra of PVDF is not terribly large (ca. 15 kHz), the spectral simplification achieved in the f_1 decoupled version of the selective COSY experiment provided information that helped in distinguishing certain resonances. The selective COSY experiment has been used extensively in other studies (*20*). Figure 4 below shows the pulse sequence used for the selective COSY experiment. The experiment was performed with continuous ^1H decoupling using WALTZ-16 modulation. For a detailed description of how the selective COSY pulse program works and its application to other fluoropolymers, see reference (*20*).

Downloaded by OHIO STATE UNIV LIBRARIES on August 28, 2012 | http://pubs.acs.org
Publication Date (Web): August 16, 2012 | doi: 10.1021/bk-2012-1106.ch012

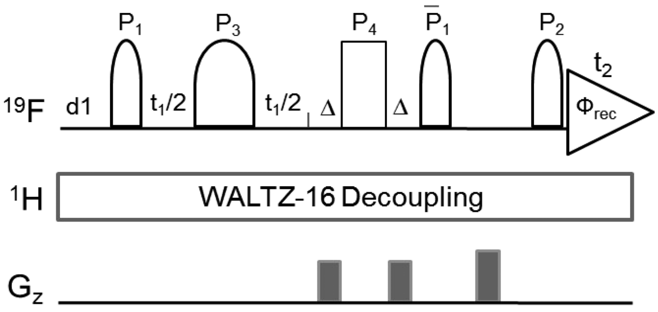

Figure 4. Pulse sequence used to obtain ^{19}F-^{19}F selective COSY spectra. The narrower symmetric shaped pulses are 90° selective pulses and the wider symmetric shaped pulse is a 180° selective inversion shaped pulse. The rectangular pulse is a non-selective 180°. Pulses are along +x axes with the exception of the following: P_1: x, -x, x, -x; P_2: $(x)_2$, $(-x)_2$; Φ_{rec}: x, -x, -x, x. EBURP1 shaped pulses were created with 9.8 μs 90° pulse width (RF field of 25.5 kHz). The gradient times were 1.0 ms, the first two gradients were 0.048 T/m and the last gradient was 0.096 T/m. Reprinted with permission from E. B. Twum, C. Gao, X. Li, E. F. McCord, P. A. Fox, D. F. Lyons and P. L. Rinaldi, Macromolecules, 2012, DOI:10.1021/ma300836. Copyright (2012) American Chemical Society.

Downloaded by OHIO STATE UNIV LIBRARIES on August 28, 2012 | http://pubs.acs.org
Publication Date (Web): August 16, 2012 | doi: 10.1021/bk-2012-1106.ch012

2D ^{19}F{^{13}C} Gradient Heteronuclear Single Quantum Coherence (gHSQC)

The ^{19}F{^{13}C} gHSQC experiments were acquired using the pulse sequence shown in Figure 5. Two experiments were performed; one with delays (Δ) optimized for one-bond couplings, and the other with delays (Δ) optimized for two-bond couplings. To accomplish this, the polarization transfer delays (Δ) were set to 0.96 ms for $^1J_{CF}$ couplings or to 8.3 ms for $^2J_{CF}$ couplings.

The one-bond C-F couplings are about an order of magnitude higher than the two-bond C-F couplings ($^1J_{CF}$ = 250-310, $^2J_{CF}$ = 25-45). One-bond correlations are suppressed in the two-bond experiment by changing the phase of the 135° pulse in the TANGO pulse train (*25*). As a consequence of the large difference between one-bond and two-bond couplings, artifact signals from one-bond leakage are minimized in the two-bond experiment and vice versa. The ^{13}C isotope shift which is observed for the ^{19}F{^{13}C} one-bond experiment also helps to distinguish one-bond leakage signals from two-bond correlations in the two-bond experiment, even if leakage does occur. For details regarding the setup and use of these experiments, see reference (*20*).

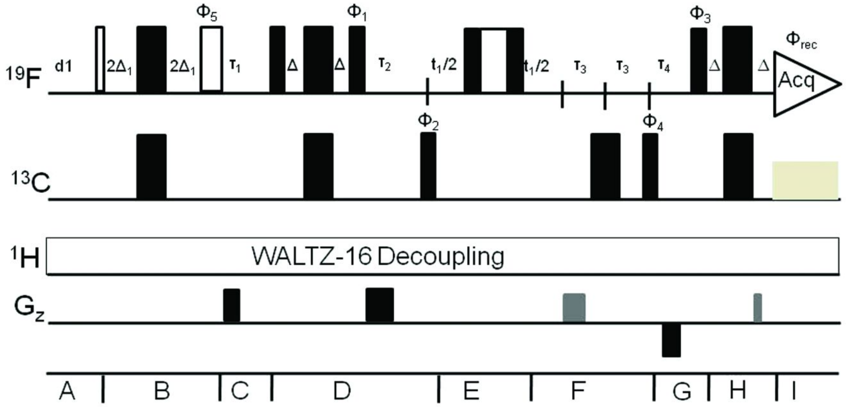

Figure 5. Diagram of the pulse sequence used to obtain the one-bond and two-bond ^{19}F{^{13}C} gHSQC spectra. The narrow and wide open rectangular symbols are 45° and 135° pulses, respectively; the narrow and wide filled rectangular symbols are 90° and 180° pulses, respectively. The three rectangular symbols in the middle of the evolution period (t_1) constitute a composite 180° pulse. The interpulse delay, $\Delta_1 = 1/(4 \times {}^1J_{CF})$ for both one-bond and two-bond experiments. The interpulse delay $\Delta = 1/(4 \times {}^nJ_{CF})$, is optimized depending on the correlations of interest. The phase cycling was: Φ_1: $(y)_2$, $(-y)_2$; Φ_2: x, -x; Φ_3: $(x)_4$, $(-x)_4$; Φ_4: $(x)_8$, $(-x)_8$; Φ_5: -x (for 1-bond experiment) and x (for 2-bond experiment); Φ_{rec}: y, $(-y)_2$, y, -y, $(y)_2$, $(-y)_2$, $(y)_2$, -y, y, $(-y)_2$, y; all other pulses were along the x axis. The τ delays were set to permit insertion of gradient pulses (for crusher and coherence selection) and short recovery delays. The amplitudes of the homospoil gradients (in black) were set to 0.098 T/m and those of the other gradients were set to 0.082 T/m (see reference (20)).

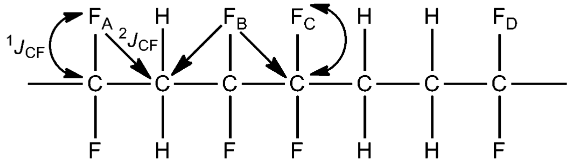

4

The $^1J_{CF}$ and $^2J_{CF}$ correlations in the gHSQC experiments also help to distinguish between $^3J_{FF}$ and $^4J_{FF}$ correlations in the ^{19}F-^{19}F gDQCOSY and/or ^{19}F-^{19}F selective COSY experiments. If in the two-bond gHSQC, both ^{19}F resonances F_A and F_B show two-bond ^{19}F-^{13}C correlations to the same CH_2 ^{13}C resonance of **4**, then this implies that the two ^{19}F resonances are correlated through a $^4J_{FF}$ correlation in the COSY spectrum. If ^{19}F resonance F_B gives a two-bond correlation to ^{13}C resonance of a carbon having a directly attached ^{19}F, then ^{19}F resonances F_B and F_C are correlated through $^3J_{FF}$ in the COSY spectrum. For example, in **4**, the resonances of carbons directly attached to F_B and F_C are identified by the one-bond gHSQC experiment, and the two-bond gHSQC experiment reveals correlations between the resonances of F_B/F_C and the resonances of each other's attached carbon. Further details regarding this sequence can be found in reference (*20*).

2D-NMR Assignment of ^{19}F Backbone Resonances

To determine fluorine and the carbon resonance assignments of atoms that are attached through one and two-bonds, a specially adapted indirect detection one-bond and two-bond $^{19}F\{^{13}C\}$ gHSQC pulse sequence described above was used; Figure 6 shows selected regions of the spectra from these experiments. The one-bond $^{19}F\{^{13}C\}$ gHSQC spectrum in Figure 6a gives detectable cross peaks correlating the resonances of ^{19}F atoms and their directly bound ^{13}C atoms for almost all the peaks (including the weak resonances from most end groups).

Due to the high sensitivity of the HSQC experiment compared to the normal ^{13}C detected 1D-NMR experiment, most resonances whose ^{13}C peaks are not seen in the ^{13}C 1D-NMR spectrum are detected in the HSQC experiment. Two-bond ^{19}F-^{13}C correlations were also observed among the resonances of fluorines and carbons in the CH_2 and CF_2 regions of the ^{13}C NMR spectrum (Figure 6b and c, respectively). As expected, ^{19}F resonances in the $0\underline{2}0$ region have two-bond correlations to only CH_2 ^{13}C resonances; while those ^{19}F resonances from the $2\underline{2}0$ region show two-bond correlations to both CF_2 and CH_2 ^{13}C resonances.

The ^{19}F resonances from the $0\underline{2}0$ region can be subdivided into two regions of peaks from different five-carbon sequences: those from $20\underline{2}02$ sequences and those from $00\underline{2}02$ sequences. In the $20\underline{2}02$ region, the two CH_2 carbons on either side of the central ^{19}F atom are in symmetric environments and hence give identical resonances. Note, however, that the two CH_2 carbons may be

Downloaded by OHIO STATE UNIV LIBRARIES on August 28, 2012 | http://pubs.acs.org
Publication Date (Web): August 16, 2012 | doi: 10.1021/bk-2012-1106.ch012

Downloaded by OHIO STATE UNIV LIBRARIES on August 28, 2012 | http://pubs.acs.org
Publication Date (Web): August 16, 2012 | doi: 10.1021/bk-2012-1106.ch012

non-identical if higher n-ads are considered. In the 00202 region, the two CH_2 carbons are in very different environments (002 and 202), and thus have very different chemical shifts. For example ^{19}F resonance D (from the 00_202 region) shows two-bond correlations to two different CH_2 carbons (correlations D-v and D-y in Figure 6b), but the ^{19}F resonances of the 20202 region (example resonances B and C) show two-bond correlations to similar CH_2 carbon resonances. The 220 ^{19}F chemical shift region can also be subdivided into two regions of peaks from different five-carbon sequences, 20220 and 02200. These two regions are distinguished based on the fact that in the 20220 region, the central CF_2 ^{19}F resonance shows a $^4J_{FF}$ correlation with another ^{19}F resonance in the COSY spectrum (Figure 7a). Referring to structure **5** (produced by a single monomer inversion), this four-bond ^{19}F-^{19}F correlation is proven from the fact that the central CF_2 ^{19}F resonance (example ^{19}F resonance E from the 20220 sequence) shows a two-bond HSQC correlation to a CH_2 carbon resonance (x). Another ^{19}F resonance (A in this case) shows a two-bond HSQC correlation to the same CH_2 carbon resonance (Figure 6b).

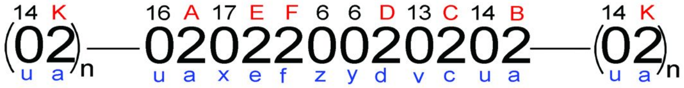

5

In the 02200 region, the central CF_2 ^{19}F resonance should not, and does not show a $^4J_{FF}$ correlation in the COSY spectrum (Figure 7). It does, however, show a weak $^3J_{FF}$ correlation with another CF_2 ^{19}F resonance in the 220 region. For example, ^{19}F resonances E and F show three-bond ^{19}F-^{19}F correlations to one another in the gDQCOSY spectrum (Figure 7c).

^{19}F resonance F has two-bond ^{19}F-^{13}C correlations with the ^{13}C resonances of carbons e and z in structure **5**. ^{19}F resonance E has two-bond correlations with the ^{13}C resonances of carbons f and x, in the $^{19}F\{^{13}C\}$ gHSQC spectrum. From the one-bond $^{19}F\{^{13}C\}$ gHSQC experiment, ^{19}F resonance E correlates with ^{13}C resonance e, while ^{19}F resonance F correlates with ^{13}C resonance f. This indicates that the resonances of the two fluorines (E and F) are correlated to each other through a three-bond coupling. This $^3J_{FF}$ correlation is detected in the gDQCOSY spectrum (Figure 7c). ^{19}F resonance D has two-bond correlations with ^{13}C resonances y and v, and ^{19}F resonance C has two-bond correlations with ^{13}C resonances u and v. From the above information, it is clear that ^{19}F resonances D and C are correlated through a four-bond coupling, as both show two-bond gHSQC correlations to ^{13}C resonance v.

The gDQCOSY spectrum shows a correlation between ^{19}F resonances D and C (Figure 7b). It is further confirmed by the gHETCOR spectrum (Figure 8a and other data not shown), which shows that both ^{19}F resonances D and C have three-bond ^{19}F-^1H correlations to the resonances of the methylene proton labeled

13 in structure **5**. The gDQCOSY spectrum (Figure 7a), shows that ^{19}F resonances F and D are correlated. Since resonances F and D show two-bond correlations to different ^{13}C resonances in Figure 6, the only logical way they can be correlated is through a $^{5}J_{FF}$ coupling. Furthermore, since ^{19}F resonance D is from the 00202 region and ^{19}F resonance F is from the $02\underline{2}00$ region, the two resonances can only be correlated through a $^{5}J_{FF}$ correlation, sharing a 00 fragment between them (see structure **5** and Figure 6). The intensity of the ^{19}F-^{19}F correlation between resonances D and F provides some support for this assignment if compared with the $^{4}J_{FF}$ correlations found in the gDQCOSY spectrum. The $^{5}J_{FF}$ correlation between ^{19}F resonances D and F (in a relatively high occurrence structure) is weaker than the $^{4}J_{FF}$ correlations between resonances from low occurrence structures (e.g. resonances B′ and C′ in Figure 7a), as expected for a correlation based on a small long range coupling.

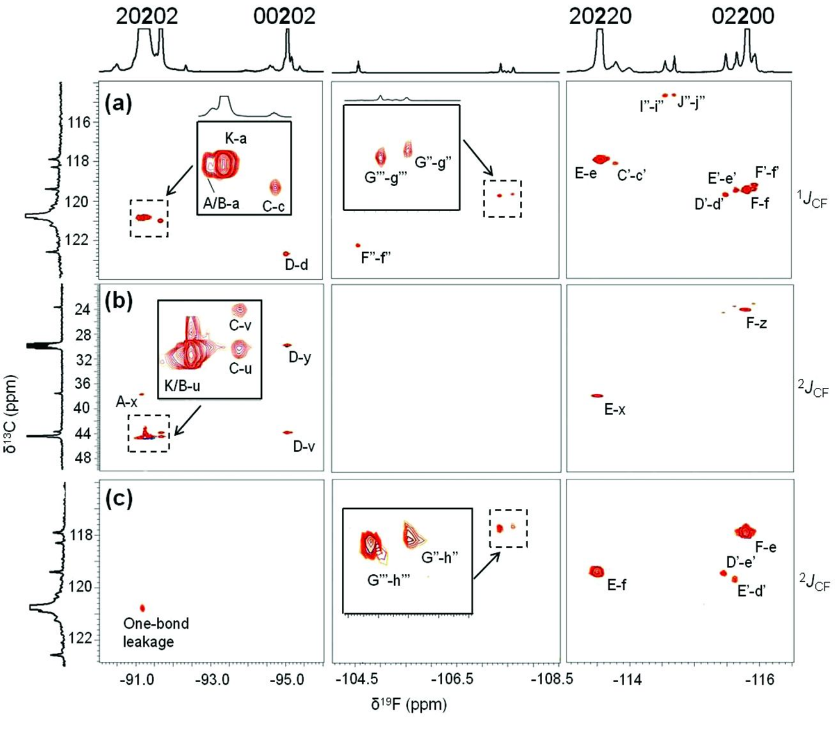

Figure 6. 470 MHz $^{19}F\{^{13}C\}$ gHSQC spectra of PVDF obtained with continuous ^{1}H decoupling : (a) selected regions from one-bond $^{19}F\{^{13}C\}$ gHSQC spectrum; (b) selected regions from two-bond $^{19}F\{^{13}C\}$ gHSQC spectrum, CH_2 carbon region; (c) selected regions from two-bond $^{19}F\{^{13}C\}$ gHSQC spectrum, CF_2 carbon region. ^{19}F and ^{13}C 1D-NMR spectra of the corresponding regions are plotted along the horizontal and vertical axes, respectively. Reprinted with permission from E. B. Twum, C. Gao, X. Li, E. F. McCord, P. A. Fox, D. F. Lyons and P. L. Rinaldi, Macromolecules, 2012, DOI:10.1021/ma300836. Copyright (2012) American Chemical Society.

Downloaded by OHIO STATE UNIV LIBRARIES on August 28, 2012 | http://pubs.acs.org
Publication Date (Web): August 16, 2012 | doi: 10.1021/bk-2012-1106.ch012

Downloaded by OHIO STATE UNIV LIBRARIES on August 28, 2012 | http://pubs.acs.org
Publication Date (Web): August 16, 2012 | doi: 10.1021/bk-2012-1106.ch012

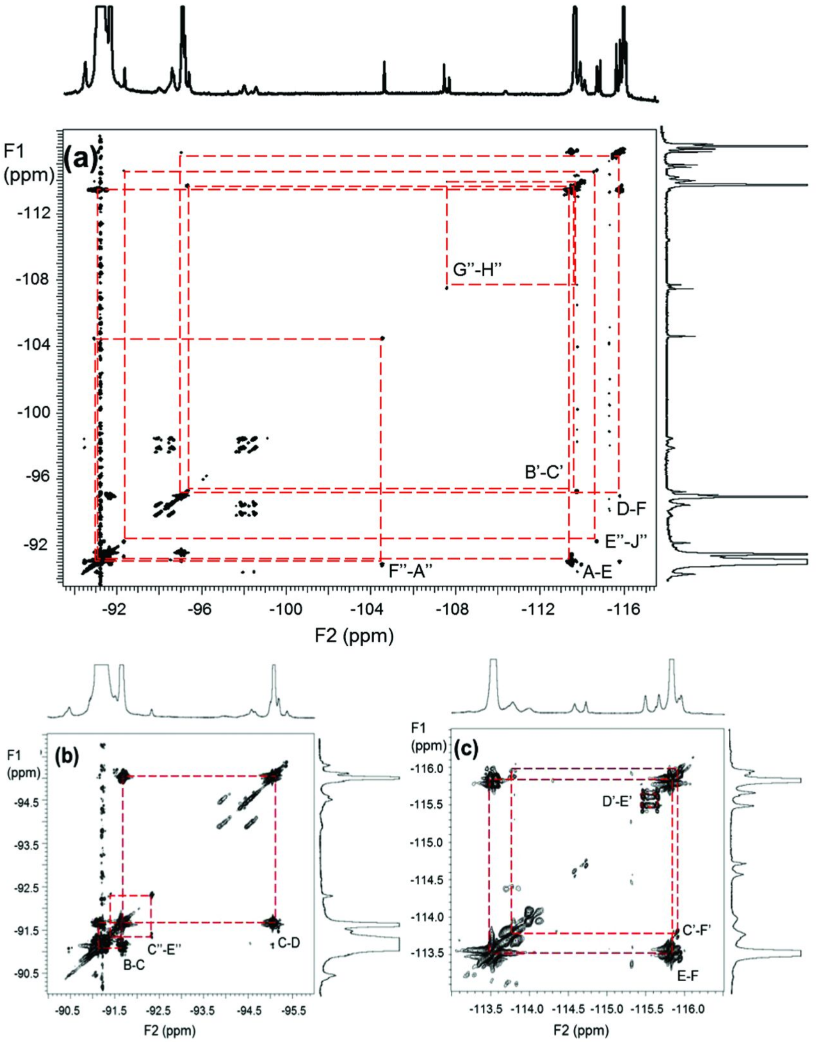

Figure 7. 470 MHz ^{19}F-^{19}F gDQCOSY spectra of PVDF: (a) full spectrum; (b) expansion around the peak region containing resonances of structures from normal addition, and (c) expansion of the -113 to -116.5 ppm region. Reprinted with permission from E. B. Twum, C. Gao, X. Li, E. F. McCord, P. A. Fox, D. F. Lyons and P. L. Rinaldi, Macromolecules, 2012, DOI:10.1021/ma300836. Copyright (2012) American Chemical Society.

Downloaded by OHIO STATE UNIV LIBRARIES on August 28, 2012 | http://pubs.acs.org
Publication Date (Web): August 16, 2012 | doi: 10.1021/bk-2012-1106.ch012

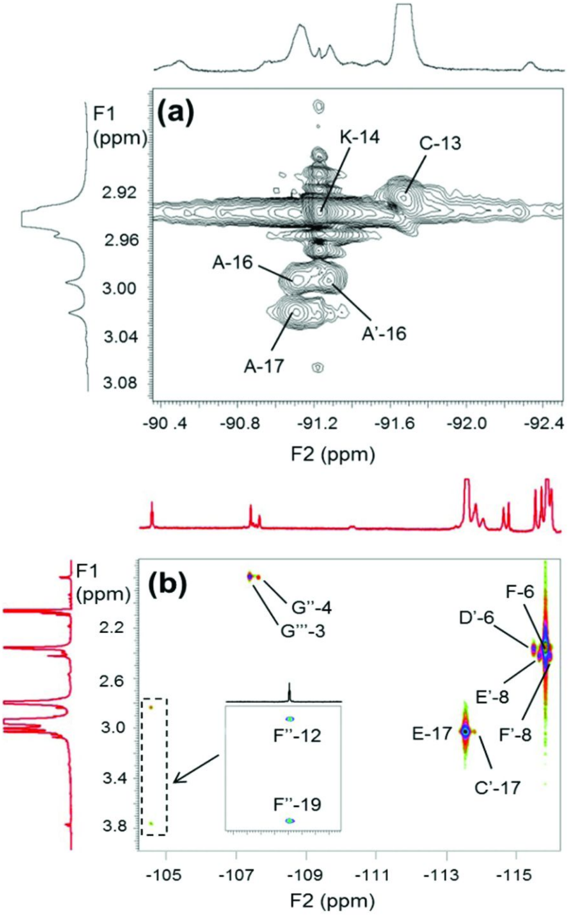

Figure 8. 470 MHz $^{19}F\{^{1}H\}$ gHETCOR spectrum of PVDF: (a) expansion around the region containing resonances from normal addition structure; (b) expansion of the -104 to -116 ppm region. The ^{19}F 1D-NMR spectrum across the top of Figure 8a was obtained with the K peak saturated.

The $^{1}H\{^{13}C\}$ gHSQC and gHMBC spectra, obtained with continuous ^{19}F decoupling (data not shown), provide evidence in support of the assignments made so far, and also help in the assignment of the ^{1}H resonances. The one-bond correlations for the major CH_2 groups are: the resonance of ^{13}C z is correlated with the resonance of methylene proton 6; the resonance of ^{13}C y is also correlated with the resonance of the methylene proton in the same region 6. Two different methylene protons have similar chemical shifts (methylenes labeled 6). While the differences in a five-carbon sequence are enough to render the carbons nonequivalent, the proton shifts are not affected as much, and their shifts are not resolved. The $^{19}F\{^{1}H\}$ gHETCOR spectrum (data not shown) also shows that ^{19}F resonances F and D have $^{3}J_{FH}$ correlations to the methylene proton resonances near position 6.

Downloaded by OHIO STATE UNIV LIBRARIES on August 28, 2012 | http://pubs.acs.org
Publication Date (Web): August 16, 2012 | doi: 10.1021/bk-2012-1106.ch012

The resonance of ^{13}C x is correlated with the resonance of methylene proton 17, and that of ^{13}C v is correlated with the resonance of methylene proton 13. Other correlations from the ^{1}H{^{13}C} gHSQC spectrum are between ^{13}C resonance u and the resonances of methylene protons 14 and 16 (data not shown). Since ^{19}F resonance K (from H-T addition) shows a two-bond ^{19}F-^{13}C correlation with the resonance of ^{13}C u, the resonance of methylene protons 14 is assigned to protons in methylene groups from normal addition. The correlation between ^{13}C resonance u and proton resonance 16 (u, 16) is assigned as the one-bond ^{1}H-^{13}C correlation near the normal addition unit (**5**). The environments of ^{13}C resonance u with one-bond ^{1}H-^{13}C correlation to methylene resonance 16, and that of ^{13}C resonance u with one-bond ^{1}H-^{13}C correlation to methylene resonance 14, are the same up to seven-carbon sequences. It is therefore not surprising that they have the same ^{13}C chemical shift. However, the two methylene proton resonances (methylenes 14 and 16) show an unexpected difference in chemical shift (0.05 ppm difference). The ^{19}F{^{1}H} gHETCOR spectrum (Figure 8), shows that ^{19}F resonance A is correlated to proton resonances 16 and 17; this proves that the correlation between ^{13}C resonances u and ^{1}H resonance 16 is a one bond correlation near a normal addition unit.

^{19}F resonances E and A are correlated in the gDQCOSY spectrum (Figure 7a). This correlation is assigned as a four-bond correlation because both resonances E and A show correlations to the proton resonance labeled 17 in the ^{19}F{^{1}H} gHETCOR spectrum (Figure 8). Furthermore, both resonances E and A have a two-bond correlation with ^{13}C resonance x Figure 6b, and their positions in the ^{19}F spectrum suggest they will be correlated by a $^{4}J_{\mathrm{FF}}$ correlation (resonance A is in the $0\underline{2}0$ region and resonance E is in the $2\underline{2}0$ region).

The gDQCOSY spectrum shows a correlation between resonances B and C (Figure 7b), and the two-bond gHSQC experiment shows that both ^{19}F resonances C and B have two-bond gHSQC correlations with ^{13}C resonance u. Putting these pieces of information together, it is evident that the correlation between ^{19}F resonances B and C is a four-bond correlation. The results from the gHMBC spectrum (data not shown) support the ^{1}H assignments thus far discussed. The complete assignments of ^{19}F resonances up to seven-carbon sequences (nine-carbon sequences in some cases) from PVDF are given in Table II. The Table also compares assignments obtained in this work to those obtained from other studies. (*6*–*8*, *13*, *14*, *26*, *27*).

One resonance whose assignment is different in this paper compared to what is commonly reported in the literature (*7*, *8*, *26*) is that of C′. In this paper, resonance C′ is assigned as $0020\underline{\mathbf{2}}2002$ based on correlations identified from 2D-NMR. In the literature, resonance C′ is assigned to the $020\underline{\mathbf{2}}202$ sequence attributed to back to back inversions of VDF monomer units. Cais and Sloane (*26*) have shown that the probability of having such a structure from VDF polymerization is very low. Russo *et al.* (*6*) rationalized that such a structure could be produced from chain termination by coupling as found in polyethylene. The possibility of producing such a structure is not contested, however, it is clear that resonance C′ is not from such a structure. If resonance C′ was from the structure $020\underline{\mathbf{2}}202$, there would be no $^{3}J_{\mathrm{FF}}$ correlation as the four ^{19}F atoms in the central 02022020 sequence would

Downloaded by OHIO STATE UNIV LIBRARIES on August 28, 2012 | http://pubs.acs.org
Publication Date (Web): August 16, 2012 | doi: 10.1021/bk-2012-1106.ch012

be equivalent. It is evident from the 2D gDQCOSY spectrum that resonance C′ shows $^3J_{FF}$ correlation to ^{19}F resonance F′.

Table II. Assignment of ^{19}F Resonances in PVDF

Peak label	*^{19}F δ (ppm) vs. $CFCl_3$*	*Assignments*	*Literature Assignments*	*References*
[a]K	-91.23	2020**2**0202	2020**2**0202	(*7*, *8*, *13*, *14*, *26*)
A	-91.14	020**2**022	020**2**022	(*7*, *8*, *13*, *14*, *26*)
[a]B	-91.14	2020**2**0202	2020**2**0202	(*13*, *14*)
C	-91.67	0020**2**0202	0020**2**0202	(*13*, *14*)
D	-95.05	200**2**020	200**2**020	(*7*, *8*, *13*, *14*, *26*)
[b]E	-113.55	20202**2**2002	20202**2**2002	(*7*, *8*, *13*, *14*, *26*)
[b]F	-115.83	02022**2**0020	02022**2**0020	(*7*, *8*, *13*, *14*, *26*)
A′	-91.28	N/A	N/A	N/A
B′	-95.36	200**2**022	200**2**022	(*7*, *8*, *26*)
[b]C′	-113.80	00202**2**2002	020**2**202	(*7*, *8*, *26*)
[b]D′	-115.50	20022**2**0020	002**2**002	(*7*, *8*, *26*)
[b]E′	-115.67	20022**2**0022	002**2**002	(*7*, *8*, *26*)
[b]F′	-115.95	02022**2**0022	N/A	N/A
A″	-90.93	In-020**2**0-	N/A	N/A
B″	-90.97	-0**2**022CH_3	N/A	N/A
C″	-91.40	-0**2**0202-H	N/A	N/A
D″	-91.53	N/A	N/A	N/A
E″	-92.33	-020**2**02-H	-0**2**02-H	(*6*, *13*, *27*)
F″	-104.55	In-0**2**020-	In-0**2**02-	(*6*, *27*)
G″	-107.60	-0202**2**CH_3	-02**2**CH_3	(*6*, *13*, *27*)
H″	-114.00	-020**2**2CH_3	-0**2**2CH_3	(*6*, *13*, *27*)
I″	-114.55	-020**2**-H	-020**2**-H	(*6*, *13*, *27*)
J″	-114.69	-02020**2**-H	-020**2**-H	(*6*, *13*, *27*)
A‴	-90.49	-0**2**02-CH(02-)2-	N/A	N/A
B‴	-93.93	-0202-CH(02-)**2**-	N/A	N/A
C‴	-94.47		N/A	
D‴	-94.58	N/A	N/A	N/A

Continued on next page.

Table II. (Continued). Assignment of ^{19}F Resonances in PVDF

Peak label	*^{19}F δ (ppm) vs. CFCl$_3$*	*Assignments*	*Literature Assignments*	*References*
E‴	-97.96	-020$\underline{\mathbf{2}}$-CH(02-)2-	N/A	N/A
F‴	-98.51		N/A	
G‴	-107.35	-02$\underline{2}$CH$_3$	N/A	N/A

[a] Nine-carbon sequences do not distinguish them. [b] Nine-carbon sequences are required to account for the difference between these resonances.

Downloaded by OHIO STATE UNIV LIBRARIES on August 28, 2012 | http://pubs.acs.org
Publication Date (Web): August 16, 2012 | doi: 10.1021/bk-2012-1106.ch012

The assignments of resonances from chain ends and branching structures are presented in Table II, without proof. The 2D-NMR experiments used in assigning these resonances will be described in detail elsewhere (*28*).

The ^{19}F detected gHSQC experiment also showed correlations for some of the ^{19}F resonances with relatively weak intensity. For ^{19}F resonances that were too weak to produce cross-peaks in the gHSQC, correlations from more sensitive experiments were employed to obtain resonance assignment. The ^{19}F-^{19}F gDQCOSY is one such experiment. For fluoropolymers, this experiment is preferred to the more common ^{1}H-^{1}H gDQCOSY experiment, as experiments with ^{19}F nuclei are both sensitive and have better spectral dispersion. The ^{19}F{^{1}H} gHETCOR and its COSY version are also very useful in providing information for the assignment of relatively weak signals.

Referring to structure **6,** the ^{19}F resonances labeled C′ and F′ are correlated in the gDQCOSY spectrum (Figure 7c). The positions of the two resonances in the ^{19}F spectrum (both are in the 2$\underline{2}$0 region) and the cross-peak intensity suggest the cross-peak is from a three-bond correlation. The three-bond ^{19}F-^{19}F correlation is confirmed by the fact that resonances C′ and F′ have different ^{19}F-^{1}H correlations in the ^{19}F{^{1}H} gHETCOR spectrum. Resonance C′ is correlated with the proton resonance labeled 17 (Figure 8b), while resonance F′ is correlated with proton resonance labeled 8. They do not show other correlations in the ^{19}F{^{1}H} gHETCOR spectrum (Figure 8b). ^{19}F resonance C′ is correlated with ^{19}F resonance B′ in the gDQCOSY spectrum (Figure 7a); ^{19}F resonance C′ is also correlated to the proton resonance labeled 17 in the ^{19}F{^{1}H} gHETCOR spectrum (see Figure 8b). Proton-fluorine correlation is also seen between ^{19}F resonance B′ and ^{1}H resonance 17, although this is not shown.

Once the 2-centered five-carbon sequences of B′ (00$\underline{2}$02) and F′ (02$\underline{2}$00) are identified, their attachment might be proven by observation of a 5-bond COSY correlation between ^{19}F resonances B′ and F′. However, these are too weak to detect. Alternatively, the ^{19}F resonances of B′ and F′ are both correlated to the ^{19}F resonance of C′, thus proving the presence of structure **6** and establishing its resonance assignments. ^{19}F resonances B′, C′ and F′ show one-bond ^{19}F-^{13}C correlations with ^{13}C resonances b′, c′ and f′ respectively. Their two-bond F-C correlations are, however, not detected because of the low probability of forming these structures. This structure results from a double monomer inversion and only occurs in ca. 0.25 % of the sequences.

Downloaded by OHIO STATE UNIV LIBRARIES on August 28, 2012 | http://pubs.acs.org
Publication Date (Web): August 16, 2012 | doi: 10.1021/bk-2012-1106.ch012

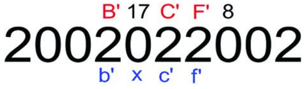

6

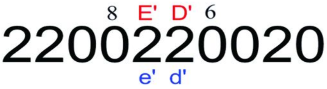

7

With respect to structure **7**, ^{19}F resonances D′ and E′ are correlated in the gDQCOSY spectrum (Figure 7c). However, they do not show common ^{19}F{^{1}H} gHETCOR correlations (Figure 8b), as ^{19}F resonance D′ is correlated with proton resonance 6, and ^{19}F resonance E′ is correlated with proton resonance 8. ^{19}F resonances D′ and E′ show one-bond correlations to ^{13}C resonances d′ and e′, respectively and two-bond correlations to ^{13}C resonances e′ and d′, respectively. Thus ^{19}F resonances D′ and E′ are correlated through three-bonds. No other correlation is seen in the gDQCOSY spectrum for ^{19}F resonances D′ and E′, as the other correlations are $^{5}J_{FF}$ correlations which are too weak to be detected. Both ^{19}F resonances D′ and E′ have the same five-carbon sequences (00**2**20). Combining two 00**2**20 sequences, taking into consideration the three-bond ^{19}F-^{19}F correlation between resonances D′ and E′ results in a 002200 sequence. This proves that the other ^{19}F-^{19}F correlations to resonances D′ and E′ are five-bond correlations.

In PVDF, 000 sequences are not possible; hence, this 002200 sequence in PVDF can be extended to 20022002. It is not possible to distinguish between ^{19}F resonances D′ and E′ based on seven-carbon sequences, nine-carbon sequences (five monomers) are required to uniquely identify ^{19}F resonances D′ and E′ (see **7** and Table II). Formation of this sequence requires two monomer inversions, and is likely to occur in ca. 0.25 % of the sequences.

Calculation of Reverse Unit Content

Since the polymerization of vinylidene fluoride (VDF) is not completely regiospecific, there is always some formation of H-H or T-T units in PVDF. The formation of the H-H or T-T units in PVDF is usually a random process and is reported to be weakly dependent on reaction temperature over a limited range (*7*). Typical values of inversion (formation of H-H or T-T units) reported for low and high molecular weight PVDF or VDF telomers range from 3-6 %. In this study two approaches were used to calculate the reverse unit content; both approaches gave very similar values. The first approach used the expression reported by Russo *et al.* (*6*), and is given in eq. 1 below; where E, F, C′, D′, E′, F′, G″, H″ and G‴ are the integral areas of resonances E, F, C′, D′, E′, F′, G″, H″ and G‴ respectively, and total area is the sum of the integrals of all NMR signals in the ^{19}F 1D -NMR spectrum. The percentage inversion was calculated as 5.2 %.

$$\%\ \text{Inversion} = \frac{\left[\frac{1}{2}(E+F)+\frac{1}{2}(D'+E')+\frac{1}{2}(C'+F')+\frac{1}{2}(G''+H'')+G'''\right]}{\text{Total area}}\ X\ 100\% \qquad (1)$$

Another approach employed to calculate the percent inversion involved comparing the measured and calculated intensities of the signals from the four triad sequences $V\ V\ V$, $V\ \overline{V}\ V$, $V\ V\ \overline{V}$ and $\overline{V}\ V\ V$, where V represents a normal addition and $\overline{V}$ represents an inversion. Of course these sequences are indistinguishable from $\overline{V}\ \overline{V}\ \overline{V}$, $\overline{V}\ V\ \overline{V}$, $\overline{V}\ \overline{V}\ V$ and $V\ \overline{V}\ \overline{V}$ tetrads, however, the latter four tetrads resulting from double and triple inversions are improbable in this polymer. Microsoft's Excel solver feature was used to find the minimum of the square of the difference between the measured and calculated intensities. Using this approach the percent inversion was calculated to be 5.1 %. Thus the two values do agree very well for the polymer studied here.

Conclusions

The presence of three NMR active nuclei ^{1}H, ^{19}F and ^{13}C, in PVDF provide a variety of single, double and triple resonance NMR experiments for extracting structure information. However, experiments that measure ^{13}C signals directly are of limited use, due to their lower sensitivity. The resonances of ^{13}C in structures with a low probability of occurrence were therefore not directly detected and assigned. The ^{1}H NMR experiments, though very sensitive, are handicapped as there is considerable overlap of the resonances; this makes ^{1}H resonance assignments difficult.

^{19}F NMR is particularly useful for analysis of fluoropolymers due to the large chemical shift dispersion, the high sensitivity of ^{19}F nuclei and the large influence of substituent effects (up to 5-bonds away) on their chemical shifts. In making resonance assignments of fluoropolymers, comparison of 1D coupled and decoupled ^{19}F and ^{1}H NMR spectra provides very useful information to aid in the assignments. Though the ^{19}F COSY experiment is very sensitive, it sometimes gives ambiguous correlations, as $^{3}J_{FF}$, $^{4}J_{FF}$ and $^{5}J_{FF}$ correlations can all be observed. The $^{19}F\{^{13}C\}$ HSQC (optimized for $^{1}J_{CF}$ or $^{2}J_{CF}$) and $^{19}F\{^{1}H\}$ COSY or HETCOR experiments help to distinguish the $^{3}J_{FF}$, $^{4}J_{FF}$ and $^{5}J_{FF}$ COSY correlations from one another; this provides unequivocal assignment of resonances.

The 2D-NMR experiments described above have been used to assign the ^{19}F resonances from PVDF. Resonances resulting from single inversion of VDF monomer and those resulting from double inversion of VDF monomer units are assigned in this work. This work confirms assignments made earlier in the literature using 1D NMR and empirical calculations; it also provides assignment of some resonances not previously assigned.

Throughout the manuscript reference is made to data not shown, in attempt to keep the length of this paper manageable. Additionally, assignments of chain end resonances are given without proof. The identification of chain-end structures and proof of their resonance assignments will appear in a companion paper (*28*). Data not shown in this paper are shared in the supplemental section of this companion paper.

Downloaded by OHIO STATE UNIV LIBRARIES on August 28, 2012 | http://pubs.acs.org
Publication Date (Web): August 16, 2012 | doi: 10.1021/bk-2012-1106.ch012

Downloaded by OHIO STATE UNIV LIBRARIES on August 28, 2012 | http://pubs.acs.org
Publication Date (Web): August 16, 2012 | doi: 10.1021/bk-2012-1106.ch012

Acknowledgments

We wish to acknowledge the support of The Ohio Board of Regents and The National Science Foundation (CHE-0341701 and DMR-0414599) for funds used to purchase the NMR instrument used for this work. We thank NSF (DMR-0905120) and E. I. du Pont de Nemours and Company for its support of this work. We wish to thank A. Zens and the probe manufacturing group at Varian Instruments for their effort in providing some of the instrument hardware used in this work. We also wish to thank the staff of the Magnetic Resonance Center at the University of Akron, especially S. Stakleff and V. Dudipala for their help in maintaining the instruments used for this work. The authors would also like to acknowledge A. Moore who prepared the original PVDF samples.

References

1. Schilling, F. C. *J. Magn. Reson.* **1982**, *47*, 61–67.
2. Tonelli, A. E.; Schilling, F. C.; Cais, R. E. *Macromolecules* **1981**, *14*, 560–564.
3. Souzy, R.; Ameduri, B.; Ahsen, S. V.; Willner, H.; Arguello, G. A. *J. Fluorine Chem.* **2003**, *123*, 85–93, and references cited therein.
4. Liu, J.; Tai, H.; Howdle, S. M. *Polymer* **2005**, *46*, 1467–1472, and references cited therein.
5. Lovinger, A. J. In *Developments in Crystalline Polymers I*; Basset, D. C, Ed.; Applied Science Publishers: London, 1982, pp 195−238.
6. Russo, S.; Behari, K.; Chengji, S.; Pianca, M.; Barchiesi, E.; Moggi, G. *Polymer* **1993**, *34*, 4777–4781.
7. Cais, R. E.; Kometani, J. M. *Macromolecules* **1985**, *18*, 1354–1357, and references cited therein.
8. Tonelli, A. E.; Schilling, F. C.; Cais, R. E. *Macromolecules* **1982**, *15*, 849–853.
9. Liepins, R.; Surles, J. R.; Morosoff, N.; Stannett, V. T.; Timmons, M. L.; Wortman, J. J. *J. Polym. Sci.: Polym. Chem. Ed.* **1978**, *16*, 3039–3044.
10. Ferguson, R. C.; Brame, E. G., Jr. *J. Phys. Chem.* **1979**, *83*, 1397–1401and references therein.
11. Herman Uno, T.; Kubono, A.; Umemoto, S.; Kikutani, T.; Okui, N. *Polymer* **1997**, *38*, 1677–1683.
12. Katoh, E.; Ogura, K.; Ando, I. *Polym. J.* **1994**, *26*, 1352–1359.
13. Wormald, P.; Ameduri, B.; Harris, R. K.; Hazendonk, P. *Polymer* **2008**, *49*, 3629–3638.
14. Wormald, P.; Apperley, D. C.; Beaume, F.; Harris, R. K. *Polymer* **2003**, *44*, 643–651.
15. *Encyclopedia of Polymer Science and Technology*, 3rd ed.; Wiley-Interscience: New York, 2003; Vol. 4, p 510.
16. Madorskaya, L. Y.; Loginova, N. N.; Panshin, Y. A.; Lobanov, A. M. *Polym. Sci. USSR* **1983**, *25*, 2490–2496.
17. Shaka, A. J.; Keeler, J.; Frenkiel, T.; Freeman, R. *J. Magn. Reson.* **1983**, *52*, 335–338.

18. Shaka, A. J.; Keeler, J.; Freeman, R. *J. Magn. Reson.* **1983**, *53*, 313–340.
19. Fu, R.; Bodenhausen, G. *J. Magn. Reson.* **1995**, *117*, 324–325.
20. Xiaohong, Li; McCord, E. F.; Baiagern, S.; Fox, P.; Howell, J. L.; Sahoo, S.; Rinaldi, P. L. *Magn. Reson. Chem.* **2011**, *49*, 413–424.
21. Rinaldi, P. L.; Baiagern, S.; Fox, P.; Howell, J. L.; Li, X. Li, L.; Lyons, D. F.; McCord, E. F.; Sahoo, S. K.; Twum, E. B.; Wyzgosksi, F. J. Advanced Solution 2D-NMR of Fluoropolymers. In *NMR Spectroscopy of Polymers: Innovative NMR Strategies for Complex Macromolecular Systems*; ACS Symposium Series 1077; Chen, H. N., Asakura, T., English, A., Eds.; American Chemical Society: Washington, DC, 2011; Chapter 21, pp 355−369.
22. States, D. J.; Haberkorn, R. A.; Ruben, D. J. *J. Magn. Reson.* **1982**, *48*, 286–292.
23. Apostolo, M.; Arcella, V.; Storti, G.; Morbidelli, M. *Macromolecules* **1999**, *32*, 989–1003.
24. Battiste, J. L.; Jing, N.; Newmark, R. A. *J. Fluorine Chem.* **2004**, *125*, 1331–1337.
25. Wimperis, S.; Freeman, R. *J. Magn. Reson.* **1984**, *58*, 348–353.
26. Cais, R. E.; Sloane, N. J. A. *Polymer* **1983**, *24*, 179–187.
27. Pianca, M.; Barchiesi, E.; Esposto, G.; Radice, S. *J. Fluorine Chem.* **1999**, *95*, 71–84.
28. Twum, E. B.; Gao, C.; Li, X.; McCord, E. F.; Fox, P. A.; Lyons, D. F.; Rinaldi, P. L. *Macromolecules* **2012**, DOI: 10.1021/ma300836.

Downloaded by OHIO STATE UNIV LIBRARIES on August 28, 2012 | http://pubs.acs.org
Publication Date (Web): August 16, 2012 | doi: 10.1021/bk-2012-1106.ch012

Subject Index

A

Aggregation behaviour, perfluorinated amphiphilic polymers, 113*f*
Aluminum nanoparticles, 132*f*
  combustion, 138*f*
  compressive strength, 139*t*
  functionalization, 135*s*, 136*f*
  in situ formation, 136*s*
  TEM, 139*f*
Aryl trifluorovinyl ethers, 12*s*

B

Biomedical applications, fluoropolymers, 4
Biphenyl perfluorocyclobutyl, 83*f*
Bridged sulfate reaction, 100*f*, 101*f*

C

Carbonate side-groups, fluorinated copolymers, 143
  DEPT ^{13}C NMR spectra, 151*f*
  ^{19}F NMR spectra, 150*f*
  fluoroolefins, 145
  GCVE monomer, 144*s*, 145, 145*f*, 146*s*
  ^{1}H NMR spectra, 149*f*
  TGA thermograms, 152*f*
  thermal properties, 148, 152*t*
Cassie-Baxter state, superoleophobic surfaces, 174*f*
Citations, fluoropolymers, 2*f*
Contact angle measurements, F-POSS, 106*t*, 107*f*
Copolymer synthesis, fluoropolymers, 3
Cotton textile, superoleophobic surfaces, 178*f*
Cyclic PFPE, 11*s*
  See also perfluoropolyethers (PFPE)

D

Disilanol reaction, 104*f*

E

Energy applications, fluoropolymers, 5
Ethanol droplet, superoleophobic surfaces, 180*f*

F

FAVE. *See* fluorinated arylene vinylene ether (FAVE) polymers
Fluorinated arylene vinylene ether (FAVE) polymers
  chromophore-modified, 19*s*
  network polymers, 22, 23*s*
  overview, 9
  polymerization, 14*s*, 15*s*
  proton exchange membranes, 19*f*
  segmented block copolymers, 22
  step-growth polymers, 13
    functionalized polymers, 18
    methodology, 13
    polymerization kinetics, 17
    thermal properties, 15
  telechelomers, 20, 20*s*
  TGA analysis, 16*f*
Fluorinated copolymers
  autoclave operations, 162
  carbonate side-groups, 143
    DEPT ^{13}C NMR spectra, 151*f*
    ^{19}F NMR spectra, 150*f*
    fluoroolefins, 145
    GCVE monomer, 144*s*, 145, 145*f*, 146*s*
    ^{1}H NMR spectra, 149*f*
    TGA thermograms, 152*f*
    thermal properties, 148, 152*t*
  characterization, 160
    differential scanning calorimetry, 161
    elemental analyses, 161
    nuclear magnetic resonance, 160
    size exclusion chromatography, 161
    thermogravimetric analyses, 161
  GCVE, 163
  methoxyoligo(ethylene oxide), 163
  methoxy-tri(ethylene oxide), 163
  oligo(ethylene oxide), 152, 154*s*
    ^{13}C NMR spectra, 158*f*
    ^{19}F NMR spectra, 157*f*
    glass transition temperature, 159*t*
    ^{1}H NMR spectra, 155*f*, 157*f*

Downloaded by 89.163.34.136 on August 28, 2012 | http://pubs.acs.org
Publication Date (Web): August 16, 2012 | doi: 10.1021/bk-2012-1106.ix002

Downloaded by 89.163.34.136 on August 28, 2012 | http://pubs.acs.org
Publication Date (Web): August 16, 2012 | doi: 10.1021/bk-2012-1106.ix002

        TGA thermograms, 159*f*
    overview, 141
    radical copolymerization, 164
        chlorotrifluoroethylene, 165
        CTFE, 146*t*, 155*t*, 164
        GCVE, 146*t*, 164
        HFP, 146*t*, 164
        PMVE, 146*t*, 164
Fluorinated homopolymers, 70*t*
Fluorinated polymers, solubility, 74*t*, 75*t*
Fluorinated vinyl ethers, 69*f*, 71*f*, 72*f*, 73*f*, 76*f*
Fluorine-containing solvents, 67*t*
Fluorine-containing star-shaped polymers, 70, 71*s*, 74*f*, 77*f*
Fluoroalkyl polyhedral oligomeric silsesquioxanes (F-POSS)
    bridged sulfate reaction, 100*f*, 101*f*
    ^{13}C NMR, 105*f*
    cage opening, 99*f*
    characterization, 97
    contact angle measurements, 106*t*, 107*f*
    disilanol reaction, 104*f*
    free radical copolymerization, 107*f*
    monomer polymerization, 98
    monomer synthesis, 98
    ORTEP, 102*f*, 103*f*
    overview, 95
    peripheral chain lengths, 96*f*
    ^{29}Si NMR, 100*f*, 101*f*, 105*f*
    x-ray crystallography data, 98
Fluorocarbons, 134
Fluorophilic-lipophilic block copolymer emulsifier synthesis, 116*s*
Fluoropolymers, 134, 135
    biomedical applications, 4
    characterization, 6
    citations, 2*f*
    composites, 4
    copolymer synthesis, 3
    energy applications, 5
    homopolymer synthesis, 3
    low energy surfaces, 5
    overview, 1
Fluorous emulsions, perfluorinated amphiphilic polymers, 114
F-POSS. *See* fluoroalkyl polyhedral oligomeric silsesquioxanes (F-POSS)
Free radical copolymerization, 107*f*

H

Homopolymer synthesis, fluoropolymers, 3

I

Interface-active substance properties, perfluorinated amphiphilic polymers, 112*t*

L

Light metals, energy densities, 130*f*
Linear PFPE, 11*s*
    See also perfluoropolyethers (PFPE)
Linear polymers, 74, 74*t*
Living cationic polymerization, 67
Lotus leaf, superoleophobic surfaces, 173*f*

M

Methoxyoligo(ethylene oxide), 163
Methoxy-tri(ethylene oxide), 163
Monomer polymerization, F-POSS, 98
Monomer synthesis, F-POSS, 98

N

Network polymers, FAVE, 22, 23*s*
Neutron reflectivity, 86*f*, 89*f*

O

Octafluorocuclopentene (OFCP), 24*f*, 25*s*
OFCP. *See* octafluorocuclopentene (OFCP)
Oligo(ethylene oxide), 152, 154*s*
    ^{13}C NMR spectra, 158*f*
    ^{19}F NMR spectra, 157*f*
    glass transition temperature, 159*t*
    ^{1}H NMR spectra, 155*f*, 157*f*
    TGA thermograms, 159*f*
Olive oil, superoleophobic surfaces, 182*f*
Oxidizers
    aluminum nanoparticles, 132*f*, 135*s*, 136*f*, 136*s*, 137*f*, 138*f*, 139*f*, 139*t*
    fluorocarbons, 134
    fluoropolymers, 134, 135
    light metals, energy densities, 130*f*
    non-PTFE, 133
    overview, 127
    PTFE, 128, 130*s*
    reactive particle composites, 135

Downloaded by 89.163.34.136 on August 28, 2012 | http://pubs.acs.org
Publication Date (Web): August 16, 2012 | doi: 10.1021/bk-2012-1106.ix002

P

Peanut oil, superoleophobic surfaces, 182*f*
Perfluorinated amphiphilic polymers
  aggregation behaviour, 113*f*
  fluorophilic-lipophilic block copolymer emulsifier synthesis, 116*s*
  fluorous emulsions, 114
  interface-active substance properties, 112*t*
  overview, 111
  polyethylene, 116*f*
  polymer stabilized metal particles, 118*f*
  polymerization, 115*f*
  polypropylene, 116*f*
  raspberry, 122*f*, 123*t*
  structures, 117*s*, 122*s*
  superhydrophobic surface preparation, 120
  surface active properties, 113*f*
  surface modification, 117
  TEM micrographs, 119*f*, 120*f*
Perfluorocycloalkene, 24*f*
Perfluorocyclobutyl (PFCB), 12*s*, 20*s*, 21*s*
Perfluoropolyethers (PFPE), 9, 10*s*, 11*s*
Peripheral chain lengths, F-POSS, 96*f*
PFCB. *See* perfluorocyclobutyl (PFCB)
PFPE. *See* perfluoropolyethers (PFPE)
Poly(IBVE), 68*f*, 72*f*, 73*f*
Poly(tetrafluoroethylene) (PTFE), 128
Polyhedral oligomeric silsesquioxane (POSS), 81
Polymer stabilized metal particles, 118*f*
Polymer-fluorodecyl POSS blends, superoleophobic surfaces, 179*f*
Polyvinylidene fluoride (PVDF)
  carbon sequences, 194*t*
  1D-NMR resonance, 195, 196*f*, 197*f*, 198*f*
  double quantum filtered COSY, 198, 205*f*
  ^{19}F backbone resonances, 202, 208*t*
  ^{19}F-^{19}F selective COSY experiment, 199, 200*f*
  gradient heteronuclear correlation, 198, 206*f*
  gradient heteronuclear single quantum coherence, 201, 201*f*, 204*f*
  homopolymerization, 193*s*
  instrumentation, 190
    1D-NMR spectra acquisition, 190
    2D-NMR spectra acquisition, 191
  overview, 187
  reverse unit content calculation, 210
  sample preparation, 190
  synthesis, 190
POSS. *See* polyhedral oligomeric silsesquioxane (POSS)
PTFE. *See* Poly(tetrafluoroethylene) (PTFE)
PVDF. *See* polyvinylidene fluoride (PVDF)

R

Rapeseed oil, superoleophobic surfaces, 177*f*

S

Segmented block copolymers, 22
Semifluorinated polyarylene copolymers
  ATR-FTIR spectra, 38*f*, 39*f*
  characterization, 33
  Diels-Alder polymerization, 31*s*
  fluorine content, 40*f*
  general polymerization procedures, 31
  ^{1}H NMR spectra, 36*f*
  ^{19}H NMR spectra, 37*f*
  overview, 29
  polymer properties, 42*t*
  sessile drop analysis, 43*f*
  thermal gravimetric analysis, 41*f*
Semifluorinated polymer thin films
  biphenyl perfluorocyclobutyl, 83*f*
  film thickness, 91*f*
  neutron reflectivity, 86*f*, 89*f*
  overview, 81
  POSS, 83*f*, 84*t*, 89*f*, 90*f*, 91*f*
  preparation, 84
Sessile drop analysis, 43*f*
Silanes, superoleophobic surfaces, 182*f*
Star polymers, 74, 74*t*, 76*t*, 77*f*
Step-growth polymers, 13
  functionalized polymers, 18
  methodology, 13
  polymerization kinetics, 17
  thermal properties, 15
Superhydrophobic surface preparation, 120
Superoleophobic surfaces
  Cassie-Baxter state, 174*f*
  cotton textile, 178*f*
  design, 174
  ethanol droplet, 180*f*
  lotus leaf, 173*f*
  olive oil, 182*f*
  overview, 171
  peanut oil, 182*f*
  polymer-fluorodecyl POSS blends, 179*f*
  rapeseed oil, 177*f*

Downloaded by 89.163.34.136 on August 28, 2012 | http://pubs.acs.org
Publication Date (Web): August 16, 2012 | doi: 10.1021/bk-2012-1106.ix002

- silanes, 182*f*
- textured surface wetting, 172
- water droplet, 180*f*
- Wenzel state, 174*f*

T

Telechelomers, 20
Temperature-induced solubility transitions, 77
Textured surface wetting, superoleophobic surfaces, 172
TFVE. *See* trifluorovinyl ether (TFVE)
Trifluorovinyl ether (TFVE), 12*s*, 14*s*

V

Vinyl ether polymers
- fluorinated homopolymers, 70*t*
- fluorinated polymers, solubility, 75, 75*t*
- fluorinated vinyl ethers, 69*f*, 71*f*, 72*f*, 73*f*, 76*f*
- fluorine-containing solvents, 67*t*
- fluorine-containing star-shaped polymers, 70, 71*s*, 74*f*, 77*f*
- linear polymers, 74, 74*t*
- living cationic polymerization, 67
- monomers, 66*c*
- overview, 65
- poly(IBVE), 68*f*, 72*f*, 73*f*
- star polymers, 74, 74*t*, 76*t*, 77*f*
- temperature-induced solubility transitions, 77

Vinylidene fluoride
- Cp_2TiCl, 55*s*, 56*t*
- overview, 47
- polymerizations, 50
- solvent effect, 51*t*
- VDF polymerizations, 51*t*, 55*s*
- VDF/HFP copolymerizations, 54*f*

W

Water droplet, superoleophobic surfaces, 180*f*
Wenzel state, superoleophobic surfaces, 174*f*